



The Institute of Oceanology of the Polish Academy of Sciences (IO PAN)

MAPPING OF OPTIMAL ENVIRONMENTAL CONDITIONS FOR
THE EXISTENCE OF SELECTED FISH SPECIES CAUGHT
INDUSTRIALLY IN THE AREA OF THE GULF OF GDAŃSK
USING NUMERICAL MODELS AND MEASUREMENT DATA

Maciej Janecki

Series of publications constituting the doctoral dissertation

The thesis prepared under
the supervision of Prof. Lidia Dzierzbicka-Głowacka

Sopot 2023



Instytut Oceanologii Polskiej Akademii Nauk

MAPOWANIE OPTYMALNYCH WARUNKÓW
ŚRODOWISKOWYCH DLA BYTOWANIA WYBRANYCH
GATUNKÓW RYB POŁAWIANYCH PRZEMYSŁOWO
W REJONIE ZATOKI GDAŃSKIEJ Z WYKORZYSTANIEM
MODELI NUMERYCZNYCH I DANYCH POMIAROWYCH

Maciej Janecki

Cykl publikacji stanowiący rozprawę doktorską

Praca przygotowana
pod kierunkiem prof. dr hab. Lidii Dzierzbickiej-Głowackiej

Sopot 2023

Contents

1	List of abbreviations	7
2	English abstract	9
2.1	Introduction	9
2.2	Material and methods	10
2.2.1	Model EcoFish	10
2.2.2	Fish Module	10
2.2.3	Study area	10
2.3	Results and discussion	11
2.3.1	Hydrodynamic part of the EcoFish model	11
2.3.2	Algorithm for determining the top of the thermocline and halocline depths	11
2.3.3	Biochemical part of the EcoFish model	11
2.3.4	Mapping the optimal environmental conditions for the habitat of sprat, herring, cod, and flounder in the Gulf of Gdańsk region	12
2.4	Summary	12
3	Streszczenie	13
3.1	Wstęp	13
3.2	Materiał i metody	14
3.2.1	Model EcoFish	14
3.2.2	Moduł Fish	16
3.2.3	Obszar badań	17
3.2.4	Dane wykorzystane do walidacji modelu EcoFish i Modułu Fish	17
3.3	Rezultaty i dyskusja	17
3.3.1	Część hydrodynamiczna modelu EcoFish	17
3.3.2	Algorytm do wyznaczania szczytu głębokości termokliny i halokliny	18
3.3.3	Część biochemiczna modelu EcoFish	18
3.3.4	Mapowanie optymalnych warunków środowiskowych dla bytowania szprota, śledzia, dorsza i storni w rejonie Zatoki Gdańskiej	19
3.4	Podsumowanie	20
	References (Bibliografia)	21
4	Series of publications constituting the PhD thesis	23
4.1	Research paper no. 1	23
4.2	Research paper no. 2	63
4.3	Research paper no. 3	79
5	Attachment	99
6	Authorship statements	119
7	Acknowledgments	133

1 List of abbreviations

Abbreviation	Explanation
3D CEMBS	three-dimensional Coupled Ecosystem Model of the Baltic Sea
AREX	Arctic Expedition
AVHRR	Advanced Very High Resolution Radiometer
BHI	Baltic Health Index
BSBD	Baltic Sea Bathymetric Database
CESM	Community Earth System Model
CHL	chlorophyll <i>a</i>
CI TASK	Centre of Informatics Tricity Academic Supercomputer and network
CICE	Community Ice CodE
CIL	cold intermediate layer
CTD	instrument used to measure the electrical conductivity, temperature, and pressure of seawater
FRAME	moving mean and moving STD sliding window
GD	Gdańsk Deep
GNS	gillnet
GPS	Global Positioning System
HELCOM	Baltic Marine Environment Protection Commission – also known as the Helsinki Commission
HP	Hel Peninsula
HSI	Habitat Suitability Index
HYPE	Hydrological Predictions for the Environment
ICES	International Council for the Exploration of the Sea
ICM UW	Interdisciplinary Centre for Mathematical and Computational Modelling of Warsaw University
IO PAN	Institute of Oceanology of the Polish Academy of Sciences
KPP	k-profile parameterization
MIDAS CTD+	Valeport’s premier Multiparameter CTD Profiler
MINSTD	profile’s minimum standard deviation
MLD	mixed layer depth
Modflow	modular finite-difference flow model
MODIS	Moderate Resolution Imaging Spectroradiometer
MovSTD	algorithm for finding the top of thermocline and halocline
MSTD	moving standard deviation
N ₂	molecular nitrogen
NaN	Not a Number
NCAR	National Center for Atmospheric Research
NH ₄	ammonia
NO ₂	nitrite
NO ₃	nitrate
NPZD	nutrient–phytoplankton–zooplankton–detritus
O ₂	oxygen
OGCM	Ocean General Circulation Model
OTB	bottom otter trawl

Abbreviation	Explanation
OTM	pelagic trawl
PCHIP	Piecewise Cubic Hermite Interpolating Polynomial
PO ₄	phosphate
POP	Parallel Ocean Program
PSU	Practical Salinity Unit
PTM	pelagic pair trawl
<i>r</i>	Pearson correlation coefficient
RMSE	root-mean-square-error
SALT	salinity
SCS	Soil Conservation Service
SiO ₃	silicate
SSH	sea surface height
SST	sea surface temperature
STD	standard deviation
SWAT	Soil & Water Assessment Tool
SY	sailing yacht
TEMP	temperature
THD	the top of halocline
THRES	threshold
TTD	the top of thermocline
UM	Unified Model
VR	Vistula River

2 English abstract

2.1 Introduction

Commercial fishing plays a vital role in the global food chain, providing a source of food for millions of people around the world. However, with technological progress and population growth, fisheries face numerous challenges and difficulties that have a significant impact on the sustainable management of fish resources (Godfray et al. 2010). The fishing industry faces several problems that threaten marine life, the environment, and the economy (Hilborn et al. 2003). Overfishing can cause a decline not only in fish populations (Myers and Worm 2003), but also lead to starvation of fish-eating birds (Camphuysen and Garthe 2000), which can have ripple effects throughout the ecosystem. At the same time, it should be remembered that fishing is driven by living people (fishers), for whom it is often the only source of income. Regulations aimed at protecting declining or endangered species and the environment make day-to-day fishing less and less profitable.

Trying to help overcome these problems, we decided to implement the project called “*Knowledge Transfer Platform FindFISH – Numerical Forecasting System for the Marine Environment of the Gulf of Gdańsk for Fisheries*” (Lidia Dzierzbicka-Głowacka, Nowicki, et al. 2018; L. Dzierzbicka-Głowacka 2023). The aim of *FindFISH* is to deal with the declining profitability of commercial fisheries, by reducing fishing time (fuel saving) and thus prevent environmental pollution. Our numerical modeling approach will enable fishers to optimize their catch and avoid bycatch. The result of the project is a user-friendly web service (www.findfish.pl) that provides accessible information regarding the physical and biochemical state of the Gulf of Gdańsk in the form of 48-hour forecasts.

One of the key components of this system is the “*Fish Module*” - algorithm designed to generate maps of the Habitat Suitability Index (HSI), indicating the locations of the best environmental conditions for fish in the Gulf of Gdańsk. It is implemented for four species: sprat (*Sprattus sprattus*), herring (*Clupea harengus*), cod (*Gadus morhua*), and flounder (*Platichthys flesus*). We expect the *Fish Module* to be the most demanded product of the *FindFISH* service.

The research conducted as part of this doctoral thesis confirmed the main research hypothesis, which posited that **it is possible to determine optimal environmental conditions for the habitat of selected fish species occurring in the southern Baltic Sea region (particularly in the Gulf of Gdańsk) by using numerical modeling.**

Four specific objectives were established to confirm the research hypothesis:

1. Characterize the structure and variability of hydrodynamic parameters in the Gulf of Gdańsk region.
2. Investigate the vertical structure of water in the Gulf of Gdańsk region with a precise determination of the thermocline and halocline, which act as barriers to fish migration.
3. Characterize the structure and variability of biochemical parameters in the Gulf of Gdańsk, and the influence of limiting factors on the primary production of phytoplankton.
4. Apply numerical modeling to identify areas where optimal conditions for the habitat of sprat, herring, cod, and flounder occur in the Gulf of Gdańsk region, based on the environmental preferences of these species.

Each of the specific objectives mentioned above has been discussed in a separate scientific articles, and their compilation forms the subject of this dissertation.

This doctoral dissertation consists of three published scientific papers in peer-reviewed journals and a manuscript attached at the end of the dissertation, which was submitted to the journal and is a consistent continuation of the research undertaken in the previous three papers.

The first paper (Janecki, Dybowski, Jakacki, et al. 2021) focuses on the description and validation of the hydrodynamic component of the *EcoFish* model. The second paper (Janecki, Dybowski, Rak, et al. 2022) presents an innovative method for determining the top depths of the thermocline and halocline. The third paper (Janecki, Dybowski, and Lidia Dzierzbicka-Głowacka 2023) presents and validates the biochemical component of the *EcoFish* model and investigates how limiting factors influence the nature and intensity of primary production of phytoplankton. The fourth manuscript (Janecki and Lidia Dzierzbicka-Głowacka 2023) is dedicated to the *Fish Module*, which utilizes fuzzy logic to create maps of the most favorable environmental conditions (Habitat Suitability Index - HSI) for commercially harvested fish species in the Gulf of Gdańsk region, namely

herring, sprat, cod (until 2021), and flounder. The largest part of the manuscript is devoted to the analysis of data from fishing expeditions and the validation of the results obtained from the *Fish Module* by comparing HSI values with catch efficiencies from fishing expeditions conducted during the project. The *Fish Module* utilizes data from the *EcoFish* model to calculate HSI score.

2.2 Material and methods

2.2.1 Model EcoFish

The *EcoFish* model is based on the source code of the Community Earth System Model (CESM), a global coupled climate model. CESM consists of five separate components with an additional module controlling time, forcing, domains, grids, and information exchange between the individual modules. Within the *FindFISH* project, CESM was downscaled and adapted for the Gulf of Gdańsk region. The horizontal resolution of the *EcoFish* model is 575 meters, and vertically it is a *z-type* model with 26 levels, each with a thickness of 5 meters. The *EcoFish* model comprises two active (performing numerical simulations) parts: the hydrodynamic and the biochemical components.

The hydrodynamic component is an ocean model, based on the source code of the Parallel Ocean Program (POP), which utilizes three-dimensional motion equations with hydrostatic and Boussinesq approximations.

The biochemical component of *EcoFish* is based on an NPZD-type model (Moore et al. 2001). The model determines the concentrations of nutrients, three types of phytoplankton (diatoms, small phytoplankton, and diazotrophs capable of directly fixing atmospheric nitrogen), chlorophyll *a*, microzooplankton, pelagic detritus, and dissolved oxygen concentration.

2.2.2 Fish Module

The *Fish Module* is a computer algorithm that constitutes the final element of the *Knowledge Transfer Platform FindFISH*. Using expert knowledge and data on water temperature, salinity, oxygen saturation, fishing depth, and catch composition and weight, we were able to determine the optimal conditions for the habitat of four commercially fished species in the Gulf of Gdańsk region. These species are herring, sprat, cod (until 2021), and flounder. Subsequently, fuzzy rules were established that connect the input variables to the preferences of each species. This fuzzy system uses the *EcoFish* model data to determine the Habitat Suitability Index (HSI) for the Gulf of Gdańsk region. The HSI indicates the habitat conditions in the studied area. The HSI score ranges from 0 to 1, where 0 indicates that the habitat does not meet the conditions for the occurrence of a particular species, while 1 describes a habitat with optimal conditions.

The determination of membership functions in the *Fish Module* involved the utilization of data defining the ranges of preferable values for each parameter governing the habitat of sprat, herring, cod, and flounder. These ranges were established based on physicochemical data (temperature, salinity, oxygen saturation, and fishing depth) and fishing data (catch composition and weight) collected during fishing expeditions.

The median of the optimal value was implemented along with a constant deviation C , and the minimum/maximum at the edges. The preferences of each species implemented in the *Fish Module* were fuzzified in a way that the central trapezoid encompassed the optimal values of the respective parameter for the species' habitat, while lower and higher values represented conditions below and above the optimal range, respectively.

2.2.3 Study area

The effective domain of the *EcoFish* model includes the extended Gulf of Gdańsk, which is the southern part of the Gdańsk Deep area, located in the Gotland Basin. A straight line connecting Cape Rozewie with Cape Taran delimits the proper Gulf of Gdańsk. This line crosses the deepest parts of the Gdańsk Deep, with a maximum depth of 118 meters. Along the coastal zone there is a wide strip of shallows widening to the west of the mouth of the Vistula River. The slope of the bottom in the coastal zone is varied. The greatest decline occurs at the headland of the Hel Peninsula, where the bottom rapidly drops to a depth of 70 meters (Majewski 1972).

2.3 Results and discussion

In this chapter, the most important results of the research are presented, while the individual results and analyzes are presented in the articles that constitute this doctoral dissertation.

2.3.1 Hydrodynamic part of the EcoFish model

The validation showed that the *EcoFish* model results for water temperature were consistent with *in situ* observations. The correlation of the *EcoFish* model with ICES data was 0.94 with the root mean square error (RMSE) of 1.33 °C. As a result of comparing the modeled temperature against the data from the database created during fishing cruises, a correlation coefficient of 0.87 was calculated. This is a satisfactory result, taking into account, the strong concentration of cruise data in the belt from the mouth of the Vistula River in the northwest direction. Thus, the data come both from the area where there is mixing of river waters (from the Vistula River) with the waters of the Gulf and from the area where the strongest currents occur in the entire domain (the belt along the Hel Peninsula).

The correlation of the model results for salinity with the ICES data at the level of 0.94 and the low root mean square error of 0.8 PSU suggest that the model copes well with the transport of water masses. It also proves that the rivers in the model have been correctly implemented and that the outgoing freshwater is correctly mixed with the saltwater of the Gulf and distributed by currents in its area.

2.3.2 Algorithm for determining the top of the thermocline and halocline depths

The second article (Janecki, Dybowski, Rak, et al. 2022) presents an innovative method called the "*MovSTD Algorithm*" for determining the top of the thermocline (TTD) and halocline (THD) depths. The method has been calibrated using an extensive set of data from the *EcoFish* model. As a result of the calibration, the values of the input parameters that allowed the correct determination of TTD and THD were established. It was confirmed by the validation carried out on the *in situ* profiles collected by the research vessel S/Y Oceania during statutory cruises in the southern Baltic Sea. The *MovSTD* algorithm was then used to analyze the seasonal variability of the vertical structure of the waters in Gdańsk Deep for temperature and salinity. The thermocline deepening speed was also estimated in the region analyzed.

The motivation behind addressing this topic was the association between the thermocline and the occurrence of fish. In some cases, the thermocline can act as a barrier to fish movement, as they prefer specific temperature ranges. In such cases, fish may gather at the thermocline boundary where suitable habitat conditions are available. Therefore, knowledge of the thermocline depth can help determine where the presence of certain fish species can be expected.

The results from the *MovSTD* algorithm when tested on model data from the Gdańsk Deep region showed that the top of the halocline depth is permanent and is located at about 50 m. Noticeable changes in the depth of the halocline can be observed in the 7-yr period analyzed. From August to November, the THD begins to form higher, at depths between 35 and 50 m. In addition, between January and February 2015 and 2016 it reached instantaneous values of 70 m deep. However, it can be said that THD does not show significant seasonal variability and the vertical structure of salinity in the Gdańsk Deep is rather stable.

The situation is different for the thermocline. We can observe a strong seasonal variability here. A fresh thermocline begins to form in May due to the heating of the surface layer (forced by air temperature and sunlight). Its deepening speed from May to September is about 2 m per month. In the following months, as a result of water mixing and increased wind forcing, the thermocline deepening accelerates, reaching greater depths at a speed of about 9 m per month. At the turn of the year, this process stops, and until April thermocline occurs at the same depth as the halocline.

2.3.3 Biochemical part of the EcoFish model

The third article (Janecki, Dybowski, and Lidia Dzierzbicka-Głowacka 2023) presented the biochemical component of the *EcoFish* model for the Gulf of Gdańsk region. The basic parameters of the marine ecosystem were determined, including the concentration of chlorophyll *a*, dissolved oxygen, and concentration of nutrients as nitrate, phosphate, and silicate. The seasonal variability of these parameters was presented, and the model data was validated by comparing it with *in situ* data from the ICES database, yielding satisfactory results.

The article also examined how limiting factors (i.e., water temperature, nutrients, light) influence the primary production of phytoplankton and demonstrated that the intensity of spring diatom blooms affects the nature of cyanobacterial blooms in the summer. The analysis of the seasonal dynamics of primary production in the waters of the Gulf of Gdańsk was crucial for the conducted research, as this process is directly linked to oxygen production and consumption. In the analysis of primary production, it was shown that geomorphological conditions and the deposition of nutrients from rivers significantly influence its character and intensity. The availability of biogenic substances can significantly alter the biomass distribution of all phytoplankton groups. An excessive reduction in nitrate deposition in river waters aimed at mitigating marine eutrophication may, consequently, lead to a situation where short and weak diatom blooms occur in spring, followed by long and intense cyanobacterial blooms in summer.

2.3.4 Mapping the optimal environmental conditions for the habitat of sprat, herring, cod, and flounder in the Gulf of Gdańsk region

Janecki and Lidia Dzierzbicka-Głowacka 2023 is the final article that utilizes the knowledge and results obtained in the previous three published works. It focuses on the *Fish Module*, which is the most important element of the Knowledge Transfer Platform *FindFISH*. Using fuzzy logic, the *Fish Module* enables the creation of maps depicting the most favorable environmental conditions (HSI - Habitat Suitability Index) for the habitats of commercially harvested fish species in the Gulf of Gdańsk region.

By calculating the mean HSI values for all the analyzed fishing expeditions and species and comparing them with fishing efficiencies, it was observed that there is a threshold HSI value below which successful catches are unlikely to occur for sprat, herring, and cod. This indicates the system's accuracy in identifying locations with favorable environmental conditions for the habitat of these three species. Fishermen are advised to select routes where the HSI is at least 0.5 for herring and sprat, and greater than 0.4 for cod. Furthermore, a slight trend was observed for these three species, indicating an increase in fishing efficiency with higher HSI values. This shows that selecting routes with sufficiently high HSI values contributes to achieving higher fishing efficiencies.

Regarding flounder, the assessment based on comparing fishing efficiency with the mean HSI from the gillnet deployment position did not provide conclusive evidence regarding the system's ability to accurately identify locations with optimal environmental conditions for this species. Although there was a substantial amount of flounder data available, its spatial coverage was not as extensive as that of sprat or herring. The nets were deployed only within three specific areas: the southern part of the Gulf of Gdańsk, the vicinity of the Vistula Spit, and both sides of the Hel Peninsula.

2.4 Summary

The application of modern measurement techniques and numerical modeling within the *FindFISH* project allowed for the determination of optimal environmental conditions for the habitats of herring, sprat, cod, and flounder in the Gulf of Gdańsk region. The development of the *Fish Module* and the availability of HSI map forecasts through an online portal can lead to more selective fishing practices and cost reductions for the fishing industry.

The implementation of the *FindFISH* platform enables the diagnosis and forecasting of marine environmental conditions in the Gulf of Gdańsk, facilitating quick access to necessary information. This can result in the reduction of unwanted catches through informed fishing location selection based on specific numerical results presented in a transparent and comprehensible format.

3 Streszczenie

3.1 Wstęp

Rybołówstwo komercyjne odgrywa istotną rolę w globalnym łańcuchu pokarmowym, zapewniając źródło pożywienia dla milionów ludzi na całym świecie. Jednak wraz z postępem technologicznym i wzrostem populacji, rybołówstwo staje przed licznymi wyzwaniami i trudnościami, które mają istotny wpływ na zrównoważone zarządzanie zasobami rybnymi (Godfray i in. 2010). Przemysł rybacki boryka się z wieloma problemami, które zagrażają życiu morskemu, środowisku naturalnemu i gospodarce (Hilborn i in. 2003). Nadmierny połów może prowadzić nie tylko do spadku populacji ryb (Myers i Worm 2003), ale także do zagłodzenia ptaków, które się nimi żywią (Camphuysen i Garthe 2000), co może mieć długofalowe negatywne skutki dla ekosystemu. Przyłów (szacowany na 40% ogólnego globalnego połowu) można traktować jako marnowanie zasobów, prowadzące do śmierci wielu organizmów morskich, w tym zagrożonych gatunków (Davies i in. 2009). Innym ważnym problemem jest degradacja środowiska morskiego spowodowana zanieczyszczeniem olejami pochodzącymi z jednostek rybackich oraz wprowadzeniem nowoczesnych metod połowowych, takich jak trałowanie denne. Według ONZ nawet 95% globalnych szkód w oceanach może być bezpośrednim rezultatem wykorzystywania tej techniki połowowej (Secretary-General 2006). Jednocześnie należy pamiętać, że rybołówstwo jest prowadzone przez ludzi (rybaków), dla których często jest to jedyne źródło dochodu. Regulacje mające na celu ochronę środowiska i znikających lub zagrożonych wyginięciem gatunków, sprawiają, że rybołówstwo staje się coraz mniej dochodowe. Wielu rybaków zmuszonych jest szukać oszczędności lub porzucić rybołówstwo poprzez zmianę zawodu.

Aby przeciwdziałać tym problemom powstał projekt o nazwie "*Platforma Transferu Wiedzy FindFISH - Numeryczny System Prognozowania warunków środowiska morskiego Zatoki Gdańskiej dla Rybołówstwa*" (Lidia Dzierzbicka-Głowacka, Nowicki i in. 2018; L. Dzierzbicka-Głowacka 2023). Głównym celem projektu *FindFISH* jest przeciwdziałanie spadającej rentowności rybołówstwa komercyjnego poprzez skrócenie czasu połowów (oszczędność paliwa), a tym samym zapobieganie zanieczyszczeniu środowiska. Podejście oparte na modelowaniu numerycznym umożliwi rybakom optymalizację połowu i unikanie niechcianych przyłówów. Ponadto projekt poprawi bezpieczeństwo morskie i warunki pracy. Dzięki złowieniu tej samej (lub większej) ilości ryb podczas krótszych wypraw, załogi statków będą mniej obciążone pracą co powinno wpłynąć na zwiększenie bezpieczeństwa na morzu. Zmniejszone zużycie paliwa przyczyni się do dodatkowych oszczędności i mniejszego zanieczyszczenia środowiska. W wyniku realizowanych w projekcie *FindFISH* prac, został stworzony przyjazny użytkownikowi serwis internetowy (www.findfish.pl), który odpowiedzialny jest za dostarczanie informacji o stanie parametrów fizycznych i biochemicznych Zatoki Gdańskiej w formie 48-godzinnych prognoz.

Jednym z kluczowych elementów tego systemu jest *Moduł Fish* - algorytm, który generuje mapy wskaźnika przydatności siedliskowej (Habitat Suitability Index - HSI), wskazując miejsca o najlepszych warunkach środowiskowych dla ryb w rejonie Zatoki Gdańskiej. *Moduł Fish* został zaimplementowany dla czterech gatunków: szprota (*Sprattus sprattus*), śledzia (*Clupea harengus*), dorsza (*Gadus morhua*) oraz storni (*Platichthys flesus*). Ocena przydatności siedliskowej jest ważnym aspektem ochrony siedlisk w pobliżu ujść rzek. W literaturze istnieje kilka metodologii stosowanych do obliczania wskaźnika przydatności siedliskowej (Beecher, Caldwell i DeMond 2002; Bovee 1986; Inglis i in. 2006; Poulos i in. 2012). Metody te wymagają dobrej znajomości preferencji analizowanych gatunków oraz opierają się na znacznej ilości bardzo dokładnych danych. W ekologii pojawia się wiele niepewności, w tym niekompletne lub niedokładne pomiary oraz wykorzystywanie oszacowań zamiast bezpośrednich pomiarów. Te ograniczenia skłoniły do zainteresowania się logiką rozmytą, która jest zdolna do efektywnego wykorzystania nieprecyzyjnych i niepewnych pomiarów oraz rozmytej wiedzy eksperckiej. Przy wykorzystaniu zbiorów rozmytych, które wyrażają niepewność symulacji siedliskowej, logika rozmyta wykorzystuje nieprecyzyjne lub niejasne informacje. Dostępna wiedza ekspercka jest reprezentowana jako zbiór danych dotyczących preferencji gatunków (Fraternali i in. 2012; Prato 2007). Modele oparte na regułach rozmytych zostały zastosowane w licznych badaniach, ponieważ są projektowane do uwzględniania wiedzy jakościowej i posiadają strukturę, która ułatwia interpretację wyników (Chou, W.-T. Lin i C.-Y. Lin 2007; Fukuda i in. 2011; Legleiter i Goodchild 2005; Mouton, De Baets i Goethals 2009; Rüger, Schlüter i Matthies 2005; Zhang i in. 2016). Cele realizowane w projekcie *FindFISH* sprawiły, że wykorzystanie logiki rozmytej było naturalnym wyborem przy projektowaniu *Modułu Fish*. Oczekujemy, że *Moduł Fish*

będzie najbardziej pożądanym produktem *Platformy Transferu Wiedzy FindFISH*.

Wykonane w ramach tej pracy doktorskiej badania potwierdziły główną hipotezę badawczą, która zakładała, że **stosując modelowanie numeryczne możliwe jest określenie optymalnych warunków środowiskowych dla bytowania wybranych gatunków ryb występujących w rejonie południowego Bałtyku (w szczególności w Zatoce Gdańskiej) oraz wskazanie obszarów występowania tych warunków.**

Dla potwierdzenia hipotezy badawczej określono cztery cele szczegółowe:

1. Scharakteryzować strukturę i zmienność parametrów hydrodynamicznych w rejonie Zatoki Gdańskiej.
2. Zbadać strukturę pionową wód w rejonie Zatoki Gdańskiej z dokładnym wyznaczeniem termokliny i halokliny, stanowiących bariery dla migracji ryb.
3. Scharakteryzować strukturę i zmienność parametrów biochemicznych w rejonie Zatoki Gdańskiej oraz wpływ czynników limitujących produkcję pierwotną fitoplanktonu.
4. Zastosować modelowanie numeryczne do wskazania obszarów, na których występują optymalne warunki dla bytowania szprota, śledzia, dorsza i storni w rejonie Zatoki Gdańskiej, na podstawie preferencji środowiskowych tych gatunków.

Każdy z powyższych celów szczegółowych został omówiony w osobnym artykule naukowym, a ich zestaw jako całość stanowi przedmiot niniejszej rozprawy.

Niniejsza praca doktorska składa się z trzech, opublikowanych w recenzowanych czasopismach, artykułów naukowych oraz manuskryptu, załączonego na końcu rozprawy, który został złożony do czasopisma i jest spójną kontynuacją badań podjętych w poprzednich trzech pracach. Pierwszy artykuł (Janecki, Dybowski, Jakacki i in. 2021) skupia się na opisie oraz walidacji części hydrodynamicznej modelu *EcoFish*. Drugi artykuł (Janecki, Dybowski, Rak i in. 2022) przedstawia nowatorską metodę wyznaczania szczytu głębokości termokliny i halokliny. W trzecim artykule (Janecki, Dybowski i Lidia Dzierzbicka-Głowacka 2023) została przedstawiona oraz poddana walidacji, część biochemiczna modelu *EcoFish* oraz zbadano w jaki sposób czynniki limitujące warunkują charakter i intensywność produkcji pierwotnej fitoplanktonu. Natomiast czwarty manuskrypt (Janecki i Lidia Dzierzbicka-Głowacka 2023) poświęcony jest *Modułowi Fish*, który przy użyciu logiki rozmytej pozwala na tworzenie map najkorzystniejszych warunków środowiskowych (Habitat Suitability Index - HSI) dla bytowania ryb poławianych w rejonie Zatoki Gdańskiej tj. śledzia, szprota, dorsza (do 2021 roku) i storni. Największa część manuskryptu poświęcona jest na analizę danych pochodzących z wypraw rybackich oraz walidację wyników uzyskiwanych z *Modułu Fish* poprzez porównanie wartości HSI z wydajnościami połowowymi pochodzącymi z wypraw rybackich prowadzonych w trakcie trwania projektu. *Moduł Fish* do tworzenia map HSI korzysta z danych pochodzących z modelu *EcoFish*.

3.2 Materiał i metody

3.2.1 Model EcoFish

Model *EcoFish* bazuje na kodzie źródłowym Community Earth System Model (CESM), który jest globalnym sprzężonym modelem klimatycznym. CESM składa się z pięciu oddzielnych komponentów z dodatkowym modułem kontrolującym czas, siły wymuszające, domeny, siatki i wymianę informacji między poszczególnymi modułami. W ramach projektu *FindFISH*, CESM został przeskalowany i przystosowany dla rejonu Zatoki Gdańskiej. Rozdzielczość pozioma modelu *EcoFish* wynosi 575 metrów. W pionie jest to model typu z, podzielony na 26 poziomów, każdy o miąższości 5 metrów. Model *EcoFish* składa się z dwóch tzw. aktywnych (przeprowadzających symulacje numeryczne) części: hydrodynamicznej i biochemicznej.

Część hydrodynamiczna to model oceanu oparty na kodzie źródłowym Parallel Ocean Program (POP), który wykorzystuje trójwymiarowe równania ruchu z przybliżeniami hydrostatycznymi i Boussinesqa. Poniżej przedstawiono główne równania hydrodynamiczne w układzie sferycznym, które są zaimplementowane w modelu.

Równania ruchu poziomego:

$$\frac{\partial u}{\partial t} + L(u) - fv = -\frac{1}{\rho_0 a \cos \phi} \frac{\partial p}{\partial \lambda} + \frac{\partial}{\partial z} \left(K_M \frac{\partial u}{\partial z} \right) + B_M \nabla_H^4 u, \quad (1)$$

$$\frac{\partial v}{\partial t} + L(v) - fu = -\frac{1}{\rho_0 a} \frac{\partial p}{\partial \phi} + \frac{\partial}{\partial z} \left(K_M \frac{\partial v}{\partial z} \right) + B_M \nabla_H^4 v. \quad (2)$$

Równanie pędu wzdłuż kierunku pionowego w przybliżeniu hydrostatycznym:

$$\frac{\partial p}{\partial z} = -\rho g. \quad (3)$$

Równanie ciągłości:

$$\frac{1}{a \cos \phi} \frac{\partial u}{\partial \lambda} + \frac{1}{a \cos \phi} \frac{\partial (v \cos \phi)}{\partial \phi} + \frac{\partial w}{\partial z} = 0 \quad (4)$$

Równanie transportu ciepła i soli:

$$\frac{\partial T}{\partial t} + L(T) = \frac{\partial}{\partial z} \left(K_D \frac{\partial T}{\partial z} \right) + B_D \nabla_H^4 T, \quad (5)$$

$$\frac{\partial S}{\partial t} + L(S) = \frac{\partial}{\partial z} \left(K_D \frac{\partial S}{\partial z} \right) + B_D \nabla_H^4 S, \quad (6)$$

Równanie stanu:

$$\rho = \rho(S, T, p). \quad (7)$$

gdzie: u, v składowe poziome prędkości; w składowa pionowa prędkości; g przyspieszenie grawitacyjne; p ciśnienie; T, S temperatura i zasolenie; ρ_0 średnia gęstość wody; λ i ϕ długość i szerokość geograficzna; a efektywny promień Ziemi; t czas; $f = 2\Omega \sin \phi$ parametr Coriolisa (Ω prędkość kątowna Ziemi); L operator adwekcyjny; ∇_H^4 horyzontalny operator biharmoniczny; K_M biharmoniczny pionowy współczynnik turbulentnej lepkości; B_D biharmoniczny horyzontalny współczynnik turbulentnej lepkości. Jako stałe przyjmuje się współczynniki B_D i B_M . Mieszanie pionowe w modelu *EcoFish* jest określane przez parametryzację KPP (Large, McWilliams i Doney 1994) określoną przez pionowe współczynniki K_D, K_M . Zastosowano ulepszenie schematu KPP z dolną warstwą graniczną (Durski, Glenn i Haidvogel 2004):

$$C_d = \kappa^2 \left(\ln \frac{dz}{z_r} \right)^{-2}, \quad (8)$$

gdzie C_d współczynnik oporu; κ stała von Karmana; dz odległość od dna do punktu siatki; z_r chropowatość określona jako 0,5 cm (wartość dostrojona na podstawie przepływu wody przez Sund w modelu 3D CEMBS).

Część biochemiczna *EcoFish* opiera się na modelu typu NPZD (Moore i in. 2001). W modelu wyznaczane są stężenia substancji biogenicznych, trzy rodzaje fitoplanktonu (okrzemki, mały fitoplankton i diazotrofy (cyjanobakterie, potrafiące wiązać azot cząsteczkowy bezpośrednio z atmosfery)), chlorofil a , zooplankton, detrytus pelagiczny, stężenie rozpuszczonego tlenu. Równaniem opisującym dynamikę zmian stężeń wielkości uwzględnianych w modelu *EcoFish*, a jednocześnie miejscem w którym następuje przekazywanie wymuszeń pomiędzy częścią hydrodynamiczną i biochemiczną jest ogólne równanie dyfuzji turbulentnej ze składnikiem adwekcyjnym:

$$\frac{\partial S}{\partial t} + (V + w_s) \nabla S - \sum_{i=1}^3 \frac{\partial}{\partial x_i} \left(K_{x_i} \frac{\partial S}{\partial x_i} \right) = F_S, \quad (9)$$

gdzie S oznacza zmienną biochemiczną. Drugi i trzeci wyraz po lewej stronie równania opisują odpowiednio adwekcję i mieszanie, gdzie $V(u, v, w)$ jest wektorem prędkości, w_s jest prędkością opadania szczątków pelagicznych, a K_{x_i} to współczynnik dyfuzji turbulentnej. Wszystkie procesy chemiczne i biologiczne są przedstawione jako jeden wyraz F_S (tzw. funkcja źródeł i strat) po prawej stronie równania, a szczegółowe równania opisane są w Lidia Dzierzbicka-Głowacka, Janecki, Nowicki i in. 2013.

Na granicy woda – atmosfera model *EcoFish* jest zasilany meteorologicznymi siłami wymuszającymi. Wymuszenia te pochodzą z modelu UM (Unified Model) rozwijanego w Interdyscyplinarnym Centrum Modelowania Uniwersytetu Warszawskiego (ICM UW). Część z otrzymanywanych parametrów (wiatr, temperatura powietrza, wilgotność, ciśnienie atmosferyczne, opady, promieniowanie) po wcześniejszej interpolacji na siatkę modelu jest bezpośrednio używana jako wymuszenia.

Brakujące parametry są natomiast wyliczane przez moduł danych atmosferycznych, stanowiący integralną część modelu *EcoFish*. W ten sposób wyznaczana jest między innymi gęstość powietrza.

W modelu *EcoFish* uwzględniono 13 rzek uchodzących do Zatoki Gdańskiej w obrębie domeny. Informacje o objętości wody słodkiej (przepływ) oraz depozycji substancji biogenych dla 6 rzek których ujścia znajdują się w rejonie Gminy Puck pochodzą z modelu SWAT (Wielgat i in. 2021), który był rozwijany w ramach projektu "*Zintegrowany Serwis Informacyjno-Predykcyjny Water-PUCK*" (Lidia Dzierzbicka-Głowacka, Janecki, Dybowski i in. 2019; Dzierzbicka-Głowacka i in. 2022). Pozostałe 7 rzek wykorzystuje dane o przepływach, które pochodzą z modelu HYPE – Hydrological Predictions for the Environment.

Domena modelu *EcoFish* od północy i północnego zachodu graniczy z otwartym Bałtykiem, co stwarza konieczność dostarczenia modelowi warunków brzegowych (otwarta granica). Wymuszenia te są przekazywane do modelu *EcoFish* z wykorzystaniem wyników pochodzących z modelu 3D CEMBS o rozdzielczości horyzontalnej 2 km (Lidia Dzierzbicka-Głowacka, Jakacki i in. 2013; Lidia Dzierzbicka-Głowacka, Janecki, Nowicki i in. 2013).

3.2.2 Moduł Fish

Moduł Fish to algorytm komputerowy, który stanowi finalny element *Platformy Transferu Wiedzy FindFISH*. Wykorzystując wiedzę ekspercką oraz dane dotyczące temperatury wody, zasolenia, natlenienia, głębokości połowu oraz jego składu i wagi, określone zostały optymalne warunki dla bytowania czterech gatunków poławianych komercyjnie w regionie Zatoki Gdańskiej. Są to śledź, szprot, dorsz (do 2021 roku) i stornia. Ustalono także rozmyte reguły, które łączą zmienne wejściowe z preferencjami każdego gatunku. Ten rozmyty system wykorzystuje wyniki z modelu *EcoFish*, aby określić wskaźnik przydatności siedliskowej (HSI) dla rejonu Zatoki Gdańskiej. HSI wskazuje warunki siedliskowe dla danego gatunku w badanym obszarze. HSI mieści się w zakresie od 0 do 1, gdzie 0 oznacza, że siedlisko nie spełnia warunków do występowania danego gatunku, a 1 opisuje siedlisko optymalne.

Do ustalenia funkcji przynależności w *Module Fish* wykorzystano dane, określające zakresy optymalnych wartości poszczególnych parametrów dla bytowania śledzia, szprota, dorsza oraz stornia ustalone na podstawie danych fizykochemicznych (temperatury, zasolenia, natlenienia i głębokości) i połowowych (skład i masa) zebranych podczas wypraw rybackich. W trakcie implementacji tego systemu przeprowadziliśmy kilka iteracji. W finalnej iteracji zastosowano medianę optymalnej wartości wraz ze stałym odchyleniem C oraz minima/maksima na krawędziach. Preferencje każdego gatunku zaimplementowanego w *Module Fish* rozmywane były tak, aby centralny trapez obejmował optymalne wartości danego parametru dla bytowania gatunku, natomiast mniejsze i większe wartości dotyczyły warunków poniżej i powyżej optymalnych.

Blok rozmytego systemu wnioskowania w *Module Fish* przeprowadza obliczenia w celu określenia funkcji przynależności wyjściowej na podstawie stopni przynależności wejściowych. Ta funkcja często ma złożony kształt, a jej określenie może być osiągnięte za pomocą różnych matematycznych metod wnioskowania. W pierwszym etapie obliczeń definiuje się zestaw funkcji przynależności w celu przekształcenia na terminy lingwistyczne. Te terminy służą jako wejścia do procesu rozmytego wnioskowania. Proces rozmywania polega na przekształceniu surowych (ostrych) wartości w ilości lingwistyczne, obejmujące zakres od niskiego do wysokiego. Każda wartość lingwistyczna posiada zakres stopni przynależności reprezentowany przez liczby rzeczywiste od 0 do 1. Ponadto, określona wartość może należeć do dwóch sąsiadujących zbiorów rozmytych. W naszym badaniu zastosowano trapezoidalne funkcje przynależności. Kolejnym krokiem w obliczeniach jest wnioskowanie z zastosowaniem logiki rozmytej i reguł rozmytych. Reguły wnioskowania łączą zmienne wejściowe (temperatura, zasolenie, natlenienie i głębokość) z warunkami środowiskowymi dotyczącymi gatunków (HSI), używając serii warunkowych instrukcji "JEŻELI-TO". Reguły rozmyte są definiowane na podstawie wiedzy eksperckiej, a rozmyte dane wejściowe są przekształcane w rozmyte dane wyjściowe przy użyciu tych reguł. Zastosowano metodę wnioskowania Maksimum-Minimum. Na podstawie bazy reguł rozmytych obliczana jest wynikowa funkcja przynależności, a następnie w procesie defuzjacji uzyskuje się wynik jako pojedynczą wartość liczbową HSI. Defuzyfikacja w *Module Fish* jest wykonywana przy użyciu metody środka ciężkości (Center of Gravity - CoG).

3.2.3 Obszar badań

Efektywna domena modelu *EcoFish* obejmuje rozszerzoną Zatokę Gdańską, która stanowi południową część akwenu Głębi Gdańskiej, znajdującego się w Basenie Gotlandzkim. Umowna, prosta linia, łącząca przylądek Rozewie z przylądkiem Taran na półwyspie Sambia, wydziela właściwą Zatokę Gdańską. Linia ta przecina najgłębsze partie dna Głębi Gdańskiej, z maksymalną głębokością 118 metrów. Wzdłuż strefy przybrzeżnej ciągnie się szeroki pas pływiczny rozszerzający się w rejonie na zachód od ujścia Wisły. Znajdują się tam stożki napływowe: w ujściu Wisły Śmiałej i Przekopu Wisły. Nachylenie dna w strefie brzegowej jest zróżnicowane. Największy spadek występuje u cypła Półwyspu Helskiego, gdzie dno opada do głębokości 70 m (Majewski 1972).

Unikalny subregion Zatoki Gdańskiej stanowi usytuowana w jej zachodniej części Zatoka Pucka. Południowo-zachodnią granicę zatoki stanowi linia brzegu – od Gdyni Orłowa, poprzez Puck do Władysławowa. Od północnego-wschodu Zatokę ogranicza Mierzeja Helska, natomiast za wschodnią granicę przyjmuje się linię łączącą Cypel Helski z Przylądkiem Orłowo. Zatoka Pucka ze względu na swoje położenie geograficzne oraz szczególne warunki hydrologiczne jest akwenem unikatowym w skali całego Morza Bałtyckiego. Swą specyfikę zawdzięcza czynnikom naturalnym: odizolowaniu od wód morza Półwyspem Helskim i rozdzieleniu przez Rybitwią Mielizną na dwie odmienne morfologicznie i środowiskowo strefy.

3.2.4 Dane wykorzystane do walidacji modelu EcoFish i Modułu Fish

Aby zweryfikować czy model *EcoFish* poprawnie odwzorowuje zmienność parametrów hydrodynamicznych oraz biochemicznych w Zatoce Gdańskiej, wykorzystano bazę danych ICES (International Council for the Exploration of the Sea). Dla temperatury i zasolenia dostępnych było 17902 pomiarów z lat od 2014 do 2019 roku. Dla lat dla których przeprowadzono walidację parametrów biochemicznych w bazie ICES w obrębie domeny modelu *EcoFish* dostępnych było 3329 pomiarów stężenia rozpuszczonego tlenu O_2 , 2370 pomiarów stężenia azotanów (NO_3), 2592 pomiarów stężenia fosforanów (PO_4), 2610 pomiarów stężenia krzemianów (SiO_3) oraz 972 pomiarów stężenia chlorofilu *a*.

Dodatkową, niezależną od ICESu, bazą danych wykorzystaną do walidacji modelu *EcoFish* były pomiary wykonane w ramach projektu *FindFISH* podczas wypraw rybackich. Do zbierania danych fizykochemicznych w morzu wykorzystywany był instrument MIDAS CDT+. Dane zbierane były z obszaru na północ od ujścia Wisły oraz w pasie na otwartym morzu, ciągnącym się równolegle do Półwyspu Helskiego. Pomiary cechowały się dużą rozdzielczością czasową i przestrzenną.

Do analizy wydajności połowowych, a następnie walidacji *Modułu Fish* wykorzystano dane pochodzące z 408 wypraw rybackich z okresu od 13 września 2018 do 9 maja 2022. Danych połowowych było więcej, jednakże część z nich została odfiltrowana. Odrzucone zostały wyprawy, które wychodziły poza domenę *Modułu Fish* oraz te podczas których wystąpiły jakiegokolwiek problemy z rejestrowaniem trasy połowu przez urządzenie GPS. Ślady GPS jednostek rybackich prowadzących połowy zostały docięte do miejsc tzw. efektywnego połowu, tzn. dla każdego połowu odfiltrowano informacje z parkowania oraz wyciągania sieci. Przeprowadzono to manualnie dla każdego profilu głębokościowego sieci. Następnie przeprowadzono walidację *Modułu Fish* poprzez zbadanie zależności pomiędzy wydajnościami połowowymi wyznaczonymi dla wypraw rybackich, a współczynnikiem Habitat Suitability Index (HSI) na trasie połowu wyznaczanym w *Module Fish*. W tym celu z danych wynikowych modelu wyciągnięty został profil pionowy HSI na trasie każdego połowu, a następnie wyznaczona została jego maksymalna i średnia wartość zgodnie z głębokościami rejestrowanymi przez sondę pomiarową przymocowaną do sieci.

3.3 Rezultaty i dyskusja

W tym rozdziale przedstawiam najważniejsze rezultaty przeprowadzonych badań, natomiast po szczegółowe wyniki oraz analizy odsyłam czytelnika do artykułów składających się na niniejszą rozprawę doktorską.

3.3.1 Część hydrodynamiczna modelu EcoFish

Walidacja pokazała, że wyniki symulacji modelu *EcoFish* dla temperatury wody cechuje duża zgodność z obserwacjami *in situ*. Korelacja między danymi eksperymentalnymi dla temperatury wody, a wynikami modelu *EcoFish* wyniosła 0.94 przy błędzie średniokwadratowym (RMSE) na poziomie 1.33 °C. Na skutek porównania modelowanej temperatury z danymi pochodzącymi z

bazy utworzonej podczas rejsów rybackich uzyskaliśmy współczynnik korelacji równy 0.87. Jest to zadowalający wynik, biorąc pod uwagę silne skupienie danych rejsowych w pasie od ujścia rzeki Wisły w kierunku północno-zachodnim. Dane pochodziły zarówno z rejonu, w którym występuje mieszanie się wód rzecznych (z Wisły) z wodami Zatoki, jak i z obszaru w którym występują najsilniejsze prądy w całej domenie (pas wzdłuż Półwyspu Helskiego). Należy również zauważyć, że większość tych danych pochodziła z głębokości połowowych, tj. od 30 do 60 metrów, na których nie widać już wpływu działania asymilacji danych satelitarnych SST.

Korelacja danych modelowych dla zasolenia z danymi ICES na poziomie 0.94 oraz niski błąd średniokwadratowy wynoszący 0.8 PSU pozwala sądzić, że model dobrze radzi sobie z transportem mas wodnych. Dowodzi to też, że rzeki w modelu zostały poprawnie zaimplementowane, a uchodząca z nich woda słodka jest poprawnie mieszana ze słonymi wodami Zatoki i roznoszona przez prądy w jej obszarze. Dodatkowo, analizując profil pionowy widać występowanie zarówno warstwy izohalinowej jak i tworzenie się halokliny na niższych poziomach głębokości, co dowodzi, że model poprawnie odwzorowuje dynamikę zmian zasolenia w kolumnie wody.

3.3.2 Algorytm do wyznaczania szczytu głębokości termokliny i halokliny

W drugim artykule (Janecki, Dybowski, Rak i in. 2022) przedstawiono nowatorską metodę nazwaną "*Algorytmem MovSTD*" do wyznaczania szczytu głębokości termokliny (TTD) i halokliny (THD). Metoda ma potencjał do stania się potężnym narzędziem do zastosowań w płytkich akwenach wodnych na całym świecie. Bazuje na średniej kroczącej z odchylenia standardowego dla profili pionowych temperatury i zasolenia, a następnie przetwarza ją w celu określenia potencjalnej głębokości, na której gwałtownie zmienia się temperatura lub zasolenie. Metoda została skalibrowana przy użyciu obszernego zestawu danych z modelu ekohydrodynamicznego *EcoFish*. W wyniku kalibracji ustalono wartości parametrów wejściowych, które pozwalają na prawidłowe wyznaczanie TTD i THD. Potwierdziła to walidacja przeprowadzona na profilach *in situ* zebranych przez statek badawczy S/Y Oceania podczas rejsów statutowych po wodach południowego Bałtyku. Algorytm *MovSTD* wykorzystano następnie do analizy sezonowej zmienności struktury pionowej wód w rejonie Głębi Gdańskiej dla temperatury i zasolenia. Oszacowane zostało także tempo zapadania się termokliny. Motywacją do podjęcia tego tematu był związek termokliny z występowaniem ryb. W niektórych przypadkach termoklina może stanowić barierę dla ruchu ryb, które preferują dany zakres temperatur. W takim przypadku ryby mogą gromadzić się na granicy termokliny, gdzie są dostępne odpowiednie warunki siedliskowe. Dlatego też, znajomość położenia termokliny może pomóc w określeniu, gdzie można spodziewać się obecności określonych gatunków ryb.

Wyniki działania algorytmu *MovSTD* na danych modelowych z regionu Głębi Gdańskiej pokazały, że szczyt głębokości halokliny (na Głębi Gdańskiej), jest ustalony i znajduje się na około 50 metrach. Zauważalne zmiany w dynamice w analizowanym 7-letnim okresie widać jednak od sierpnia do listopada, kiedy to haloklina zaczyna formować się wyżej, na głębokościach między 35 a 50 metrów, oraz między styczniem a lutym, kiedy w latach 2015 i 2016 znajdowała się na głębokości 70 metrów. Można jednak powiedzieć, że THD nie wykazuje dużej zmienności sezonowej, i struktura pionowa zasolenia na Głębi Gdańskiej jest dość stabilna.

Sytuacja wygląda inaczej w przypadku termokliny. Widać tu wyraźną zmienność sezonową. Świeża termoklina zaczyna się formować w maju w związku z nagrzewaniem się warstwy powierzchniowej na skutek warunków atmosferycznych (wysokie temperatury powietrza i nasłonecznienie). Prędkość jej zapadania w miesiącach od maja do września wynosi około 2 metry na miesiąc. W kolejnych miesiącach, na skutek mieszania się wód i wzmożonych oddziaływań wiatrowych, zapadanie się TTD przyspiesza, osiągając większe głębokości z prędkością około 9 metrów na miesiąc. Na przełomie roku opadanie termokliny zatrzymuje się i do kwietnia znajduje się ona na tej samej głębokości co haloklina.

Algorytm *MovSTD* jest dobrą metodą do wyznaczania TTD i THD dla wód Morza Bałtyckiego. Dzięki swojej małej złożoności obliczeniowej można go stosować do dużej ilości danych (profilu) i uzyskiwać odpowiedź w bardzo krótkim czasie, co jest szczególnie istotne przy przetwarzaniu danych modelowych o dużej rozdzielczości horyzontalnej jak i czasowej.

3.3.3 Część biochemiczna modelu *EcoFish*

W artykule Janecki, Dybowski i Lidia Dzierzbicka-Głowacka 2023 zaprezentowana została część biochemiczna modelu *EcoFish* dla rejonu Zatoki Gdańskiej. Określone zostały podstawowe para-

metry ekosystemu morskiego, m.in. stężenie chlorofilu *a*, stężenie rozpuszczonego tlenu oraz parametry chemiczne, m.in. stężenie substancji biogennych takich jak azotany, fosforany i krzemiany. Przedstawiono zmienność sezonową tych parametrów oraz przeprowadzono walidację danych modelowych poprzez porównanie ich z danymi *in situ* z bazy ICES. Uzyskano zadowalające wyniki. Najistotniejszym parametrem poddanym walidacji było stężenie rozpuszczonego tlenu z uwagi na fakt, iż jest to parametr wejściowy do *Modułu Fish*, w którym wyznaczane są mapy HSI (Wskaźnik Przydatności Siedliska/Habitat Suitability Index) na podstawie preferencji ryb. W artykule zbadano również to w jaki sposób czynniki limitujące (tj. temperatura wody, substancje biogenne, światło) wpływają na produkcję pierwotną fitoplanktonu i wykazano, że intensywność wiosennych zakwitów okrzemek wpływa na charakter zakwitów sinic latem.

Analiza dynamiki zmienności sezonowej procesu produkcji pierwotnej, w wodach Zatoki Gdańskiej, była niezwykle istotna w ramach prowadzonych badań, gdyż jest to proces bezpośrednio związany z produkcją i konsumpcją tlenu. Przy analizie produkcji pierwotnej wykazano, że warunki geomorfologiczne oraz depozycja substancji biogennych z rzek ma ogromne znaczenie na jej charakter i intensywność. Dostępność substancji biogennych może w znaczny sposób zmienić rozkład biomasy wszystkich grup fitoplanktonu. Nastawienie na zbyt silne ograniczanie depozycji azotanów w wodach rzecznych w celu zahamowania eutrofizacji wód morskich, może w konsekwencji prowadzić do sytuacji odwrotnej, gdzie po krótkich i słabych zakwitach okrzemek na wiosnę, występują długie i intensywne zakwity sinic latem. Jest to zgodne z wynikami uzyskanymi dla eksperymentu numerycznego przeprowadzonego dla Zatoki Puckiej przez Dybowski i Lidia Dzierzbicka-Głowacka 2023. Rozsądne podejście do jakichkolwiek decyzji legislacyjnych w tym aspekcie jest szczególnie ważne w dobie zmian klimatycznych i podwyższania się temperatury wód w morzach i oceanach, co jeszcze bardziej wydłuży okres, z optymalną temperaturą do zakwitów tego toksycznego i niechcianego gatunku (z punktu widzenia specyfiki regionu nastawionego na turystykę).

3.3.4 Mapowanie optymalnych warunków środowiskowych dla bytowania szprota, śledzia, dorsza i storni w rejonie Zatoki Gdańskiej

Janecki i Lidia Dzierzbicka-Głowacka 2023 to finalny artykuł, wykorzystujący wiedzę i wyniki uzyskane w poprzednich trzech, opublikowanych już pracach. Jest on skupiony wokół *Modułu Fish*. *Moduł Fish* to najważniejszy element Platformy Transferu Wiedzy – *FindFISH*, który przy użyciu logiki rozmytej pozwala na tworzenie map najkorzystniejszych warunków środowiskowych (HSI - Habitat Suitability Index) dla bytowania ryb poławianych w rejonie Zatoki Gdańskiej.

Poprzez obliczenie średnich wartości HSI dla wszystkich analizowanych wypraw rybackich i gatunków oraz porównanie ich z wydajnością połowową, stwierdzono, że istnieje próg wartości HSI, poniżej którego trudno jest uzyskać udany połów szprota, śledzia i dorsza. Wskazuje to na zdolność systemu do poprawnej identyfikacji lokalizacji o korzystnych warunkach środowiskowych dla siedlisk tych trzech gatunków. Zaleca się, aby rybacy wybierali trasy, gdzie HSI wynosi co najmniej 0.5 podczas połowów szprota i śledzia oraz powyżej 0.4 przy połowach dorsza. Ponadto, zaobserwowano lekką tendencję dla tych trzech gatunków, wskazującą na wzrost efektywności połowowej przy wyższych wartościach HSI. Oznacza to, że wybór tras o dostatecznie wysokich wartościach HSI przyczynia się do osiągnięcia wyższej efektywności połowowej.

W odniesieniu do storni, ocena oparta na porównaniu wydajności połowowej z średnią wartością HSI z pozycji wystawienia narzędzia nie dostarczyła jednoznacznych dowodów na zdolność systemu do dokładnego identyfikowania lokalizacji o optymalnych warunkach środowiskowych dla tego gatunku. Chociaż dostępne były znaczne ilości danych dotyczących storni, ich pokrycie przestrzenne nie było tak rozległe jak w przypadku szprota czy śledzia. Narzędzia stawne były wystawiane tylko w trzech wąskich obszarach: w południowej części Zatoki Gdańskiej, okolicach Mierzei Wiślanej i po obu stronach Półwyspu Helskiego.

Analiza wykazuje również, że średni czas efektywnego połowu dla szprota i śledzia wynosił od pięciu do sześciu godzin. Porównując czas trwania poszczególnych wypraw rybackich z obfitością połowów szprota i śledzia, staje się jasne, że długie wyprawy nie gwarantują sukcesu połowowego. Podobne ilości ryb poławiano zarówno podczas krótkich trzygodzinnych wyprawach, jak i tych trwających ponad siedem godzin. Te wyniki podkreślają, że kluczowym czynnikiem w planowaniu połowów nie jest czas trwania wyprawy, ale wybór odpowiedniej trasy z korzystnymi warunkami środowiskowymi sprzyjającymi bytowaniu ryb. Podkreśla to zasadnicze znaczenie *Platformy Transferu Wiedzy FindFISH* i *Modułu Fish*, które prawidłowo wykorzystywane, mogą wspierać rybaków w działaniach połowowych.

3.4 Podsumowanie

Zastosowanie nowoczesnych technik pomiarowych i modelowania numerycznego, w ramach projektu *FindFISH*, pozwoliło określić optymalne warunki środowiskowe dla bytowania śledzia, szprota, dorsza i storni w rejonie Zatoki Gdańskiej. Stworzenie narzędzia *Moduł Fish* oraz portalu internetowego na którym dostępne są prognozy map HSI może oprowadzić do bardziej selektywnego rybołówstwa i zmniejszenia kosztów dla przemysłu rybnego.

Wdrożenie platformy *FindFISH* umożliwi diagnozowanie i prognozowanie warunków środowiska morskiego Zatoki Gdańskiej i ułatwi szybki dostęp do niezbędnych informacji, co może przełożyć się na ograniczenie niepożądanych połowów poprzez świadomy wybór miejsca połowu na podstawie konkretnych wyników liczbowych przedstawionych w przejrzystej i czytelnej formie.

References (Bibliografia)

- Beecher, Hal A., Brad A. Caldwell, and S. Brett DeMond (2002). "Evaluation of Depth and Velocity Preferences of Juvenile Coho Salmon in Washington Streams". en. In: *North American Journal of Fisheries Management* 22.3, pp. 785–795. ISSN: 1548-8675. DOI: 10.1577/1548-8675(2002)022<0785:EODAVP>2.0.CO;2.
- Bovee, Ken D. (1986). *Development and evaluation of habitat suitability criteria for use in the in-stream flow incremental methodology*. Other Report FWS/OBS-86/7. Washington, D.C.: USDI Fish and Wildlife Service, p. 235. URL: <http://pubs.er.usgs.gov/publication/70121265>.
- Camphuysen, C.J. and S. Garthe (2000). "Sea birds and commercial fisheries: population trends of piscivorous seabirds explained?" In: *Effects of Fishing on Non-Target Species and Habitats*. Oxford: Blackwell Science, pp. 163–184.
- Chou, Wen-Chieh, Wen-Tzu Lin, and Chao-Yuan Lin (2007). "Application of fuzzy theory and PROMETHEE technique to evaluate suitable ecotechnology method: A case study in Shihmen Reservoir Watershed, Taiwan". en. In: *Ecological Engineering* 31.4, pp. 269–280. ISSN: 0925-8574. DOI: 10.1016/j.ecoleng.2007.08.004.
- Davies, R. W. D. et al. (2009). "Defining and estimating global marine fisheries bycatch". en. In: *Marine Policy* 33.4, pp. 661–672. ISSN: 0308-597X. DOI: 10.1016/j.marpol.2009.01.003.
- Durski, Scott M., Scott M. Glenn, and Dale B. Haidvogel (2004). "Vertical mixing schemes in the coastal ocean: Comparison of the level 2.5 Mellor-Yamada scheme with an enhanced version of the K profile parameterization". en. In: *Journal of Geophysical Research: Oceans* 109.C1. ISSN: 2156-2202. DOI: 10.1029/2002JC001702.
- Dybowski, Dawid and Lidia Dzierzbicka-Głowacka (Apr. 2023). "Analysis of the impact of nutrients deposited from the land side on the waters of Puck Lagoon (Gdańsk Basin, Southern Baltic): A model study". In: *Oceanologia* 65.2, pp. 386–397. ISSN: 0078-3234. DOI: 10.1016/j.oceano.2022.11.005. URL: <https://www.sciencedirect.com/science/article/pii/S0078323422001075>.
- Dzierzbicka-Głowacka, L. (2023). *Platforma transferu wiedzy FindFISH – Numeryczny System Prognozowania warunków środowiska morskiego Zatoki Gdańskiej dla Rybołówstwa*. pl. Gdynia: Wydawnictwo Uniwersytetu Morskiego w Gdyni. ISBN: 978-83-7421-447-6. URL: <https://doi.org/10.26408/FindFISH>.
- Dzierzbicka-Głowacka, Lidia, Jaromir Jakacki, et al. (Aug. 2013). "Activation of the operational ecohydrodynamic model (3D CEMBS) – the hydrodynamic part". pl. In: *Oceanologia* 55.3, pp. 519–541. ISSN: 0078-3234. DOI: 10.5697/oc.55-3.519. URL: <https://www.sciencedirect.com/science/article/pii/S0078323413500285> (visited on 03/08/2023).
- Dzierzbicka-Głowacka, Lidia, Maciej Janecki, Dawid Dybowski, et al. (2019). "A New Approach for Investigating the Impact of Pesticides and Nutrient Flux from Agricultural Holdings and Land-Use Structures on Baltic Sea Coastal Waters". In: *Pol. J. Environ. Stud.* 28.4, pp. 2531–2539. ISSN: 1230-1485. DOI: 10.15244/pjoes/92524. URL: <https://doi.org/10.15244/pjoes/92524>.
- Dzierzbicka-Głowacka, Lidia, Maciej Janecki, Artur Nowicki, et al. (2013). "Activation of the operational ecohydrodynamic model (3D CEMBS) – the ecosystem module". In: *Oceanologia* 55.3, pp. 543–572. ISSN: 0078-3234. DOI: <https://doi.org/10.5697/oc.55-3.543>. URL: <https://www.sciencedirect.com/science/article/pii/S0078323413500297>.
- Dzierzbicka-Głowacka, Lidia, Artur Nowicki, et al. (2018). "Structure of the FindFish Knowledge Transfer Platform". pl. In: *Fisheries & Aquatic Life* 26.3, pp. 193–197. DOI: 10.2478/aopf-2018-0021.
- Dzierzbicka-Głowacka, Lidia et al. (Apr. 2022). "Modelling the impact of the agricultural holdings and land-use structure on the quality of inland and coastal waters with an innovative and interdisciplinary toolkit". en. In: *Agricultural Water Management* 263, p. 107438. ISSN: 0378-3774. DOI: 10.1016/j.agwat.2021.107438. URL: <https://www.sciencedirect.com/science/article/pii/S0378377421007150> (visited on 03/08/2023).
- Fraternali, P. et al. (2012). "Putting humans in the loop: Social computing for Water Resources Management". en. In: *Environmental Modelling & Software* 37, pp. 68–77. ISSN: 1364-8152. DOI: 10.1016/j.envsoft.2012.03.002.
- Fukuda, Shinji et al. (2011). "Effect of model formulation on the optimization of a genetic Takagi-Sugeno fuzzy system for fish habitat suitability evaluation". en. In: *Ecological Modelling* 222.8, pp. 1401–1413. ISSN: 0304-3800. DOI: 10.1016/j.ecolmodel.2011.01.023.

- Godfray, H. Charles J. et al. (2010). “Food Security: The Challenge of Feeding 9 Billion People”. In: *Science* 327.5967, pp. 812–818. DOI: 10.1126/science.1185383.
- Hilborn, Ray et al. (2003). “State of the World’s Fisheries”. In: *Annual Review of Environment and Resources* 28.1, pp. 359–399. DOI: 10.1146/annurev.energy.28.050302.105509.
- Inglis, Graeme J. et al. (2006). “Using Habitat Suitability Index and Particle Dispersion Models for Early Detection of Marine Invaders”. en. In: *Ecological Applications* 16.4, pp. 1377–1390. ISSN: 1939-5582. DOI: 10.1890/1051-0761(2006)016[1377:UHSIAP]2.0.CO;2.
- Janecki, Maciej, Dawid Dybowski, and Lidia Dzierzbicka-Głowacka (2023). “The influence of biochemical parameters on primary production in the Gulf of Gdańsk region: A model study”. en. In: *Oceanologia*. ISSN: 0078-3234. DOI: 10.1016/j.oceano.2023.05.001.
- Janecki, Maciej, Dawid Dybowski, Jaromir Jakacki, et al. (2021). “The Use of Satellite Data to Determine the Changes of Hydrodynamic Parameters in the Gulf of Gdańsk via EcoFish Model”. en. In: *Remote Sensing* 13.18, p. 3572. ISSN: 2072-4292. DOI: 10.3390/rs13183572.
- Janecki, Maciej, Dawid Dybowski, Daniel Rak, et al. (2022). “A New Method for Thermocline and Halocline Depth Determination at Shallow Seas”. EN. In: *Journal of Physical Oceanography* 52.9, pp. 2205–2218. ISSN: 0022-3670, 1520-0485. DOI: 10.1175/JPO-D-22-0008.1.
- Janecki, Maciej and Lidia Dzierzbicka-Głowacka (2023). “Fish Module - A Prognostic Tool for Modeling the Optimal Environmental Conditions for Fish in the Gulf of Gdańsk (Southern Baltic Sea)”. In: *submitted to Fish and Fisheries Journal*.
- Large, W. G., J. C. McWilliams, and S. C. Doney (1994). “Oceanic vertical mixing: A review and a model with a nonlocal boundary layer parameterization”. en. In: *Reviews of Geophysics* 32.4, pp. 363–403. ISSN: 1944-9208. DOI: 10.1029/94RG01872.
- Legleiter, Carl J. and Michael F. Goodchild (2005). “Alternative representations of in-stream habitat: classification using remote sensing, hydraulic modeling, and fuzzy logic”. In: *International Journal of Geographical Information Science* 19.1, pp. 29–50. ISSN: 1365-8816. DOI: 10.1080/13658810412331280220.
- Majewski, A. (1972). “Hydrological characteristics of estuarine waters at the Polish Coast”. pl. In: *Prace Panstw. Inst. Hydrol.- Meteorol.* 105, pp. 3–40.
- Moore, J. Keith et al. (2001). “An intermediate complexity marine ecosystem model for the global domain”. en. In: *Deep Sea Research Part II: Topical Studies in Oceanography*. The US JGOFS Synthesis and Modeling Project: Phase 1 49.1, pp. 403–462. ISSN: 0967-0645. DOI: 10.1016/S0967-0645(01)00108-4.
- Mouton, A. M., B. De Baets, and P. L. M. Goethals (2009). “Knowledge-based versus data-driven fuzzy habitat suitability models for river management”. en. In: *Environmental Modelling & Software* 24.8, pp. 982–993. ISSN: 1364-8152. DOI: 10.1016/j.envsoft.2009.02.005.
- Myers, Ransom A. and Boris Worm (2003). “Rapid worldwide depletion of predatory fish communities”. en. In: *Nature* 423.6937, pp. 280–283. ISSN: 1476-4687. DOI: 10.1038/nature01610.
- Poulos, HM. et al. (2012). “Ensemble forecasting of potential habitat for three invasive fishes”. In: *Proceedings of the 17th International Conference on Aquatic Invasive Species*. San Diego, USA, pp. 59–72. DOI: <https://doi.org/10.3391/ai.2012.7.1.007>.
- Prato, Tony (2007). “Assessing ecosystem sustainability and management using fuzzy logic”. en. In: *Ecological Economics* 61.1, pp. 171–177. ISSN: 0921-8009. DOI: 10.1016/j.ecolecon.2006.08.004.
- Rüger, Nadja, Maja Schlüter, and Michael Matthies (2005). “A fuzzy habitat suitability index for *Populus euphratica* in the Northern Amudarya delta (Uzbekistan)”. en. In: *Ecological Modelling* 184.2, pp. 313–328. ISSN: 0304-3800. DOI: 10.1016/j.ecolmodel.2004.10.010.
- Secretary-General, UN (2006). “Impacts of fishing on vulnerable marine ecosystems :: actions taken by States and regional fisheries management organizations and arrangements to give effect to paragraphs 66 to 69 of General Assembly resolution 59/25 on sustainable fisheries, regarding the impact of fishing on vulnerable marine ecosystems : report of the Secretary-General”. en. In.
- Wielgat, Paweł et al. (Feb. 2021). “Towards a multi-basin SWAT model for the migration of nutrients and pesticides to Puck Bay (Southern Baltic Sea)”. en. In: *PeerJ* 9. Publisher: PeerJ Inc., e10938. ISSN: 2167-8359. DOI: 10.7717/peerj.10938. URL: <https://peerj.com/articles/10938> (visited on 06/12/2023).
- Zhang, Heyue et al. (2016). “Fuzzy Logic Method for Evaluating Habitat Suitability in an Estuary Affected by Land Reclamation”. en. In: *Wetlands* 36.1, pp. 19–30. ISSN: 1943-6246. DOI: 10.1007/s13157-014-0606-2.

4 Series of publications constituting the PhD thesis

4.1 Research paper no. 1

Janecki, M., Dybowski, D., Jakacki, J., Nowicki, A., Dzierzbicka-Głowacka, L., 2021. *The Use of Satellite Data to Determine the Changes of Hydrodynamic Parameters in the Gulf of Gdańsk via EcoFish Model*. *Remote Sensing* 13, 3572. <https://doi.org/10.3390/rs13183572>

(IF¹ = 5.786; MEiN² = 100)

¹Journal 5-Year Impact Factor (IF) according to the Journal Citation Reports

²Journal score according to the list of the Polish Ministry of Education and Science



Article

The Use of Satellite Data to Determine the Changes of Hydrodynamic Parameters in the Gulf of Gdańsk via EcoFish Model

Maciej Janecki ^{1,*} , Dawid Dybowski ¹ , Jaromir Jakacki ² , Artur Nowicki ¹
and Lidia Dzierzbicka-Glowacka ¹

- ¹ Ecohydrodynamics Laboratory, Physical Oceanography Department, Institute of Oceanology Polish Academy of Sciences, Powstańców Warszawy 55, 81-712 Sopot, Poland; ddybowski@iopan.pl (D.D.); anowicki@iopan.pl (A.N.); dzierzb@iopan.pl (L.D.-G.)
- ² Ocean and Atmosphere Numerical Modelling Laboratory, Physical Oceanography Department, Institute of Oceanology Polish Academy of Sciences, Powstańców Warszawy 55, 81-712 Sopot, Poland; jjakacki@iopan.pl
- * Correspondence: mjanecki@iopan.pl; Tel.: +48-587-311-912

Abstract: Using mathematical models alone to describe the changes in the parameters characterizing the analyzed reservoir may be insufficient due to the complexity of ocean circulation. One of the ways to improve the accuracy of models is to use data assimilation based on remote sensing methods. In this study, we tested the EcoFish numerical model that was developed for the Gulf of Gdańsk area, under the FindFish Knowledge Transfer Platform. In order to improve the model results and map local phenomena occurring in the studied water, which would be difficult to simulate using only mathematical equations, EcoFish was extended with a satellite data assimilation module that assimilates the sea surface temperature data from a medium-resolution imaging spectroradiometer and an advanced ultrahigh-resolution radiometer. EcoFish was then statistically validated, which resulted in high correlations for water temperature and salinity as well as low errors in comparison with in situ experimental data.

Keywords: FindFish; Gulf of Gdańsk; EcoFish model; satellite data assimilation



Citation: Janecki, M.; Dybowski, D.; Jakacki, J.; Nowicki, A.; Dzierzbicka-Glowacka, L. The Use of Satellite Data to Determine the Changes of Hydrodynamic Parameters in the Gulf of Gdańsk via EcoFish Model. *Remote Sens.* **2021**, *13*, 3572. <https://doi.org/10.3390/rs13183572>

Academic Editor: Simone Cosoli

Received: 7 July 2021

Accepted: 3 September 2021

Published: 8 September 2021

Publisher's Note: MDPI stays neutral with regard to jurisdictional claims in published maps and institutional affiliations.



Copyright: © 2021 by the authors. Licensee MDPI, Basel, Switzerland. This article is an open access article distributed under the terms and conditions of the Creative Commons Attribution (CC BY) license (<https://creativecommons.org/licenses/by/4.0/>).

1. Introduction

The Baltic Sea is a shallow inland sea connected to the North Sea by narrow (4–28 km wide) straits. The topography of these straits, and in particular their low depth (around 5–6 m in most shallow points), impedes the free exchange of waters between the Baltic and the North Sea, causing significant water exchanges between these seas only during large infusions [1,2]. The Gulf of Gdańsk is the southern part of the Baltic Sea and is less affected by infusions, but it is exposed to influences from the land. The highly urbanized and industrialized coast has a huge impact on the environmental conditions of the Gulf in addition to the waters coming from the Vistula River [3,4]. An additional obstacle in the exchange of the Bay's waters with the open sea is the Hel Peninsula. It serves as a natural land barrier, marking the border between the Puck Bay and the Gdańsk Basin.

The morphometric conditions of the Gulf of Gdańsk favor the heterogeneity in salinity. Visible differences can be observed between the shallow coastal area hydrologically belonging to the surface layer of the Baltic Sea and the remaining deeper zone of the gulf [5,6]. However, smaller differences exist between the deep water region of the Gulf of Gdańsk and the open sea, where a typical for the Baltic Sea, layered water structure can be observed [7].

Comprehensive understanding and description of processes occurring in water is possible through the combined use of mathematical models, modern in situ research, and observational techniques in the form of satellite remote sensing [8–11].

In order to increase the intensity of knowledge transfer and the use of scientific potential by fishermen, and consequently contribute to the sustainable development of fisheries while increasing the protection of the Gulf's ecosystem, a three-dimensional, prognostic ecohydrodynamic model named EcoFish was built. The EcoFish model is configured for the Gulf of Gdańsk area and being developed under the project "FindFish Knowledge Transfer Platform—Numerical Forecasting System for the Marine Environment of the Gulf of Gdańsk for Fisheries" [12]. The main goal of the project is to create a platform from which users (in particular fishermen and scientists) will be able to obtain knowledge and information about the physical and biological conditions of the Gulf of Gdańsk. The EcoFish model will be an essential tool in achieving this goal.

The most important modeled variables (especially water temperature, salinity, and dissolved oxygen concentration) that determine the state of the Gulf of Gdańsk ecosystem will also serve as input data for the Fish Module. Output information from this module, together with the data on fish preferences and expert knowledge, will allow the creation of maps of the most favorable environmental conditions for the occurrence of industrial pelagic fish in the Gulf of Gdańsk region, i.e., herring, sprat, and flounder.

The implementation of the satellite data assimilation module for sea surface temperature (SST), and also for chlorophyll *a* later in the biological part, in the EcoFish model will ensure that the obtained model results will be even more accurate (close to reality) and the model will correctly reflect the state of the Gulf of Gdańsk environment. In this study, the results from the EcoFish model were statistically validated.

2. Materials and Methods

2.1. Study Area

The domain of the EcoFish model includes the extended Gulf of Gdańsk (Figure 1), which is the southern part of the Gdańsk Deep area, located in the Gotland Basin. A straight line connecting Cape Rozewie with Cape Taran delimits the proper Gulf of Gdańsk. This line crosses the deepest parts of the Gdańsk Deep, with a maximum depth of 118 m. Along the coastal zone, there is a wide strip of shallows widening to the west of the mouth of the Vistula River. The slope of the bottom in the coastal zone is varied. The greatest decline occurs at the headland of the Hel Peninsula, where the bottom rapidly drops to a depth of 70 m [13].

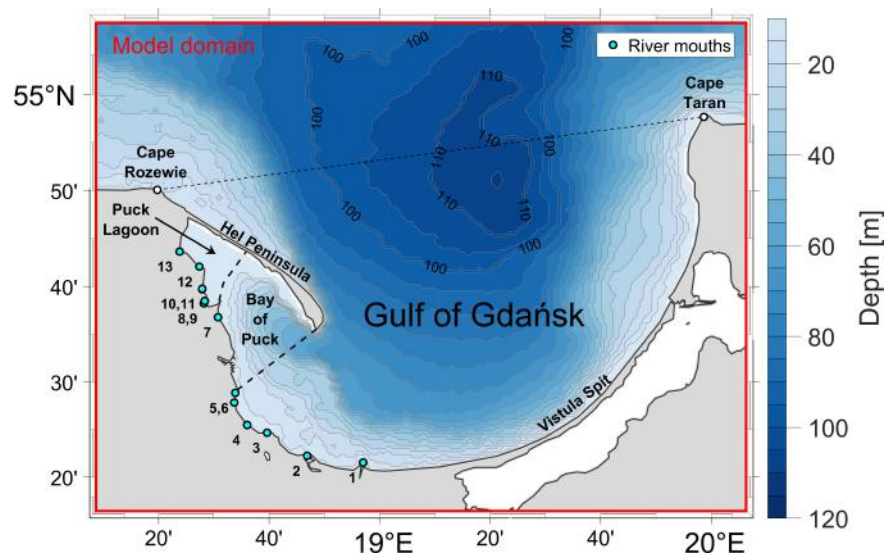


Figure 1. EcoFish model domain with topography. Numbers 1–13 indicates mouths of rivers (Section 2.5).

The Bay of Puck is a shallow area of the Gulf of Gdańsk located in its western part [14,15]. Due to its geographical location and special hydrological conditions, the Bay

of Puck is a reservoir unique in the scale of the entire Baltic Sea. It owes its specificity to natural factors: isolation from the sea waters by the Hel Peninsula and separation into two morphologically and environmentally different zones—the part known as outer Bay of Puck and the semienclosed, inner part called Puck Lagoon to the northwest.

2.2. EcoFish Model Configuration

EcoFish origins from Community Earth System Model (CESM) coupled global climate model <http://www.cesm.ucar.edu/models/ccsm4.0>, accessed on 1 June 2018 by NCAR. CESM is a state-of-the-art model system consisting of five separate components with an additional coupler controlling time, exciting forces, domains, grids, and information exchange between the models. For the purpose of the FindFish project, CESM was down-scaled and adapted for the Gulf of Gdańsk region for further development at the Institute of Oceanology, Polish Academy of Sciences.

EcoFish's horizontal resolution is 575 m (1/192°). The vertical resolution is 5 m for each layer with a total of 26 layers (Table 1). The vertical discretization uses the z formulation and the bottom topography is based on the Baltic Sea Bathymetric Database (BSBD) from the Baltic Sea Hydrographic Commission [16]. The bathymetric data were interpolated into the model grid using the Kriging method.

Table 1. EcoFish model vertical resolution.

Model Level	Thickness [m]	Low-Depth [m]	Mid-Depth [m]
1	5.0	5.0	2.5
2	5.0	10.0	7.5
3	5.0	15.0	12.5
4	5.0	20.0	17.5
5	5.0	25.0	22.5
6	5.0	30.0	27.5
7	5.0	35.0	32.5
8	5.0	40.0	37.5
9	5.0	45.0	42.5
10	5.0	50.0	47.5
11	5.0	55.0	52.5
12	5.0	60.0	57.5
13	5.0	65.0	62.5
14	5.0	70.0	67.5
15	5.0	75.0	72.5
16	5.0	80.0	77.5
17	5.0	85.0	82.5
18	5.0	90.0	87.5
19	5.0	95.0	92.5
20	5.0	100.0	97.5
21	5.0	105.0	102.5
22	5.0	110.0	107.5
23	5.0	115.0	112.5
24	5.0	120.0	117.5
25	5.0	125.0	122.5
26	5.0	130.0	127.5

The EcoFish model consists of two active and two passive components. The active prognostic models are Parallel Ocean Program (POP) and Community Ice Code (CICE). The passive components are responsible for providing atmospheric data fields and fresh water from catchment area. The main part of this system is the ocean model in which horizontal mixing is represented by biharmonic operator that is implemented by applying the Laplacian operator twice. It is performed in both viscosity and diffusion schemes; however, the mixing coefficients are different and equal to -3×10^{14} and 0.3×10^{14} ,

respectively (note: the sign was omitted). Vertical mixing used by authors in EcoFish system is called *k*-profile parametrization (KPP) [17]. Shear instability is parameterized in terms of the gradient Richardson number, while diffusivity (active tracers) and viscosity (momentum) are parameterized as diapycnal. Each active component has its own time step. The CICE time step is 10 min and it is equal to the coupling time step. Ocean model has typically two mods and time step is divided into two parts. The baroclinic part makes one step in 60 s. Because the model has linear free surface formulation, it is not needed to make substeps for the barotropic part. CESM is intended for use in global applications; thus, it was adapted for this purpose. Barotropic equation has been modified for possibility of assimilation of sea level at the boundaries [18]. Additionally, at the boundary area, salinity has been forced to have values from external model using restoring. The restoring time scale is not constant and depends on distance from the boundaries. Exactly at the boundaries, the restoring time scale is in the range of days and it increases to infinity toward the center of the domain at a distance of about 20 km (40 model cells). Similar models were already presented in [18,19].

2.3. Open Boundary

The results from the EcoFish model analyzed in this paper were spatially limited to the Gulf of Gdańsk area. However, the entire domain of the model is slightly larger and borders on the west and north with the open Baltic. Therefore, it is necessary to provide the model with boundary conditions. Apart from water temperature and salinity, it is necessary to prepare the data of sea surface height and barotropic components of sea currents. The data to the model boundary are provided by a 3D CEMBS [20,21] model with a horizontal resolution of 2 km. Since the exact determination of the data range on the border required trials with different settings, it was decided to prepare data on the entire FindFish domain, not only on its border. This allows the use of the same data regardless of the finally adopted settings. The fact that the results of the 3D CEMBS model are used as the source of boundary conditions means that 3D CEMBS's calculations must be performed prior to EcoFish.

2.4. Atmosphere Forcing

At the water–atmosphere border, the EcoFish model is fed with meteorological forcing. These data come from the UM (Unified Model) developed at the Interdisciplinary Modeling Center of the University of Warsaw (ICM UW). Parameters directly used as inputs are as follow:

- 10 m wind speed,
- 2 m air temperature,
- specific humidity,
- sea level pressure,
- precipitation (convective and large-scale),
- downward shortwave and longwave radiation

Missing parameters are calculated by the atmospheric data module, which is an integral part of the EcoFish model. Air density and scattered and direct shortwave radiation in the visible and near-infrared range are determined that way.

2.5. River Discharge

Due to the fact that modeling of surface runoff requires the use of a hydrological model, The Soil & Water Assessment Tool (SWAT) software was used [22–24]. SWAT is a small watershed to river basin-scale model used to simulate the quality and quantity of surface and ground water and predict the environmental impact of land use, land management practices, and climate change. This adaptation of SWAT was developed under the WaterPUCK—Integrated Information and Prediction Service project [11]. Meteorological data (precipitation, wind, temperature, and atmospheric pressure) comprise a key element of any water balance model. The SWAT hydrological model is based on real-time

observations (local meteorological station) as well as shorter weather forecasts (ICM UW website). The conversion of rainfall data into surface runoff is accomplished using the SCS (Soil Conservation Service) Curve Number procedure through the cumulative runoff volume and concentration time. SWAT covers sedimentation in surface and groundwater, and the transport model also includes snow cover. Additionally, the transport of nutrients and pesticides was taken into account for use at a later stage related to the launch of the biochemical part of the EcoFish model.

The SWAT model was created for six rivers (numbered 8–13) from the described domain (Table 2). For the remaining seven rivers (numbered 1–7), information on the runoff volume was taken from the Hydrological Predictions for the Environment (HYPE) model. It is a physics-based semidispersed catchment model that simulates the flow of water and substances as they travel from precipitation to discharge into the sea. We used historical time series from 1980–2010 for the geographic domain of Europe available as daily averages. Spatial resolution is determined by dividing the land area into catchments for which the HYPE data represent mean values at the estuary. The volumes for the years 2014 to 2020 have been calculated as the multiyear average over the available 30-year period.

Table 2. Rivers mouths' locations included within the EcoFish model domain and mean runoff.

	Source	River	Longitude	Latitude	Mean Runoff [m ³ /s]
1	HYPE	Vistula	18.95	54.35	1064
2	HYPE	Bold Vistula	18.78	54.37	2.05
3	HYPE	Still Vistula	18.66	54.41	6.06
4	HYPE	Oliwski Stream	18.60	54.42	0.31
5	HYPE	Kamienny Stream	18.56	54.46	0.45
6	HYPE	Kacza	18.56	54.48	0.29
7	HYPE	Ściekowy Canal	18.51	54.61	0.21
8	SWAT	Zagórska Stream	18.47	54.63	0.11
9	SWAT	Reda	18.47	54.64	0.48
10	SWAT	Mrzezino Canal	18.46	54.66	0.20
11	SWAT	Gizdepka	18.46	54.66	0.30
12	SWAT	Żelistrzewo Canal	18.45	54.70	0.17
13	SWAT	Plutnica	18.39	54.72	0.91

2.6. Simulation Run

The EcoFish model was validated using the results of a seven-year simulation from 1 January 2014 to 31 December 2020, preceded by a two-year model spin-up. This run was calculated using the above-described model configuration with satellite data assimilation for surface temperature. Results were recorded four times a day as 6-h averages. The simulation results and model validation are presented in Section 4.

Additionally, in order to verify the correctness of the assimilation module itself, the same simulation was carried out without the assimilation of satellite data for the surface temperature. Both runs were then compared against satellite data.

2.7. Data Sets Used for Evaluation

Two in situ databases were used for the statistical analysis of the EcoFish model. Detailed descriptions are provided below.

2.7.1. ICES

The main in situ database that was used to validate the water temperature and salinity in the EcoFish model is the hydrochemical database provided online by the International Council for the Exploration of the Sea (ICES) via the <https://ocean.ices.dk/HydChem/>, accessed on 1 February 2021 website. 17,902 measurements from 2014 to 2019 were used for comparison. Data for 2020 was not yet available in the database at the day of this validation.

Most of the data was from 2014 (6130 measurements) and 2015 (6848 measurements). From 2016 to 2019, 1055 to 1444 measurements per year were available. ICES measurements covered almost the entire domain (Figure 2), except its eastern part, which covers areas along the Vistula Spit to the easterly coast of Gulf of Gdańsk. The region with the densest measurement grid was the strip along the 19°E meridian.

ICES measurements were relatively uniformly distributed throughout the water column. In the surface layer from 0 to 5 m, 1082 measurements were available, in the layer from 5 to 30 m—5429, in the layer from 30 to 80 m—8987 and 2404 measurements for depths greater than 80 m.

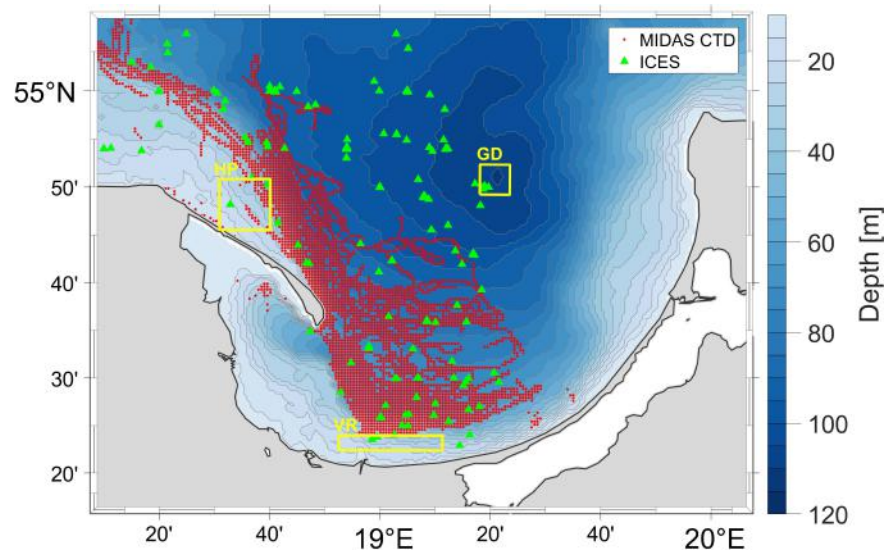


Figure 2. Locations of in situ data collected with the MIDAS CTD instrument during cruises and data from the ICES database used to validate the EcoFish model. Rectangles mark the regions (HP—Hel Peninsula, GD—Gdańsk Deep, VR—Vistula River) used in the description of the sea currents.

2.7.2. Fishing Cruises

We had an additional database that was used to validate the model. It was a set of measurements taken under the FindFish project during fishing cruises. Valeport MIDAS CTD model 500 and GPS 73 Worldwide by GARMIN were used for this purpose. Recording of physicochemical data was carried out during fishing with towed and set gears. The following parameters were saved in the device memory:

- water temperature,
- salinity,
- pressure,
- turbidity,
- saturation,
- pH.

Data from the MIDAS CTD instrument were collected in the area north of the Vistula River mouth and in the strip in the open sea, parallel to the Hel Peninsula (Figure 2). The measurements have a high temporal and spatial resolution. Therefore, they were averaged to match the model mesh. After this operation, we had 15,312 records. The highest density of measurements (8533 values) were from 30 to 60 m deep layer. It was closely related to the optimal fishing depth. The first data was collected on 22 May 2018 during pelagic fishing. To date, 422 hauls/releases have been made, of which 306 were harvested with towed gear and 116 with set gear. Most of the data was collected in 2020 (7293 measurements) and 2019 (5954 measurements). The remaining 2065 measurements were taken in 2018. The months with the highest amount of data collected were April (3150) and March (2395). Measurements were taken from the decks of 10 vessels, and the schedule of

their cruises was determined on an ongoing basis in relation to the frequency of occurrence of fish species being the target of the catch. In addition, meteorological data were also recorded, including air temperature, wind strength and direction, cloud cover, and sea state, which were collected in the form of questionnaires completed by skippers.

3. Assimilation of Satellite Data in the EcoFish Model

3.1. Satellite Data Acquisition and Processing Module

The satellite sea surface temperature data (SST) used along with EcoFish model come from the SatBałtyk project database [8,9] and are based on measurements from a medium-resolution imaging spectroradiometer (MODIS AQUA) and an advanced ultrahigh-resolution radiometer (AVHRR). These data are calibrated to local conditions in the Baltic region and subjected to atmospheric correction and filtration. Raw maps are linked in space, geometrically corrected for changes in satellite position, and radiometrically corrected in case of numerical errors in data transmission. Data in the SatBałtyk system have a horizontal resolution of 1 km and cover the entire area of the Baltic Sea. Daily average values obtained from the combination of all satellite images available on a given day are used for assimilation. Assimilation takes place during the assimilation window with the peak of the window set to 12:00. This is taken into the account during the process of combining data using weighted averaging. The data acquisition management module automatically detects the presence of new data, downloads new files to a local storage, processes the data, and saves the result together with control files and metadata. Data processing consists of their interpolation onto the 575 m grid of EcoFish model and saving in the file format compliant with the model requirements. Thanks to the aforementioned control files, the module managing the entire system can monitor the status of satellite data on an ongoing basis and, if available, start assimilation.

3.2. Satellite Data Assimilation Module

The assimilation module is based on modified and extended CESM model [25,26] components that are an integral part of the EcoFish model. This allowed for smooth introduction of satellite information to computed data with each time step. In addition, it allowed the reuse of a number of settings and functionalities already available in the CESM, e.g., parameterization of the length of the assimilation window currently set to 24 h, the frequency of assimilation (each time step) and the modules for reading and processing data by the model. The method of assimilation selected in the EcoFish model takes as input the values of a given variable V_{mod} obtained from the calculations of the model and satellite measurements V_{sat} . Moreover, the method accepts a number of parameters that control its behavior and describe the data source. The most important of them are:

- *data_type*—allows you to specify the frequency with which data for assimilation appears, e.g., annually, monthly, every N hours [value used: N hours].
- *data_inc*—in the case of data appearing every N hours, specifies the number of N [value used: 24].
- *interp_freq*—determines how often information from assimilated data is entered into the model calculations, e.g., every N hours, every time step [value used: every time step].
- *interp_type*—defines the way in which assimilation data are interpolated between the frequency resulting from *data_type* and the one resulting from *interp_freq*. The possible options are nearest neighbor algorithm, linear interpolation, and third-order polynomial interpolation using the four nearest points on the timeline [value used: Linear].
- *interp_inc*—parameter specifying the frequency with which the differences between the model and measurement data are calculated [value used: 1 h].
- *restore_tau*—this is a parameter that specifies the time after which the model results should reach a value consistent with the measurement data [value used: 0.1 day].

With each calculation step, each assimilation module checks, on the basis of the *data_type* and *data_inc* parameters, whether new assimilation data should appear in a given

step. If so, it loads the next file with assimilated data V_{sat} . For the sake of example, let us assume that data appears every 24 h. Of course, these data should not be entered into the model at once, in one time step, as this would disrupt the continuity of equations and the equilibrium of the system. Hence, using the *interp_freq* parameter, one can choose that the data should be entered gradually, e.g., every 0.5 h. Using the *restore_tau* parameter, one can specify that the model should reach the assimilated values after a period of 12 h. Having these parameters, the module divides the current difference between V_{sat} and V_{mod} into the number of steps resulting from *interp_freq* that fall within the *restore_tau* period, i.e., in this case by 24.

$$dV_{step} = (V_{sat} - V_{mod}) / (\text{restore_tau} / \text{interp_freq}) \quad (1)$$

$$= dV / (\text{restore_tau} / \text{interp_freq}), \quad (2)$$

Here, dV_{step} is a partial increment introduced to the model in a given assimilation step (0.5 h in this example). The value of a given model variable depends on many factors, e.g., transport, radiation, biological processes, etc. Therefore, the difference dV calculated at the beginning between the model data and the measurement data must be constantly corrected to obtain the expected value at the end. Hence, it is updated at the frequency specified by the *interp_inc* parameter. The resulting value of the assimilated variable is calculated by adding the calculated increment to the model result:

$$V_{assim} = V_{mod} + dV_{step}, \quad (3)$$

The figures below present the application of the satellite data assimilation module in the EcoFish model for two selected days from the simulation period. On the left side, one can see the satellite image for the surface temperature, in the middle, the model result with visible effect of assimilation, and on the right side, the results from the model version without the assimilation. The first scene (Figure 3) was taken on 28 April 2019. On that day, due to the heavy cloud cover, the satellite image was severely restricted and provided information only about a small area within the domain (Figure 3a). As a result of the assimilation module, the surface temperature in the vicinity of the Hel Peninsula and the eastern coast of the Gulf decreased, which can be seen in the Figure 3b. Figure 3c shows the surface temperature from the version of the model without the assimilation.

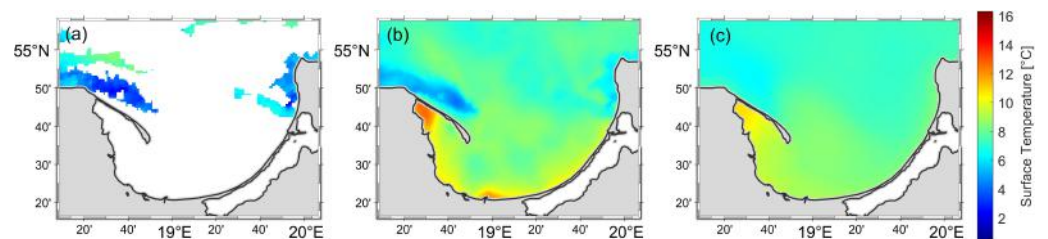


Figure 3. Application of the satellite data assimilation module in the EcoFish model for 28 April 2019. On the left, (a) a satellite image of the surface temperature. In the middle, (b) the result from the EcoFish model with a visible effect of assimilation. On the right, (c) the result from the EcoFish model without assimilation.

In the next figure (Figure 4) for 3 May 2019, the satellite image is more complete and almost the entire visible domain has been assimilated.

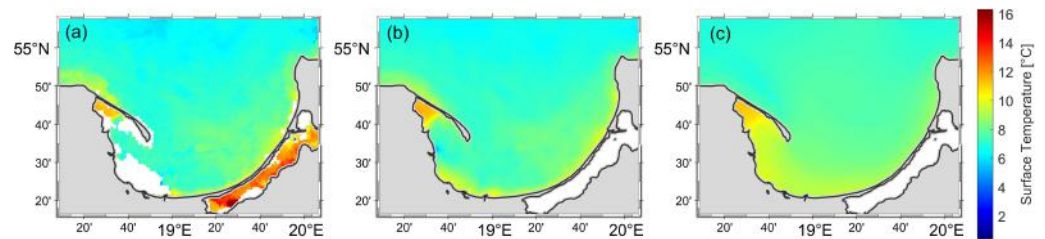


Figure 4. Application of the satellite data assimilation module in the EcoFish model for 3 May 2019. On the left, (a) a satellite image of the surface temperature. In the middle, (b) the result from the EcoFish model with a visible effect of assimilation. On the right, (c) the result from the EcoFish model without assimilation.

4. Results

4.1. EcoFish Model Validation

The accuracy of the EcoFish model results, in the period from January 2014 to December 2020, for water temperature (Section 4.1.1) and salinity (Section 4.1.2) was checked by comparing them with available in situ observations from the ICES database and measurements made with the MIDAS CTD instrument during fishing cruises. This was conducted for the two versions of the EcoFish model—one with the assimilation module enabled (EcoFish+A) and one without assimilation (EcoFish−A). The most important statistical quantities were determined, such as Pearson’s correlation coefficients (r), root mean square errors (RMSE), standard deviations (STD), and biases (in relation to means), which illustrate the tendency of the model to systematically overstate or underestimate the result.

4.1.1. Water Temperature

At first, we wanted to verify the impact of the assimilation of satellite SST module itself. Therefore, the surface temperature was validated for 2018 using two separate versions of the EcoFish model—one without (EcoFish−A) and one with satellite data assimilation (EcoFish+A). All other model parameters were identical. Results from both runs were then compared against assimilated satellite data. Table 3 provides a statistical summary of the temperature obtained from all three sources to give a better overview of its characteristics. Table 4 contains comparison of both model versions against satellite data used for assimilation.

Table 3. Statistical description of SST from model and satellite.

Source	Mean [°C]	Median [°C]	STD [°C]
Satellite	12.55	13.24	6.39
EcoFish−A	11.42	11.83	5.67
EcoFish+A	11.99	12.42	6.16

Table 4. Statistical verification of SST from model calculations vs. satellite measurements.

Source	Pearson’s r	RMSE [°C]	Bias [°C]
EcoFish−A vs. Satellite	0.95	2.31	−1.12
EcoFish+A vs. Satellite	0.98	1.45	−0.56

As one can observe, the differences between model and the satellite are larger in case of the model without assimilation (Table 4). Pearson’s correlation coefficient (r) increased from 0.95 to 0.98. The root mean square error (RMSE) decreased by almost 1 °C from 2.31 °C to 1.45 °C, and the tendency of the EcoFish model to systematically underestimate the results by −1.12 °C for the nonassimilated version decreased to −0.56 °C for the assimilated version. This confirms that the assimilation mechanism itself was designed and implemented properly and it yields significant changes in obtained results. It is worth

noticing that the assimilation does not result in 100% agreement between satellite and model data. This can be contributed to several factors. Most importantly, in order to save disk space, results saved by the model are averaged over the period of 6 h. Satellite data are also averaged over the assimilation period, but the assimilation is designed to have the peak alignment of the data precisely at 12:00. Apart from that, the model surface layer is much thicker than the surface layer measured by satellites. Because of that, it would be wrong to exactly replicate satellite results in the model. The assimilation module is parameterized to leave some level of freedom between model and satellite data. Last, one must take into the account that even though satellite data are assimilated with every time step, each water cell in the model is subjected to vertical and horizontal currents that dissipate the assimilated information. Given the above, obtained results are satisfactory and prove that the assimilation module works as expected.

In order to additionally emphasize the impact of assimilation on the improvement of the model results, a separate comparison of the temperature in the surface layer itself (from 0 to 5 m) with the data from the ICES database was made. For the surface, within the model domain, 1082 observations from the ICES database were available. The result of this analysis is presented in the Taylor diagram (Figure 5) in the form of normalized statistical coefficients. Absolute statistical values are presented in tabular form (Table 5).

Table 5. Statistical comparison of modeled surface temperature with the reference data from ICES.

Database	Pearson's r	RMSE [°C]	STD [°C]	Bias [°C]
ICES (EcoFish+A)	0.99	0.70	5.75	0.01
ICES (EcoFish−A)	0.99	0.93	5.32	−0.40

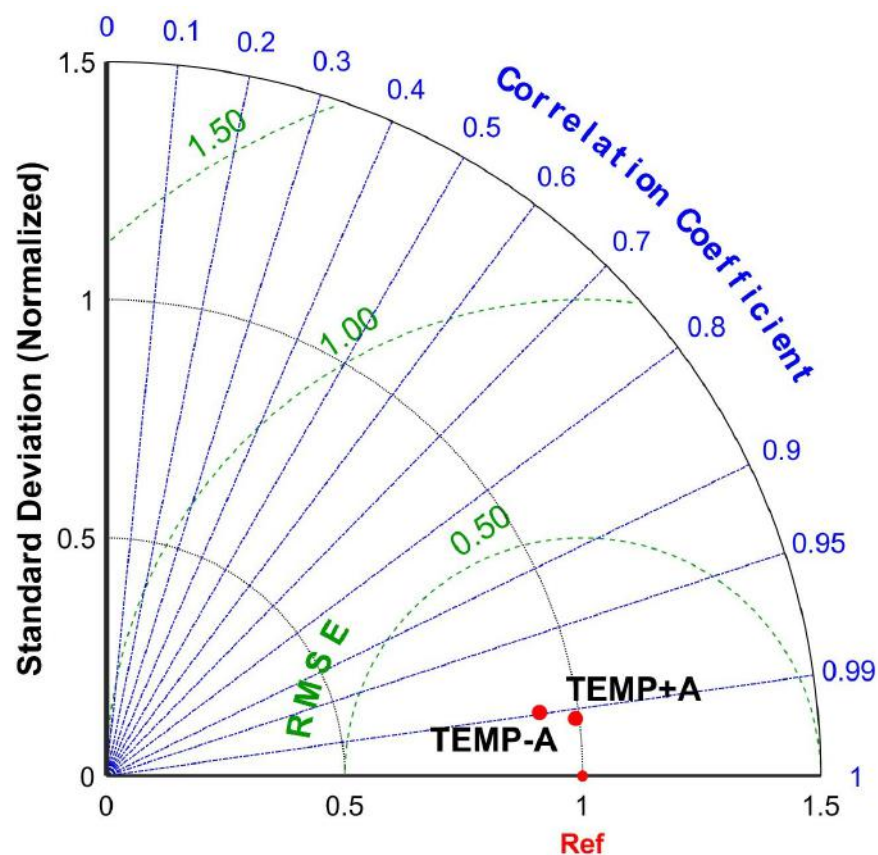


Figure 5. Taylor diagram for surface temperature from EcoFish model with (TEMP+A) and without (TEMP−A) assimilation versus ICES database.

The ability of the EcoFish model (with an active SST satellite data assimilation module and without) to correctly project the real environment conditions was verified by comparing the model results for temperature with all available observations at all depths. The result of this validation is presented in the Taylor diagram [27] (Figure 6) in the form of normalized statistical coefficients. Absolute statistical values are presented in tabular form (Table 6).

Table 6. Statistical comparison of modeled temperature on all depths with the reference data from ICES and MIDAS CTD.

Database	Pearson's r	RMSE [°C]	STD [°C]	Bias [°C]
ICES (EcoFish+A)	0.94	1.33	3.66	−0.36
ICES (EcoFish−A)	0.95	1.22	3.52	−0.28
MIDAS CTD (EcoFish+A)	0.87	1.83	3.57	−0.34
MIDAS CTD (EcoFish−A)	0.85	2.03	3.84	−0.25

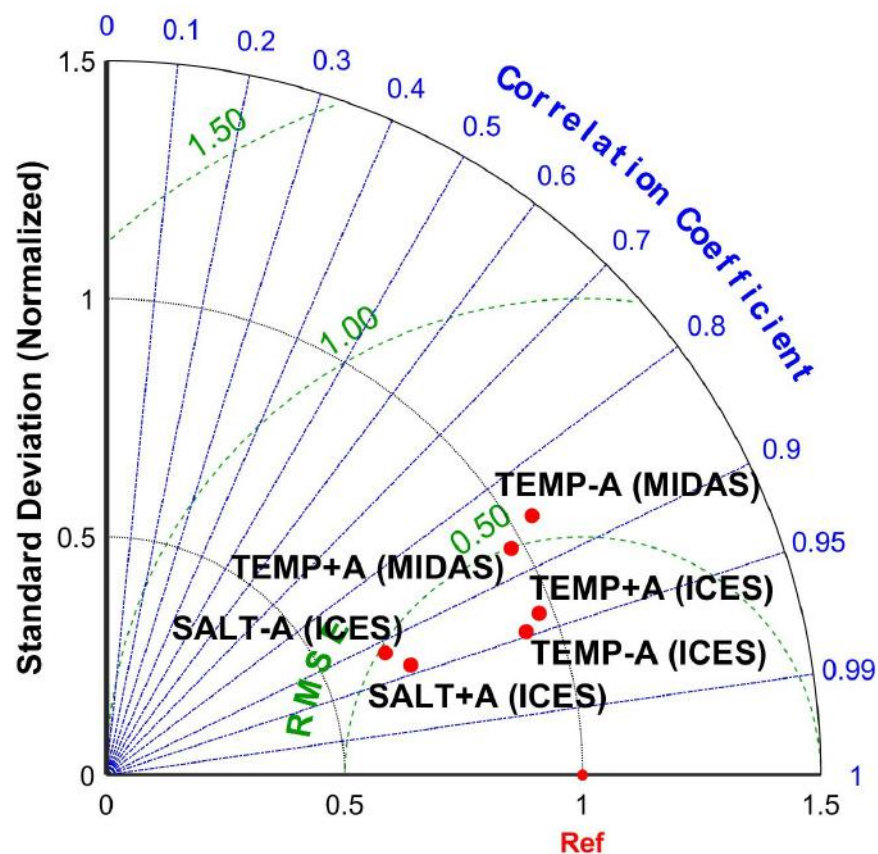


Figure 6. Taylor diagram for temperature and salinity using all available in situ data.

The Pearson correlation coefficient (r) calculated between the assimilated model (EcoFish+A) and the data from the ICES database was 0.94. When compared with data from fishing cruises using the MIDAS CTD instrument, it took the value of 0.87. The decline may be related to the varying density of in situ data from surface to bottom. ICES data was relatively homogeneously distributed in the water column, while the cruise data most often occurred at fishing depths, i.e., 30 to 60 m. Due to the use of assimilation, the model better reflects the temperature closer to the surface, as indicated by high correlations that slightly decrease with depth.

Table 6 shows also that when comparing to ICES data, a nonassimilated version of the model (EcoFish−A) produced slightly better statistics than the assimilated version (EcoFish+A). This might be related to the database itself and should not be taken as a sign that assimilation worsened the results. It is opposite in the case of MIDAS CTD

data in which statistics for EcoFish+A are better than for the version without assimilation. Summarizing, high correlations and low RMSEs were received from both versions of the model.

The mean square error (RMSE) for EcoFish+A is 1.33 °C when compared with ICES data and 1.83 °C when compared with cruise data. The model has a similar bias for both in situ databases of -0.36 °C and -0.34 °C, respectively. This means that the model tends to systematically underestimate the results slightly. The standard deviation for both databases used during the validation is similar and amounts to 3.66 °C for ICES data and 3.57 °C for data from the MIDAS CTD instrument (Table 6).

When analyzing the vertical profile (Figure 7), created while taking all observations from the ICES database into account, compared to the corresponding values from the EcoFish model (with and without assimilation), a high correlation can be seen, lasting from the surface up to about the 13th level of the model (to a depth of 80 m).

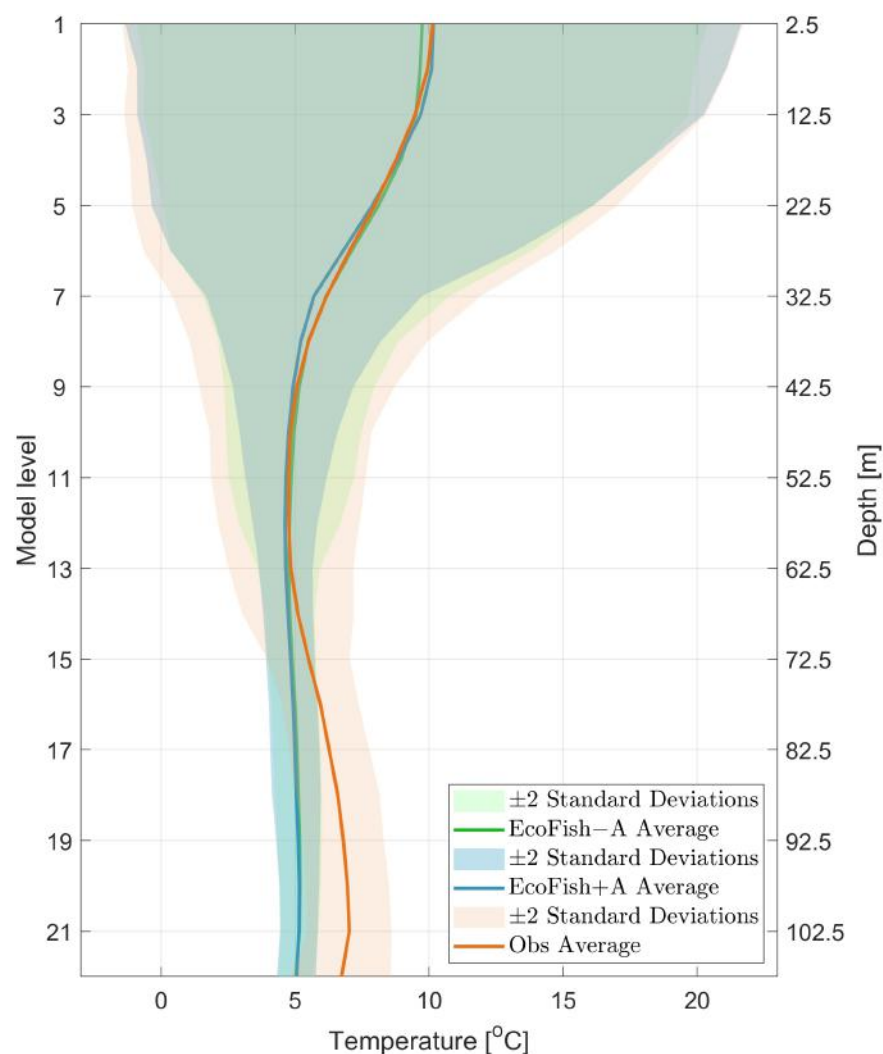


Figure 7. Temperature vertical profile for all ICES observations compared with EcoFish values.

Below the 13th level, the data are less correlated and the EcoFish model has a tendency to slightly underestimate the results. The reason for this is that the POP model has KPP implemented for surface layer only. Since it is designed for global issues, the vertical mixing scheme has been modified for better representation of surface layer in the Baltic Sea. Small changes of the interior shear mixing, suggested by Durski et al. [28], have been introduced. For better reproduction of the bottom layer, the dependence of the quadratic drag formula on thickness of the lowest model cells was applied (the logarithmic profile of

roughness height). There is no turbulent closure though that will cover the bottom layer, which results in the underestimation of temperature (Figure 7) and salinity (Figure 8) in the bottom layers.

The most important thing is that the model correctly reflects the temperature drop in the thermocline layer (on average from the 3rd to the 9th depth level). Not only is a high correlation visible, but close and overlapping ranges of the double standard deviations are also visible. Only below the 7th level (below the depth of 35 m) are the model data characterized by a smaller standard deviation than the observational data from the ICES database.

Therefore, it can be concluded that, despite the slight discrepancies between the model results and the observations (mostly at greater depths), the vertical mixing in the EcoFish model has been correctly implemented, and the model itself reflects real conditions well.

4.1.2. Salinity

Another physical variable derived from the EcoFish model that we validated is salinity. Salinity is a good parameter to check if the model is capable of handling water masses, as it does not undergo any transformations (gains and losses) in the marine environment. Salinity results from both versions (with and without assimilation) of the model were compared with available in situ observations from the ICES database using the same locations as for temperature (Figure 2). The result of this comparison is presented in the Taylor diagram (Figure 6) in the form of normalized statistical coefficients, as well as in the form of absolute values in table (Table 7).

Table 7. Statistical comparison of modeled salinity with the reference data from ICES.

Database	Pearson's r	RMSE [PSU]	STD [PSU]	Bias [PSU]
ICES (EcoFish+A)	0.94	0.80	1.27	−0.01
ICES (EcoFish−A)	0.92	0.91	1.20	0.01

The Pearson correlation coefficient (r) calculated between the model data (EcoFish+A) and the observations from the ICES database took the value of 0.94, which is better than in the case of the nonassimilated version of the model. The root mean square error (RMSE) was 0.8 PSU; this is a satisfactory result, while having relatively large standard deviation of 1.27 PSU. The model has a low negative mean bias of −0.01 PSU, which could signify that it responds well to changes in salinity. However, this is largely due to the fact that at low and medium depths (from the surface to about 14th level), the model results for salinity are slightly higher than the ICES observational values, followed by a trend that reverses. At higher depths, the model begins to underestimate salinity from about 0.5 up to 2.0 PSU. This was demonstrated on a vertical salinity profile (Figure 8) created using all observations from the ICES database.

When analyzing the vertical profile, several characteristic zones in the water column can be seen. On the surface, we observe an increased standard deviation, both for model data and observations. It is the result of mixing fresh waters from river runoff with sea waters, causing increased salinity dynamics on the surface. Then, between 10 and 40 m deep (up to 60 m depending on the location), the isohaline layer stretches, which is noticeable both at a constant average salinity of about 7–8 PSU and the size of the standard deviation, which in this layer is the smallest throughout the entire water column. Below 35 m, the STD begins to rise gradually, reaching about 2 PSU by 70 m and remaining at this value to the bottom. Below the isohaline layer, there is a transition layer with a clearly delineated halocline, especially for the curve determined using ICES observations. Average salinity starts to increase systematically from about 55 m (11th level) and stabilizes only at a depth of 100 m (20th level). The curve determined using the model data also shows the presence of a halocline, but it is not so clearly marked. The model results do not have the same dynamics as in situ data, which is especially visible in a much smaller

STD than in the case of observations. In the water layer from the 12th level to the bottom, the salinity obtained from the EcoFish model increases from about 9 PSU to 12 PSU, while the increase in salinity for the experimental data is greater and goes from 8 PSU to 13 PSU (Figure 8). The highest salinity values seen in the experimental data can be related to the infusion effect, while decreases can occur during periods of long-term stagnation.

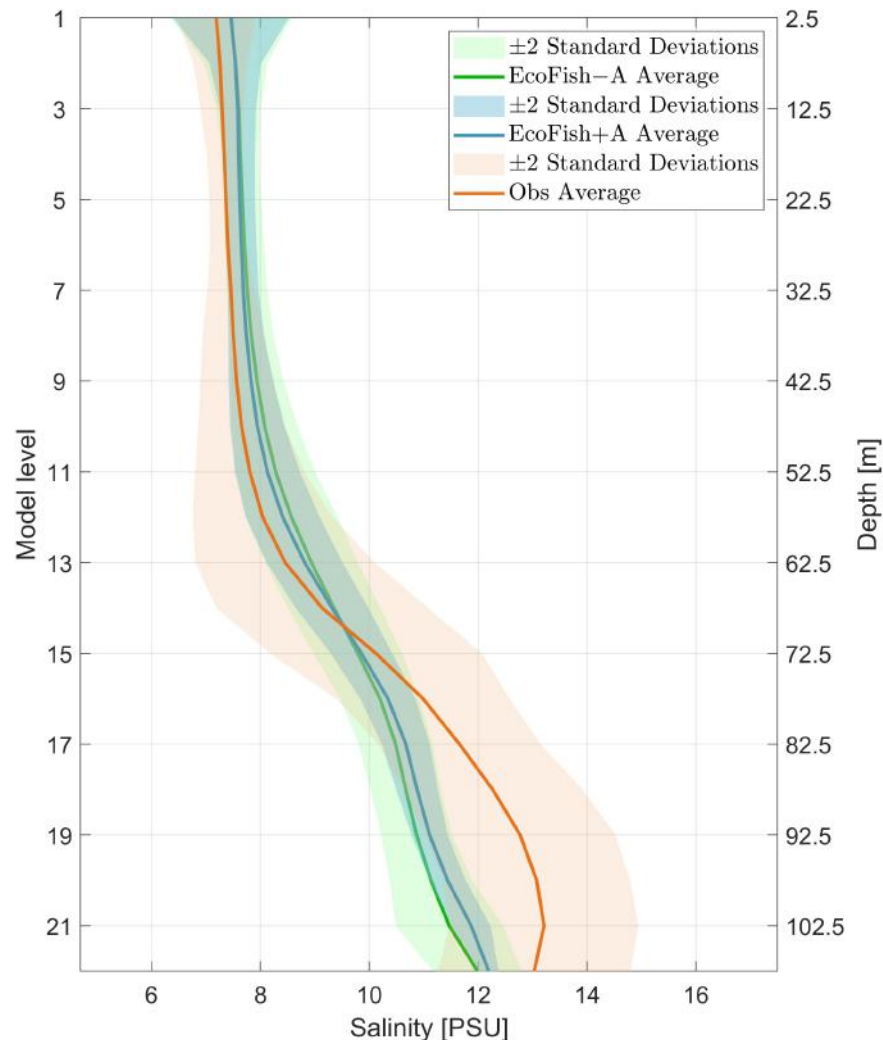


Figure 8. Salinity vertical profile for all ICES observations compared with EcoFish values.

4.2. EcoFish Model Simulation Results

In this section, we present the average monthly temperatures, salinity, sea surface height, and currents in the surface layer for EcoFish model with an active SST satellite data assimilation module. The averages reflect the simulation period from 2014 to 2020. The results for individual months have been transferred to the Appendix A section (Figures A1–A8 and Tables A1–A23). Additionally, figures with the differences between the monthly averages of parameters from the models with (EcoFish+A) and without (EcoFish–A) assimilation are presented.

4.2.1. Water Temperature

The model domain is characterized by a strong seasonal variability of the surface temperature (Figure 9) for each year from the seven-year simulation (2014–2020). The greatest dynamics occurs in the southern part of the domain, which includes the southern part of the Gulf of Gdańsk and the Bay of Puck, which has the greatest number of low-depth coastal areas that react quickly to atmospheric forcing. The remaining regions are characterized by relatively lower seasonal variability of the surface temperature.

The mean water surface temperature for the entire analyzed model domain was 10.43 °C. The months with the lowest average temperature are generally February and March, and the coldest month in the simulation period was March 2018 with an average temperature of 2.05 °C. The warmest months are usually the summer ones, i.e., July and August with the record-breaking August 2018, in which the average water temperature in the surface layer reached 21.23 °C (Figures A1 and A2 and Table A1).

Temperature extremes for single model cells were most common in shallow coastal regions. The most characteristic is the shallow inner Bay of Puck called Puck Lagoon (Figure 1), which is not only separated from the open sea by the Hel Peninsula, but in its eastern part, there is a characteristic bathymetric anomaly in the form of shallow water (marked with curved dashed line), which additionally limits the exchange of water masses with the outer Bay of Puck (and whole Gulf), influencing to local temperature extremes. The lowest temperatures were in January and February 2014, falling to -0.43 °C (Table A2), and the highest were in July 2014 and 2018, when the temperature exceeded 28 °C (Table A3).

The lowest standard deviations ranging from 0.34 °C to 0.81 °C (0.53 °C on average) were obtained by the model for February and March. It is the period before spring when the surface layer is cooled down after winter, and both air temperature and sunlight do not yet reach high values to cause significant local changes. The largest deviations from the mean surface temperature appear in May and June (1.22 °C to 3.11 °C) with values exceeding 3 °C in May 2017 and 2018 (Table A4).

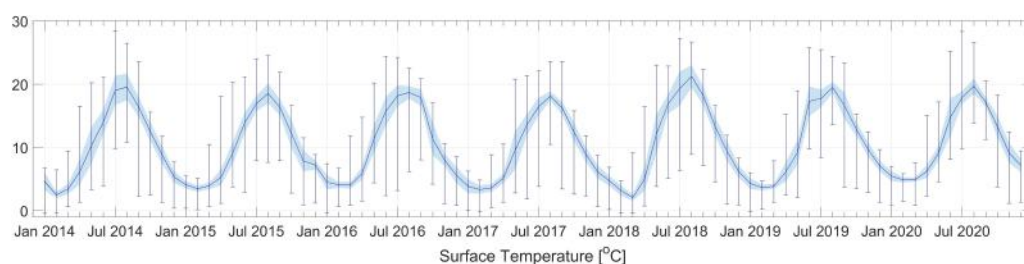


Figure 9. Monthly mean surface temperature for the entire model domain. Error bars represent extreme values. The shaded area represents standard deviation.

The picture below (Figure 10) presents the average monthly surface temperature for the period 2014 to 2020. It can be seen that there are four characteristic periods of temperature variation in the domain. The longest, five-month cold period, lasting from December to April, when the average surface temperature is low and relatively stable, ranging only from about 3 °C to 7 °C. Then, a four-month warm period lasting from June to September with average temperatures ranging from about 15 °C to 19 °C. There are also two transitional periods. The first transition (uptrend) period is May, when the temperature rises sharply from 5 °C in April to 15 °C recorded in June. The second transition period (downward) is October and November, when the water cools down quickly from an average of 17 °C in September to 6 °C in December (Table A1).

The reservoir that responds most quickly to external factors is the aforementioned Puck Lagoon. Thanks to its specific location and bottom topography, it has the greatest variability of the surface temperature and the minimum and maximum temperature achieved. In winter, local ice cover is observed, while in summer, it is exposed to toxic algae blooms stimulated by high temperatures and the deposition of inorganic phosphate from rivers.

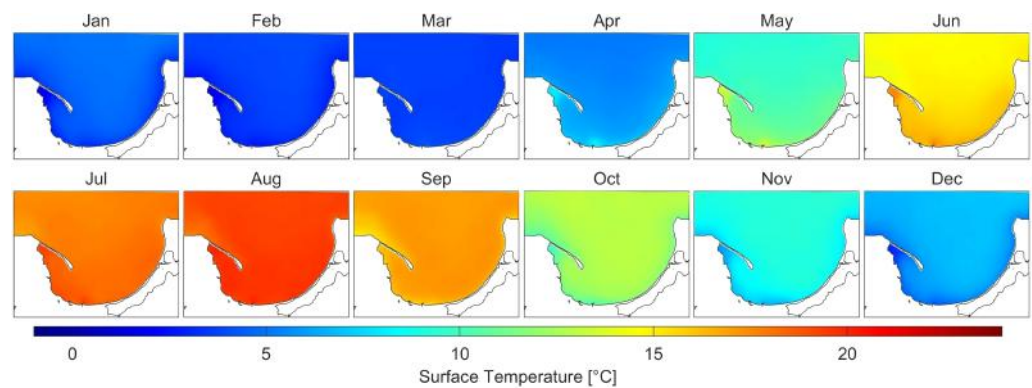


Figure 10. Average monthly water temperatures for the surface layer in 2014–2020.

Looking at Figure 11, that shows the difference in the monthly average SST values between the model with (EcoFish+A) and without assimilation (EcoFish–A), it can be seen that the assimilation influences the increase of the temperature in the warm season (from May to August) and the decrease in the cold one (from October to January). It is related to the vertical resolution of the model, and more precisely to the thickness of the first (surface) layer, which is 5 m.

It is more than the actual surface layer for which the SST is measured from satellite instruments. A thicker layer responds slower to atmospheric forcing, as it has a higher heat capacity. Assimilation of the satellite data into the model adjusts the surface layer temperature to the atmospheric conditions faster; hence, it responds faster to the changes.

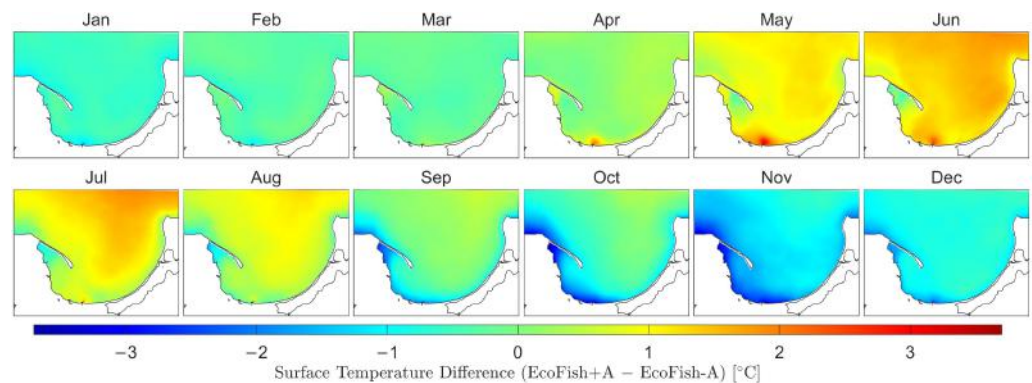


Figure 11. Average monthly water temperature differences for the surface layer in 2014–2020 between two versions of the model: with and without SST assimilation enabled.

4.2.2. Salinity

During the seven-year-long simulation, the average monthly salinity in the surface layer was between 7.31 PSU and 7.76 PSU, which gives an average of 7.47 PSU for the entire time period (Figures 12 and 13). The annual course of salinity in the study area is usually established assuming lower values in the warm/summer months (minimum for April 2014) and higher values in the cold/winter season (maximum in February 2014) (Figures A3 and A4 and Table A9).

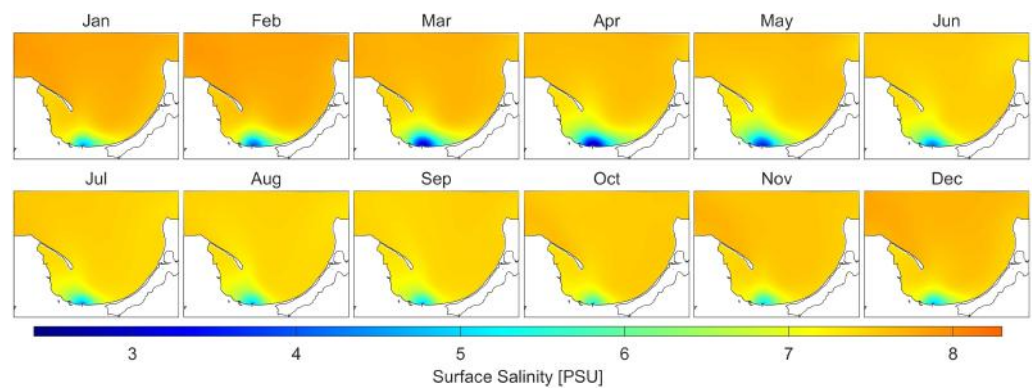


Figure 12. Average monthly salinity for the surface layer in 2014–2020.

Figure 14 shows that there are differences in surface salinity distribution when comparing models with and without SST assimilation. The model with assimilation (EcoFish+A) gives almost 1 PSU higher salinity in the south area of Gulf of Gdansk from May to August. The reason for that is the increase in water circulation (Section 4.2.4) leading to more salty waters located in the deeper bottom layers being transported to the surface as a result of mass conservation law.

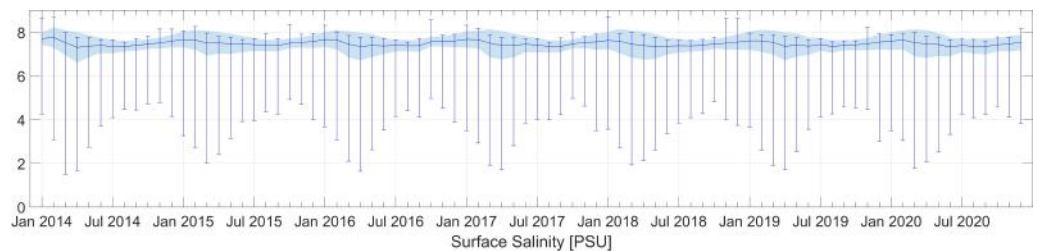


Figure 13. Average monthly surface salinity for the entire model domain. Error bars represent extreme values. The shaded area represents standard deviation.

The lowest seasonal fluctuations in salinity occur in the open sea, which is confirmed by small standard deviations (Table A12), rarely exceeding 0.3 PSU. In the southern part of the domain, which includes the mouth of the Vistula River, salinity can fluctuate from about 2 PSU to even 8 PSU in the summer months (Figure 13). The lowest salinity recorded in the model for the simulation period, amounting to 1.51 PSU, was recorded in March 2014 (Table A10). It was the result of the spring rise and runoff from the Vistula River. The highest of 8.70 PSU was obtained for January 2018 at open sea (Table A11).

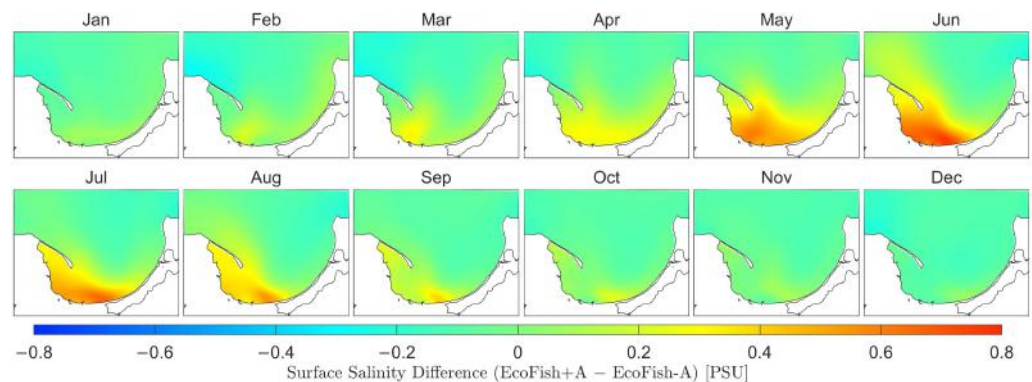


Figure 14. Average monthly salinity differences for the surface layer in 2014–2020 between two versions of the model: with and without SST assimilation enabled.

The dynamics of changes in salinity along the surface layer is influenced by a number of factors. Among others, it is the amount of river runoff, seasonal changes in the thermal

structure of water or changing meteorological conditions. However, in the bottom layer, the salinity distribution over the year seems to be relatively uniform, strongly related to the bathymetry (Figure 15). The highest salinity at the bottom (12.66 PSU on average) occurs in areas of great depth, in particular in the Gdańsk Deep. Possible fluctuations there, are no longer the result of cyclical processes with a seasonal frequency, but rather, of irregular events such as sea inflow. Only in 3 out of 84 considered months, the average monthly salinity at the bottom exceeded 13 PSU (Table A15). This situation occurred in March 2014 (13.04 PSU), September 2017 (13.15 PSU) and November 2015 (13.19 PSU).

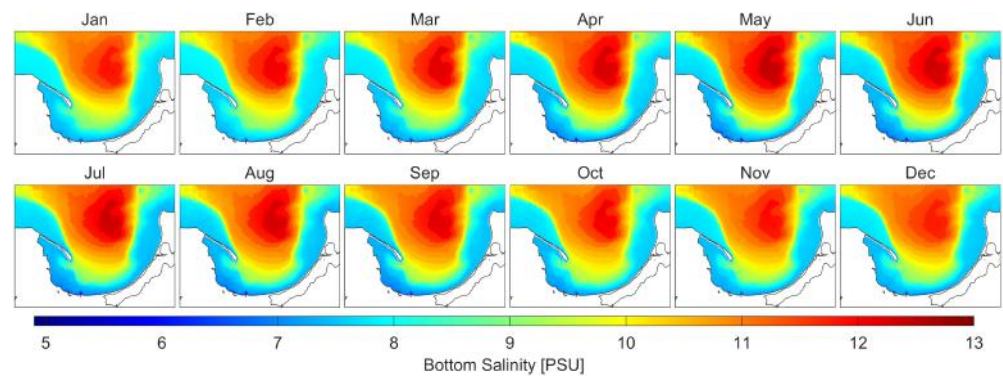


Figure 15. Average monthly salinity for the bottom layer in 2014–2020.

4.2.3. Sea Surface Height

The lowest values of sea surface height determined in the model were -29.58 cm in November 2015 and -31.09 cm in October 2016 (Table A18). The highest, 60.19 cm and 77.21 cm, were obtained for March 2020 and January 2015, respectively (Table A19).

The average sea surface height was 1.50 cm (Figure 16 and Table A17). Individual monthly averages are characterized by higher standard deviations (between 4.96 cm and 6.47 cm) in the months from October to February (Table A20). In the remaining months, the average standard deviations are usually smaller and reach values of about 3 cm (Figure 17).

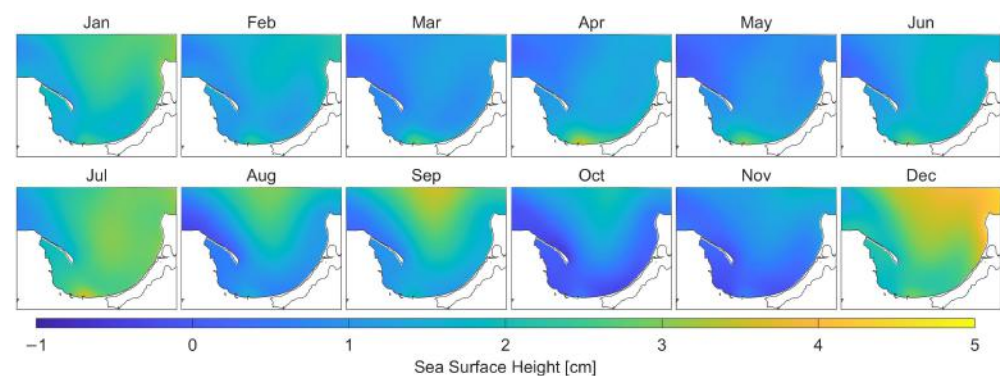


Figure 16. Average monthly sea surface height in 2014–2020.

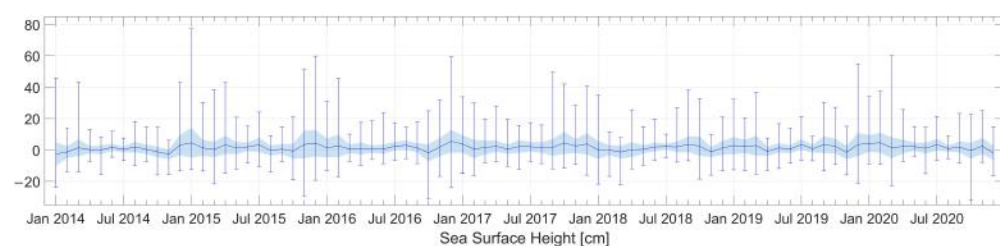


Figure 17. Average monthly sea surface heights for the entire model domain. Error bars represent extreme values. The shaded area represents standard deviation.

The process of SST assimilation has minor but noticeable influence on sea level (Figure 18). The increase of salinity in the coastal area (Figure 14) results in higher density, which has direct impact on pressure distribution. Therefore, an increase in salinity causes a decrease in sea level, keeping the hydrostatic balance of the system.

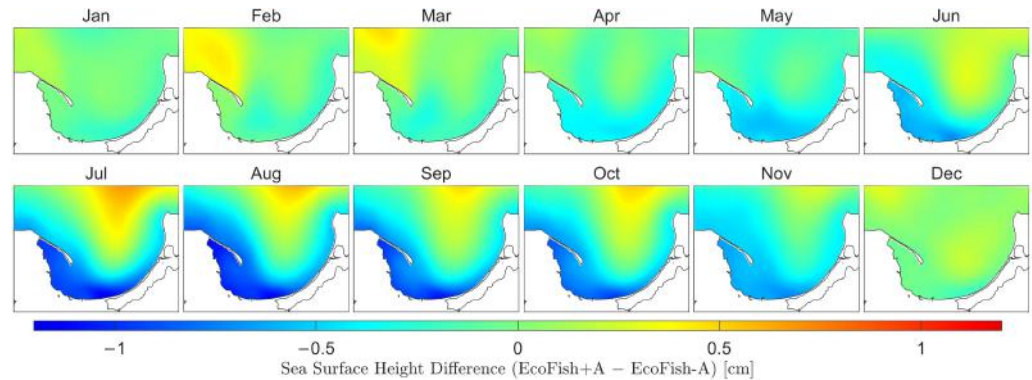


Figure 18. Average monthly sea surface height differences in 2014–2020 between two versions of the model: with and without SST assimilation enabled.

4.2.4. Currents

The spatial distribution of sea currents inside the domain is much more characteristic and repeatable than in the case of sea surface height. The average current velocity in the surface layer for 2014–2020 was $6.73 \text{ cm}\cdot\text{s}^{-1}$ with an average standard deviation of $5.23 \text{ cm}\cdot\text{s}^{-1}$ (Figure 19 and Tables A21 and A23). The strongest currents were obtained for December 2016 and January 2015 and reached the speed of $104.45 \text{ cm}\cdot\text{s}^{-1}$ and $120.09 \text{ cm}\cdot\text{s}^{-1}$ (Table A22), respectively.

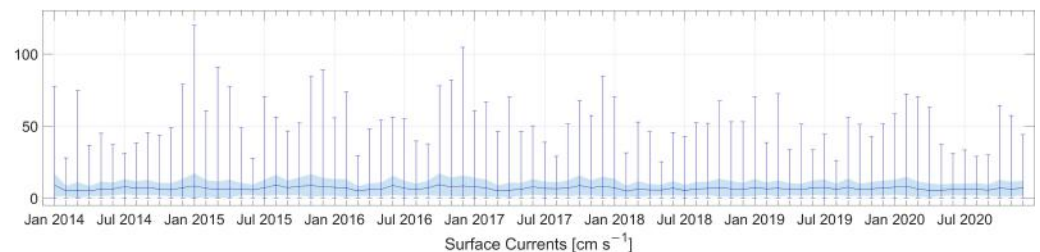


Figure 19. Average monthly currents velocity on the sea surface for the entire model domain. Error bars represent extreme values. The shaded area represents standard deviation.

Inside the domain, a characteristic area can be distinguished in which the strongest currents exceeding $20 \text{ cm}\cdot\text{s}^{-1}$ were modeled. It is a coastal strip stretching along the entire Hel Peninsula from the open sea (Figure 20).

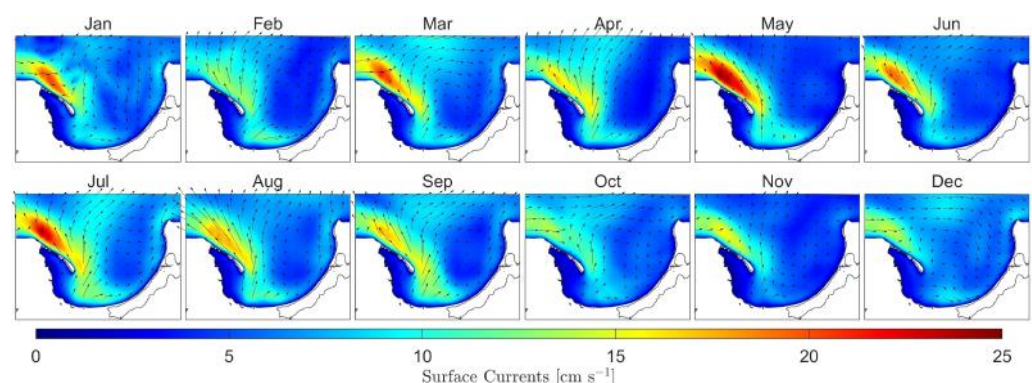


Figure 20. Average monthly currents in the surface layer in 2014–2020.

This is also an area of frequent coastal upwelling, which causes cold water masses to rise from the bottom to the surface. The process responsible for this phenomenon is the Ekman transport, associated with the persistence of the southeastern wind running along the Hel Peninsula. For example, the August 2015 current map (Figure A8) shows a strong northwesterly current along the peninsula due to winds blowing in August, resulting in upwelling. The surface temperature map from 25 August 2015 (Figure 21) shows a large horizontal gradient. Gradients observed in this region are often reaching up to $5\text{ }^{\circ}\text{C}\cdot\text{km}^{-1}$ [29].

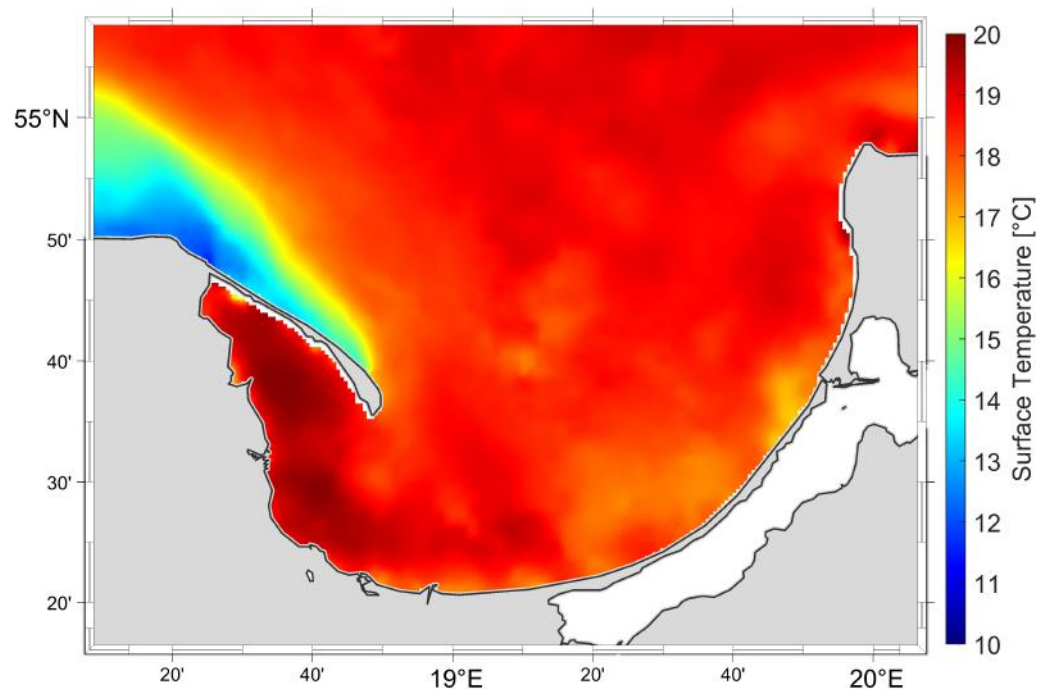


Figure 21. Surface temperature on 25 August 2015 with visible upwelling.

Temperature has a direct effect on the density of water, and the density becomes lower as the temperature increases. As the result of such modification, the same wind stress gives stronger currents because of the second law of dynamics, which is presented as the difference between assimilated and nonassimilated sea currents (Figure 22). Consequently, bigger sea currents increase water circulation in the coastal areas of Gulf of Gdansk.

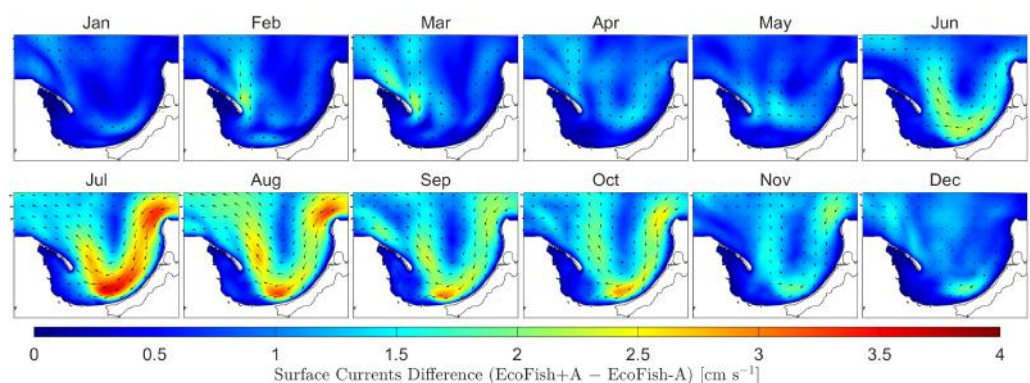


Figure 22. Average monthly currents differences for the surface layer in 2014–2020 between two versions of the model: with and without SST assimilation enabled.

Images of current roses in the surface layer for selected three characteristic regions within the domain (Figure 2) are presented below.

The VR region (Vistula River) covers the coastal and shallow, southern part of the Gulf of Gdansk within the mouth of the Vistula River. Monthly averages of surface currents in

this area rarely exceed $16 \text{ cm}\cdot\text{s}^{-1}$ (Figure 23). In this region, eastern currents constitute the dominant part of directions. In the months from December to April, they have 39% and a greater share of all directions. Such current direction causes that the water flowing out of the Vistula has a difficult outflow and is distributed to the east along the shore of the Gulf. The long-term presence of such currents limits the spread of river waters and reduces the zone of fresh and sea water mixing.

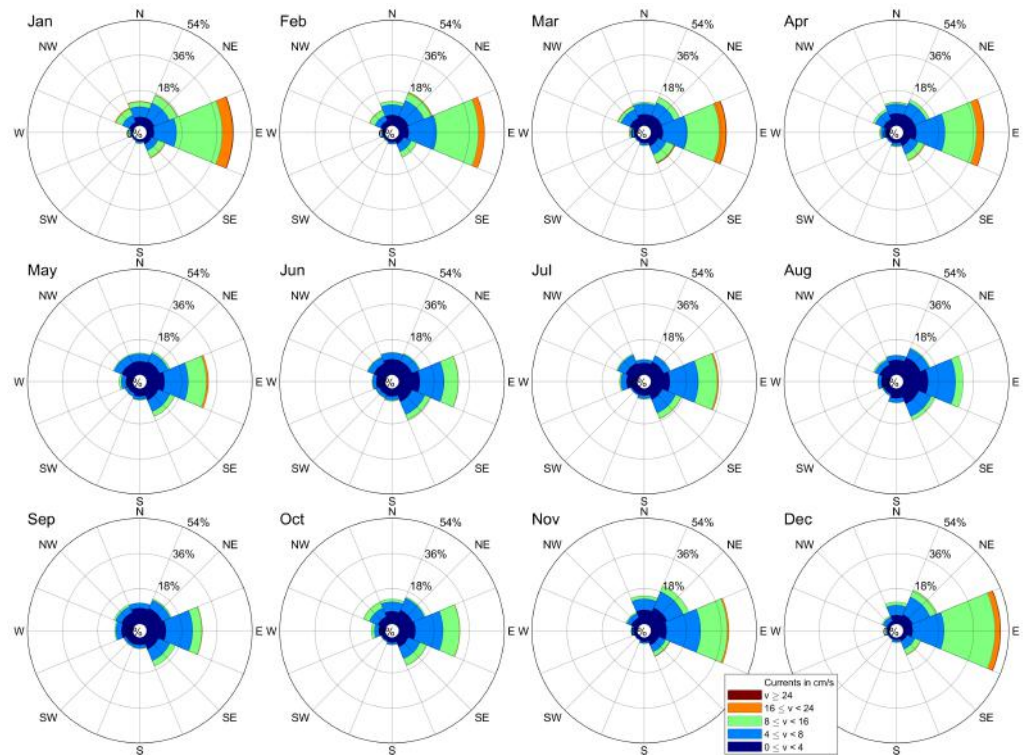


Figure 23. Rose of sea currents in the surface layer for the VR region (Vistula River)—monthly averages.

In the GD region (Gdańsk Deep), which covers the deepwater area of the domain, located directly above the Gdańsk Deep, both the distribution of average velocities and directions is much more homogeneous than in the case of other regions (Figure 24). This is due to the high variability of wind directions and velocities over this area. Moreover, due to the great depths occurring here, the bathymetry does not have such a strong influence on the distribution of currents as in the case of areas close to the coast. From November to February, statistically more often there are currents heading in the eastern, northeastern and southeastern directions (about 60% of cases), but in the remaining months, the situation is less diversified. For example, in the summer months (from June to September), the southeast, south and southwest are dominant directions. They account for 48.6% in June, 57% in July, 58.3% in August, and 53.6% in September. In this region, the average monthly current speeds are comparable to those obtained for the VR region. Currents with speeds in the range $4\text{--}16 \text{ cm}\cdot\text{s}^{-1}$ often constitute even 60–70% of all velocities here. Moreover, in each month, a small share of current velocities exceeding $16 \text{ cm}\cdot\text{s}^{-1}$, and sometimes even $24 \text{ cm}\cdot\text{s}^{-1}$, can be found.

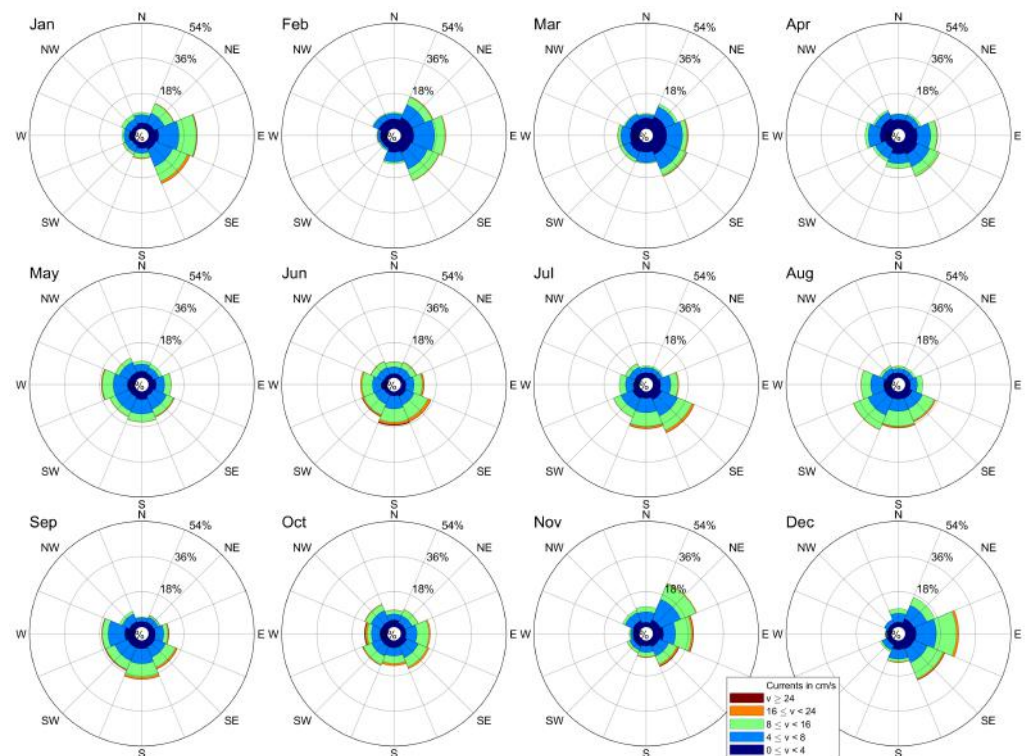


Figure 24. Rose of sea currents in the surface layer for the GD region (Gdańsk Deep)–monthly averages.

In the model results for HP (Hel Peninsula) region, we observe the highest average monthly current velocities in the entire domain (Figure 25). Average values exceeding $24 \text{ cm}\cdot\text{s}^{-1}$ appear here every month and constitute from 3 to 22% of all speed ranges. The directions of surface currents are specific in this region. In each month, the dominant directions are northwest (prevailing in the warm months, from May to November) and southeast (in other months). Together, they constitute over 60% of all currents in each month. Such structure of surface currents enables rapid movement of water masses along the Hel Peninsula, mixing together the Gulf of Gdańsk and Baltic Proper waters. The surface current distribution in the vicinity of Hel Peninsula is mostly induced by dominating westerly winds [30], but also depends on the large-scale internal water cycle in the Baltic Sea [31].

The current velocities in the bottom layer along the VR and HP regions rarely exceed $4 \text{ cm}\cdot\text{s}^{-1}$. Only in GD they have a higher share of over 10%, especially from October to February. The rose of currents for the Gdańsk Deep indicates the existence of a dominant northern bottom current (Figure 26). This suggests that the waters at the bottom are most often pushed toward the Gotland Basin. On the monthly average maps (Figure A9), from December to March, however, the dominance of the southern current can be observed. It moves the water masses in the shallow-water direction of the southern part of the Gulf of Gdańsk.

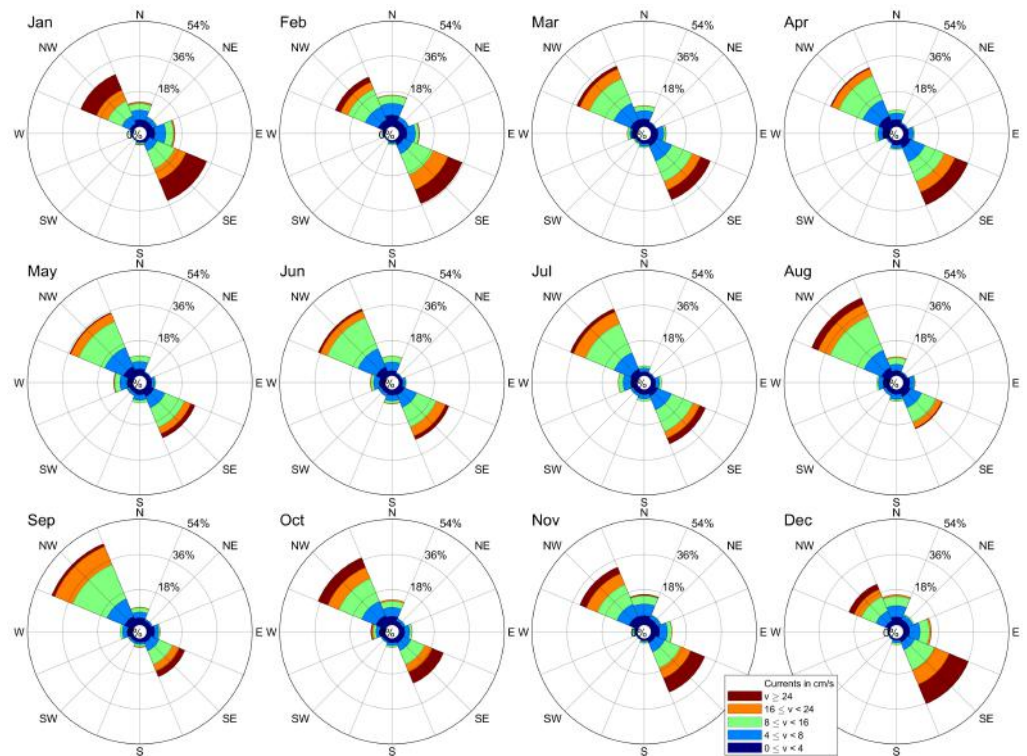


Figure 25. Rose of sea currents in the surface layer for the HP region (Hel Peninsula)—monthly averages.

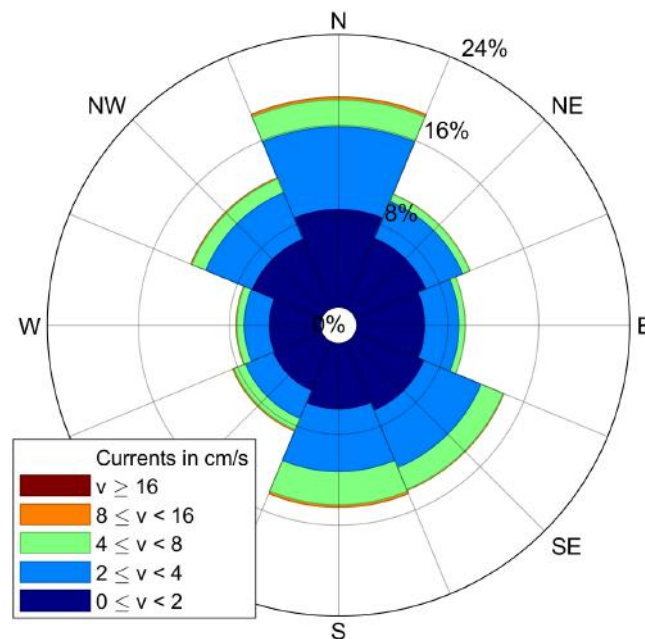


Figure 26. Rose of sea currents in the bottom layer of the Gdańsk Deep—annual average.

5. Discussion

This paper presents the hydrodynamic part of the three-dimensional numerical model EcoFish. The model has been used to simulate the hydrodynamics of the Gulf of Gdańsk. EcoFish has a satellite data assimilation module for SST, which uses data from the SatBałtyk project database, consisting of photos from a medium-resolution imaging spectroradiometer (MODIS AQUA) and an advanced ultrahigh-resolution radiometer (AVHRR). The task of this module is to assimilate the available surface temperature satellite data into the model domain in order to improve the simulation results, allowing for better determination of the dynamics of changes in physical parameters. The EcoFish model covers the South

Baltic Sea and, more precisely, the entire Gulf of Gdańsk together with the Bay of Puck. The model domain is connected via an open boundary with the Baltic Sea from the west and the north.

The article presents statistical validation of the EcoFish model, which allowed to verify the correctness of the results obtained from it in terms of seasonal and spatial variability of the simulated water temperature and salinity. For this purpose, the available in situ observations from the ICES databases were used, along with the database created during fishing cruises carried out under the tasks of the FindFish Knowledge Transfer Platform. For the entire analyzed simulation period from January 2014 to December 2020, basic statistical values were determined, such as root mean square errors (RMSE), standard deviations (STD), and Pearson correlation coefficients (Section 4.1).

The validation showed that the EcoFish model results for water temperature were consistent with in situ observations. To confirm this, two experimental databases were used. Almost 18,000 measurements were available in the ICES database, distributed relatively evenly throughout the domain, except for the shallow region along the coast where no monitoring was carried out, or at least data from this region were not publicly available (Figure 2). The correlation of the EcoFish model with these data (ICES) was 0.94 with the root mean square error (RMSE) of 1.33 °C. As a result of comparing the modeled temperature against the data from the database created during fishing cruises, a correlation coefficient of 0.87 were calculated. This is a satisfactory result, taking the strong concentration of cruise data in the belt from the mouth of the Vistula River in the northwest direction into account. Thus, the data come both from the area where there is mixing of river waters (from the Vistula River) with the waters of the Gulf and from the area where the strongest currents occur in the entire domain (the belt along the Hel Peninsula). It should also be noted that most of these data came from fishing depths, i.e., 30 to 60 m, where the impact of SST satellite data assimilation is no longer visible.

The correlation of the model results for salinity with the ICES data at the level of 0.94 and the low root mean square error of 0.8 PSU suggest that the model copes well with the transport of water masses. It also proves that the rivers in the model have been correctly implemented and that the outgoing freshwater is correctly mixed with the saltwater of the Gulf and distributed by currents in its area. Additionally, when analyzing the vertical profile (Figure 8), both the isohaline layer and the formation of a halocline at lower depth levels can be seen, which proves that the model correctly reflects the dynamics of salinity changes in the water column.

When analyzing the seven-year simulation period of the EcoFish model (from January 2014 to December 2020), it can be observed that the temperature of the Gulf of Gdańsk waters is subject to strong seasonal changes and depends mainly on changes in air temperature and solar radiation. They are also largely influenced by convection processes and wind-induced mixing. The changes in the water temperature of the Gulf also show the influence of the Vistula River, whose waters increase the temperature in the Gulf in spring and summer and lower it in autumn. The lowest values of surface water temperature occur in January and remain at the level of about 0.1 °C (Table A2). On the other hand, the lowest average values of surface water temperature in the entire domain occur in February (Table A1). During this month, the surface waters of the entire reservoir are characterized by a similar temperature, and the differences do not exceed 2.5 °C. In the following months, the temperature of surface waters increases (the fastest in the coastal zone). The highest spatial differentiation is observed in the model results for May and June (differences amounting to about 7 °C). The highest average surface water temperatures occur in August (Table A1).

The location of the Gulf of Gdańsk and its specific bottom topography favor the occurrence of salinity diversification. Significant differences in its distribution occur between the shallow coastal area and the deeper part of the Gulf, which resembles the waters with a layered structure typical of the Baltic Sea (with the presence of a halocline and a thermocline). The shallow-water coastal zone of the Gulf of Gdańsk is influenced by fresh

waters entering it from rivers and other types of surface runoff. The Vistula River has the greatest impact on changes in salinity, with huge volumes of fresh water flowing out (average flow exceeding $1000 \text{ m}^3/\text{s}$), causing local salinity drops below 7 PSU. Its influence is also noticeable in the surface layer of the deep-water part of the Gulf of Gdańsk, mainly in the spring season, when, due to currents, river waters mix with sea waters and are carried into the Gulf.

When analyzing the distribution of currents in the studied domain, a characteristic area can be distinguished, stretching along the Hel Peninsula. The strongest surface currents occur there, often exceeding $20 \text{ cm}\cdot\text{s}^{-1}$. Two directions dominate there, depending on the season. Northwestern currents are mainly observed in the model results for the summer months, pushing the water from the Gdańsk Basin toward the open sea and are accompanied by the formation of coastal upwelling and downwelling. In the remaining months, southeastern currents predominate in this region, carrying waters toward the inner Gulf of Gdańsk. The distribution of surface currents around the mouth of the Vistula is also peculiar, where the most common is the eastern current, which distributes the waters flowing out of the Vistula along the shore of the Gulf. Its long-term presence limits the spread of the Vistula waters and reduces the zone of mixing fresh water with sea water. HP and VR regions are two specific regions along the Polish coastline where coastal up- and downwelling events occur. This is induced by several factors, which the most important are the dominating westerly winds [30], bathymetry and vicinity of the coastal formation. In the HP region, in addition, the large-scale circulation of the Baltic Sea with the surface current pushing waters along the Hel Peninsula into the Gulf of Gdańsk [31] is responsible for the currents distribution.

The factor that has the greatest impact on changes in the sea surface height is wind. Certain areas can be distinguished with the greatest variation in the SSH. These are coastal areas, in particular around the Hel Peninsula, the southern coast stretching from the Bay of Puck, along the Vistula Spit, as well as the eastern shore of the Gulf of Gdańsk (Figures A5 and A6).

6. Conclusions

In this paper, we present a numerical model of the Gulf of Gdańsk EcoFish model with an active module of satellite data assimilation for surface temperature. This version of the EcoFish model is being developed and used within the framework of the project “FindFish Knowledge Transfer Platform—Numerical Forecasting System for the Marine Environment of the Gulf of Gdańsk for Fisheries”. EcoFish is the basic element of the platform that provides fishermen and scientists with the current and forecast hydrodynamic, chemical, and biological conditions of the Gulf of Gdańsk. It also produces forecasts determining the most favorable environmental conditions for the occurrence of industrial pelagic fish in the South Baltic region. The aim of this research and development project is to increase the intensity of knowledge transfer and the use of scientific potential by fishermen, and consequently contribute to the sustainable development of sea fisheries and increase the protection of the Gulf of Gdańsk ecosystem.

To verify the correctness of the EcoFish model, a statistical analysis was carried out by comparing the model results with the in situ observations for the simulation period from January 2014 to December 2020. Satisfactory results were obtained and the compliance of the model results for water temperature and salinity with the available observations was confirmed. Correct mapping of the physical conditions inside the domain allows the model to be used for further simulations with an active part of the ecosystem. To do this, it is required to have a model that correctly simulates the physical conditions of mixing in a water body and heat exchange, controlling the heating and cooling of water masses. This is of great importance for the simulation of biochemical factors and the primary production process that will be conducted by the biochemical part of the EcoFish model.

The decision to validate the model for water temperature and salinity resulted from the fact that these two parameters serve as input data for the Fish Module, in which the

Habitat Suitability Index maps are determined based on the environmental preferences of fish. The final product of the project will be sharing the FindFish platform as a website that will provide all the results and forecasts in operational mode.

Author Contributions: Conceptualization, M.J. and L.D.-G.; methodology, M.J., D.D., J.J. and L.D.-G.; software, M.J. and A.N.; validation, M.J.; formal analysis, M.J. and L.D.-G.; investigation, M.J. and D.D.; resources, M.J. and D.D.; data curation, M.J., D.D. and A.N.; writing—original draft preparation, M.J. and L.D.-G.; writing—review and editing, M.J. and L.D.-G.; visualization, M.J. and D.D.; supervision, L.D.-G.; project administration, L.D.-G.; funding acquisition, L.D.-G. All authors have read and agreed to the published version of the manuscript.

Funding: Partial support for this study was provided by the project “Knowledge transfer platform FindFish—Numerical Forecasting System for the Marine Environment of the Gulf of Gdańsk for Fisheries”, funded by the European Union through European Regional Development Fund contract No. RPPM.01.01.01-22-0025/16-00.

Institutional Review Board Statement: Not applicable.

Informed Consent Statement: Not applicable.

Data Availability Statement: Publicly available datasets were analyzed in this study. This data (ICES database) can be found here: <https://ocean.ices.dk/HydChem/>, accessed on 1 February 2021. All of the model results and MIDAS CTD database presented in this study are available on request from the corresponding author. The data are not yet publicly available due to the FindFish project being still work in progress. Some of the additional model results (monthly means) presented in this study are available in Appendix A in forms of maps and tables.

Acknowledgments: Calculations were carried out at the Academic Computer Centre in Gdańsk. We are grateful to the anonymous reviewers for valuable comments on earlier versions of the manuscript.

Conflicts of Interest: The authors declare no conflict of interest.

Abbreviations

The following abbreviations are used in this manuscript:

ICES	International Council for the Exploration of the Sea
VR	Vistula River
HP	Hel Peninsula
GD	Gdańsk Deep
SST	Sea Surface Temperature
SSH	Sea Surface Height
CESM	Community Earth System Model

Appendix A

In the main part of the article, there are only figures presenting the monthly averages and averaged statistical values of validation. Detailed maps for separate months, years, and statistics have been moved to the Appendix section.

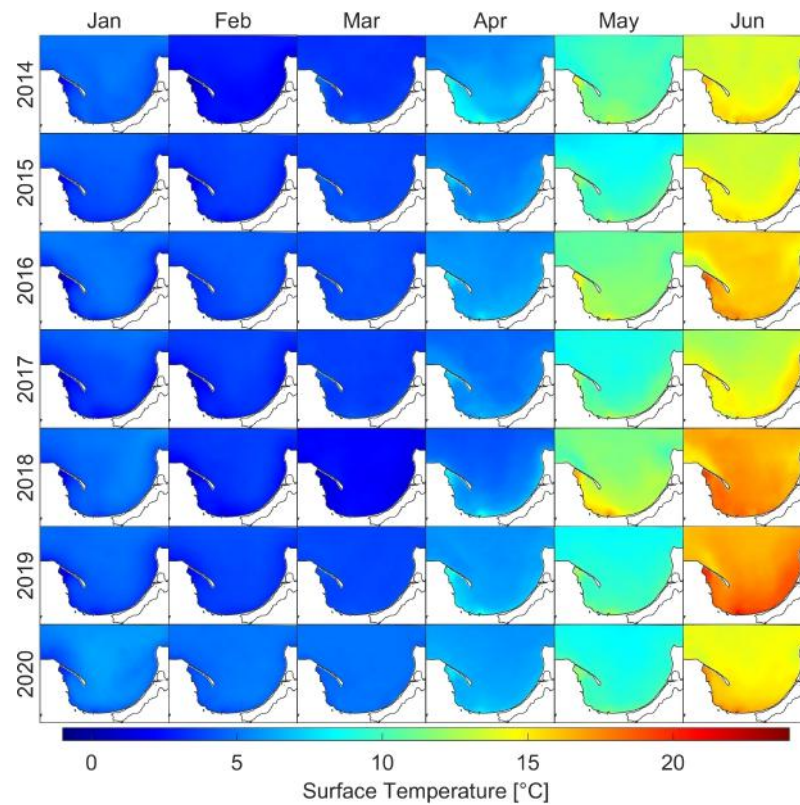
Appendix A.1. Surface Temperature

Figure A1. Monthly means for surface temperature from January to June for the years 2014–2020.

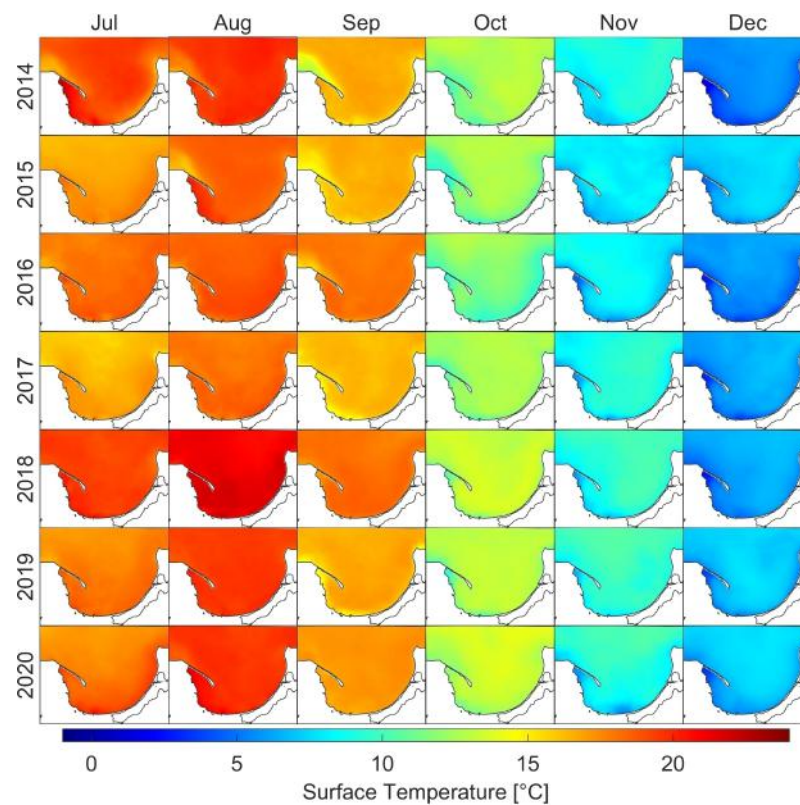


Figure A2. Monthly means for surface temperature from July to December for the years 2014–2020.

Table A1. Monthly means for surface temperature for the years 2014–2020.

Year\Month	January	February	March	April	May	June	July	August	September	October	November	December
2014	4.62	2.48	3.43	6.17	10.36	14.02	19.02	19.56	16.39	12.44	8.77	5.33
2015	4.09	3.48	3.92	5.28	9.11	13.84	16.94	18.52	16.36	12.13	7.85	7.22
2016	4.48	4.08	4.02	5.90	11.34	15.69	18.16	18.67	17.88	11.34	8.02	5.62
2017	3.85	3.34	3.61	5.12	9.52	13.58	16.46	18.12	16.21	12.42	8.94	6.16
2018	4.71	3.17	2.05	4.98	12.08	16.86	19.32	21.23	18.13	13.29	9.45	6.17
2019	4.28	3.66	3.84	6.10	9.20	17.28	17.74	19.47	16.58	12.92	9.70	7.05
2020	5.45	4.85	4.90	6.19	9.11	14.77	17.89	19.68	17.18	13.30	9.13	7.13
mean	4.50	3.58	3.68	5.68	10.10	15.15	17.93	19.32	16.96	12.55	8.84	6.38

Table A2. Monthly minimums for surface temperature for the years 2014–2020.

Year\Month	January	February	March	April	May	June	July	August	September	October	November	December
2014	−0.43	−0.43	0.60	1.33	3.28	3.94	9.81	10.81	2.24	2.48	1.29	0.38
2015	0.38	0.14	0.67	1.13	3.77	2.91	7.94	7.62	7.94	2.78	0.89	1.17
2016	−0.40	0.66	0.82	1.54	4.37	2.37	3.17	6.19	8.04	4.18	1.10	0.83
2017	0.05	−0.19	0.46	1.30	2.79	1.82	3.83	10.48	3.41	2.60	2.29	0.64
2018	0.17	−0.38	−0.41	0.74	3.81	5.07	6.39	8.85	7.14	4.49	1.06	0.88
2019	−0.20	0.22	1.30	2.47	2.05	9.74	8.40	13.60	3.70	3.53	2.86	1.27
2020	0.78	1.48	0.81	2.26	4.55	8.09	9.80	13.86	11.22	3.75	1.12	1.33
mean	0.05	0.21	0.60	1.54	3.52	4.85	7.05	10.20	6.24	3.40	1.52	0.93

Table A3. Monthly maximums for surface temperature for the years 2014–2020.

Year\Month	January	February	March	April	May	June	July	August	September	October	November	December
2014	6.75	6.44	9.42	16.51	20.22	21.08	28.45	26.47	23.56	15.56	11.78	7.73
2015	5.46	5.12	10.47	18.06	20.32	21.15	23.96	24.50	21.87	16.71	11.50	8.85
2016	7.42	6.71	11.78	14.77	20.19	24.40	24.23	22.58	20.85	17.05	10.60	8.50
2017	6.23	4.83	8.84	10.54	20.79	21.35	22.15	23.60	23.60	15.78	11.84	8.76
2018	6.87	4.71	9.13	16.41	23.02	22.86	27.26	26.69	22.32	16.65	11.92	8.29
2019	5.95	4.73	7.88	15.25	18.93	25.85	25.48	24.43	23.35	15.29	12.48	9.65
2020	6.95	5.84	7.54	15.04	17.19	25.16	28.31	26.66	20.53	18.24	12.45	9.46
mean	6.52	5.48	9.29	15.22	20.09	23.12	25.69	24.99	22.30	16.47	11.80	8.75

Table A4. Monthly standard deviations for surface temperature for the years 2014–2020.

Year\Month	January	February	March	April	May	June	July	August	September	October	November	December
2014	1.41	0.50	0.81	2.01	2.89	1.94	2.35	2.11	1.58	1.52	1.42	0.98
2015	0.59	0.50	0.53	1.26	1.74	1.65	1.22	1.55	1.26	2.24	1.65	0.75
2016	1.14	0.45	0.55	0.97	2.18	2.27	1.65	0.98	1.34	2.58	1.02	1.29
2017	1.10	0.64	0.63	0.79	3.04	1.69	1.43	0.72	1.03	1.49	1.16	1.06
2018	0.79	0.82	0.49	1.83	3.11	1.53	2.71	1.76	1.50	1.47	1.65	0.94
2019	0.84	0.48	0.36	1.50	1.90	2.36	1.42	0.84	2.12	1.08	1.16	0.85
2020	0.79	0.42	0.34	1.02	1.22	2.99	1.03	1.21	0.80	1.72	1.58	1.08
mean	0.95	0.54	0.53	1.34	2.30	2.06	1.69	1.31	1.37	1.73	1.38	0.99

Appendix A.2. Bottom Temperature

Table A5. Monthly means for bottom temperature for the years 2014–2020.

Year\Month	January	February	March	April	May	June	July	August	September	October	November	December
2014	4.90	4.19	4.41	4.76	5.26	6.26	6.39	7.21	6.81	6.51	6.06	5.39
2015	4.78	4.52	4.68	5.10	6.04	7.08	7.99	7.34	6.95	6.55	6.31	6.13
2016	5.21	4.88	4.92	5.42	6.17	6.60	7.82	8.29	7.68	6.58	6.54	5.82
2017	5.08	4.95	4.93	5.38	5.84	7.47	7.78	7.71	7.62	7.26	6.50	5.49
2018	4.92	4.42	4.26	4.78	5.35	6.09	7.05	7.57	7.50	7.13	5.77	5.23
2019	4.72	4.69	4.79	5.22	5.93	6.64	8.31	7.66	8.01	7.42	6.37	5.72
2020	5.15	4.99	5.01	5.37	6.17	6.65	8.13	7.90	8.16	7.08	6.53	6.08
mean	4.97	4.66	4.71	5.15	5.82	6.68	7.64	7.67	7.53	6.93	6.30	5.69

Table A6. Monthly standard deviations for bottom temperature for the years 2014–2020.

Year\Month	January	February	March	April	May	June	July	August	September	October	November	December
2014	0.94	1.27	0.81	0.84	1.77	3.44	4.09	5.08	3.98	2.73	1.50	0.76
2015	0.87	1.01	0.75	0.68	1.80	3.32	4.63	4.38	3.55	2.46	1.30	0.78
2016	1.15	0.84	0.78	0.65	1.80	2.90	4.47	5.10	4.65	2.40	1.10	0.95
2017	1.41	1.44	1.22	0.69	1.61	3.51	4.13	4.51	4.15	2.98	1.71	0.87
2018	0.63	0.96	1.22	0.93	1.98	3.67	5.03	6.06	5.40	3.96	2.15	0.85
2019	0.86	1.02	0.82	0.75	1.45	3.21	4.82	4.57	4.37	3.22	1.85	0.82
2020	0.54	0.35	0.28	0.64	1.77	2.87	5.00	4.94	4.66	2.78	1.43	0.79
mean	0.91	0.98	0.84	0.74	1.74	3.27	4.59	4.95	4.39	2.93	1.58	0.83

Table A7. Monthly minimums for bottom temperature for the years 2014–2020.

Year\Month	January	February	March	April	May	June	July	August	September	October	November	December
2014	−0.43	−0.43	0.99	2.26	3.53	3.77	3.88	4.05	4.24	4.35	1.84	0.47
2015	0.80	0.41	1.22	1.87	4.37	4.37	4.43	4.47	4.62	3.08	1.51	1.77
2016	−0.40	1.44	1.62	2.68	4.35	4.30	4.05	4.45	4.65	4.74	1.98	1.12
2017	0.27	−0.05	0.94	2.38	3.39	4.56	4.27	4.38	3.99	3.73	2.99	0.92
2018	0.33	−0.24	−0.40	1.03	3.42	3.49	3.52	3.70	3.86	3.98	1.92	1.24
2019	0.03	0.25	1.98	2.84	3.06	4.56	4.51	4.51	4.89	4.82	3.52	2.28
2020	1.24	1.76	2.07	3.17	4.81	4.76	4.83	4.89	4.86	4.49	2.40	2.30
mean	0.26	0.45	1.20	2.32	3.85	4.26	4.21	4.35	4.44	4.17	2.31	1.44

Table A8. Monthly maximums for bottom temperature for the years 2014–2020.

Year\Month	January	February	March	April	May	June	July	August	September	October	November	December
2014	7.19	5.86	7.41	12.37	18.76	19.77	25.34	24.42	18.87	14.89	11.43	7.68
2015	6.58	5.68	6.23	10.89	14.08	17.64	20.52	22.49	19.11	15.60	10.82	8.79
2016	7.64	6.38	6.74	9.61	16.64	21.21	21.84	21.04	20.03	16.70	10.41	8.15
2017	6.60	6.49	6.88	8.48	17.38	18.80	19.87	20.31	19.14	15.30	11.05	8.98
2018	6.47	5.63	6.07	11.31	19.19	21.40	24.05	25.44	19.91	16.78	11.57	8.27
2019	7.13	6.79	6.80	12.44	14.78	22.47	21.71	21.74	22.23	15.13	12.00	8.72
2020	7.00	6.02	6.21	10.62	14.20	22.29	22.17	22.65	20.55	16.63	11.90	9.12
mean	6.94	6.12	6.62	10.82	16.43	20.51	22.21	22.58	19.98	15.86	11.31	8.53

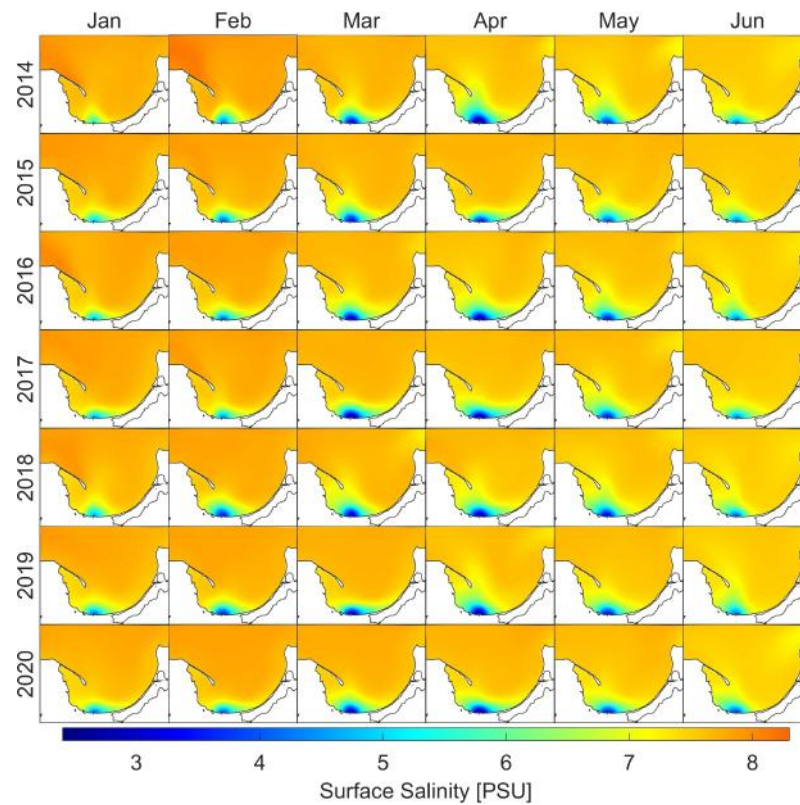
Appendix A.3. Surface Salinity

Figure A3. Monthly means for surface salinity from January to June for the years 2014–2020.

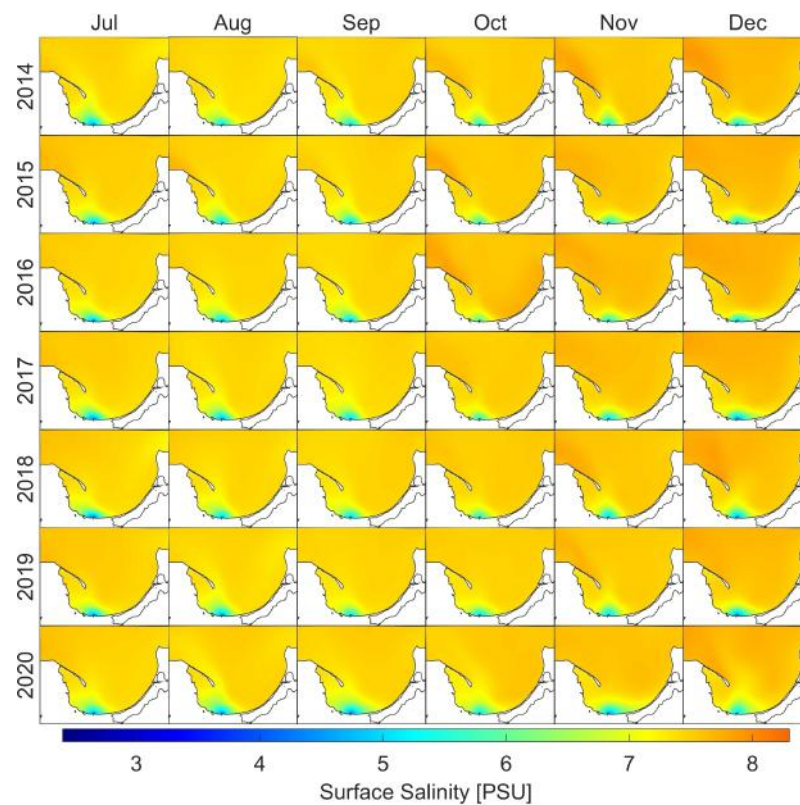


Figure A4. Monthly means for surface salinity from July to December for the years 2014–2020.

Table A9. Monthly means for surface salinity for the years 2014–2020.

Year\Month	January	February	March	April	May	June	July	August	September	October	November	December
2014	7.71	7.76	7.52	7.31	7.36	7.40	7.35	7.35	7.40	7.46	7.51	7.59
2015	7.67	7.65	7.50	7.52	7.47	7.46	7.43	7.39	7.39	7.50	7.54	7.58
2016	7.67	7.66	7.45	7.35	7.40	7.37	7.40	7.38	7.38	7.57	7.58	7.61
2017	7.67	7.66	7.49	7.40	7.40	7.45	7.41	7.35	7.35	7.47	7.54	7.56
2018	7.63	7.60	7.45	7.39	7.35	7.37	7.38	7.38	7.39	7.47	7.50	7.55
2019	7.61	7.61	7.54	7.35	7.42	7.37	7.44	7.35	7.40	7.42	7.47	7.55
2020	7.59	7.65	7.52	7.46	7.44	7.33	7.40	7.36	7.35	7.43	7.47	7.53
mean	7.65	7.66	7.50	7.40	7.40	7.39	7.40	7.37	7.38	7.48	7.51	7.57

Table A10. Monthly minimums for surface salinity for the years 2014–2020.

Year\Month	January	February	March	April	May	June	July	August	September	October	November	December
2014	4.25	3.08	1.51	1.67	2.74	3.71	4.09	4.47	4.44	4.73	4.79	4.15
2015	3.27	2.73	1.99	2.40	3.13	3.92	3.96	4.37	4.24	4.92	4.70	4.00
2016	3.67	3.07	2.10	1.64	2.63	3.54	4.15	4.43	4.12	4.98	4.53	3.88
2017	3.50	2.92	1.92	1.72	2.81	3.85	4.03	4.01	4.23	4.97	4.62	3.50
2018	3.57	2.70	1.93	2.13	2.62	3.38	3.85	4.09	4.28	4.83	4.03	3.74
2019	3.64	2.59	1.89	1.72	2.55	3.57	4.13	4.27	4.60	4.55	4.46	3.01
2020	3.48	3.05	1.78	2.08	2.52	3.33	4.24	4.09	4.23	4.61	4.11	3.81
mean	3.62	2.88	1.87	1.91	2.72	3.61	4.06	4.25	4.31	4.80	4.46	3.73

Table A11. Monthly maximums for surface salinity for the years 2014–2020.

Year\Month	January	February	March	April	May	June	July	August	September	October	November	December
2014	8.65	8.70	7.98	7.77	7.75	7.67	7.66	7.55	7.70	7.81	8.15	8.15
2015	8.06	8.26	7.96	7.81	7.76	7.67	7.72	7.95	7.71	8.33	7.90	7.96
2016	8.32	8.02	7.85	7.76	7.75	7.73	7.63	7.56	7.71	8.56	7.86	7.91
2017	8.32	8.18	7.88	7.77	7.78	7.71	7.71	7.53	7.74	7.98	7.80	7.91
2018	8.70	7.95	8.00	7.89	7.75	7.63	7.62	7.62	7.68	7.77	8.65	8.66
2019	7.96	7.88	7.87	7.82	7.75	7.65	7.72	7.56	7.61	7.61	8.23	7.95
2020	7.89	7.93	7.99	7.81	7.78	7.66	7.68	7.67	7.58	7.78	7.74	8.16
mean	8.27	8.13	7.93	7.80	7.76	7.67	7.68	7.63	7.68	7.98	8.05	8.10

Table A12. Monthly standard deviations for surface salinity for the years 2014–2020.

Year\Month	January	February	March	April	May	June	July	August	September	October	November	December
2014	0.29	0.46	0.57	0.70	0.50	0.35	0.32	0.24	0.25	0.22	0.25	0.29
2015	0.36	0.45	0.57	0.49	0.46	0.37	0.30	0.26	0.27	0.22	0.24	0.30
2016	0.35	0.44	0.60	0.64	0.53	0.37	0.28	0.26	0.27	0.22	0.24	0.29
2017	0.37	0.40	0.65	0.65	0.54	0.37	0.32	0.28	0.26	0.20	0.27	0.35
2018	0.39	0.56	0.62	0.64	0.57	0.39	0.32	0.26	0.26	0.21	0.29	0.35
2019	0.42	0.50	0.55	0.64	0.53	0.40	0.29	0.29	0.23	0.24	0.28	0.34
2020	0.40	0.43	0.62	0.63	0.52	0.43	0.30	0.33	0.37	0.30	0.35	0.35
mean	0.37	0.47	0.60	0.63	0.52	0.38	0.30	0.28	0.27	0.23	0.27	0.32

Appendix A.4. Bottom Salinity

Table A13. Monthly means for bottom salinity for the years 2014–2020.

Year\Month	January	February	March	April	May	June	July	August	September	October	November	December
2014	9.46	9.72	9.47	9.64	9.70	9.55	9.63	9.55	9.61	9.62	9.67	9.57
2015	9.24	9.45	9.53	9.39	9.58	9.58	9.52	9.64	9.63	9.63	9.39	9.40
2016	9.56	9.35	9.49	9.60	9.64	9.63	9.52	9.51	9.63	9.70	9.43	9.24
2017	9.25	9.49	9.36	9.48	9.65	9.50	9.50	9.57	9.54	9.39	9.34	9.38
2018	9.59	9.47	9.60	9.65	9.69	9.60	9.53	9.56	9.55	9.38	9.63	9.60
2019	9.28	9.46	9.31	9.68	9.65	9.64	9.48	9.61	9.48	9.47	9.60	9.51
2020	9.34	9.34	9.35	9.47	9.59	9.61	9.55	9.52	9.50	9.51	9.44	9.48
mean	9.39	9.47	9.44	9.56	9.64	9.59	9.53	9.57	9.56	9.53	9.50	9.45

Table A14. Monthly minimums for bottom salinity for the years 2014–2020.

Year\Month	January	February	March	April	May	June	July	August	September	October	November	December
2014	5.33	5.49	3.82	3.62	4.02	4.71	5.56	5.45	5.32	5.90	6.69	5.16
2015	5.29	4.12	3.87	3.56	4.38	5	5.16	5.69	5.23	5.79	5.80	5.33
2016	5.10	4.73	3.48	3.50	4.61	4.71	5.25	5.24	5.45	5.72	5.37	5.17
2017	4.95	4.87	3.39	3.04	4.18	4.40	4.89	5.52	5.48	5.81	5.56	4.77
2018	4.84	4.13	4.71	3.66	4.06	4.86	5.20	5.59	5.55	5.86	6.19	5.13
2019	4.70	4.13	3.50	4.34	4.07	4.99	5.30	5.59	5.71	5.64	5.83	4.39
2020	4.66	4.89	3.53	3.67	3.91	4.97	5.36	5.05	4.62	5.44	5.21	5.05
mean	4.98	4.62	3.76	3.63	4.18	4.81	5.25	5.45	5.34	5.74	5.81	5.00

Table A15. Monthly maximums for bottom salinity for the years 2014–2020.

Year\Month	January	February	March	April	May	June	July	August	September	October	November	December
2014	12.45	12.52	13.04	12.62	12.71	12.62	12.64	12.67	12.61	12.75	12.45	12.82
2015	12.92	12.54	12.99	12.96	12.84	12.77	12.85	12.59	12.62	12.82	13.19	12.82
2016	12.55	12.71	12.61	12.72	12.73	12.62	12.59	12.61	12.76	12.80	12.50	12.83
2017	12.52	12.54	12.59	12.79	12.82	12.70	12.63	12.74	13.15	12.82	12.42	12.44
2018	12.70	12.39	12.59	12.80	12.75	12.70	12.57	12.85	12.85	12.89	12.43	12.51
2019	12.44	12.48	12.80	12.59	12.68	12.61	12.59	12.60	12.74	12.84	12.48	12.93
2020	12.40	12.58	13.21	12.67	12.75	12.81	12.76	12.58	12.59	12.11	11.91	11.40
mean	12.57	12.54	12.83	12.73	12.76	12.69	12.66	12.66	12.76	12.72	12.48	12.54

Table A16. Monthly standard deviations for bottom salinity for the years 2014–2020.

Year\Month	January	February	March	April	May	June	July	August	September	October	November	December
2014	1.39	1.47	1.59	1.68	1.74	1.74	1.69	1.74	1.66	1.59	1.54	1.62
2015	1.51	1.55	1.57	1.72	1.76	1.75	1.74	1.64	1.67	1.56	1.62	1.60
2016	1.50	1.54	1.60	1.72	1.73	1.68	1.73	1.75	1.68	1.55	1.64	1.61
2017	1.54	1.54	1.61	1.75	1.70	1.75	1.73	1.71	1.71	1.63	1.62	1.63
2018	1.54	1.53	1.51	1.68	1.74	1.74	1.73	1.72	1.70	1.57	1.54	1.59
2019	1.57	1.58	1.64	1.64	1.75	1.72	1.74	1.69	1.70	1.64	1.58	1.62
2020	1.58	1.60	1.56	1.70	1.79	1.72	1.77	1.64	1.60	1.42	1.49	1.33
mean	1.52	1.54	1.58	1.70	1.74	1.73	1.73	1.70	1.67	1.57	1.58	1.57

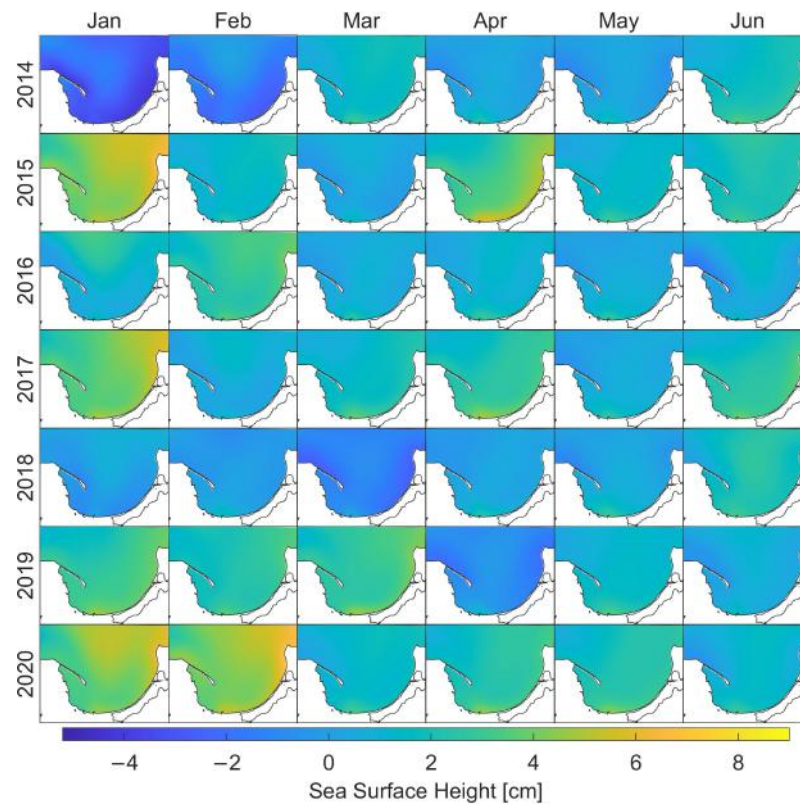
Appendix A.5. Sea Surface Height

Figure A5. Monthly means for sea surface height from January to June for the years 2014–2020.

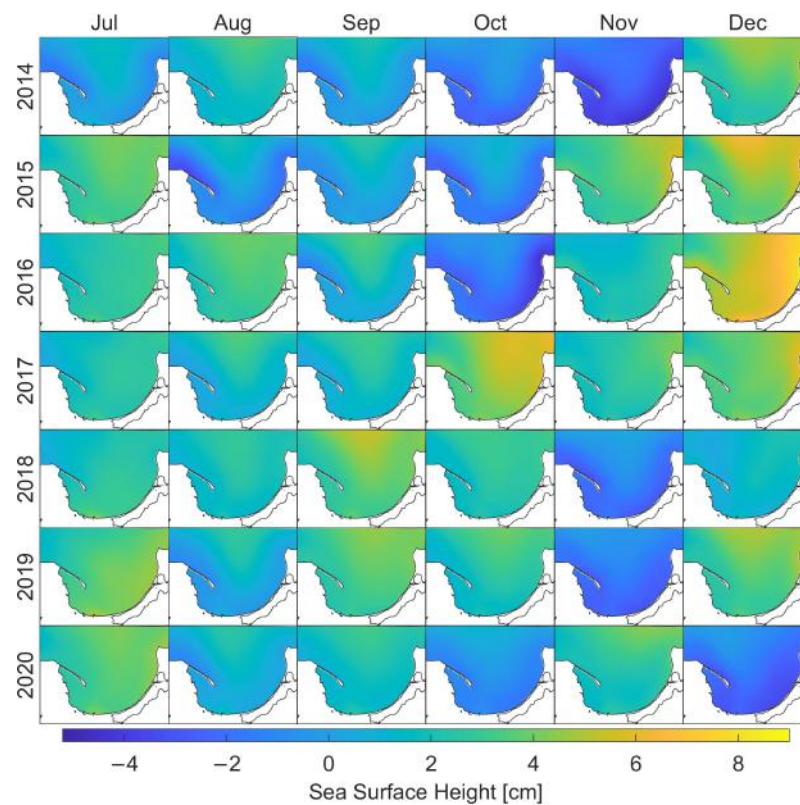


Figure A6. Monthly means for sea surface height from July to December for the years 2014–2020.

Table A17. Monthly means for sea surface height for the years 2014–2020.

Year\Month	January	February	March	April	May	June	July	August	September	October	November	December
2014	−2.58	−1.27	1.46	0.27	0.14	1.69	0.28	1.93	0.47	−1.21	−2.73	3.20
2015	4.59	1.37	0.37	3.26	1.23	2.00	3.25	−0.29	0.58	−0.76	3.57	4.34
2016	1.35	2.67	0.62	0.98	0.53	0.59	2.44	3.00	1.35	−1.81	1.96	5.54
2017	3.86	0.69	1.57	2.39	0.55	2.20	2.11	1.57	1.75	4.49	2.53	3.88
2018	0.09	−0.11	−1.34	0.22	0.40	1.93	2.23	1.95	3.66	2.41	−1.27	1.30
2019	2.79	2.27	2.84	−0.83	1.32	0.59	3.45	0.78	3.34	2.41	−1.56	3.49
2020	4.20	4.55	1.39	2.28	2.14	1.12	3.38	0.92	1.91	−0.48	2.55	−1.82
mean	2.04	1.45	0.99	1.22	0.90	1.44	2.45	1.41	1.87	0.72	0.72	2.85

Table A18. Monthly minimums for sea surface height for the years 2014–2020.

Year\Month	January	February	March	April	May	June	July	August	September	October	November	December
2014	−23.84	−13.86	−14.12	−7.34	−15.87	−4.55	−6.76	−9.82	−7.45	−15.93	−15.70	−13.04
2015	−12.53	−13.46	−21.62	−14.91	−12.23	−8.29	−10.68	−14.11	−7.47	−19.00	−29.58	−19.20
2016	−13.14	−16.97	−7.40	−9.86	−5.65	−8.77	−6.39	−5.45	−8.66	−31.09	−16.76	−23.97
2017	−14.86	−16.38	−8.11	−7.56	−10.31	−12.32	−7.46	−8.61	−12.05	−11.56	−9.23	−16.03
2018	−21.75	−16.80	−22.01	−12.01	−9.55	−6.52	−4.71	−7.78	−6.83	−18.41	−16.05	−13.08
2019	−12.71	−13.03	−15.27	−12.87	−11.73	−8.40	−6.49	−6.89	−13.27	−9.23	−15.90	−21.19
2020	−8.80	−9.19	−22.77	−7.21	−4.12	−15.11	−6.59	−5.57	−8.24	−31.79	−7.82	−16.38
mean	−15.37	−14.24	−15.90	−10.25	−9.92	−9.14	−7.01	−8.32	−9.14	−19.57	−15.86	−17.55

Table A19. Monthly maximums for sea surface height for the years 2014–2020.

Year\Month	January	February	March	April	May	June	July	August	September	October	November	December
2014	45.86	13.67	43.37	13.11	8.38	11.86	7.68	18.14	14.61	14.65	6.26	43.04
2015	77.21	30.20	38.32	43.02	20.88	15.22	24.09	9.21	14.85	21.09	51.51	59.79
2016	31.17	45.59	10.15	17.59	18.70	23.84	17.29	14.55	18.14	24.84	31.78	59.41
2017	33.82	29.94	19.70	27.80	19.65	15.75	17.50	15.95	49.66	42.08	28.32	40.60
2018	34.89	11.46	7.89	25.70	14.86	19.77	10.17	27.11	38.23	32.82	10.03	21.01
2019	32.40	20.54	36.61	7.64	16.73	13.90	21.35	8.73	30.37	27.21	15.10	54.94
2020	34.10	37.47	60.19	25.78	14.99	14.54	21.37	8.79	23.26	22.65	24.96	14.91
mean	41.35	26.98	30.89	22.95	16.31	16.41	17.06	14.64	27.02	26.48	23.99	41.96

Table A20. Monthly standard deviations for sea surface height for the years 2014–2020.

Year\Month	January	February	March	April	May	June	July	August	September	October	November	December
2014	7.61	3.81	5.29	2.35	2.84	2.27	1.90	3.47	2.97	3.34	3.07	6.57
2015	9.46	5.11	4.87	5.81	3.87	2.73	4.63	3.26	3.20	4.67	8.82	8.41
2016	5.94	7.20	2.74	3.83	2.32	3.10	2.77	2.95	2.95	5.52	5.80	7.27
2017	5.56	5.84	4.48	3.66	3.00	4.07	3.09	3.38	5.38	7.14	4.49	6.75
2018	5.73	3.14	4.07	4.71	2.73	2.77	1.80	3.50	5.09	6.18	3.21	4.40
2019	5.46	4.29	6.40	2.99	3.02	2.54	3.39	2.50	5.38	4.75	4.27	7.35
2020	5.36	6.46	6.59	4.48	2.57	3.53	3.73	2.04	3.55	5.07	5.06	4.52
mean	6.45	5.12	4.92	3.97	2.91	3.00	3.04	3.01	4.07	5.24	4.96	6.47

Appendix A.6. Surface Currents

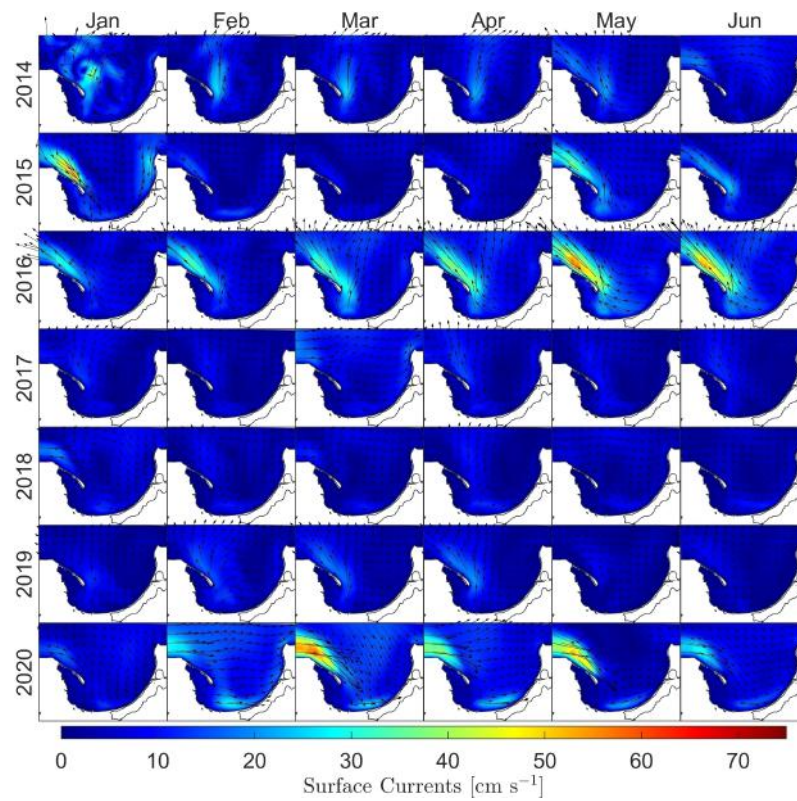


Figure A7. Monthly means for surface currents from January to June for the years 2014–2020.

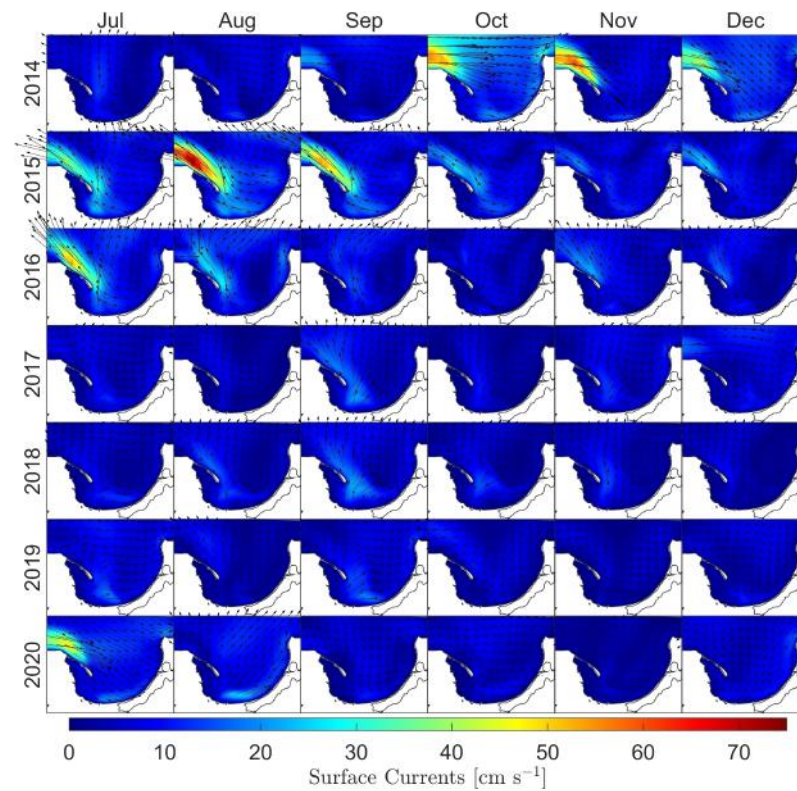


Figure A8. Monthly means for surface currents from July to December for the years 2014–2020.

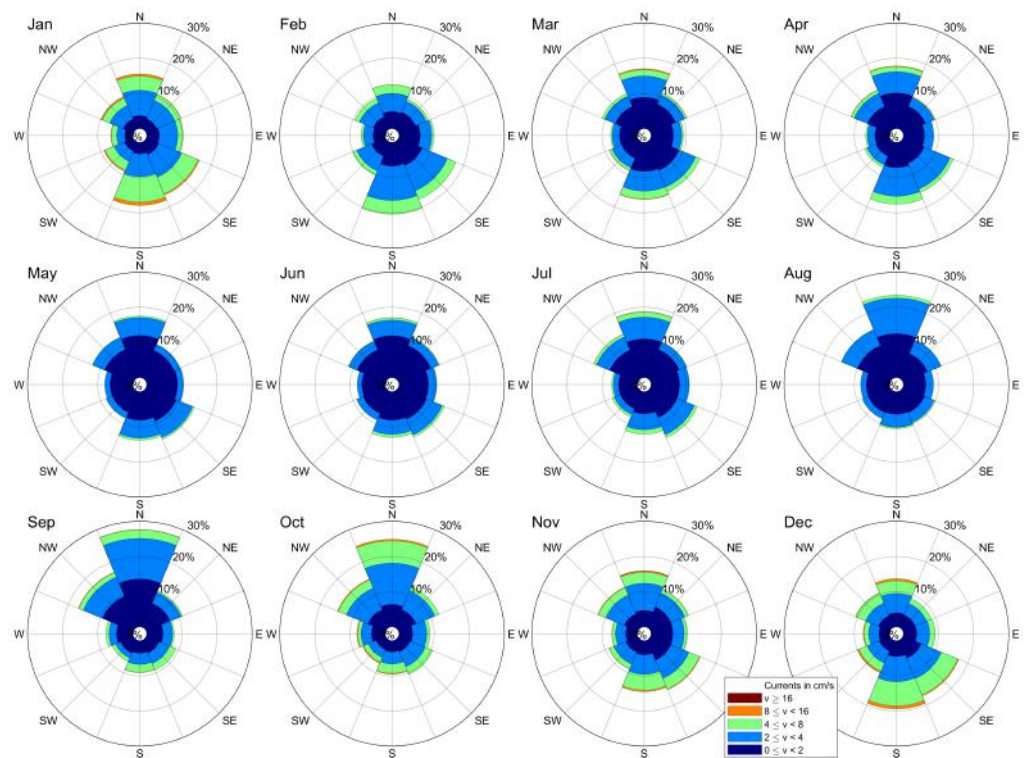


Figure A9. Rose of sea currents in the bottom layer of the Gdańsk Deep—monthly averages.

Table A21. Monthly means for surface currents for the years 2014–2020.

Year\Month	January	February	March	April	May	June	July	August	September	October	November	December
2014	8.98	5.02	5.48	4.94	6.33	6.25	7.88	6.78	7.39	6.18	5.72	7.18
2015	8.43	6.76	5.87	6.56	6.23	5.69	7.10	9.13	7.12	8.18	8.71	7.86
2016	7.41	6.95	4.91	5.97	6.03	8.83	6.76	5.90	6.98	9.31	7.72	8.43
2017	7.84	6.97	4.90	5.58	6.11	7.75	6.65	6.52	6.83	8.78	7.12	8.08
2018	7.18	4.80	6.23	5.66	5.59	6.91	5.34	6.39	6.61	7.32	6.40	5.88
2019	7.41	6.42	6.72	6.14	5.78	7.20	7.40	6.05	7.53	5.82	6.32	7.02
2020	7.52	8.20	6.25	5.34	5.49	5.96	5.88	6.13	5.54	6.82	6.30	6.94
mean	7.82	6.44	5.77	5.74	5.94	6.94	6.72	6.70	6.86	7.49	6.90	7.34

Table A22. Monthly maximums for surface currents for the years 2014–2020.

Year\Month	January	February	March	April	May	June	July	August	September	October	November	December
2014	77.33	27.82	74.57	36.57	44.93	37.04	30.96	38.19	45.39	43.46	48.85	78.88
2015	120.09	60.55	90.82	77.49	48.70	27.68	70.34	56.30	46.57	52.13	84.40	89.04
2016	55.58	73.70	29.52	48.28	53.90	56.06	55.10	39.51	37.75	77.81	81.79	104.45
2017	60.38	66.74	46.19	70.15	46.20	50.08	38.65	28.88	51.69	67.66	57.29	84.60
2018	70.18	31.45	52.83	45.94	25.20	45.54	42.67	52.24	51.98	67.29	52.96	52.90
2019	70.52	38.52	72.50	33.80	51.43	33.49	44.28	26.03	55.87	51.12	42.51	51.77
2020	58.32	72.23	70.19	63.05	37.54	30.77	33.34	28.82	29.95	64.21	57.21	43.93
mean	73.20	53.00	62.37	53.61	43.98	40.10	45.05	38.57	45.60	60.53	60.71	72.22

Table A23. Monthly standard deviations for surface currents for the years 2014–2020.

Year\Month	January	February	March	April	May	June	July	August	September	October	November	December
2014	7.95	3.60	5.60	3.44	4.97	4.43	5.24	4.95	5.31	4.33	4.63	6.12
2015	8.72	5.73	5.66	6.20	4.32	3.60	5.72	6.91	5.07	6.28	7.85	6.20
2016	5.83	6.12	3.47	4.30	4.74	6.60	5.23	4.08	5.02	7.87	6.30	7.41
2017	6.18	5.97	4.00	5.04	4.38	5.49	4.89	4.47	5.40	6.95	5.27	6.73
2018	6.20	3.82	5.45	4.12	3.71	4.96	3.88	4.69	4.76	6.11	5.46	4.60
2019	5.97	4.27	5.61	4.18	4.14	5.02	5.56	4.03	6.04	4.17	4.73	5.17
2020	5.15	6.56	5.23	4.81	3.95	4.11	4.07	4.35	3.85	5.81	5.10	5.05
mean	6.57	5.15	5.00	4.59	4.32	4.89	4.94	4.78	5.06	5.93	5.62	5.90

References

- Matthäus, W.; Franck, H. Characteristics of major Baltic inflows—A statistical analysis. *Cont. Shelf Res.* **1992**, *12*, 1375–1400. [\[CrossRef\]](#)
- Fischer, H.; Matthäus, W. The importance of the Drogden Sill in the Sound for major Baltic inflows. *J. Mar. Syst.* **1996**, *9*, 137–157. [\[CrossRef\]](#)
- Kowalkowski, T.; Pastuszek, M.; Igras, J.; Buszewski, B. Differences in emission of nitrogen and phosphorus into the Vistula and Oder basins in 1995–2008—Natural and anthropogenic causes (MONERIS model). *J. Mar. Syst.* **2012**, *89*, 48–60. [\[CrossRef\]](#)
- Pastuszek, M.; Kowalkowski, T.; Kopyński, J.; Doroszewski, A.; Jurga, B.; Buszewski, B. Long-term changes in nitrogen and phosphorus emission into the Vistula and Oder catchments (Poland)—Modeling (MONERIS) studies. *Environ. Sci. Pollut. Res.* **2018**, *25*, 29734–29751. [\[CrossRef\]](#)
- Jankowska, H.; Matciak, M.; Nowacki, J. Salinity variations as an effect of groundwater seepage through the seabed [Puck Bay, Poland]. *Oceanologia* **1994**, *36*, 33–46.
- Kruk-Dowgiałło, L.; Szaniawska, A. Gulf of Gdańsk and Puck Bay. In *Ecology of Baltic Coastal Waters*; Schiewer, U., Ed.; Ecological Studies; Springer: Berlin/Heidelberg, Germany, 2008; pp. 139–165.
- Dargahi, B.; Kolluru, V.; Cvetkovic, V. Multi-Layered Stratification in the Baltic Sea: Insight from a Modeling Study with Reference to Environmental Conditions. *J. Mar. Sci. Eng.* **2017**, *5*, 2. [\[CrossRef\]](#)
- Woźniak, B.; Bradtke, K.; Darecki, M.; Dera, J.; Dudzińska-Nowak, J.; Dzierzbicka-Głowacka, L.; Ficek, D.; Furmańczyk, K.; Kowalewski, M.; Krężel, A.; et al. SatBałtyk—A Baltic environmental satellite remote sensing system—An ongoing project in Poland. Part 1: Assumptions, scope and operating range. *Oceanologia* **2011**, *53*, 897–924. [\[CrossRef\]](#)
- Woźniak, B.; Bradtke, K.; Darecki, M.; Dera, J.; Dudzińska-Nowak, J.; Dzierzbicka-Głowacka, L.; Ficek, D.; Furmańczyk, K.; Kowalewski, M.; Krężel, A.; et al. SatBałtyk—A Baltic environmental satellite remote sensing system—An ongoing project in Poland. Part 2: Practical applicability and preliminary results. *Oceanologia* **2011**, *53*, 925–958. [\[CrossRef\]](#)
- Konik, M.; Kowalewski, M.; Bradtke, K.; Darecki, M. The operational method of filling information gaps in satellite imagery using numerical models. *Int. J. Appl. Earth Obs. Geoinf.* **2019**, *75*, 68–82. [\[CrossRef\]](#)
- Dzierzbicka-Głowacka, L.; Janecki, M.; Dybowski, D.; Szymczycha, B.; Obarska-Pempkowiak, H.; Wojciechowska, E.; Zima, P.; Pietrzak, S.; Pazikowska-Sapota, G.; Jaworska-Szulc, B.; et al. A New Approach for Investigating the Impact of Pesticides and Nutrient Flux from Agricultural Holdings and Land-Use Structures on Baltic Sea Coastal Waters. *Pol. J. Environ. Stud.* **2019**, *28*, 2531–2539. [\[CrossRef\]](#)
- Dzierzbicka-Głowacka, L.; Nowicki, A.; Janecki, M.; Szymczycha, B.; Piotrowski, P.; Piekiel, P.; Łukasiewicz, G. Structure of the FindFish Knowledge Transfer Platform. *Fish. Aquat. Life* **2018**, *26*, 193–197. [\[CrossRef\]](#)
- Majewski, A. Hydrological characteristics of estuarine waters at the Polish Coast. *Pr. Państw. Inst. Hydrol.-Meteorol.* **1972**, *105*, 3–40.
- Osowiecki, A. *Kierunki Wieloletnich Zmian w Strukturze Makrozoobentosu Zatoki Puckiej*; Centrum Biologii Morza PAN: Gdynia, Poland, 2000; p. 134.
- Bolałek, J.; Falkowska, L.; Korzeniewski, K. Hydrochemia Zatoki. In *Zatoka Pucka*; Fundacja Rozwoju Uniwersytetu Gdańskiego: Gdańsk, Poland, 1993; pp. 222–281.
- Baltic Sea Hydrographic Commission. Baltic Sea Bathymetry Database Version 0.9.3. 2013. Available online: <http://data.bshc.pro/#2/52.8/20.4> (accessed on 15 February 2020).
- Large, W.G.; McWilliams, J.C.; Doney, S.C. Oceanic vertical mixing: A review and a model with a nonlocal boundary layer parameterization. *Rev. Geophys.* **1994**, *32*, 363–403. [\[CrossRef\]](#)
- Jakacki, J.; Meler, S. An evaluation and implementation of the regional coupled ice-ocean model of the Baltic Sea. *Ocean Dyn.* **2019**, *69*, 1–19. [\[CrossRef\]](#)
- Dybowski, D.; Jakacki, J.; Janecki, M.; Nowicki, A.; Rak, D.; Dzierzbicka-Głowacka, L. High-Resolution Ecosystem Model of the Puck Bay (Southern Baltic Sea)—Hydrodynamic Component Evaluation. *Water* **2019**, *11*, 2057. [\[CrossRef\]](#)

20. Dzierzbicka-Głowacka, L.; Jakacki, J.; Janecki, M.; Nowicki, A. Activation of the operational ecohydrodynamic model (3D CEMBS)—The hydrodynamic part *. *Oceanologia* **2013**, *55*, 519–541. [[CrossRef](#)]
21. Dzierzbicka-Głowacka, L.; Janecki, M.; Nowicki, A.; Jakacki, J. Activation of the operational ecohydrodynamic model (3D CEMBS)—The ecosystem module*. *Oceanologia* **2013**, *55*, 543–572. [[CrossRef](#)]
22. Kalinowska, D.; Wielgat, P.; Kolerski, T.; Zima, P. Effect of GIS parameters on modelling runoff from river basin. The case study of catchment in the Puck District. *E3S Web Conf.* **2018**, *63*, 00005. [[CrossRef](#)]
23. Kalinowska, D.; Wielgat, P.; Kolerski, T.; Zima, P. Model of Nutrient and Pesticide Outflow with Surface Water to Puck Bay (Southern Baltic Sea). *Water* **2020**, *12*, 809. [[CrossRef](#)]
24. Wielgat, P.; Kalinowska, D.; Szymkiewicz, A.; Zima, P.; Jaworska-Szulc, B.; Wojciechowska, E.; Nawrot, N.; Matej-Lukowicz, K.; Dzierzbicka-Głowacka, L.A. Towards a multi-basin SWAT model for the migration of nutrients and pesticides to Puck Bay (Southern Baltic Sea). *PeerJ* **2021**, *9*, e10938. [[CrossRef](#)] [[PubMed](#)]
25. Smith, R.; Gent, P. *Reference manual for the Parallel Ocean Program (POP), Ocean Component of the Community Climate System Model (CCSM2.0)*; Los Alamos National Laboratory Technical Report; National Center For Atmospheric Research: Boulder, Colorado, 2002.
26. Los Alamos National Laboratory. Parallel Ocean Program (POP) User Guide. 2003. Available online: https://www.cesm.ucar.edu/models/cesm2/ocean/doc/users/POPusers_main.html (accessed on 20 August 2021).
27. Taylor, K.E. Summarizing multiple aspects of model performance in a single diagram. *J. Geophys. Res. Atmos.* **2001**, *106*, 7183–7192. [[CrossRef](#)]
28. Durski, S.M.; Glenn, S.M.; Haidvogel, D.B. Vertical mixing schemes in the coastal ocean: Comparison of the level 2.5 Mellor-Yamada scheme with an enhanced version of the K profile parameterization. *J. Geophys. Res. Ocean.* **2004**, *109*. [[CrossRef](#)]
29. Krezel, A.; Ostrowski, M.; Szymelfenig, M. Sea surface temperature distribution during upwelling along the Polish Baltic coast. *Oceanologia* **2005**, *47*, 415–432.
30. Kowalewski, M.; Ostrowski, M. Coastal up- and downwelling in the southern Baltic. *Oceanologia* **2005**, *47*, 453–475.
31. BACC Author Team. Baltic Sea Oceanography. In *Assessment of Climate Change for the Baltic Sea Basin; Regional Climate Studies*; Springer: Berlin/Heidelberg, Germany, 2008; pp. 379–385. [[CrossRef](#)]

4.2 Research paper no. 2

Janecki, M., Dybowski, D., Rak, D., Dzierzbicka-Glowacka, L., 2022. *A New Method for Thermocline and Halocline Depth Determination at Shallow Seas*. *Journal of Physical Oceanography* 52, 2205–2218. <https://doi.org/10.1175/JPO-D-22-0008.1>

(IF¹ = 4.327; MEiN² = 140)

¹Journal 5-Year Impact Factor (IF) according to the Journal Citation Reports

²Journal score according to the list of the Polish Ministry of Education and Science

A New Method for Thermocline and Halocline Depth Determination at Shallow Seas

MACIEJ JANECKI,^a DAWID DYBOWSKI,^a DANIEL RAK,^b AND LIDIA DZIERZBICKA-GŁOWACKA^a

^a *Ecohydrodynamics Laboratory, Physical Oceanography Department, Institute of Oceanology, Polish Academy of Sciences, Sopot, Poland*

^b *Observational Oceanography Laboratory, Physical Oceanography Department, Institute of Oceanology, Polish Academy of Sciences, Sopot, Poland*

(Manuscript received 10 January 2022, in final form 26 May 2022)

ABSTRACT: This paper introduces a new method for finding the top of thermocline (TTD) and halocline (THD) depths that may become a powerful tool for applications in shallow marine basins around the world. The method calculates the moving average of the ocean vertical profile's short-scale spatial variability (standard deviation) and then processes it to determine the potential depth at which temperature or salinity rapidly changes. The method has been calibrated using an extensive set of data from the ecohydrodynamic model EcoFish. As a result of the calibration, the values of the input parameters that allowed the correct determination of TTD and THD were established. It was confirmed by the validation carried out on the in situ profiles collected by the research vessel S/Y *Oceania* during statutory cruises in the southern Baltic Sea. The "MovSTD" algorithm was then used to analyze the seasonal variability of the vertical structure of the waters in Gdańsk Deep for temperature and salinity. The thermocline deepening speed was also estimated in the region analyzed.

KEYWORDS: Ocean; Mixed layer; Thermocline; Ocean models

1. Introduction

The existence of a well-mixed surface layer where temperature, salinity, and density are almost homogeneous is a characteristic and almost universal feature of water bodies such as seas and oceans. Wind-driven interactions and heat flux exchange at the water–atmosphere boundary cause strong turbulent mixing processes within this layer.


The depth of this mixed layer shows high seasonal variability. It may be located close to the surface or be not present at all during the warm summer months. However, in winter, because of the deep convection stimulated by surface heat loss, the boundary of the mixed layer is observed at great depths. In selected ocean locations, it can reach 2000 m (Marshall and Schott 1999), while in shallow seas, an example of which is the Baltic Sea, it is observed at depths of tens of meters (Leppäranta and Myrberg 2009).

The correct determination of the mixed layer depth (MLD) is of key importance in oceanographic research. This knowledge is used in the development, parameterization improvements and validation of ocean general circulation models (OGCMs), which are used to simulate the physical and thermodynamic processes that occur in the ocean (Chen et al. 1994; Masson et al. 2002; Noh et al. 2002; Kara et al. 2003; Zhang and Zebiak 2002). Furthermore, since a significant proportion of biological activity occurs in the upper ocean (in the euphotic zone), the mixed layer is also important for work related to biological processes

(Morel and André 1991; Longhurst 1995; Polovina et al. 1995).

The concept of a mixed layer is arbitrary and can be based on various parameters (e.g., temperature, density, salinity). The most commonly used criteria for defining a mixed layer are threshold methods, where MLD is the depth at which the temperature (or density) changes by a predetermined threshold value with respect to the one at a reference depth close to the surface. The choice of reference depth and threshold is usually arbitrary (de Boyer Montégut et al. 2004; Thomson and Fine 2003; Weller and Plueddemann 1996; Obata et al. 1996; Thompson 1976; Spall et al. 2000; Foltz et al. 2003; Rao et al. 1989); however, there are also studies in which it is based on a detailed analysis of thousands of profiles (Sprintall and Roemmich 1999), statistical analysis (Kara et al. 2000), water mass characteristics (Monterey and Levitus 1997), or other criteria (Schneider and Müller 1990). Gradient methods are also widely used, which, like threshold methods, are based on the assumption that there is a strong gradient at the base of the mixed layer and focus on finding its critical value (Lukas and Lindstrom 1991; Dong et al. 2008).

The limitation of these methods is their dependence on the reference depth and the threshold value. The consequence of the universal use of single parameterization for all profiles is overestimating (especially in those based on the temperature criterion) or underestimating the depth of the mixed layer. Due to the existence of salinity barrier layers, the density criterion was found to be better than the temperature one (Lukas and Lindstrom 1991); however, the availability of the density profiles is much lower than the temperature ones (Lorbacher et al. 2006). Due to these limitations, more complex methods of determining the MLD have developed. Examples can be the "curvature method" proposed by Lorbacher (Lorbacher et al. 2006), the "split and merge" (Thomson and Fine 2003), as well as a hybrid algorithm based on the

 Supplemental information related to this paper is available at the Journals Online website: <https://doi.org/10.1175/JPO-D-22-0008.s1>.

Corresponding author: Maciej Jannecki, mjannecki@iopan.pl

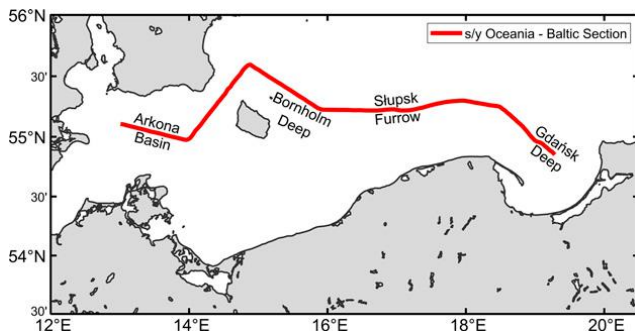


FIG. 1. S/Y *Oceania* section. Regular CTD measuring section of S/Y *Oceania*.

combined use of several methods to find the best MLD fit (Holte and Talley 2009).

The MLD determination methods presented above have been tested and applied on a number of water bodies (including the Global Ocean, Pacific Ocean, Atlantic Ocean, Indian Ocean), which all have a common feature of great depth. We could not find any papers with these methods dedicated and calibrated to semiclosed, shallow, and brackish seas such as the Baltic Sea. There are many factors that influence changes in water temperature in these types of seas, among others: diurnal variability (Karagali et al. 2012), strong winds, upwelling phenomenon, or freshwater inflow from rivers (Grelowska et al. 2018). These processes can impede the accurate and precise determination of TTD/THD.

The region of our particular interest is the Gulf of Gdańsk and Gdańsk Deep with a maximum depth of 118 m located in its northern part. It is related to the ongoing project “FindFish—Numerical Forecasting System for the Marine Environment of the Gulf of Gdańsk for Fisheries” (Dzierzbicka-Głowacka et al. 2018). Being aware of the applicability limitations of the existing methods and having the need to analyze the vertical structure of the waters of the Gulf of Gdańsk, we decided to develop our own method of determining the mixed layer depth and called it the “MovSTD” algorithm. We think that thanks to the methodology we used

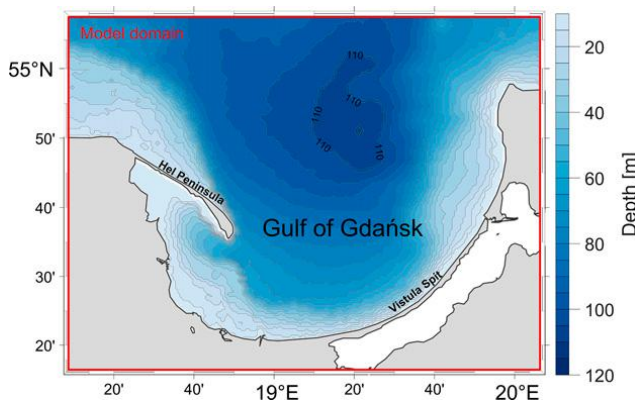


FIG. 2. Model domain. Topography of the EcoFish model domain with the analyzed 110-m isobath region emphasized.

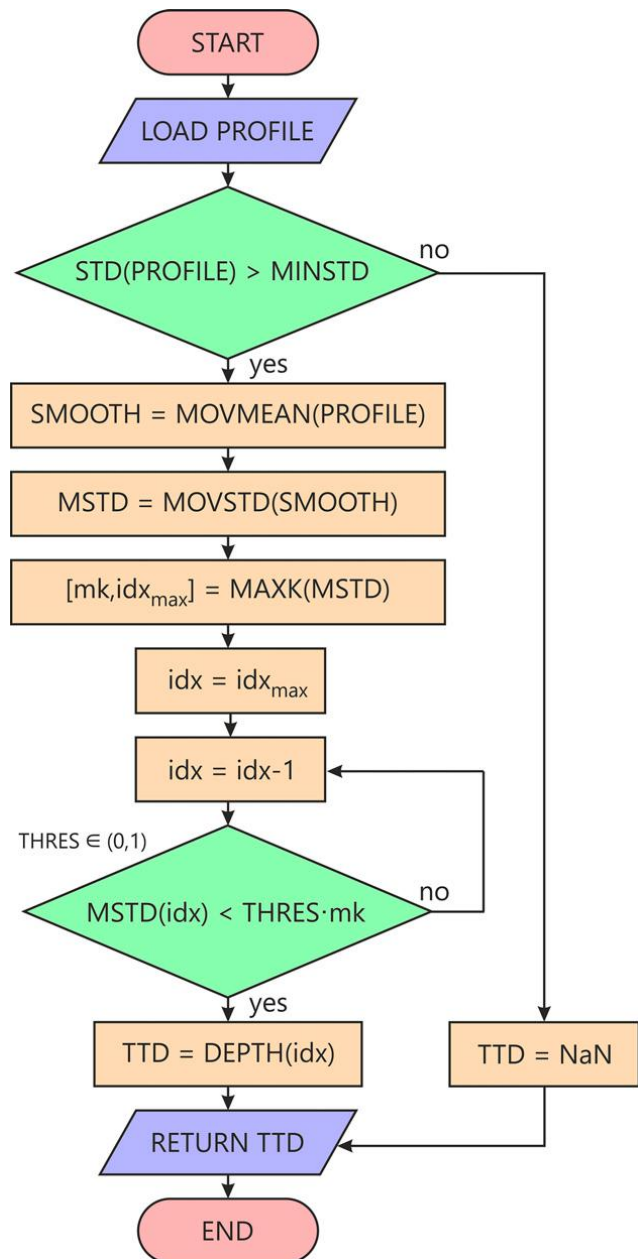


FIG. 3. The flow diagram of the MovSTD algorithm.

and its low computational complexity, the MovSTD algorithm will fill the knowledge gap and become a powerful tool for applications in shallow marine basins around the world.

The MovSTD algorithm was calibrated and then validated against in situ profiles of temperature and salinity. After visually confirming that the method correctly determines the depth of the mixing layer, it was used to analyze the mechanism of thermocline and halocline formation in the Gdańsk Deep, using EcoFish model data from 1 January 2014 to 31 December 2020. Using the proposed method, we were able to analyze MLD in the waters of the Baltic Sea by determining the top of the thermocline (TTD) and halocline (THD) depths.

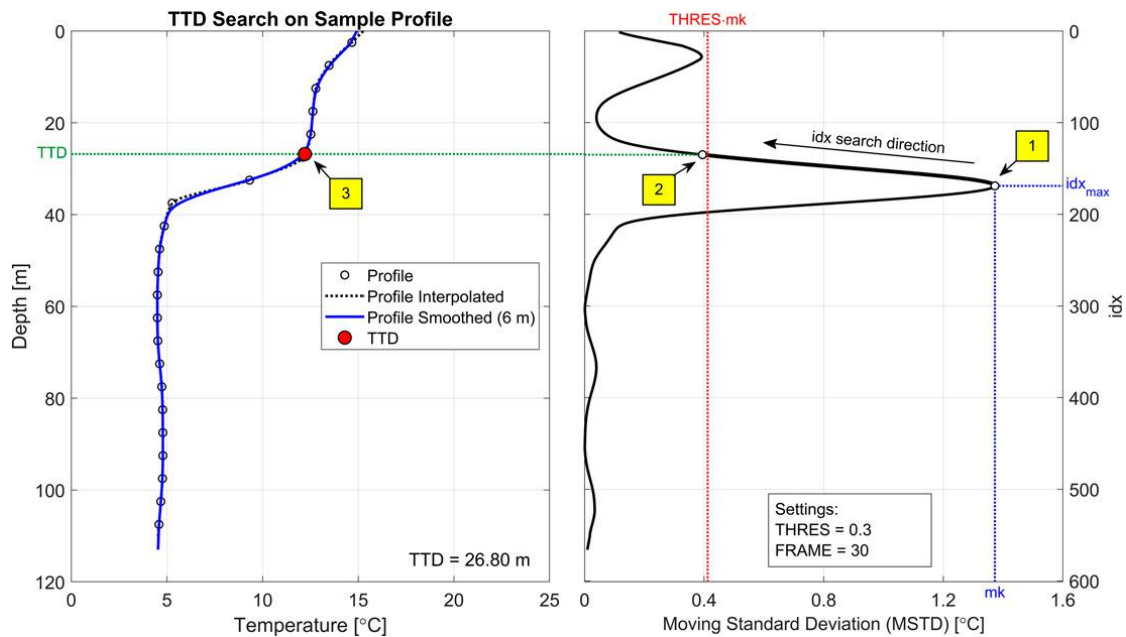


FIG. 4. An example of finding a TTD using the MovSTD algorithm. (left) Sample temperature profile and (right) the moving standard deviation of the profile. The yellow squares indicate 1) the maximum value of the MSTD curve, 2) the first index that meets the cutoff search condition of Eq. (1), and 3) the top of thermocline depth in the profile (TTD).

2. Materials and methods

a. Field data

This research uses in situ hydrographic data obtained by the Institute of Oceanology, Polish Academy of Sciences, during regular cruises of the research vessel *S/Y Oceania* (Rak and Wiczorek 2012). Data were recorded using a CTD (conductivity–temperature–depth) probe on a fixed measurement section extending between 13° and 20°E. The measuring section starts at Gdańsk Basin and then runs through the Słupsk Furrow toward Bornholm Basin and further to the Arkona Basin (Fig. 1).

The data used here were collected between January 2014 and December 2020. During this period, 15 research cruises were made. Seven of them were held in the fall (one in September, two in October, and four in November). Four cruises were carried out in winter (two in January and two in February). In spring there were also four cruises (all in May). There are no summer campaigns due to the ship’s participation in the Arctic Expedition (AREX). For the purposes of this study, vertical profiles were averaged every 0.5 m. The data were used to validate the MovSTD algorithm.

b. EcoFish model

Detailed information on the EcoFish model is provided in (Janecki et al. 2021). Besides an extensive description, it includes a chapter on the validation of water temperature and salinity profiles used in this research. Here, we present only a brief summary and description of the model results that were used in this research.

EcoFish’s horizontal resolution is 575 m (1/192°). The vertical resolution is 5 m for each layer with a total of 26 layers. Vertical discretization uses the z formulation, and the bottom topography is based on the Baltic Sea Bathymetric Database (BSBD) of the Baltic Sea Hydrographic Commission (Baltic Sea Hydrographic Commission 2013).

The EcoFish model domain covers an extended Gulf of Gdańsk region (Fig. 2). The data come from a 7-yr simulation of the model from 1 January 2014 to 31 December 2020. The simulation was preceded by a 2-yr spinup. EcoFish model has active satellite data assimilation for surface temperature. The results were recorded four times a day as 6-h averages and then converted to daily average.

c. MovSTD algorithm

This section introduces the MovSTD algorithm for determining the TTD and THD depths. In brief, the algorithm smooths the analyzed profile to eliminate short-term fluctuations and bimodal distribution, and then it creates a moving average of the smoothed profile’s standard deviation (STD) to find its maximum value and the index (depth) for which it occurs. It proceeds to scan the STD curve upward for a value that meets the condition specified by Eq. (1). The index of the first point returned from the method indicates TTD/THD. The source code of the MovSTD algorithm is provided in the online supplemental material.

The result of this calculation depends on the values of three predefined parameters that, together with the analyzed individual profile, serve as input arguments for the method. The values of these parameters that are suitable

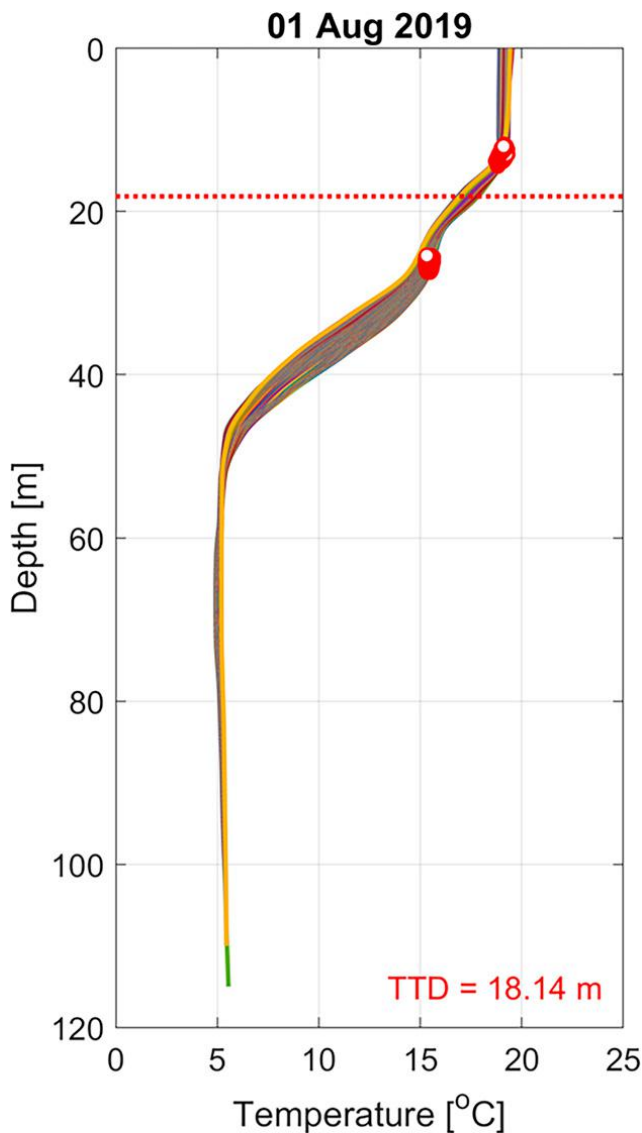


FIG. 5. Bimodal distribution of TTD. A group of temperature profiles of the EcoFish model with a visible bimodal distribution of TTD for 1 Aug 2019. Multicolored curves (orange, purple, green, etc.) represent individual vertical profiles. Red–white circles are the TTDs of the individual profiles. The dashed red line marks the average TTD for that day in the region analyzed.

for the Baltic Sea conditions were determined at the calibration stage, which is described in next section. The parameters are as follows:

- moving mean and moving STD sliding window (FRAME),
- standard deviation threshold (THRES), and
- profile's minimum standard deviation (MINSTD).

The flow diagram (Fig. 3) shows the step-by-step mechanism of finding TTD/THD in the MovSTD algorithm. The initial step is to cache the individual vertical profile of the variable analyzed (temperature or salinity). The precision of the MovSTD algorithm is closely related to the spatial resolution of the profile. If it is too coarse, the interpolation should be performed first. In this study, both the profiles from the

EcoFish model and the in situ data were interpolated at a resolution of 0.2 m. The choice of this resolution was the result of our expert judgment. It is adequate to eliminate local spikes of in situ data and capture temperature/salinity variation at the same time. Calibration of the MovSTD algorithm was performed with this resolution selected. Therefore, the parameter values determined during the calibration stage will be appropriate for this data density. If one tries to use the MovSTD algorithm for profiles with a resolution other (mostly coarser) than 0.2 m, the FRAME parameter should be recalibrated.

In the next step, the STD condition is checked across the entire profile. If it is less than MINSTD, the algorithm returns not a number (NaN), which signals that the profile is homogeneous (isothermal or isohaline) and there is no visible thermocline/halocline. An attempt to use MovSTD here may result in receiving an erroneous value related to the local change in temperature/salinity, not the fact that there is a wedge in the profile analyzed.

If the above condition is met (when the STD of the profile is greater than MINSTD), the algorithm begins to smooth the profile using a moving average, with a step defined by the FRAME parameter.

We calculate the moving standard deviation (MSTD) of the smoothed vertical profile, which is the most important operation in the presented method. The result of this operation is used to determine the position where the greatest changes in value occur.

Now we find the maximum of the MSTD mk and the corresponding index idx_{max} . The idx is the depth measurement index from the surface ($idx = 1$) to the bottom ($idx = N$). In a profile reaching 120 m with a vertical resolution of 0.2 m, $idx = 1$ is 0-m depth, $idx = 2$ is 0.2 m, $idx = 3$ is 0.4 m, and so on up to $idx = 601$ for a depth of 120 m.

The index number idx_{max} is used as the starting point for the MSTD curve search. At this stage, the algorithm starts to check the cutoff condition in the direction of decreasing depth indexes (toward the surface). For each subsequent index, it is checked whether the MSTD value has fallen below the value of the product mk and the threshold parameter THRES [Eq. (1)]. The first index that meets this condition indicates the TTD (for the temperature profile) or THD (for the salinity profile):

$$MSTD(idx) < THRES \times mk; \text{ where } THRES \in (0, 1). \quad (1)$$

Here we present the description of the algorithm's steps on the sample temperature profile. The method works similarly for salinity profiles.

The analyzed sample temperature profile (Fig. 4) is an EcoFish model result for 3 October 2014 from the Gdańsk Deep location. Due to the coarse vertical resolution (5 m), it is subjected to the piecewise cubic Hermite interpolating polynomial (PCHIP) method with nodes every 0.2 m (black dotted line in Fig. 4). The interpolated value at a query point is based on a shape-preserving piecewise cubic interpolation of the values at neighboring grid points.

Since the profile's STD is 3.74°C, the condition of MINSTD = 0.7°C is met, which means that the profile is not isothermal and we can proceed to determine the TTD. In the next step, the profile is smoothed (solid blue line in Fig. 4) using a moving average with a sampling width of 30 indexes

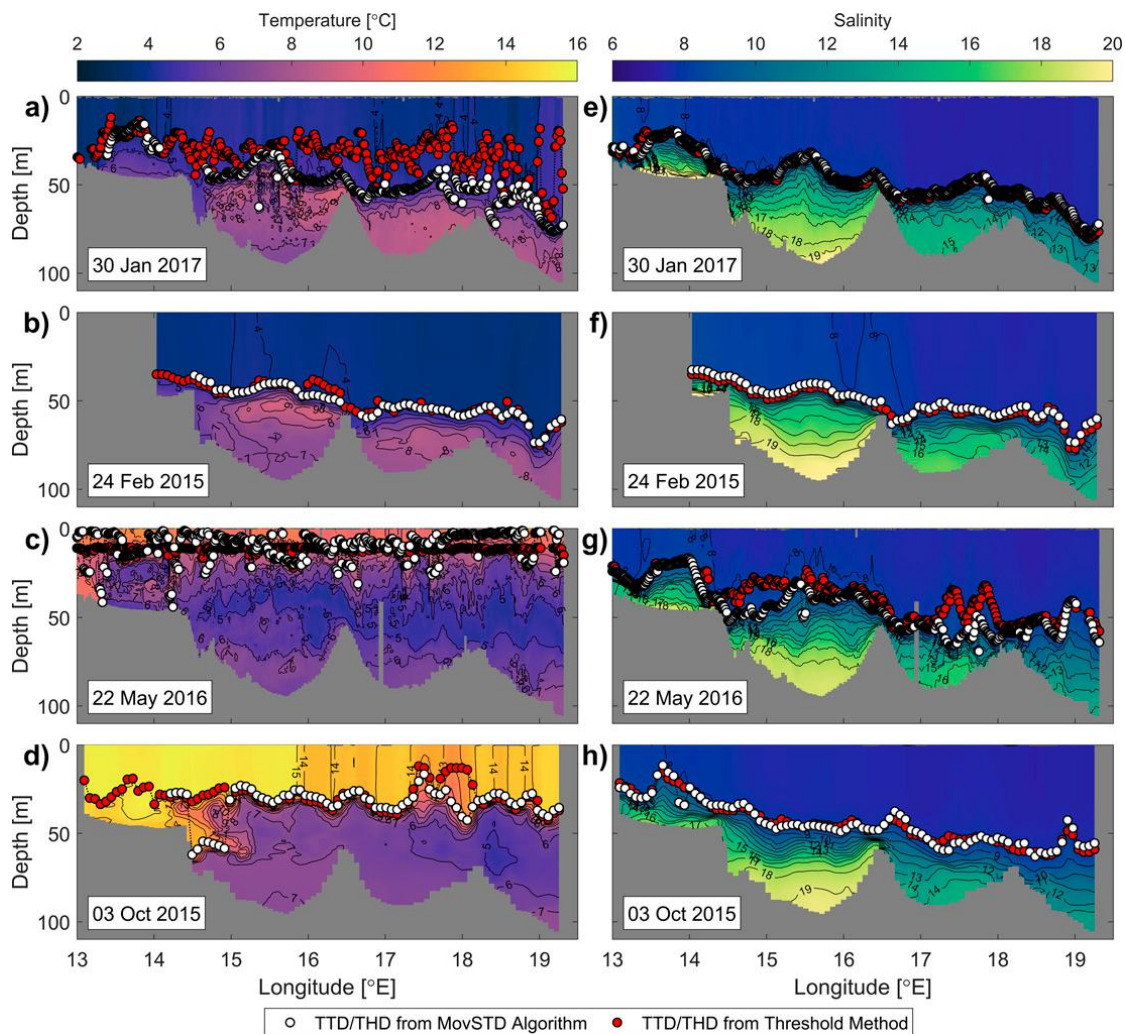


FIG. 6. MovSTD validation. Algorithm validation for temperature and salinity profiles from four representative S/Y Oceania cruises, which took place in January, February, May, and October. (a)–(d) Temperature profiles with TTDs marked. (e)–(h) Salinity profiles with THDs marked. The white dots are the results of the MovSTD algorithm. The red dots were obtained using the threshold method with $\Delta T = 0.2^\circ\text{C}$, $\Delta S = 0.5$.

(FRAME = 30), which corresponds to a width of 6 m for a profile resolution of 0.2 m. For the smoothed profile, the moving standard deviation (MSTD) is calculated using the same sampling width.

The algorithm determines the maximum value mk on the MSTD curve, which for the analyzed profile is 1.3725 and the corresponding depth index idx_{\max} equal to 169 (yellow square 1 in Fig. 4). The MSTD curve is scanned from idx_{\max} in the upward direction (descending indexes). The algorithm begins to search for the first index that meets the conditions of Eq. (1). After substituting the numerical values, we get

$$\text{MSTD}(idx) < 0.3 \times 1.3725 = 0.4118. \quad (2)$$

The first index that meets the conditions is $idx = 135$, for which the MSTD is 0.3945 (yellow square 2 in Fig. 4). The index is then returned from the MovSTD algorithm, indicating that the top of the thermocline is located at a depth of 26.8 m (yellow square 3 in Fig. 4).

d. Parameterization

This section presents the parameterization and calibration process of the MovSTD algorithm. The TTD and THD depth values returned by the MovSTD algorithm depend on three input parameters. The appropriate selection of these parameters has a significant impact on the results obtained.

The FRAME parameter is responsible for smoothing the individual vertical profiles and the shape of the MSTD curve. The reason for its use is the need to eliminate the erroneous results obtained from the algorithm, related to the existence of inversions inside the profiles (especially temperature ones). The MovSTD method is based on the assumption that the presence of thermocline and halocline is associated with a strong gradient and unimodal distribution. Profiles with a multimodal (usually bimodal) distribution (Fig. 5) can be observed during the months when the seasonal thermocline starts to form. These additional modes, although relatively

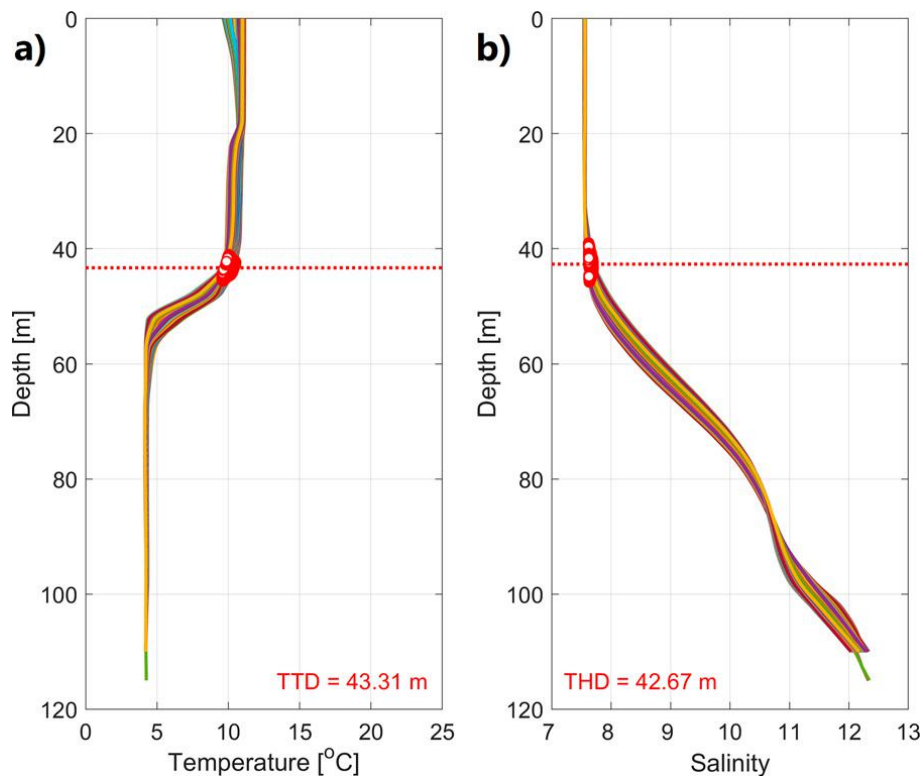


FIG. 7. Sample results from the MovSTD algorithm. EcoFish model (a) temperature and (b) salinity vertical profiles, 18 Nov 2018. Multicolored curves (orange, purple, green, etc.) represent individual vertical profiles. Red–white circles are the TTD/THD of the individual profiles. The dashed red line marks the average TTD/THD value for that day in the Gdańsk Deep region (110-m isobath).

narrow, may have a greater temperature gradient than that found in the thermocline. The use of a moving average of the profile and moving standard deviation allows to eliminate these additional modes and transform the profile into unimodal.

Selecting a FRAME that is too small can result in insufficient elimination of additional modes. However, a large value smooths the profile too much, causing the thermocline/halocline to stretch and making it difficult for the algorithm to find the correct depth of its top.

The THRES parameter is directly responsible for the step when MovSTD algorithm stops scanning the MSTD curve and returns the index indicating the top of thermocline/halocline

depth. Selecting a THRES too high will meet the condition [Eq. (1)] too fast and terminate the TTD/THD search inside the thermocline/halocline rather than at their top, causing the depth to be overestimated (area between yellow square 1 and 2 on Fig. 4). On the other hand, a small THRES may cause an underestimation of the depth by terminating the MSTD curve search process too late, above the thermocline/halocline layer (left of yellow square 2 on Fig. 4). The correct determination of this parameter was the result of a visual examination of hundreds of profiles while using different THRES and choosing a value that would place the TTD/THD on the correct depth.

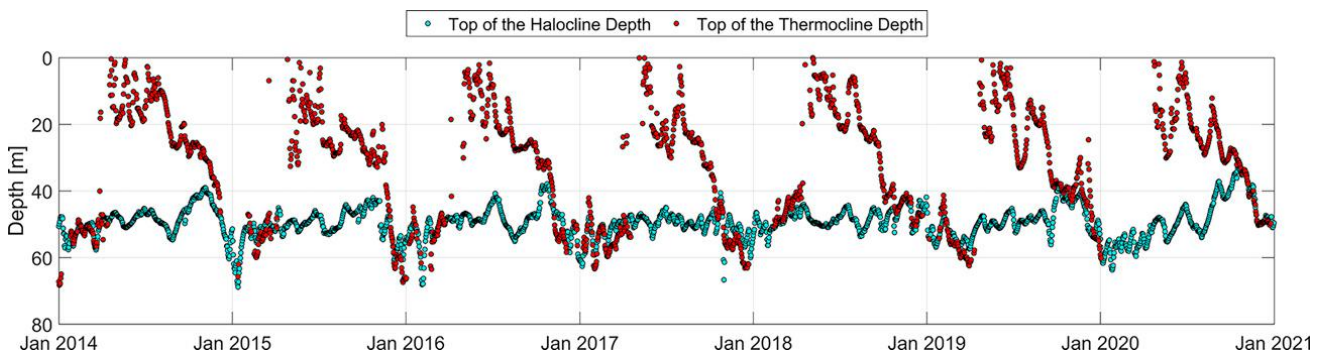


FIG. 8. TTD and THD time series. Top of thermocline (TTD) and halocline (THD) depth values time series obtained from MovSTD algorithm.

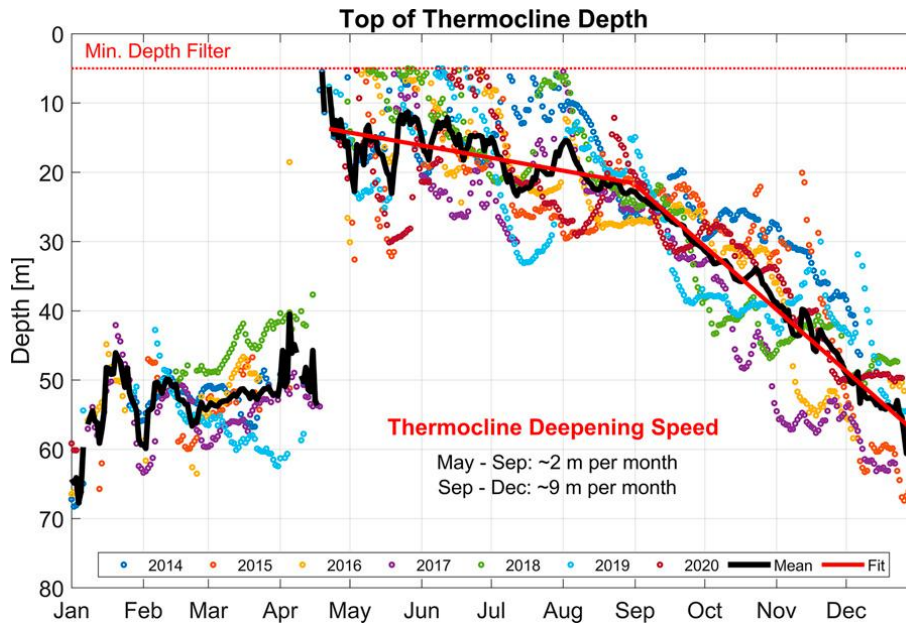


FIG. 9. Seasonal variability of the thermocline. Seasonal variability of the average TTD values from the MovSTD algorithm for the Gdańsk Deep region in the 2014–20 period.

The MINSTD parameter protects the method against returning erroneous values by omitting the search in homogeneously mixed profiles without thermocline (or halocline). If the STD of the data in the profile is less than MINSTD, the MovSTD algorithm does not start a search for TTD/THD and returns NaN.

e. Calibration

MovSTD algorithm calibration was carried out with the use of modeled temperature and salinity vertical profiles from the Gdańsk Deep region.

First, we used the MovSTD algorithm to obtain the TTDs/THDs of all individual profiles on each day in the 7-yr data interval. The next step was to calculate the region mean TTD/THD for each day and its standard deviation. After that we took all the daily STD values and calculated their mean. Since we did not analyze a single location, but the entire region of Gdańsk Deep, we assumed that there is a background daily STD related to the fact that the profiles in the analyzed area were not homogeneous. The addition to the daily STD value comes from the fact that for a given group of profiles,

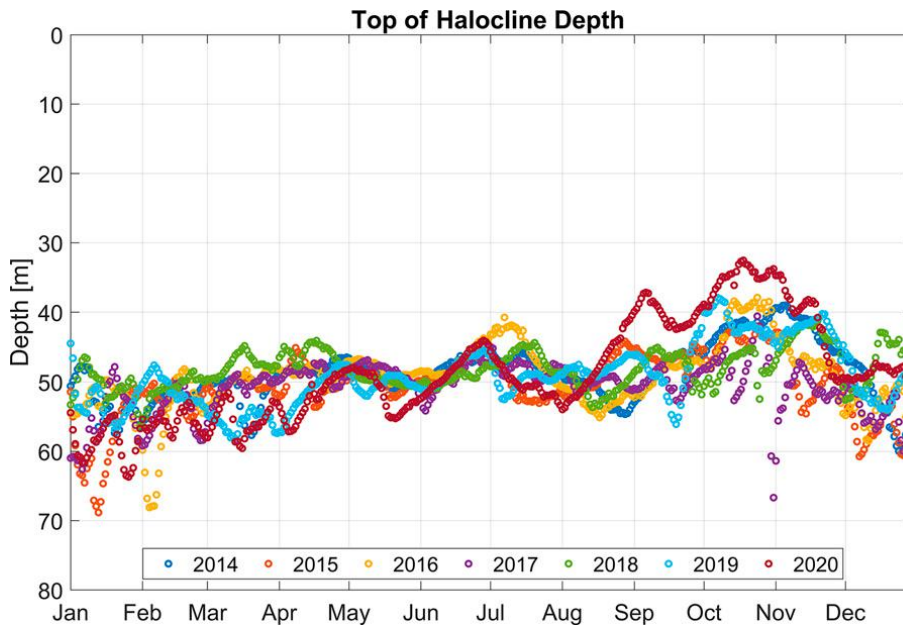


FIG. 10. Seasonal variability of the halocline. Seasonal variability of the average THD values from the MovSTD algorithm for the Gdańsk Deep region in the 2014–20 period.

TABLE A1. MovSTD algorithm calibration table. Boldface italic entries denote potential candidates for parameter values choice. Boldface non-italic entries are the combination of values that were chosen as the best set of input parameters for the MovSTD algorithm.

Pick	Parameters			Mean STD (m)	
	FRAME	THRES	MINSTD	TTD	THD
	20 (4 m)	0.20	0.60	1.76	1.62
	20 (4 m)	0.25	0.60	1.77	1.83
	20 (4 m)	0.30	0.60	1.77	2.25
	20 (4 m)	0.20	0.65	1.71	1.62
	20 (4 m)	0.25	0.65	1.73	1.83
	20 (4 m)	0.30	0.65	1.72	2.25
	20 (4 m)	0.20	0.70	1.65	1.62
	20 (4 m)	0.25	0.70	1.66	1.83
	20 (4 m)	0.30	0.70	1.67	2.25
	25 (5 m)	0.20	0.60	1.76	1.47
	25 (5 m)	0.25	0.60	1.68	1.61
	25 (5 m)	0.30	0.60	1.69	1.93
	25 (5 m)	0.20	0.65	1.70	1.47
	25 (5 m)	0.25	0.65	1.62	1.61
	25 (5 m)	0.30	0.65	1.64	1.93
	25 (5 m)	0.20	0.70	1.65	1.47
	25 (5 m)	0.25	0.70	1.56	1.61
	25 (5 m)	0.30	0.70	1.58	1.93
THD	30 (6 m)	0.20	0.60	1.75	1.37
	30 (6 m)	0.25	0.60	1.67	1.44
	30 (6 m)	0.30	0.60	1.63	1.66
	30 (6 m)	0.20	0.65	1.70	1.37
	30 (6 m)	0.25	0.65	1.61	1.44
	30 (6 m)	0.30	0.65	1.57	1.66
	30 (6 m)	0.20	0.70	1.63	1.37
	30 (6 m)	0.25	0.70	1.56	1.44
TTD	30 (6 m)	0.30	0.70	1.51	1.66

the MovSTD algorithm returned two groups of possible TTDs/THDs, creating a bimodal distribution (Fig. 5). Therefore, it was advisable to find a combination of input parameters such that the mean STD was as small as possible. For calibration, we choose three values for each parameter in the range that gave satisfactory results during the initial visual examination of the results. Table A1 in the appendix summarizes all combinations of parameters and mean STD values calculated using these parameters. The three sets of parameters with the smallest mean STD for salinity and temperature were selected as potential candidates for parameter determination and subjected to further examination to select the best combination of values. After analyzing the results, we decided that the MovSTD algorithm gives the most plausible estimations of TTDs/THDs using the following parameters:

For determining the TTD:

- FRAME: 30 (6 m),
- THRES: 0.3,
- MINSTD: 0.7°C.

For determining the THD:

- FRAME: 30 (6 m),
- THRES: 0.2,
- MINSTD: 0.6.

3. Results and discussion

a. MovSTD algorithm validation and comparison with the threshold method

The MovSTD algorithm was validated on data from all 15 available Baltic cruises on S/Y *Oceania* (Rak and Wieczorek 2012). This section presents the results for a selection of four representative cruises that occurred in January/February, late February, May, and early October (Fig. 6). The validation results for all cruises are in the appendix (Figs. A1–A5).

Validation revealed that the MovSTD algorithm correctly determines TTDs in the winter months (Figs. 6a,b), when there is a semi-isothermal cold water structure in the mixed layer, and a visible, well-established thermocline at greater depths. Very good results are also obtained for the October cruise (Fig. 6d), when the warm mixed water that has heated up in summer is in the upper layers, and then a rapid temperature drop is observed with a relatively thin thermocline. MovSTD algorithm gives satisfactory results in May (Fig. 6c), when the seasonal thermocline begins to form due to the heating of the surface layer; however, it should be noted that in these months a strong temperature variability is observed, which can sometimes cause underestimation or overestimation (visible spikes) of TTD.

Halocline does not have the same seasonal characteristics as thermocline. It is relatively constant for the entire section in each of the cruises, and the THDs are well determined. The increases in salinity that occur in the analyzed cruises are so strong and homogeneous (no bimodal distribution) that the MovSTD algorithm produces highly reliable results (Figs. 6e–h).

The MovSTD algorithm was compared with the threshold method. It is another common and fast way for determining the top of thermocline and halocline depths. It starts at the surface reference depth and continues to search the vertical profile, until a level is found where the water temperature (or salinity) differs from the reference value by a fixed threshold.

In this comparison, we used a surface reference depth of 10 m and a fixed threshold of 0.2°C (0.5 for salinity) proposed by de Boyer Montégut et al. (2004). These values were established for global climatology, and we acknowledge that we did not proceed with a dedicated calibration of this method for the Baltic Sea. Therefore, it was possible that it had performed worse than the MovSTD algorithm that was specifically calibrated for the Gdańsk Deep area.

The results obtained from the threshold method are similar to those from the MovSTD algorithm only in the case of a very clearly delineated thermocline. This is especially visible in the October section (Fig. 6d) and during the February cruise (Fig. 6b). For the May section, where a freshly formed thermocline can be observed, the threshold method fails. It yields the result practically in the first meters below the reference depth due to rapid local temperature fluctuations (Fig. 6c). The MovSTD algorithm is better in this case by adjusting to the nature and dynamics of the profile. The threshold method also fails for the January section (Fig. 6a), when it underestimates the thermocline, marking its top several meters above the actual TTD. In the case of salinity profiles, there is greater

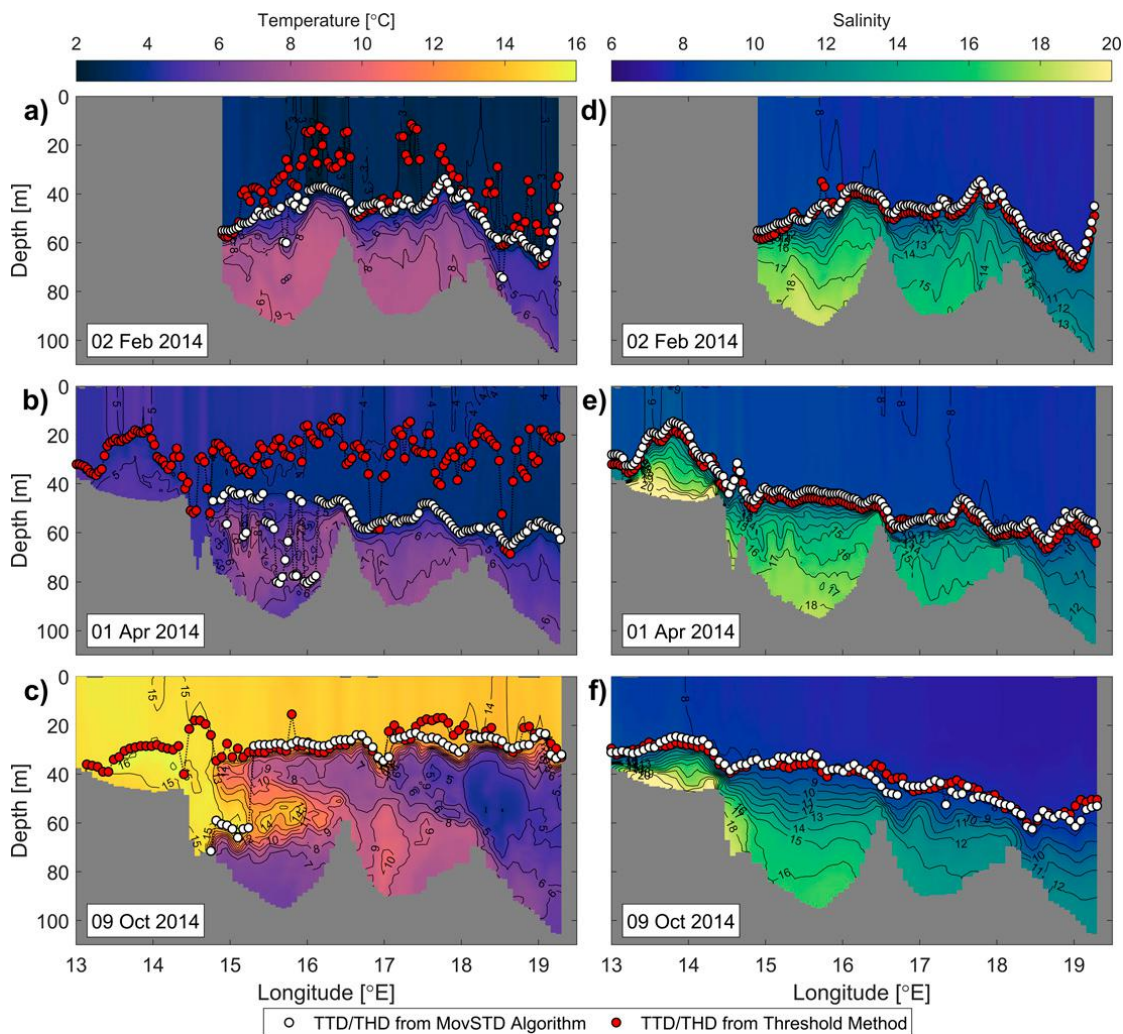


FIG. A1. MovSTD algorithm validation. Method validation using temperature and salinity profiles from S/Y *Oceania* cruises, which took place in February 2014, April 2014, and October 2014. (a)–(c) Temperature profiles with TTDs marked. (d)–(f) Salinity profiles with THDs marked. The white dots are the results of the MovSTD algorithm. The red dots were obtained using the threshold method with $\Delta T = 0.2^\circ\text{C}$, $\Delta S = 0.5$.

compatibility between the methods, although there are also discrepancies in favor of the MovSTD algorithm, especially during the May cruise (Fig. 6g).

b. Seasonal variability of the Gdańsk deep water vertical structure

Here, we analyze the seasonal variability of the water temperature and salinity in the Gdańsk Deep region with the use of model data. The analyzed profiles were taken from a 7-yr simulation of the EcoFish model for the period from 1 January 2014 to 31 December 2020 (Janecki et al. 2021). The border of the analyzed region is marked by the 110-m isobath (Fig. 2).

This region includes 1123 individual vertical profiles. Nine of them are profiles from the strict Gdańsk Deep, with a depth of 115 m, while the remaining 1114 are 110 m deep. The MovSTD algorithm was used to calculate TTDs and THDs for all individual profiles on each day from 1 January

2014 to 31 December 2020. We then calculated the mean TTD/THD to obtain one value per day for the entire region (Fig. 7).

As a result of these operations, a time series was created for the top of thermocline and halocline depths in the analyzed 7-yr period (Fig. 8).

To track the seasonal variability, the results are presented in one graph on a monthly scale, separately for the thermocline (Fig. 9) and the halocline (Fig. 10).

We filtered the results from 0- to 5-m depth on the TTD plot (Fig. 9). This procedure is related to the vertical resolution of the EcoFish model. The extreme near-surface interpolation node was the value for a depth of 2.5 m. Values from the layer between 0 and 2.5 m were obtained by linear extrapolation. Due to this, the algorithm’s estimation of such a shallow TTD was a method error related to the postextrapolation large temperature gradient in this thin layer, rather than the fact that a real thermocline was present.

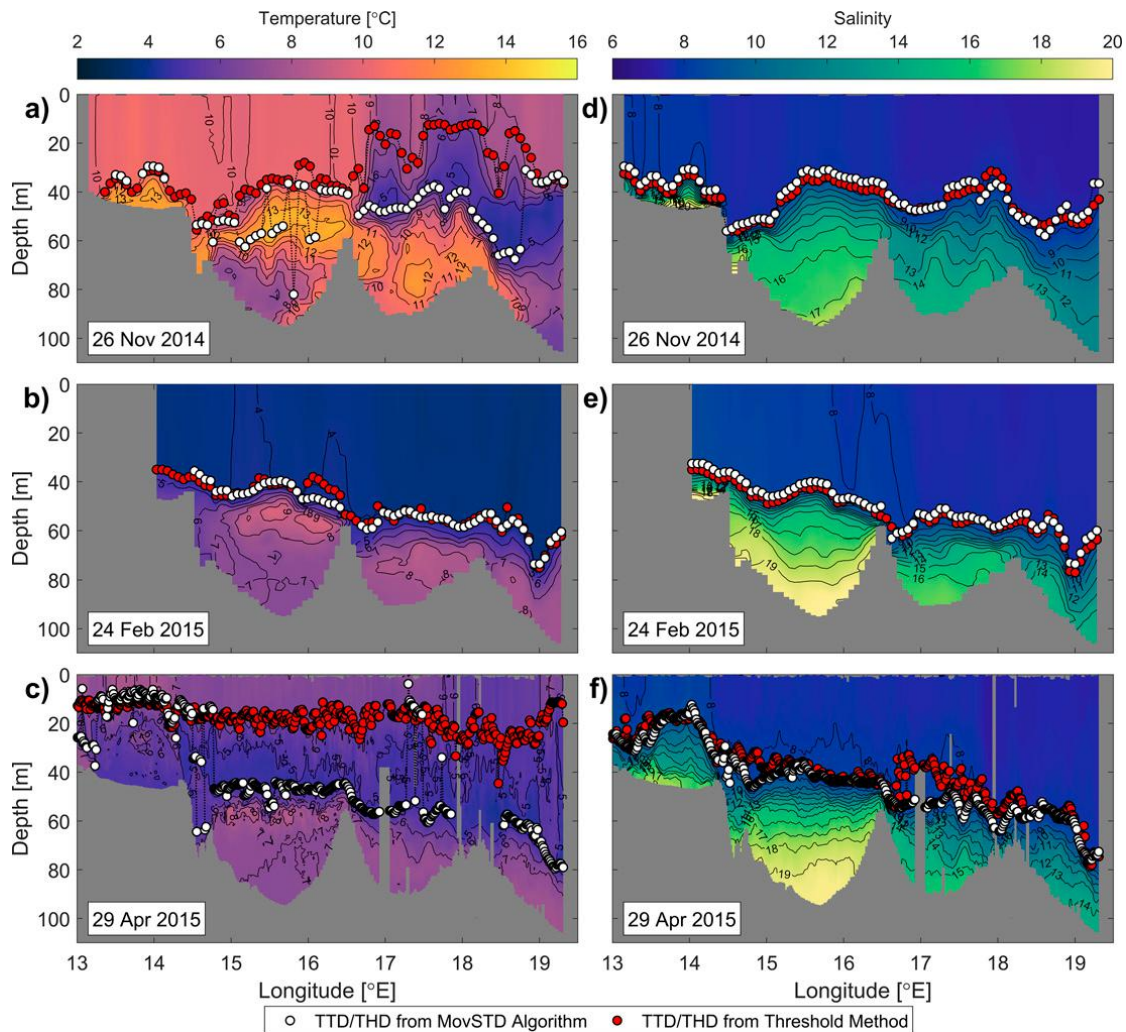


FIG. A2. MovSTD algorithm validation. Method validation using temperature and salinity profiles from *S/Y Oceania* cruises, which took place in November 2014, February 2015, and April 2015. (a)–(c) Temperature profiles with TTDs marked. (d)–(f) Salinity profiles with THDs marked. The white dots are the results of the MovSTD algorithm. The red dots were obtained using the threshold method with $\Delta T = 0.2^\circ\text{C}$, $\Delta S = 0.5$.

Supplying heat energy to the upper layers of the sea creates a thermocline (Fig. 9). In the analyzed region of the southern Baltic, the thermocline starts to form in May. As a result of further heating of the upper layers and mixing processes, the thermocline systematically deepens until it reaches the maximum depth defined by the halocline, which happens around December (Fig. 8). The deepening speed of the thermocline is not constant. Due to the slow heating of the upper layers and the influence of the cold intermediate layer (CIL), the initial deepening occurs at a speed of about 2 m month^{-1} . From September to December, after reaching the depth of the CIL, the deepening of the thermocline accelerates and occurs at a speed of about 9 m month^{-1} . When the upper layers are mixed by winter storms, they become homogeneous. This, with calm deep water below the thermocline, creates a two-layer structure visible from January to mid-April.

The top of halocline, which marks the maximum depth of the thermocline and is the lower limit of the CIL, is

most stable in the summer months of May–September. However, as the intensity and strength of the winds that force the advection processes increase, the halocline becomes unstable, rapidly changing its depth. The change in the depth of the halocline top in Gdańsk Deep is about $50 \pm 15 \text{ m}$ (Fig. 10).

4. Conclusions

The MovSTD algorithm works correctly both on in situ data, as confirmed by validation on the *S/Y Oceania* sections, and for model data from the EcoFish model.

The results from the MovSTD algorithm when tested on model data from the Gdańsk Deep region showed that the top of the halocline depth is relatively permanent and is located at about 50 m. Noticeable changes in the depth of the halocline can also be observed in the 7-yr period analyzed. From August to November, the THD begins to appear higher, at depths between 35 and 50 m. In addition, between

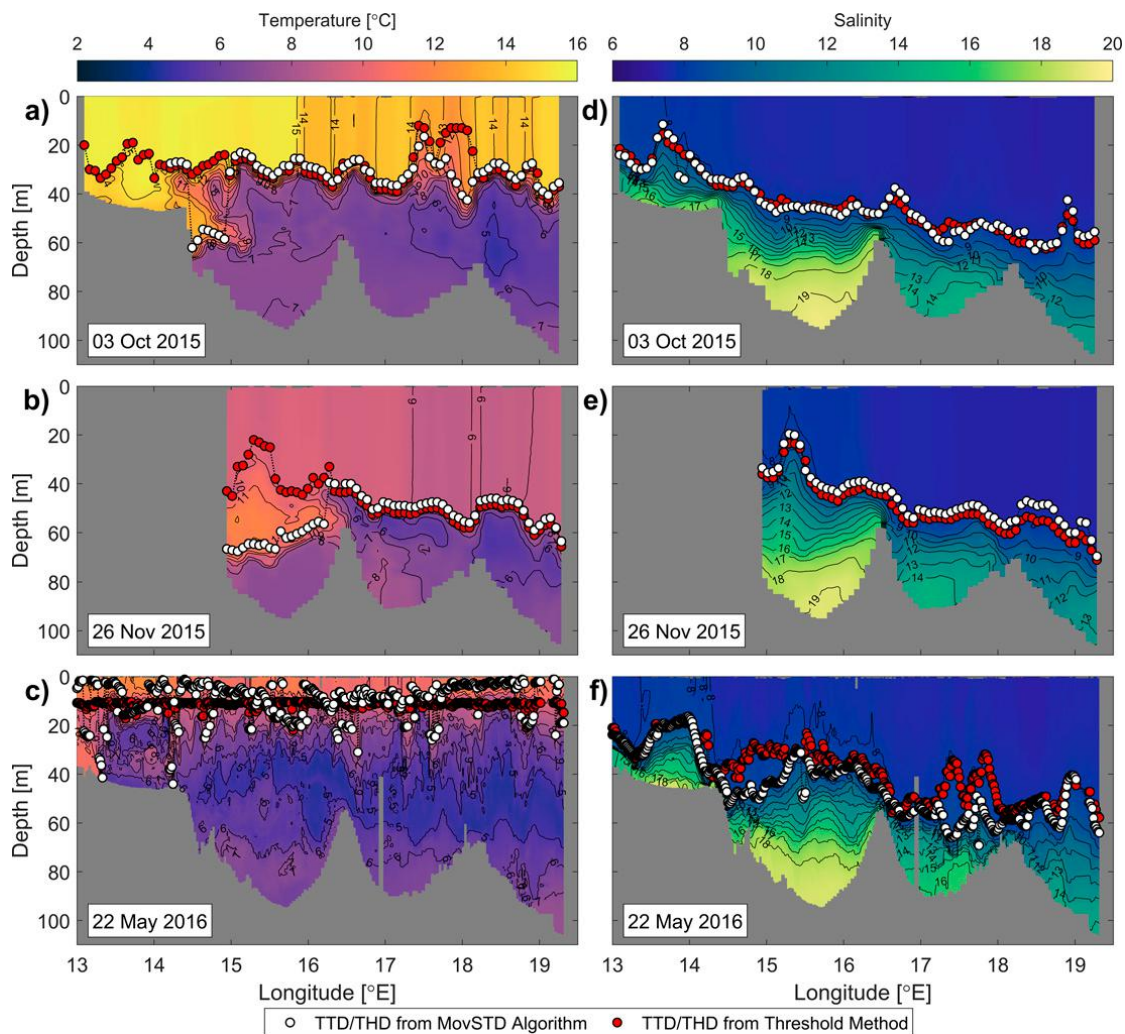


FIG. A3. MovSTD algorithm validation. Method validation using temperature and salinity profiles from S/Y *Oceania* cruises, which took place in October 2015, November 2015, and May 2016. (a)–(c) Temperature profiles with TTDs marked. (d)–(f) Salinity profiles with THDs marked. The white dots are the results of the MovSTD algorithm. The red dots were obtained using the threshold method with $\Delta T = 0.2^{\circ}\text{C}$, $\Delta S = 0.5$.

January and February 2015 and 2016 it reached instantaneous values of 70 m deep. However, it can be said that THD does not show significant seasonal variability and the vertical structure of salinity in the Gdańsk Deep is rather stable.

The situation is different for the thermocline. We can observe a strong seasonal variability here. A fresh thermocline begins to form in May due to the heating of the surface layer (forced by air temperature and sunlight). Its deepening speed from May to September is about 2 m month^{-1} . In the following months, as a result of water mixing and increased wind forcing, the thermocline deepening accelerates, reaching greater depths at a speed of about 9 m month^{-1} . At the turn of the year, this process stops, and until April thermocline occurs at the same depth as the halocline.

The values of the three predefined parameters (FRAME, THRES, and MINSTD) determined at the calibration stage are optimal for use in the Gulf of Gdańsk area. The one-to-one transfer of these values to other locations (different

seas) may reduce the accuracy and/or correctness of the results obtained from the MovSTD algorithm. However, they can be used as an initial estimate and then refined by repeating the calibration steps described in section 2e. Still, the method's versatility, combined with its low computational complexity, makes the algorithm a fast and robust tool for processing large amounts of data with high horizontal and temporal resolution.

This method can also be easily extended with additional functionality that allows the determination of the bottom of the thermocline and halocline depth. It can be accomplished by searching the MSTD curve toward greater depth instead of toward the surface. Extending the algorithm to such an element will consequently allow for the calculation of thermocline and halocline thickness. When properly calibrated, it is also possible to use the algorithm to analyze dissolved oxygen concentration profiles and further to detect hypoxic and anoxic zones. This work will be the subject of upcoming papers.

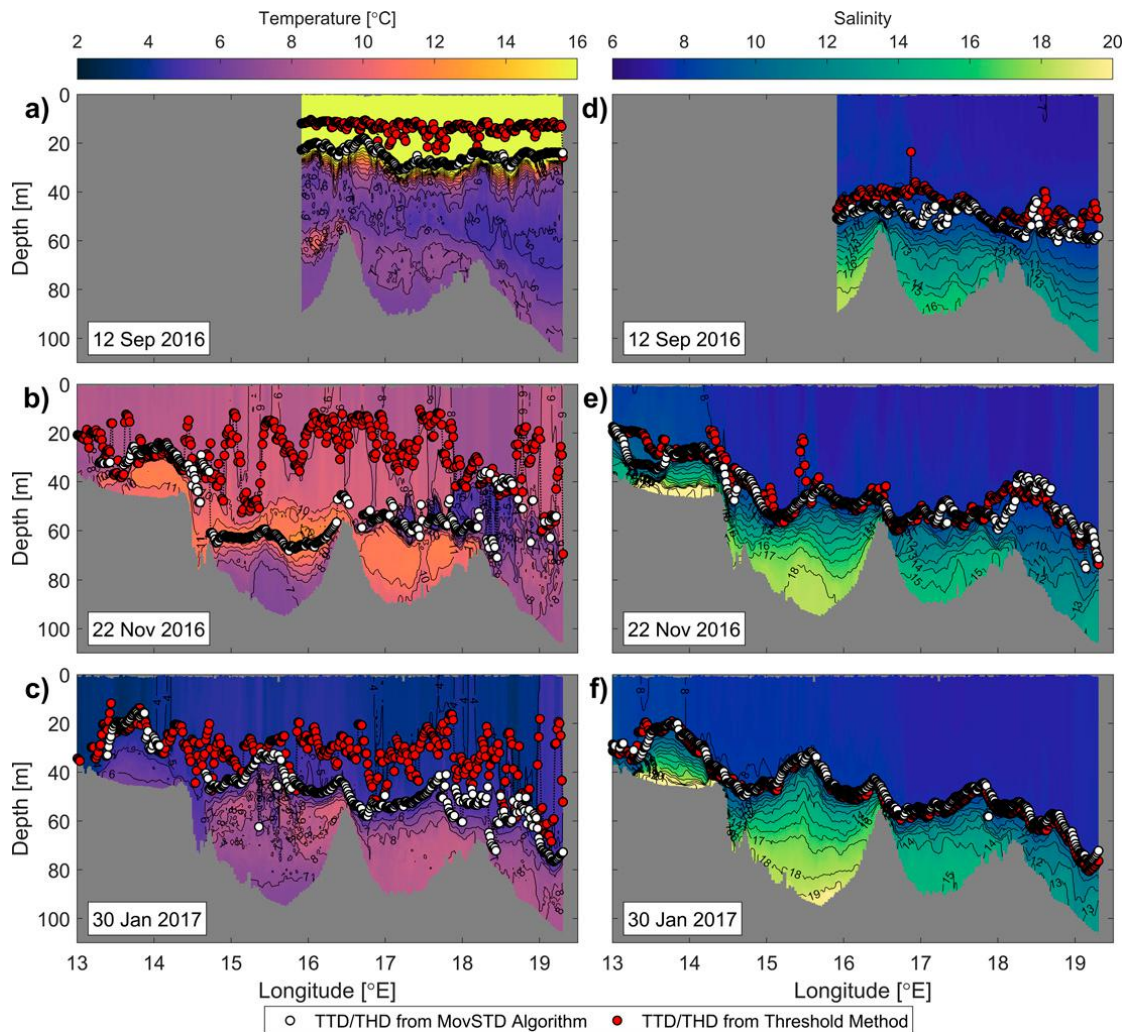


FIG. A4. MovSTD algorithm validation. Method validation using temperature and salinity profiles from S/Y *Oceania* cruises, which took place in September 2016, November 2016, and January 2017. (a)–(c) Temperature profiles with TTDs marked. (d)–(f) Salinity profiles with THDs marked. The white dots are the results of the MovSTD algorithm. The red dots were obtained using the threshold method with $\Delta T = 0.2^\circ\text{C}$, $\Delta S = 0.5$.

The lack of a separate calibration for the threshold method in the comparison (section 3a) may seem unfair and provoke the feeling that this was done deliberately to exalt the MovSTD algorithm. However, this was not our intention. Our creation of a new method was, in fact, dictated by the fact that the threshold method was not well suited to the Gulf of Gdańsk area. Nevertheless, our goal was not to replace the threshold method with a better one, but rather to propose an additional tool to the set of methods for determining the TTD/THD already available in the literature. A tool that in some regions may be a better choice (and worse in others) than the available methods.

Acknowledgments. Partial support for this study was provided by the project “Knowledge transfer platform Find-Fish—Numerical Forecasting System for the Marine Environment of the Gulf of Gdańsk for Fisheries,” funded by the

European Union through European Regional Development Fund Contract RPPM.01.01.01-22-0025/16-00. Some elements of the EcoFish model (i.e., river runoff data) are based on the solutions developed during the WaterPUCK project funded by National Centre for Research and Development of Poland within the BIOSTRATEG III program BIOSTRATEG3/343927/3/NCBR/2017. Calculations were carried out at the Academic Computer Centre in Gdańsk. The authors declare that they have no competing interests. We are grateful to the anonymous reviewers for valuable comments on earlier versions of the manuscript.

Data availability statement. All EcoFish model results and S/Y *Oceania* database presented in this study are available on request from the corresponding author. All other data and code are present in the paper, the online supplemental material, and section 2.

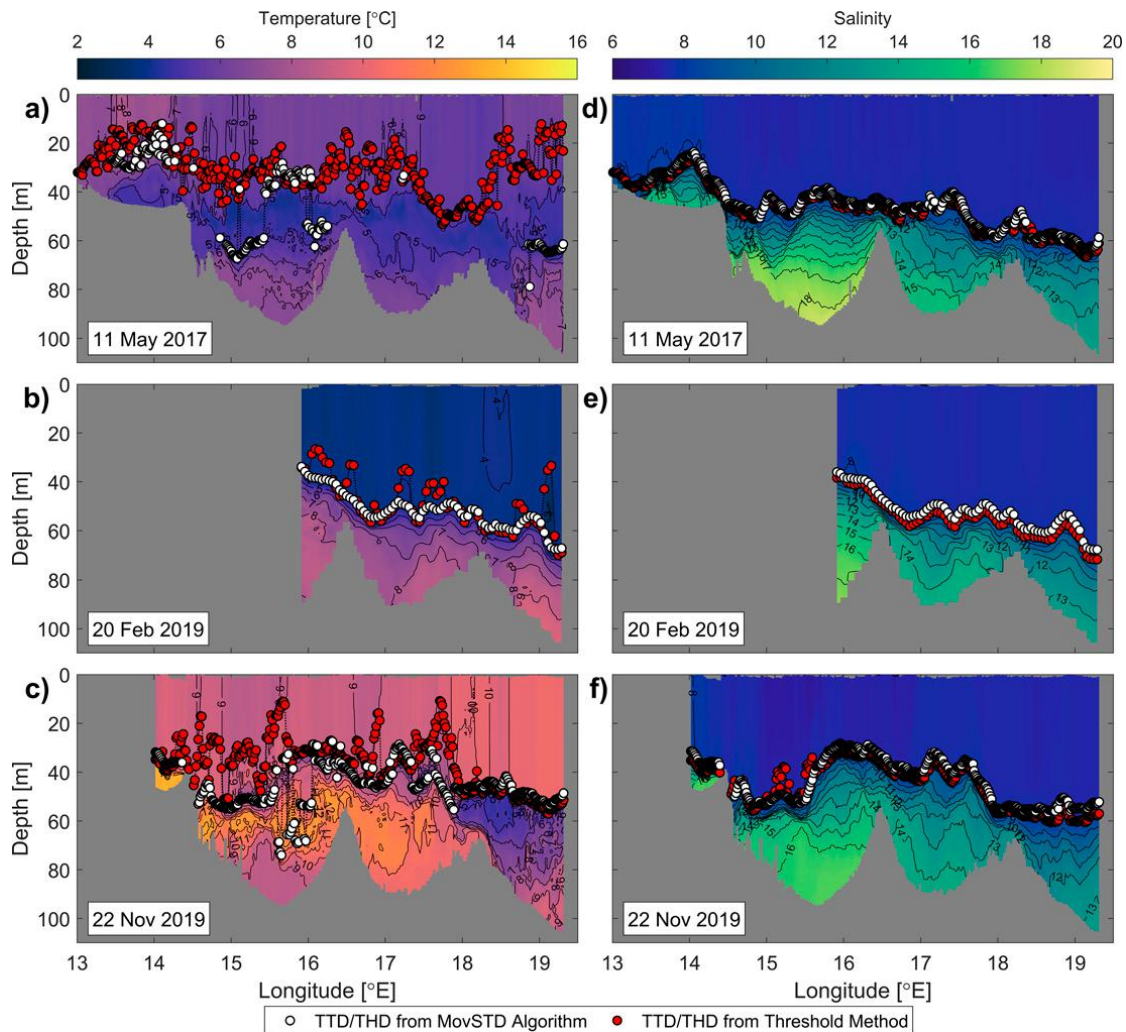


FIG. A5. MovSTD algorithm validation. Method validation using temperature and salinity profiles from S/Y *Oceania* cruises, which took place in May 2017, February 2019, and November 2019. (a)–(c) Temperature profiles with TTDs marked. (d)–(f) Salinity profiles with THDs marked. The white dots are the results of the MovSTD algorithm. The red dots were obtained using the threshold method with $\Delta T = 0.2^\circ\text{C}$, $\Delta S = 0.5$.

APPENDIX

MovSTD Calibration and Validation

Here we present a calibration table (Table A1) that allowed for a correct determination of MovSTD algorithm input parameters. Figures A1–A5 show MovSTD algorithm validation. It was carried out using temperature and salinity profiles from all S/Y *Oceania* cruises that took place between January 2014 and December 2020.

REFERENCES

Baltic Sea Hydrographic Commission, 2013: Baltic Sea Bathymetry Database Version 0.9.3. <http://data.bshc.pro/#2/58.6/16.2>.
 Chen, D., A. J. Busalacchi, and L. M. Rothstein, 1994: The roles of vertical mixing, solar radiation, and wind stress in a model simulation of the sea surface temperature seasonal cycle in the tropical Pacific Ocean. *J. Geophys. Res.*, **99**, 20345–20359, <https://doi.org/10.1029/94JC01621>.

De Boyer Montégut, C., G. Madec, A. S. Fischer, A. Lazar, and D. Iudicone, 2004: Mixed layer depth over the global ocean: An examination of profile data and a profile-based climatology. *J. Geophys. Res.*, **109**, C12003, <https://doi.org/10.1029/2004JC002378>.
 Dong, S., J. Sprintall, S. T. Gille, and L. Talley, 2008: Southern ocean mixed-layer depth from Argo float profiles. *J. Geophys. Res.*, **113**, C06013, <https://doi.org/10.1029/2006JC004051>.
 Dzierzbicka-Głowacka, L., A. Nowicki, M. Janecki, B. Szymczycha, P. Piotrowski, P. Piecki, and G. Łukasiewicz, 2018: Structure of the FindFish Knowledge Transfer Platform. *Fish. Aquat. Life*, **26**, 193–197, <https://doi.org/10.2478/aopf-2018-0021>.
 Foltz, G. R., S. A. Grodsky, J. A. Carton, and M. J. McPhaden, 2003: Seasonal mixed layer heat budget of the tropical Atlantic Ocean. *J. Geophys. Res.*, **108**, 3146, <https://doi.org/10.1029/2002JC001584>.
 Grelowska, G., E. Kozaczka, and D. Witos-Okrasińska, 2018: Vertical temperature stratification of the Gulf of Gdansk

- water. *2018 Joint Conf. - Acoustics*, Ustka, Poland, Institute of Electrical and Electronics Engineers, 1–6, <https://doi.org/10.1109/ACOUSTICS.2018.8502387>.
- Holte, J., and L. Talley, 2009: A new algorithm for finding mixed layer depths with applications to Argo data and subantarctic mode water formation. *J. Atmos. Oceanic Technol.*, **26**, 1920–1939, <https://doi.org/10.1175/2009JTECHO543.1>.
- Janecki, M., D. Dybowski, J. Jakacki, A. Nowicki, and L. Dzierzbicka-Glowacka, 2021: The use of satellite data to determine the changes of hydrodynamic parameters in the Gulf of Gdańsk via Ecofish model. *Remote Sens.*, **13**, 3572, <https://doi.org/10.3390/rs13183572>.
- Kara, A. B., P. A. Rochford, and H. E. Hurlburt, 2000: An optimal definition for ocean mixed layer depth. *J. Geophys. Res.*, **105**, 16 803–16 821, <https://doi.org/10.1029/2000JC900072>.
- , A. J. Wallcraft, and H. E. Hurlburt, 2003: Climatological SST and MLD predictions from a global layered ocean model with an embedded mixed layer. *J. Atmos. Oceanic Technol.*, **20**, 1616–1632, [https://doi.org/10.1175/1520-0426\(2003\)020<1616:CSAMPF>2.0.CO;2](https://doi.org/10.1175/1520-0426(2003)020<1616:CSAMPF>2.0.CO;2).
- Karagali, I., J. Høyer, and C. Hasager, 2012: SST diurnal variability in the North Sea and the Baltic Sea. *Remote Sens. Environ.*, **121**, 159–170, <https://doi.org/10.1016/j.rse.2012.01.016>.
- Leppäranta, M., and K. Myrberg, 2009: Topography and hydrography of the Baltic Sea. *Physical Oceanography of the Baltic Sea*, Springer, 41–88, https://doi.org/10.1007/978-3-540-79703-6_3.
- Longhurst, A., 1995: Seasonal cycles of pelagic production and consumption. *Prog. Oceanogr.*, **36**, 77–167, [https://doi.org/10.1016/0079-6611\(95\)00015-1](https://doi.org/10.1016/0079-6611(95)00015-1).
- Lorbacher, K., D. Dommenges, P. P. Niiler, and A. Köhl, 2006: Ocean mixed layer depth: A subsurface proxy of ocean-atmosphere variability. *J. Geophys. Res.*, **111**, C07010, <https://doi.org/10.1029/2003JC002157>.
- Lukas, R., and E. Lindstrom, 1991: The mixed layer of the western equatorial Pacific ocean. *J. Geophys. Res.*, **96**, 3343–3357, <https://doi.org/10.1029/90JC01951>.
- Marshall, J., and F. Schott, 1999: Open-ocean convection: Observations, theory, and models. *Rev. Geophys.*, **37**, 1–64, <https://doi.org/10.1029/98RG02739>.
- Masson, S., P. Delecluse, J.-P. Boulanger, and C. Menkes, 2002: A model study of the seasonal variability and formation mechanisms of the barrier layer in the eastern equatorial Indian Ocean. *J. Geophys. Res.*, **107**, 8017, <https://doi.org/10.1029/2001JC000832>.
- Monterey, G., and S. Levitus, 1997: Seasonal variability of mixed layer depth for the World Ocean. NOAA Atlas NESDIS 14, 96 pp.
- Morel, A., and J.-M. André, 1991: Pigment distribution and primary production in the western Mediterranean as derived and modeled from coastal zone color scanner observations. *J. Geophys. Res.*, **96**, 12 685–12 698, <https://doi.org/10.1029/91JC00788>.
- Noh, Y., C. J. Jang, T. Yamagata, P. C. Chu, and C.-H. Kim, 2002: Simulation of more realistic upper-ocean processes from an OGCM with a new ocean mixed layer model. *J. Phys. Oceanogr.*, **32**, 1284–1307, [https://doi.org/10.1175/1520-0485\(2002\)032<1284:SOMRUO>2.0.CO;2](https://doi.org/10.1175/1520-0485(2002)032<1284:SOMRUO>2.0.CO;2).
- Obata, A., J. Ishizaka, and M. Endoh, 1996: Global verification of critical depth theory for phytoplankton bloom with climatological in situ temperature and satellite ocean color data. *J. Geophys. Res.*, **101**, 20 657–20 667, <https://doi.org/10.1029/96JC01734>.
- Polovina, J. J., G. T. Mitchum, and G. T. Evans, 1995: Decadal and basin-scale variation in mixed layer depth and the impact on biological production in the central and north Pacific, 1960–88. *Deep-Sea Res. I*, **42**, 1701–1716, [https://doi.org/10.1016/0967-0637\(95\)00075-H](https://doi.org/10.1016/0967-0637(95)00075-H).
- Rak, D., and P. Wieczorek, 2012: Variability of temperature and salinity over the last decade in selected regions of the southern Baltic Sea. *Oceanologia*, **54**, 339–354, <https://doi.org/10.5697/oc.54-3.339>.
- Rao, R. R., R. L. Molinari, and J. F. Festa, 1989: Evolution of the climatological near-surface thermal structure of the tropical Indian Ocean: 1. Description of mean monthly mixed layer depth, and sea surface temperature, surface current, and surface meteorological fields. *J. Geophys. Res.*, **94**, 10 801–10 815, <https://doi.org/10.1029/JC094iC08p10801>.
- Schneider, N., and P. Müller, 1990: The meridional and seasonal structures of the mixed-layer depth and its diurnal amplitude observed during the Hawaii-to-Tahiti Shuttle experiment. *J. Phys. Oceanogr.*, **20**, 1395–1404, [https://doi.org/10.1175/1520-0485\(1990\)020<1395:TMASSO>2.0.CO;2](https://doi.org/10.1175/1520-0485(1990)020<1395:TMASSO>2.0.CO;2).
- Spall, M. A., R. A. Weller, and P. W. Furey, 2000: Modeling the three-dimensional upper ocean heat budget and subduction rate during the subduction experiment. *J. Geophys. Res. Oceans*, **105**, 26 151–26 166, <https://doi.org/10.1029/2000JC000228>.
- Sprintall, J., and D. Roemmich, 1999: Characterizing the structure of the surface layer in the Pacific Ocean. *J. Geophys. Res.*, **104**, 23 297–23 311, <https://doi.org/10.1029/1999JC900179>.
- Thompson, R. O. R. Y., 1976: Climatological numerical models of the surface mixed layer of the ocean. *J. Phys. Oceanogr.*, **6**, 496–503, [https://doi.org/10.1175/1520-0485\(1976\)006<0496:CNMOTS>2.0.CO;2](https://doi.org/10.1175/1520-0485(1976)006<0496:CNMOTS>2.0.CO;2).
- Thomson, R. E., and I. V. Fine, 2003: Estimating mixed layer depth from oceanic profile data. *J. Atmos. Oceanic Technol.*, **20**, 319–329, [https://doi.org/10.1175/1520-0426\(2003\)020<0319:EMLDFO>2.0.CO;2](https://doi.org/10.1175/1520-0426(2003)020<0319:EMLDFO>2.0.CO;2).
- Weller, R. A., and A. J. Plueddemann, 1996: Observations of the vertical structure of the oceanic boundary layer. *J. Geophys. Res.*, **101**, 8789–8806, <https://doi.org/10.1029/96JC00206>.
- Zhang, R.-H., and S. E. Zebiak, 2002: Effect of penetrating momentum flux over the surface boundary/mixed layer in a z-coordinate OGCM of the tropical Pacific. *J. Phys. Oceanogr.*, **32**, 3616–3637, [https://doi.org/10.1175/1520-0485\(2002\)032<3616:EOPMFO>2.0.CO;2](https://doi.org/10.1175/1520-0485(2002)032<3616:EOPMFO>2.0.CO;2).

4.3 Research paper no. 3

Janecki, M., Dybowski, D., Dzierzbicka-Głowacka, L., 2023. *The influence of biochemical parameters on primary production in the Gulf of Gdańsk region: A model study.* Oceanologia. <https://doi.org/10.1016/j.oceano.2023.05.001>

(IF¹ = 2.778; MEiN² = 100)

¹Journal 5-Year Impact Factor (IF) according to the Journal Citation Reports

²Journal score according to the list of the Polish Ministry of Education and Science

Available online at www.sciencedirect.com

ScienceDirect

journal homepage: www.journals.elsevier.com/oceanologia

ORIGINAL RESEARCH ARTICLE

The influence of biochemical parameters on primary production in the Gulf of Gdańsk region: A model study

Maciej Janecki*, Dawid Dybowski, Lidia Dzierzbicka-Głowacka

Ecohydrodynamics Laboratory, Physical Oceanography Department, Institute of Oceanology, Polish Academy of Sciences, Sopot, Poland

Received 31 March 2023; accepted 23 May 2023

Available online xxx

KEYWORDSGulf of Gdańsk;
Biochemical
parameters;
Primary production;
Phytoplankton;
Numerical modelling

Abstract Understanding the changing levels of biochemical parameters and the factors that influence them throughout the seasons is crucial for comprehending the dynamics of marine ecosystems. It also helps us identify potential threats that could harm their condition, aiding decision-making processes related to their protection. This study focuses on examining the variations in nutrients (such as nitrates, phosphates, and silicates), dissolved oxygen, and phytoplankton within the Gulf of Gdańsk. Additionally, we analyze the primary production process at three representative locations. To achieve this, we used data from the *EcoFish* biochemical numerical model. To ensure the model's accuracy, we compared its results with *in situ* data from the ICES database. The comparison revealed high correlations and minimal errors. Furthermore, we investigated how limiting factors impact primary phytoplankton production and demonstrated how the intensity of spring diatom blooms influences the nature of cyanobacterial blooms in the summer.

© 2023 Institute of Oceanology of the Polish Academy of Sciences. Production and hosting by Elsevier B.V. This is an open access article under the CC BY-NC-ND license (<http://creativecommons.org/licenses/by-nc-nd/4.0/>).

* Corresponding author: Ecohydrodynamics Laboratory, Physical Oceanography Department, Institute of Oceanology Polish Academy of Sciences, Powstańców Warszawy 55, 81-712 Sopot, Poland. Tel.: (+48) 587-311-912.

E-mail addresses: mjanecki@iopan.pl (M. Janecki), dwybowski@iopan.pl (D. Dybowski), dzierzb@iopan.pl (L. Dzierzbicka-Głowacka).

Peer review under the responsibility of the Institute of Oceanology of the Polish Academy of Sciences.

<https://doi.org/10.1016/j.oceano.2023.05.001>

0078-3234/© 2023 Institute of Oceanology of the Polish Academy of Sciences. Production and hosting by Elsevier B.V. This is an open access article under the CC BY-NC-ND license (<http://creativecommons.org/licenses/by-nc-nd/4.0/>).



Production and hosting by Elsevier

Please cite this article as: M. Janecki, D. Dybowski and L. Dzierzbicka-Głowacka, The influence of biochemical parameters on primary production in the Gulf of Gdańsk region: A model study, *Oceanologia*, <https://doi.org/10.1016/j.oceano.2023.05.001>

1. Introduction

Primary production in marine environments is associated with the process of photosynthesis, in which organisms such as phytoplankton (and other photosynthesizing organisms) use sunlight, water, and carbon dioxide to produce organic matter. Phytoplankton is a key component of the marine food web and plays an important role in shaping the ecosystem of the Gulf of Gdańsk (Verity and Smetacek, 1996). It serves as the primary source of food for many organisms, such as zooplankton (for example invertebrates) or small fish, which then are consumed by larger fish, birds, and marine mammals. Various factors, including water temperature, nutrient availability, and sunlight, influence primary production in the Gulf of Gdańsk. Its location at the mouth of the Vistula River (and other smaller rivers), which provides nutrient-rich freshwater, makes it a particularly productive area (Tomczak et al., 2016).

The Baltic Sea is exposed to a range of natural processes and anthropogenic stressors (Hans von Storch, 2021). These include climate change, rising sea levels, coastal processes, excessive nutrient loads resulting in eutrophication, hypoxia, acidification, agriculture, fisheries, organic pollution, sunken munitions, marine litter, underwater noise and tourism (Reckermann et al., 2021; Szymczycha et al., 2019).

During the latest socioecological assessment, the Baltic Sea achieved a Baltic Health Index (BHI) score of 76 out of 100, indicating that its overall condition is suboptimal and achieving management objectives and associated targets requires significant effort (Blenckner et al., 2021). Regionally, the Gulf of Gdańsk achieved the lowest BHI score of 55 among all regions considered, mainly due to a low assessment in relation to contaminants, carbon storage, and lasting special places. Therefore, continuous monitoring of the state of the Gulf of Gdańsk and appropriate management of human maritime activities is particularly important to minimize their negative impact on the condition of its waters.

The project *Knowledge transfer platform FindFISH* (short: *FindFISH*) (Dzierzbicka-Głowacka et al., 2018) is perfectly suited to the implementation of the aforementioned tasks (monitoring and management of human activities). The project aimed to develop a user-friendly platform to provide fishermen and scientists with accessible knowledge and information regarding the Gulf of Gdańsk's physical and biological state. As part of the project, a *Fish Module* was designed to generate maps indicating the best environmental conditions for specific commercially caught fish species in the Gulf of Gdańsk, such as herring, sprat, and flounder. This tool enables targeted fishing, reducing unintended catch and minimizing pollution caused by fishing expeditions, thus promoting environmental protection.

The heart of *FindFISH* is the 3D prognostic ecohydrodynamic model *EcoFish*, developed within the project. The *EcoFish* model (www.findfish.pl) operates in real-time mode, creating 48-hour forecasts of hydrodynamic parameters (water temperature, salinity, sea currents, sea surface height) and biochemical parameters (nitrate, phosphate, silicate, chlorophyll *a*, phytoplankton and microzooplankton biomass, dissolved oxygen and dissolved organic carbon concentration).

The hydrodynamic part of the *EcoFish* model was described in separate papers (Janecki et al., 2021, 2022), along with the analysis of the variability of the physical parameters, confirming a very good agreement between the model results and environmental data. In this work, we focus on the biochemical part of the *EcoFish* model. The following chapters present the results for the biochemical parameters, their variability, and a comparison with in situ data from the ICES database.

One of the three groups of phytoplankton implemented in the *EcoFish* model is Cyanobacteria. Cyanobacteria are prokaryotes but have historically been grouped with eukaryotic "algae" and at varying times have been referred to as "blue-greens" or "blue-green algae" (Carmichael, 2008; O'Neil et al., 2012). This name does not reflect any relationship between cyanobacteria and other organisms called algae. Cyanobacteria are a distinct group of bacteria that perform oxygenic photosynthesis, and it is only the chloroplast in eukaryotic algae to which the cyanobacteria are related (Sato, 2021).

Although we are aware of the updated classification of Cyanobacteria, for the purposes of our study, we have chosen to treat Cyanobacteria as a component of phytoplankton as it was traditionally understood. This decision is motivated by the need to maintain consistency with previous studies and the existing literature, ensuring comparability and facilitating model-based analyses. By acknowledging the revised systematic position of Cyanobacteria while using the term "phytoplankton" within the scope of our research, we aim to strike a balance between the historical perspective and the contemporary scientific understanding.

The purpose of the paper is not only to prove, that the *EcoFish* model provides reliable results on biochemical variables for the Gulf of Gdańsk. By analyzing the variability of nutrients (nitrates, phosphates and silicates), dissolved oxygen and phytoplankton in the Gulf of Gdańsk, we wanted to describe their impact on the pattern and intensity of the primary production. The rich nutrient deposition from rivers can significantly alter the biomass distribution of all phytoplankton groups.

The analysis of the seasonal variability dynamics of the primary production process is extremely important in the context of the conducted research, as it is a process directly related to the production and consumption of oxygen in the waters of the Gulf of Gdańsk. Dissolved oxygen concentration is one of the four parameters (along with temperature, salinity, and depth) that constitute an input variable crucial for the *Fish Module*.

2. Material and methods

2.1. Study area

The *EcoFish* model domain encompasses an enlarged area of the Gulf of Gdańsk (Figure 1). It is one of the most important coastal areas in the southern part of the Baltic Sea, with unique oceanographic and hydrological conditions. The western part of the Gulf of Gdańsk can be divided into a shallow part called the Puck Bay, and further west into the semiclosed Puck Lagoon (Majewski, 1972). The Vistula, which is the largest river flowing into the bay and carry-

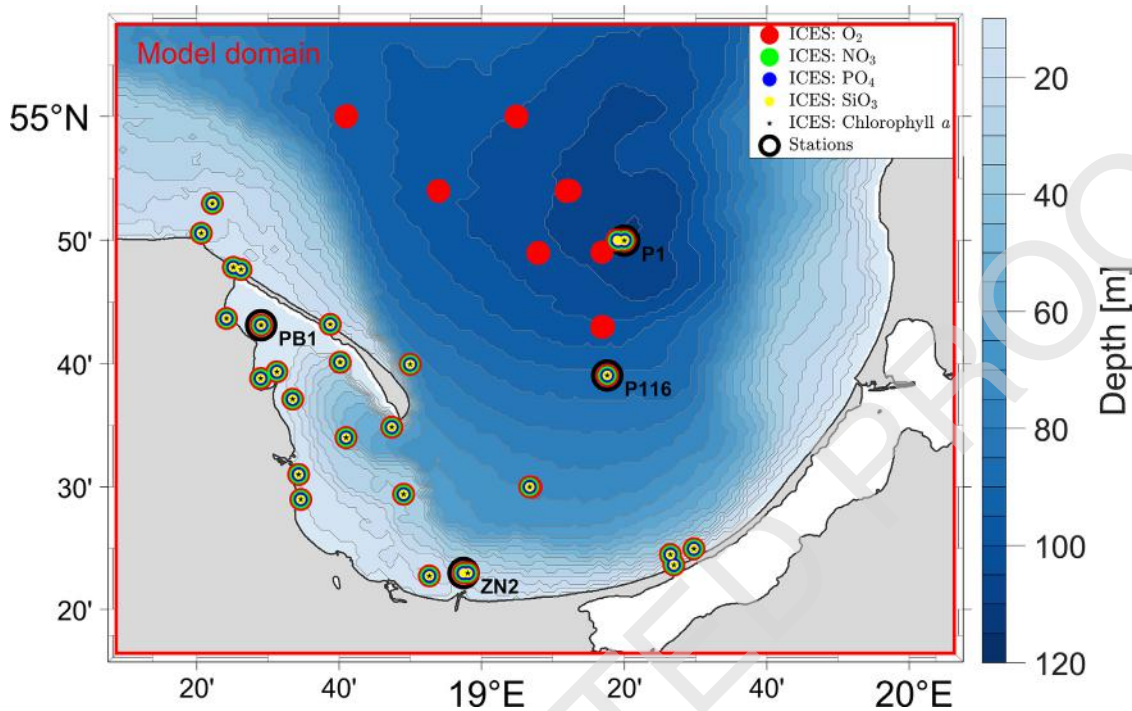


Figure 1 The *EcoFish* model domain with bathymetry, the location of environmental data from the ICES database, and the stations where primary production was investigated.

119 ing nutrients and other substances originating from industry
 120 and other human activities, has a significant impact on the
 121 hydrology of the Gulf of Gdansk (Voss et al., 2005; Witek
 122 et al., 1997). The Gulf of Gdansk also contains the largest
 123 Polish ports, such as Gdansk and Gdynia, which have a signif-
 124 icant impact on its environment due to pollution, maritime
 125 transport, and fishing (HELCOM, 2010).

126 2.2. In situ data

127 To verify whether the *EcoFish* model accurately reproduces
 128 the variability of biochemical parameters in the Gulf of
 129 Gdansk, the International Council for the Exploration of the
 130 Sea¹ (ICES) database was used. The ICES database for the
 131 years 2017–2020 contained 3329 measurements of oxygen
 132 (O_2), 2370 measurements of nitrate (NO_3), 2592 measure-
 133 ments of phosphate (PO_4), 2610 measurements of silicate
 134 (SiO_3), and 972 measurements of chlorophyll *a*. Most of the
 135 data originated from the shallow waters in the Puck Bay
 136 area and the southern part of the Gulf of Gdansk. Only
 137 a small fraction (mainly for oxygen concentration) was lo-
 138 cated at greater depths in the open sea (Figure 1).

139 2.3. The *EcoFish* model

140 2.3.1. Configuration

141 The *EcoFish* model is a three-dimensional, numerical prog-
 142 nostic model of the Gulf of Gdansk ecosystem with a hor-
 143 izontal resolution of 575 m, which was developed as part

of the *FindFISH* project. The model is divided into 26 verti-
 cal levels, each with a thickness of 5 m. The *EcoFish* model
 consists of:

- Hydrodynamic component – this is an ocean model based
 on the Parallel Ocean Program (POP) code, which has
 been described and validated (for water temperature
 and salinity) in a separate article (Janecki et al., 2021);
- Biochemical component – this is an NPZD-type biochemi-
 cal model, which is described and validated in this paper;
- *Fish Module* – this is an additional element created
 within the *FindFISH* project, which, based on data from
 the hydrodynamic and biochemical components, allows
 for the creation of maps of optimal environmental condi-
 tions for the habitat of fish (sprat, herring, and flounder)
 commercially caught in the Gulf of Gdansk region.

In addition to the three main components in which sim-
 ulations are conducted, the *EcoFish* model includes dedi-
 cated modules for processing input and output data, data
 assimilation modules (for surface temperature and chloro-
 phyll *a*), and a module coordinating the model in the oper-
 ational mode. Its task is to control the components, handle
 errors, and transmit data between modules.

146 2.3.2. Water – water border

The *EcoFish* model domain is connected with the Baltic Sea
 from the north and northwest, which creates the need to
 provide the model with boundary conditions (open bound-
 ary). These forcings are transmitted to the *EcoFish* model
 using the results from the 3D CEMBS model with a horizontal
 resolution of 2 km (Dzierzbicka-Głowacka et al., 2013a,b).

¹ <https://data.ices.dk>.

Table 1 Rivers mouths' locations included within the *EcoFish* model domain and mean runoff.

	Source	River name	Longitude	Latitude	Mean runoff [$\text{m}^3 \text{s}^{-1}$]
1	HYPE	Vistula	18.95	54.35	1064
2	HYPE	Bold Vistula	18.78	54.37	2.05
3	HYPE	Still Vistula	18.66	54.41	6.06
4	HYPE	Oliwski Stream	18.60	54.42	0.31
5	HYPE	Kamienny Stream	18.56	54.46	0.45
6	HYPE	Kacza	18.56	54.48	0.29
7	HYPE	Sewage Canal	18.51	54.61	0.21
8	SWAT	Zagórska Stream	18.47	54.63	0.11
9	SWAT	Reda	18.47	54.64	0.48
10	SWAT	Mrzezino Canal	18.46	54.66	0.20
11	SWAT	Gizdepka	18.46	54.66	0.30
12	SWAT	Żelistrzewo Canal	18.45	54.70	0.17
13	SWAT	Plutnica	18.39	54.72	0.91

173 2.3.3. Atmosphere forcing

174 At the water-atmosphere boundary, the *EcoFish* model is
 175 driven by meteorological forcing. These forcings are derived
 176 from the UM (Unified Model)², developed at the Interdisciplinary
 177 Centre for Mathematical and Computational Modelling of the University
 178 of Warsaw (ICM UW). Some of the obtained parameters (wind speed,
 179 air temperature, specific humidity, atmospheric pressure, precipitation,
 180 radiation) are directly used as forcings after interpolation onto the
 181 *EcoFish* model grid. The missing parameters are calculated by the
 182 atmospheric data module, which is an integral part of the *EcoFish*
 184 model.

185 2.3.4. Land-water linkage

186 In the *EcoFish* model, 13 rivers that flow into the Gulf of
 187 Gdańsk are taken into account (Table 1). Information about the
 188 volume of freshwater (runoff) and nutrients deposition for six rivers
 189 whose mouths are located in the area of the Puck Commune comes
 190 from the SWAT model (Kalinowska et al., 2020, 2018; Wielgat et al.,
 191 2021). SWAT was developed as part of the *Integrated Information-Predictive Service*
 192 *WaterPUCK* project (Dybowski et al., 2019; Dzierzbicka-Głowacka
 193 et al., 2019, 2022). The remaining seven rivers use runoff data from
 194 the Hydrological Predictions for the Environment (HYPE) model
 195 (Arheimer et al., 2012; Donnelly et al., 2016). Data on the amount
 196 of nutrient deposition in the HYPE model were available only in the
 197 form of monthly averages for the period 1980–2010. As a result of
 198 the HELCOM directives, the actual amounts of these substances
 199 entering the Baltic Sea from the territory of the Republic of Poland
 200 have been significantly reduced over the past 30 years (Pastuszak
 201 et al., 2018). The use of 30-year averages would lead to overestimation
 202 and distortion of the actual flow. Therefore, nutrient deposition for
 203 HYPE rivers was set based on the work of Pastuszak et al. (2018).
 204 Nitrate concentrations were established at 0.9 mg dm^{-3} , ammonia at
 205 0.07 mg dm^{-3} , phosphate at 0.07 mg dm^{-3} , and silicate at
 206 1.1 mg dm^{-3} . Concentrations were linked to daily volumes

of freshwater introduced by these rivers, obtaining a satisfactory
 210 estimate of deposition (Dybowski et al., 2020). 211

212 2.3.5. NPZD-type biochemical model

213 The implementation of environmental variables in the *EcoFish*
 214 model was carried out by determining the source and sink functions
 215 for four types of nutrients (phosphates – PO_4 , nitrates – NO_3 ,
 216 ammonia – NH_4 , and silicates – SiO_3), three groups of phytoplankton
 217 and microzooplankton. There are two things that the general equation
 218 of turbulent diffusion with an advection component does in the
 219 *EcoFish* model (Equation (1)). First, it describes the dynamics
 220 of changes in concentrations. Second, it serves as the link where
 221 the transfer of forcings between the hydrodynamic and biochemical
 222 components takes place. 223

$$\frac{\partial S}{\partial t} + (V + w_s) \cdot \nabla S = \frac{\partial}{\partial z} \left(K_z \frac{\partial S}{\partial z} \right) + \sum_{i=1}^2 \frac{\partial}{\partial x_i} \left(K_{x_i} \frac{\partial S}{\partial x_i} \right) + F_s \quad (1)$$

224 where S is each model variable, $V(u, v, w)$ is the velocity
 225 vector, w_s is the sinking velocity of pelagic detritus, K_z ,
 226 K_{x_i} , are vertical and horizontal turbulent diffusion coefficients
 227 and F_s is the biogeochemical source-sink term which describes
 228 possible sources and losses of the diffusing substance in the
 229 space being studied.

230 The source code of the biochemical part was filled with
 231 interrelated dependencies describing the variability of the primary
 232 production of phytoplankton biomass, as well as the concentration
 233 of chlorophyll a , microzooplankton biomass, nutrients concentrations
 234 (phosphates, nitrates, ammonia and silicates), dissolved oxygen,
 235 pelagic and benthic detritus (for NO_3 and PO_4). Source and sink
 236 functions were determined based on knowledge of the biological
 237 and chemical processes that occur in the marine environment and
 238 their mutual relationships (Dzierzbicka-Głowacka et al., 2013b;
 239 Moore et al., 2001). 240

241 The biochemical component of the *EcoFish* model requires
 242 information about the state and physical conditions of the ecosystem
 243 it represents. Therefore, it depends on the hydrodynamic component
 244 and operates in the same domain (Figure 1). 245

² www.meteo.pl.

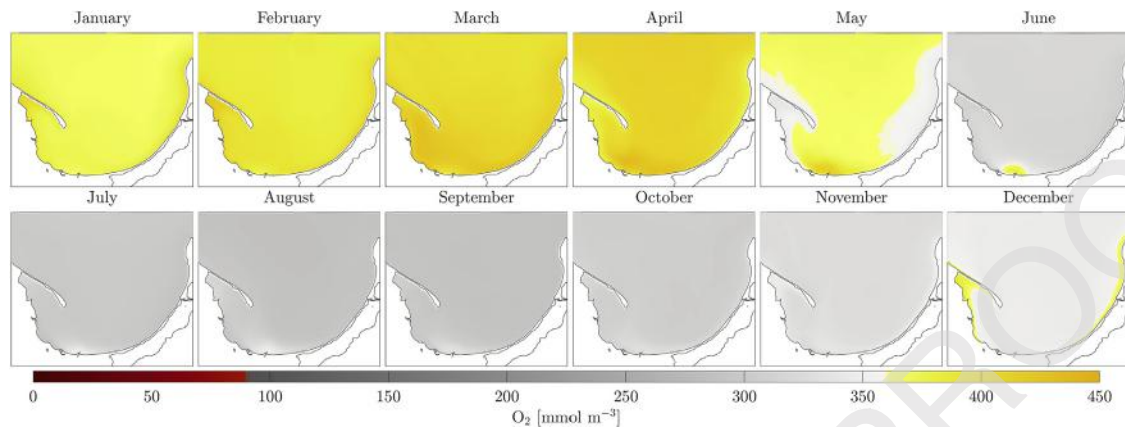


Figure 2 Average monthly concentrations of dissolved oxygen (O_2) in the surface layer for the period 2017–2020.

246 3. Results

247 In the following chapters, we present monthly average con-
 248 centrations of dissolved oxygen (O_2), nitrate (NO_3), phos-
 249 phate (PO_4), silicate (SiO_3), and phytoplankton (as chloro-
 250 phyll *a*) for a four-year period from January 1, 2017 to De-
 251 cember 31, 2020.

252 Furthermore, each biochemical variable was validated by
 253 comparing it with the available measurements from the ICES
 254 database (Figure 1). Basic statistical measures were deter-
 255 mined: means, standard deviations (STD), Pearson's correla-
 256 tion coefficients (r) and root mean square errors (RMSE).

257 In the *EcoFish* model, all depth levels have a thickness
 258 of 5 meters. However, the ICES data had non-uniform sam-
 259 pling density in the water column (e.g., 0 m, 1 m, 2.5 m,
 260 4 m, 5 m, 10 m, 20 m). This resulted in several ICES mea-
 261 surements that differed from each other but corresponded
 262 to the same *EcoFish* model value, or an ICES measurement
 263 was taken from a depth at the boundary of two adjacent
 264 model levels. This could cause unnatural distortion of the
 265 validation results. To eliminate the negative impact of the
 266 non-uniform data density, interpolation (and extrapolation)
 267 between *EcoFish* model levels with a step of 0.1 m was ap-
 268 plied. Among the available methods of interpolation and ex-
 269 trapolation, the third-order simplified Hermite polynomial
 270 method (PCHIP) was chosen, which interpolates both the
 271 function and its first derivative.

272 3.1. Dissolved oxygen – O_2

273 Seasonal changes in water oxygenation are influenced by
 274 both climatic factors and primary production. Maximum
 275 concentrations of dissolved oxygen occur in the winter-
 276 spring season, with the combination of low water tempera-
 277 ture and the beginning of the phytoplankton bloom period
 278 (Figure 2). The maximum monthly average concentration of
 279 dissolved oxygen in the surface layer of the *EcoFish* model
 280 (calculated for the entire domain area) occurred in March
 281 and April, and was $398.79 \text{ mmol m}^{-3}$ and $401.03 \text{ mmol m}^{-3}$,
 282 respectively. In the following months, as the temperature
 283 increases, the solubility decreases, and so the oxygen con-
 284 centration in the water drops. However, there are areas
 285 where an increase in dissolved oxygen is noticeable as a
 286 result of intensive primary production. The minimum con-

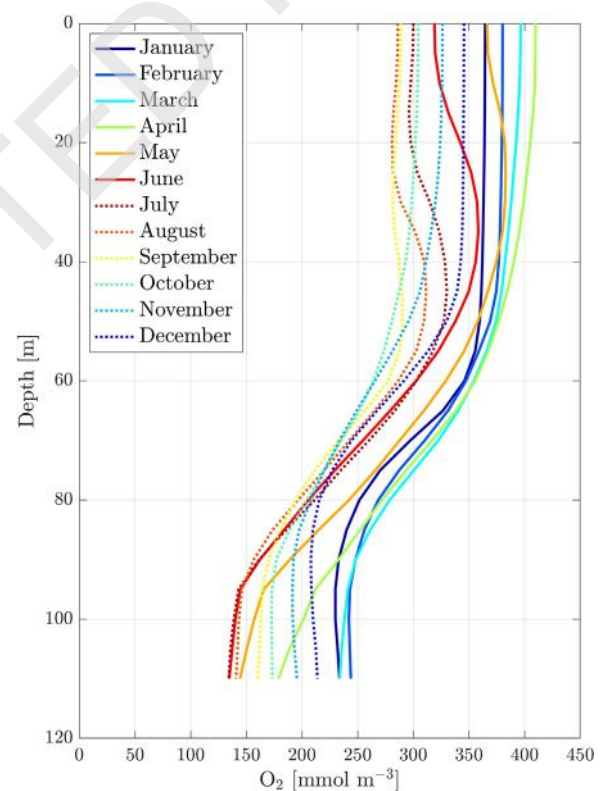


Figure 3 Vertical profiles of the mean monthly dissolved oxygen concentrations (O_2) for the period 2017–2020.

287 concentration of dissolved oxygen in the surface layer occurred
 288 in August with a mean value of $269.50 \text{ mmol m}^{-3}$. The average
 289 annual concentration of dissolved oxygen in the surface
 290 layer was $344.07 \text{ mmol m}^{-3}$ with a standard deviation of
 291 $40.33 \text{ mmol m}^{-3}$.

292 When examining the vertical profiles of mean monthly
 293 oxygen concentrations (Figure 3) at station P1 situated in
 294 the Gdańsk Deep area (Figure 1), it becomes apparent that
 295 there is a distinct variation as depth increases. In all months
 296 except summer months (May, June, July, and August), the
 297 oxygen concentration remains constant (homogeneous) un-
 298 til a depth of approximately 40–50 meters. Then it begins

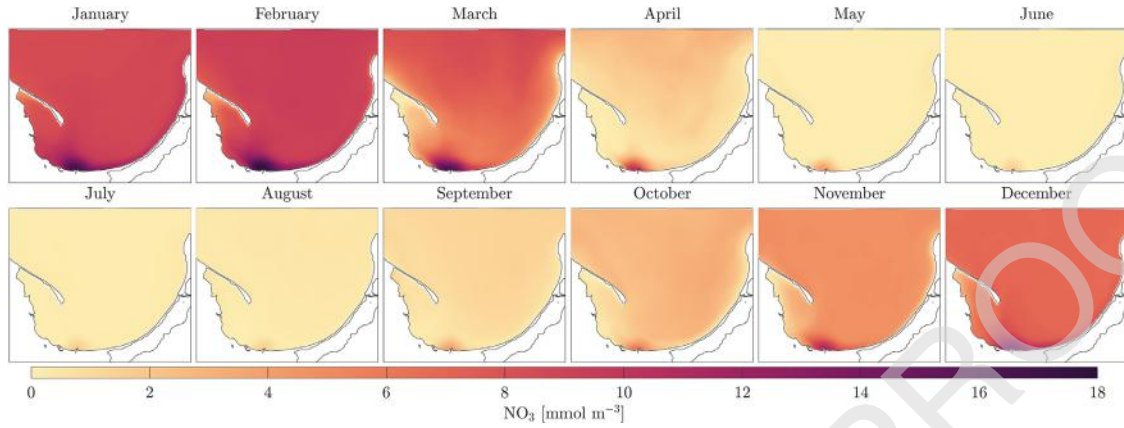


Figure 4 Average monthly concentrations of nitrates (NO_3) in the surface layer for the period 2017–2020.

299 to drop with increasing depth until it stabilizes at a depth of
 300 about 90 meters. In the winter months, this stable concentra-
 301 tion at the greatest depths is higher (up to approximately
 302 250 mmol m^{-3} in February). This is due to stronger vertical
 303 mixing, pushing the cold, oxygenated water from the sur-
 304 face to greater depths. In the summer, such strong vertical
 305 mixing does not occur, and the average oxygen concentra-
 306 tion at greater depths drops to 150 mmol m^{-3} and below.

307 The concentration of dissolved oxygen is the most impor-
 308 tant modeled variable that needed to be verified for accu-
 309 racy. This is because it is used as an input parameter for
 310 the *Fish Module*. In the ICES database for the years 2017–
 311 2020, there were 3329 measurements available within the
 312 *EcoFish* model domain. After comparing ICES measurements
 313 with their corresponding values from the *EcoFish* model, a
 314 good reproduction of oxygen concentration variability was
 315 obtained for high O_2 concentrations. However, for measure-
 316 ments from great depths with concentrations dropping be-
 317 low 200 mmol m^{-3} the *EcoFish* model tended to slightly
 318 overestimate the results. The validation results for oxygen
 319 are presented in Table S1. Pearson's correlation coefficients
 320 ranged from 0.70 to 0.80 and RMSE from 61.14 to 86.85
 321 mmol m^{-3} . For the entire period 2017–2020, a Pearson cor-
 322 relation coefficient of 0.75 and a root mean square error of
 323 $70.86 \text{ mmol m}^{-3}$ were obtained.

324 3.2. Nitrates – NO_3

325 The highest concentrations of nitrates in the *EcoFish* model
 326 were observed in winter and early spring, before the start
 327 of the growing season. The lowest concentrations were ob-
 328 served in the summer months (Figure 4). The highest aver-
 329 age monthly concentration of nitrates in the surface layer of
 330 the *EcoFish* model (calculated for the entire domain area)
 331 occurred in February (8.66 mmol m^{-3}), and the lowest in
 332 June (0.03 mmol m^{-3}).

333 By examining the vertical profiles of the nitrate concentra-
 334 tions at station P1 (Figure 5), we can observe that the
 335 highest amounts of this compound (concentrations greater
 336 than 9 mmol m^{-3}) accumulate at depths from 60 meters to
 337 the seabed. Nitrates are also present closer to the surface,
 338 but there is a clear seasonal variability associated with the
 339 intensity of primary production and phytoplankton blooms.
 340 Nitrates in the euphotic zone begin to decline in the spring

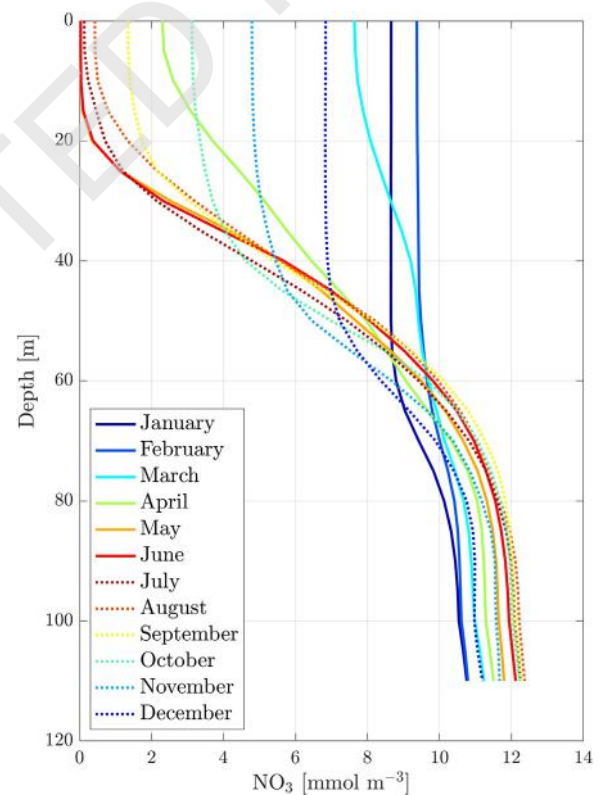


Figure 5 Vertical profiles of mean monthly concentrations of nitrates (NO_3) for the period 2017–2020.

341 due to diatom blooms, and subsequently decrease until July,
 342 when they are completely depleted in the layer to about
 343 20 meters. In September, slow extraction of nitrates from
 344 deeper layers to the surface occurs because of fall storms,
 345 causing an increase in their concentrations. In October, due
 346 to low primary production, nitrate concentrations in the
 347 surface layer can reach values greater than 3 mmol m^{-3} .
 348 In the following months, nitrate concentrations on the sur-
 349 face gradually increase, reaching their maximum of around
 350 9 mmol m^{-3} in January and February.

351 In the ICES database for the years 2017–2020, there were
 352 2370 nitrate concentration measurements available. After

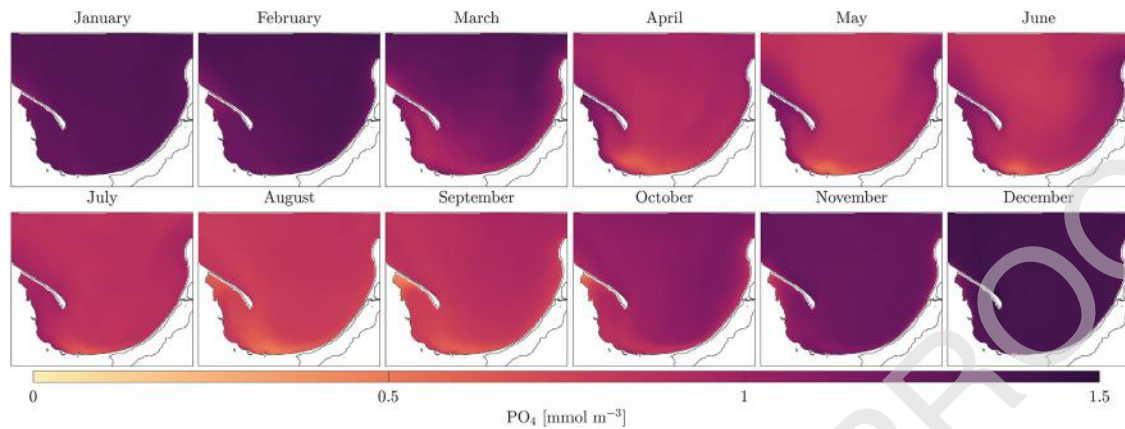


Figure 6 Average monthly concentrations of phosphates (PO_4) in the surface layer for the period 2017–2020.

353 comparing the ICES measurements with their corresponding
 354 values from the *EcoFish* model, a moderately good repre-
 355 sentation of the dynamics of nitrate concentrations was ob-
 356 tained. This is because the ICES measurements came mainly
 357 from locations that are under strong pressure from the land,
 358 in the form of nutrient deposition from rivers flowing into
 359 the Puck Bay and Gulf of Gdańsk. The results of the nitrate
 360 validation are presented in Table S2. Pearson's correlation
 361 coefficients ranged from 0.40 to 0.59 and the root mean
 362 square errors ranged from 3.28 to 4.02 mmol m^{-3} . For the
 363 entire period 2017–2020, a Pearson correlation coefficient
 364 of 0.46 and a mean squared error of 3.77 mmol m^{-3} were
 365 obtained.

366 3.3. Phosphates – PO_4

367 The highest average monthly concentration of phosphates
 368 in the surface layer of the *EcoFish* model (calculated for
 369 the entire domain area) occurred in December (1.34 mmol
 370 m^{-3}), while the lowest occurred in August (0.89 mmol m^{-3})
 371 (Figure 6).

372 The vertical profiles of the monthly mean concentrations
 373 of phosphates at station P1 (Figure 7) have a similar char-
 374 acter to that of nitrates. The largest amounts of this com-
 375 pound (concentrations of about 2 mmol m^{-3} and higher) also
 376 lie at great depths (below 60 meters). Variations in this pa-
 377 rameter in the euphotic zone are related to primary produc-
 378 tion and the vegetative cycle of phytoplankton. Phosphorus
 379 is a limiting factor for the growth of all groups of phyto-
 380 plankton, which means that it is consumed more or less in-
 381 tensively throughout the year.

382 The decrease in phosphate concentrations in the eu-
 383 photic zone begins in March with the beginning of diatom
 384 blooms and lasts until August, when the highest inten-
 385 sity of primary production associated with cyanobacterial
 386 blooms occurs (caused by the highest water temperatures
 387 in the surface layer). From September, phosphate concen-
 388 trations begin to systematically increase (as water tempera-
 389 ture drops) until December, when they reach their maximum
 390 value for the whole year (approximately 1.4 mmol m^{-3}).

391 In the bottom layer, the situation is reversed. The highest
 392 concentrations occur in summer due to the settling of dead
 393 organic matter. There, as a result of the mineralization pro-
 394 cess, phosphorus is released back into the water column by

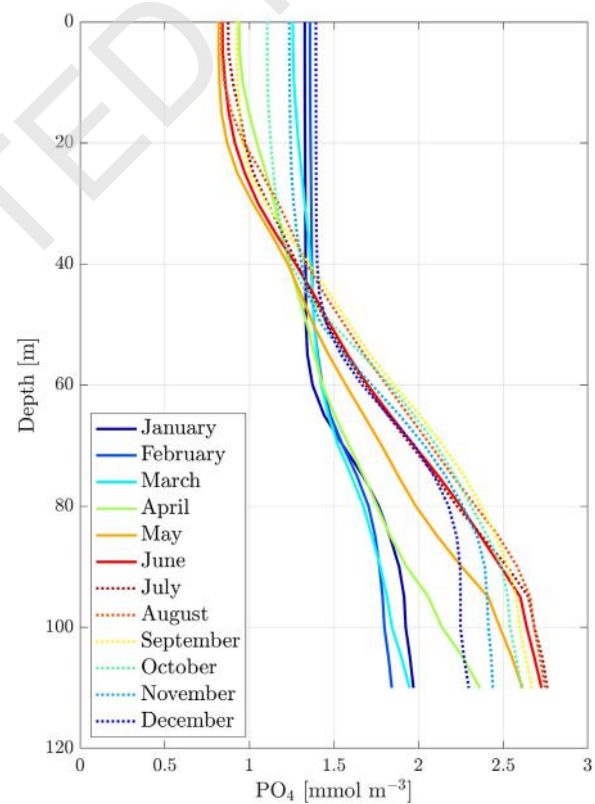


Figure 7 Vertical profiles of mean monthly concentrations of phosphates (PO_4) for the period 2017–2020.

395 microorganisms, leading to elevated concentrations. In win-
 396 ter months, because of vertical mixing, phosphate deposits
 397 are transported to the surface, replenishing the resources
 398 used after the vegetative period of phytoplankton.

399 In the ICES database for the years 2017–2020, there
 400 were 2592 phosphate concentration measurements avail-
 401 able. After comparing the ICES measurements with the
 402 corresponding values from the *EcoFish* model, we observed
 403 that the model systematically overestimates phosphate con-
 404 centrations. Despite this, high correlations were obtained
 405 in individual years, as well as acceptable RMSEs. The results
 406 of the phosphate validation are presented in Table S3.

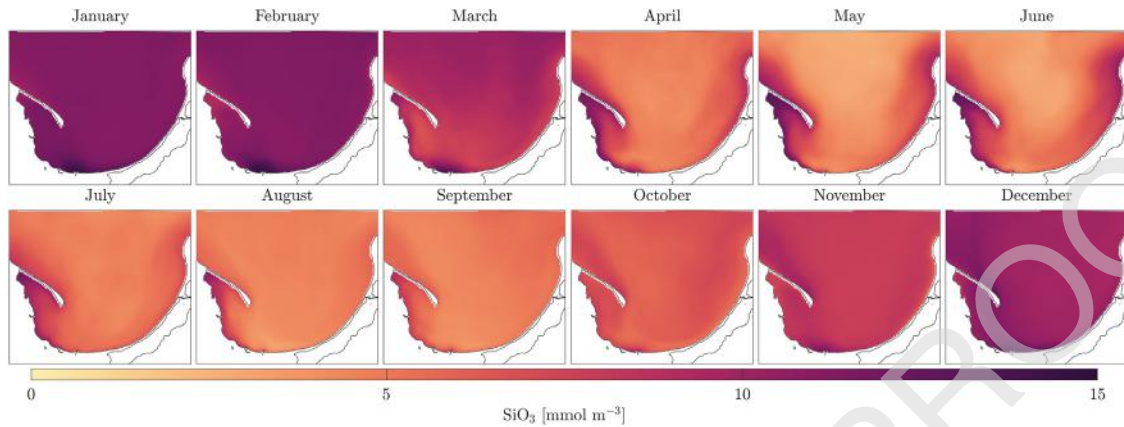


Figure 8 Average monthly concentrations of silicates (SiO_3) in the surface layer for the period 2017–2020.

407 Pearson's correlation coefficients were in the range of 0.66
 408 to 0.77, and the root mean squared errors ranged from
 409 0.37 to 0.75 mmol m^{-3} . For the entire comparison period
 410 (2017–2020), we obtained a Pearson correlation coefficient
 411 of 0.65 and a root mean square error of 0.63 mmol m^{-3} .

412 3.4. Silicates – SiO_3

413 Nitrogen and phosphorus are the main factors that limit bi-
 414 ological production, however, the primary production of di-
 415 atoms is also limited by silicates. The *EcoFish* model shows
 416 the highest concentrations of silicates in winter and early
 417 spring, before the start of the growing season (Figure 8).
 418 In March, when intense spring diatom blooms begin, silicate
 419 concentrations begin to decrease and remain at lower levels
 420 until autumn. The highest average monthly concentrations
 421 of silicates in the surface layer occurred in February (10.69
 422 mmol m^{-3}) and January (10.67 mmol m^{-3}), while the lowest
 423 occurred in May (6.49 mmol m^{-3}).

424 Analysis of vertical profiles of mean monthly silicate con-
 425 centrations at station P1 reveals large differences between
 426 values at depths below 80 meters (Figure 9). Silicate con-
 427 centrations from May to August are up to twice as high as
 428 concentrations in winter months (from December to March).
 429 In the layer between 40 and 60 meters, silicates remain at
 430 similar levels (usually between 10 and 15 mmol m^{-3}) regard-
 431 less of the month analyzed. In the euphotic layer, there is an
 432 inverse relationship compared to the bottom. Silicate con-
 433 centrations are higher in the winter months, outside of the
 434 phytoplankton growing season. Lower values are observed
 435 from spring to fall and are closely related to their con-
 436 sumption in the primary production process to increase the
 437 biomass of diatoms.

438 In the ICES database for the years 2017–2020, there were
 439 2610 silicate concentration measurements available. A com-
 440 parison of in situ data from the ICES database with the cor-
 441 responding values from the *EcoFish* model confirmed that
 442 the model performs well in reproducing the dynamics of
 443 silicate concentrations, although there is a noticeable ten-
 444 dency to underestimate the results, mainly for high SiO_3
 445 concentrations above 40 mmol m^{-3} . The results of the sil-
 446 icate validation are presented in Table S4. Pearson correla-
 447 tion coefficients ranged from 0.51 to 0.74, and root mean
 448 square errors ranged from 7.45 to 12.58 mmol m^{-3} . For the

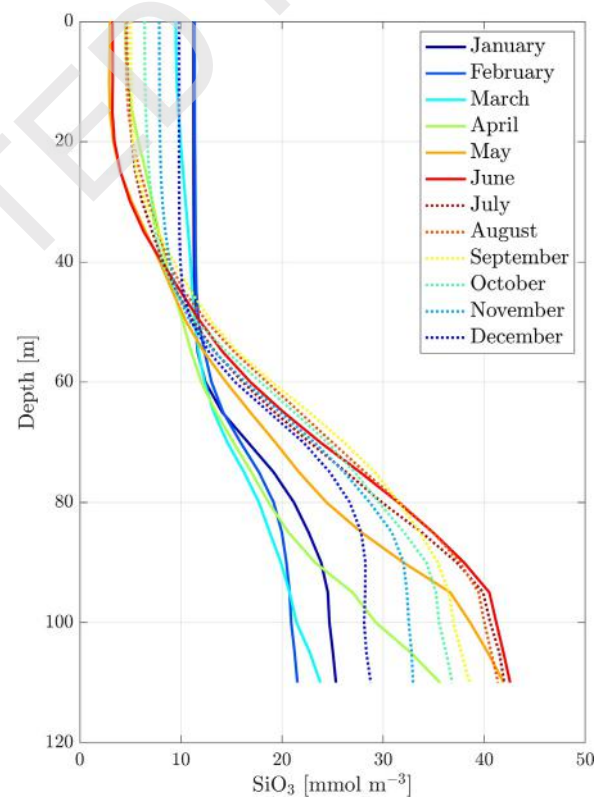


Figure 9 Vertical profiles of mean monthly concentrations of silicates (SiO_3) for the period 2017–2020.

entire comparison period (2017–2020), we obtained a Pear- 449
 son correlation coefficient of 0.62 and a root mean square 450
 error of 10.32 mmol m^{-3} . 451

452 3.5. Chlorophyll a

453 In the *EcoFish* model, phytoplankton is divided into three 454
 groups. The first group represents nano- and pico-sized phy- 455
 toplankton, whose growth is limited by nitrogen, phospho- 456
 rus, temperature, and light. The second group represents 457
 large phytoplankton, mainly diatoms, whose production is 458
 limited by the same factors plus silica. The third group is 459

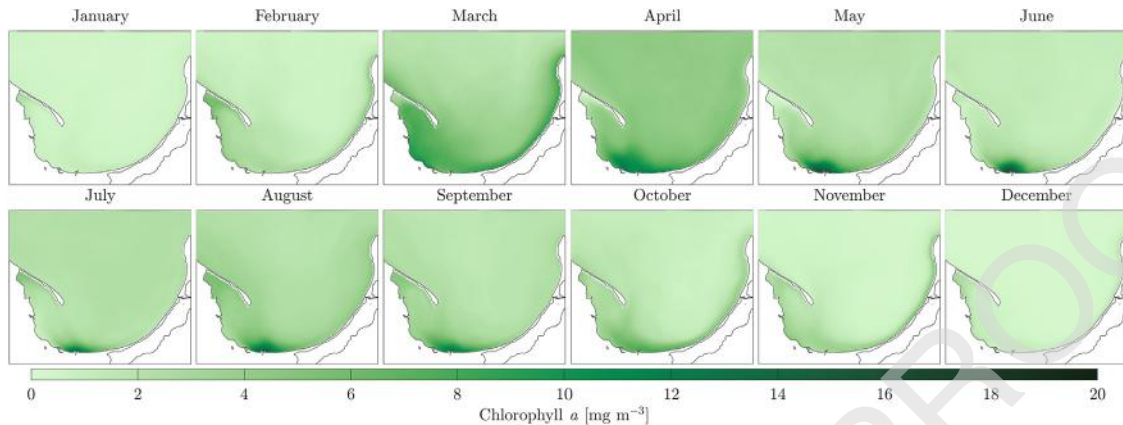


Figure 10 Average monthly concentrations of chlorophyll *a* in the surface layer for the period 2017–2020.

459 cyanobacteria, which have the ability to fix nitrogen di-
 460 rectly from the atmosphere and whose production is limited
 461 only by phosphorus, light, and temperature.

462 The highest concentrations of chlorophyll *a* are observed
 463 relatively close to the shore, where the access to nutrients
 464 is greatest due to the deposition of biogenic substances
 465 carried by rivers. The highest modeled monthly mean chloro-
 466 phyll *a* concentration for the period 2017–2020 in the sur-
 467 face layer occurred in April and was 3.91 mg m^{-3} (Figure 10).
 468 The lowest concentrations were observed in the winter
 469 months, with a minimum of 0.29 mg m^{-3} (in December).

470 In vertical distribution, chlorophyll *a* concentrations
 471 reach their highest values in the upper layer of the wa-
 472 ter column. Then the concentration values decrease with
 473 depth. Below 60 meters deep, chlorophyll *a* occurs in negli-
 474 gible amounts or is not detected at all (Figure 11).

475 The highest chlorophyll *a* concentration values occur in
 476 spring (in April and March) when there is a maximum in phy-
 477 toplankton biomass due to the spring diatom bloom and in
 478 July due to the growth of cyanobacteria. In months with
 479 primary production, concentrations rapidly decrease with
 480 depth. This is particularly visible in summer. There are no
 481 longer nitrates in the euphotic zone, and cyanobacteria
 482 grow only in the surface layer, where they are in direct con-
 483 tact with nitrogen fixed from the atmosphere.

484 In the ICES database for the years 2017–2020, only 972
 485 chlorophyll *a* concentration measurements were available.
 486 Most of the measurements were taken in the area of Puck
 487 Bay and the southern part of the Gulf of Gdansk, close
 488 to the coast (Figure 1). After comparing the ICES mea-
 489 surements with the corresponding values from the *EcoFish*
 490 model, we obtained a moderately good representation of
 491 the chlorophyll *a* variability. The results of the chlorophyll
 492 *a* validation are presented in Table S5. Pearson's correlation
 493 coefficients ranged from 0.50 to 0.63, and root mean square
 494 errors ranged from 1.77 to 3.63 mg m^{-3} . For the entire
 495 comparison period (2017–2020), we obtained a Pearson
 496 correlation coefficient of 0.50 and a root mean square error
 497 of 2.77 mg m^{-3} .

498 3.6. Primary production

499 An important aspect studied in this article is primary pro-
 500 duction, which is a key function of marine ecosystems. Pri-

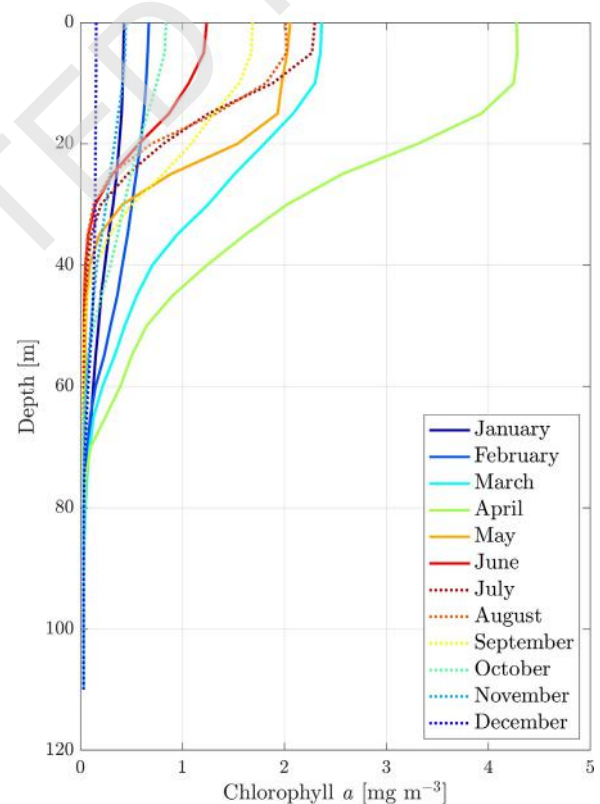


Figure 11 Vertical profiles of mean monthly concentrations of chlorophyll *a* for the period 2017–2020.

501 mary production is a process in which photosynthetic organ-
 502 isms, such as phytoplankton, use solar energy to produce or-
 503 ganic compounds. In this way, primary production forms the
 504 basis for the entire marine food chain, providing energy and
 505 organic compounds for zooplankton and other marine organ-
 506 isms. Studying the seasonal variability of primary production
 507 in the Gulf of Gdansk is important to understand the impact
 508 of climate change and other factors on marine ecosystems
 509 and their ability to adapt to changing conditions.

510 Primary production in the water column was calculated
 511 for each of the modeled phytoplankton groups at three se-
 512 lected locations (Figure 1).

- 513 • PB1 – (54°43'N, 18°29'E) – the inner part of the Puck
- 514 Bay, depth of about 10 m,
- 515 • ZN2 – (54°22'N, 18°57'E) – the mouth of the Vistula
- 516 River, depth of about 20 m,
- 517 • P116 – (54°39'N, 19°17'E) – the central part of the Gulf
- 518 of Gdańsk, depth of about 90 m.

519 The location PB1 comes from a very shallow area (inner
520 part of Puck Bay), which is geographically limited from the
521 northeast by the Hel Peninsula and from the east by the
522 Rybitwia Mielizna, effectively preventing the mixing of wa-
523 ter from Puck Bay with both the open Baltic Sea and the
524 Outer Puck Bay. Six rivers flow into the inner part of Puck
525 Bay (Zagórska Stream, Reda, Mrzezino Canal, Gizdepka,
526 Żelistrzewo Canal and Płutnica), causing the PB1 station to
527 be regularly supplied with moderate amounts of nutrients.

528 The ZN2 station is located in the shallow coastal part of
529 the Gulf of Gdańsk, close to the mouth of the Vistula River.
530 The Vistula is the largest river in the region and carries more
531 than 1000 m³ s⁻¹ of freshwater on average, along with huge
532 amounts of nutrients, strongly affecting the primary produc-
533 tion of phytoplankton at this location.

534 The P116 station, with a depth of approximately 90 me-
535 ters, is located in the open waters of the central part of the
536 Gulf of Gdańsk. It is located far from the river mouths and
537 is not geographically constrained by any factors.

538 The rate of primary production in the chosen locations
539 was determined from the *EcoFish* model for a one-year pe-
540 riod, from January 1 to December 31, 2021. Production val-
541 ues were calculated for the entire water column and com-
542 pared with the limiting functions. The temperature of the
543 water, the availability of light and the phosphates are lim-
544 ing factors for the growth of all phytoplankton groups im-
545 plemented in the *EcoFish* model. The growth of the group
546 representing nano- and pico-sized phytoplankton is addition-
547 ally limited by the availability of nitrates, while the growth of
548 diatoms is additionally limited by the availability of nitrates
549 and silicates.

550 The beginning of phytoplankton bloom in the first weeks
551 of the year is primarily dependent on the amount of light
552 available. At station PB1, the annual cycle of primary pro-
553 duction begins in mid-February with a low intensity (up to
554 1000 mg C m⁻² d⁻¹) and a short-lived diatom bloom, which
555 ends in the first days of March (Figure 12a). This is due to the
556 shallow depth at this location. All available nitrogen in the
557 water column is rapidly depleted and reaches zero values at
558 the end of February (Figure 12d). As a result of such a short
559 diatom bloom period, a very small amount of phosphate is
560 consumed. It remains in the water column in large amounts
561 until mid-June, when a bloom of cyanobacteria begins due
562 to the appropriately high water temperature (Figure 12b).
563 Due to favorable conditions (available light, high water tem-
564 perature, and a large amount of phosphates), this process is
565 very intense (more than 2000 mg C m⁻² d⁻¹) and lasts until
566 mid-September, when it is stopped due to decreasing water
567 temperature and replaced by a bloom of small phytoplank-
568 ton (Figure 12c). The cycle of primary production at this
569 station in 2021 slows down in the first days of November,
570 which is due to a low amount of available light and a drop
571 in the water temperature. The period of unfavorable condi-
572 tions for phytoplankton bloom, which lasts until next spring,
573 allows the replenishment of the nutrient fields (Figure 12d).

574 In the P116 station, the annual cycle of primary produc-
575 tion (similar to the PB1 station) begins in mid-February. It
576 is initiated by the appearance of appropriately strong light
577 and favorable water temperature (Figure 13a). However,
578 unlike station PB1, this bloom does not end in the first half
579 of March due to the depletion of available nitrate. Station
580 P116 is located at a great depth in the central part of the
581 Gulf of Gdańsk. Because of the vertical mixing, nitrates are
582 carried from greater depths toward the surface, sustaining
583 the bloom of diatoms until mid-April. Then, the nitrate re-
584 sources are depleted (Figure 13d), leading to a slowdown
585 in production (around 200 to 300 mg C m⁻² d⁻¹), but not
586 enough to completely stop it (Figure 13a). Diatoms remain
587 in the water column at a level of around 10–20 mmol C
588 m⁻³ until the first days of July. In mid-July, a cyanobacte-
589 rial bloom begins (Figure 13b). This is a month later than
590 at the PB1 station (Figure 12b), which is a consequence of
591 the lower water temperature in the open water. The shal-
592 low, enclosed coastal zone where station PB1 is located
593 heats up much faster than the deep waters of the central
594 part of the Gulf of Gdańsk. However, cyanobacterial pro-
595 duction is not as intense as at station PB1. In addition to the
596 lower water temperature, the decisive factor here may be a
597 smaller amount of available phosphate (Figure 13d), which
598 was partially consumed during the diatom bloom that began
599 in mid-February. In 2021, small phytoplankton practically
600 does not occur at this station (Figure 13c), which is also re-
601 lated to lower levels of phosphate in summer compared to
602 the PB1 station and competition for access to nitrogen and
603 phosphorus with diatoms.

604 At the ZN2 station located at the mouth of the Vistula
605 River, the diatom bloom begins in a period similar to that of
606 the other stations, i.e., in mid-February (Figure 14a). The
607 highest intensity of diatom primary production occurs here
608 in May and June, reaching rates of up to 4000 mg C m⁻² d⁻¹.
609 In July 2021, diatom production is slowed and a very intense
610 bloom of small phytoplankton begins, which lasts until the
611 end of October, with peak production in August.

612 However, the cyanobacteria bloom has a completely dif-
613 ferent pattern than at the other stations. The station is lo-
614 cated in a shallow coastal area, which means that the water
615 temperature is high enough for the cyanobacterial blooms
616 to start in mid-May (Figure 14b). However, cyanobacteria
617 do not appear until the end of July, competing for phos-
618 phate with small phytoplankton (Figure 14c) that grow at
619 the same time. This leads to a very low primary production
620 rate associated with this species (below 1000 mg C m⁻² d⁻¹)
621 causing suppression of cyanobacterial blooms. The produc-
622 tion of cyanobacteria ends in October because the water
623 temperature is too low.

624 It should be noted that station ZN2 is located at the
625 mouth of the Vistula River. Nitrates and silicates do not
626 deplete here after spring diatom bloom and are available
627 throughout the year (Figure 14d). This is related to the mas-
628 sive deposition of nutrients from the Vistula.

629 4. Discussion

630 4.1. *EcoFish* Model Evaluation

631 The article presents the biochemical component of the
632 three-dimensional numerical model *EcoFish*, which was

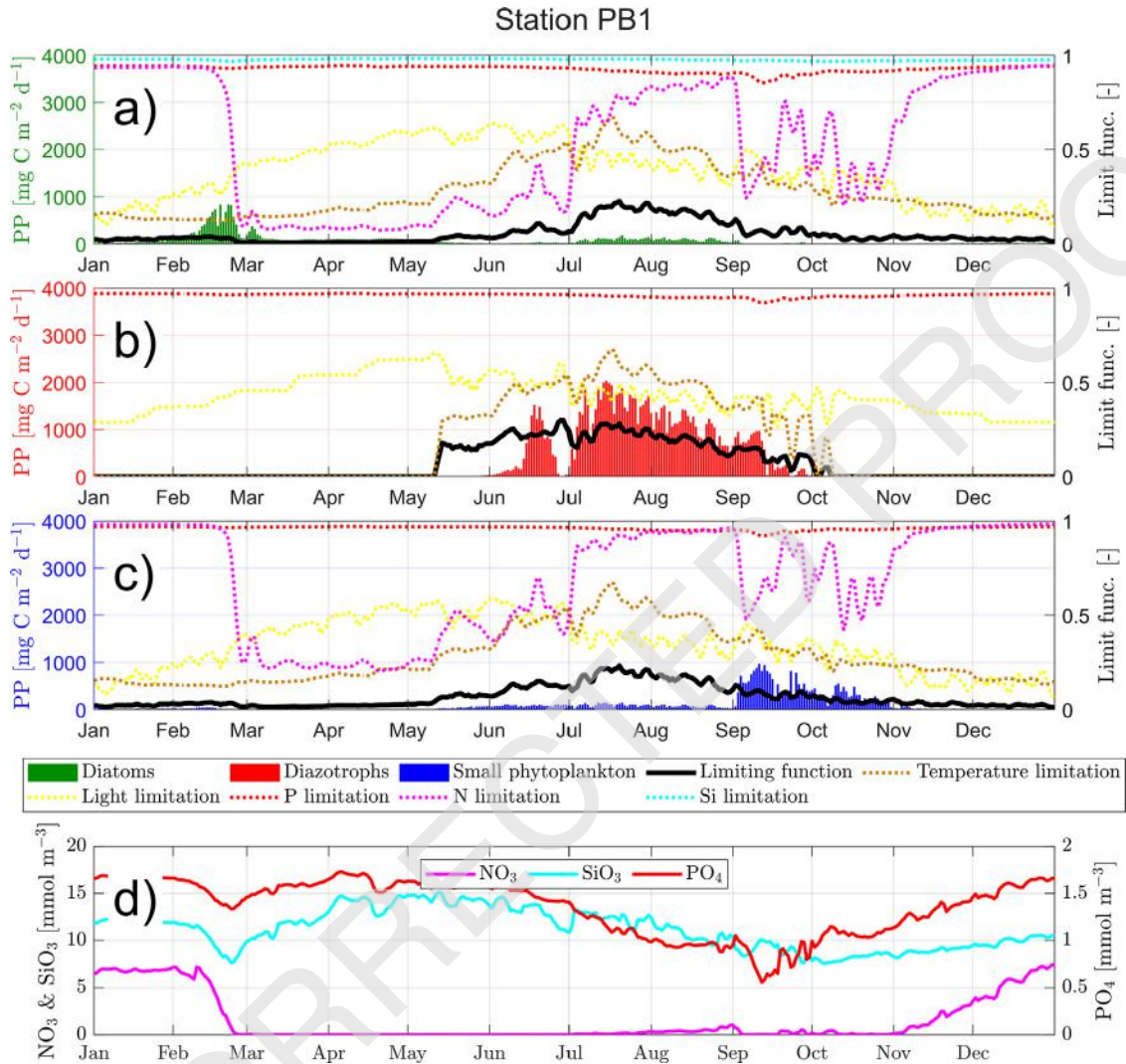


Figure 12 Primary production rate in 2021 for the entire water column at PB1 station for a) diatoms, b) cyanobacteria, and c) small phytoplankton, compiled with limiting factors, and d) concentrations of nutrients.

633 used to analyze the basic biochemical parameters that char- 634
 634 acterize the dynamics of the Gulf of Gdańsk ecosystem. To 635
 635 increase the accuracy of the results obtained in the *EcoFish* 636
 636 model, a module was implemented to assimilate satellite 637
 637 data for SST and chlorophyll *a*. The source of these data is 638
 638 the *SatBaltyk*³ system (Woźniak et al. 2011a,b).

639 Statistical validation of the *EcoFish* model, allowed us 640
 640 to verify the accuracy of the results in terms of the spa- 641
 641 tiotemporal variability of nitrate, phosphate, silicate, dis- 642
 642 solved oxygen, and chlorophyll *a* concentrations. Validation 643
 643 was carried out using available in situ data from the ICES 644
 644 database for the period from January 1, 2017 to December 645
 645 31, 2020, and basic statistical quantities were determined.

646 The *EcoFish* model tends to systematically overestimate 647
 647 (for oxygen, nitrates, and phosphates) and underestimate 648
 648 (for chlorophyll *a* and silicates) the results. However, these 649
 649 values are not significantly different from the measurement 650
 650 data and are acceptable after careful examination of the

651 causes. The main reason for the lower correlations, espe- 652
 652 cially in the validation of chlorophyll *a* and nitrates, is the 653
 653 specificity of the ICES experimental database itself. The 654
 654 map with the distribution of measurements for individual 655
 655 variables (Figure 1) shows that the vast majority of mea- 656
 656 surements come from shallow coastal areas with depths that 657
 657 generally do not exceed 30 meters. Approximately half of 658
 658 all measurements were taken within 2 km from the shore. 659
 659 Only a small number of points are located in the open sea 660
 660 or at greater depths. More open-water measurements can 661
 661 only be found in the ICES database for oxygen concentra- 662
 662 tion, resulting in the highest correlation (0.75) between all 663
 663 biochemical variables we analyzed.

664 Another cause is the construction of the numerical model 665
 665 itself. The *EcoFish* model is a *z*-type model. It means that 666
 666 the model maintains the thickness of layers in a cell rather 667
 667 than the number of layers, in contrast to sigma-type mod- 668
 668 els, where the same number of layers exists at each point, 669
 669 but they differ in their thickness. *z*-type models are less 670
 670 capable of dealing with shallow water areas, where the 671
 671 water column often consists of only two or three layers.

³ www.satbaltyk.pl.

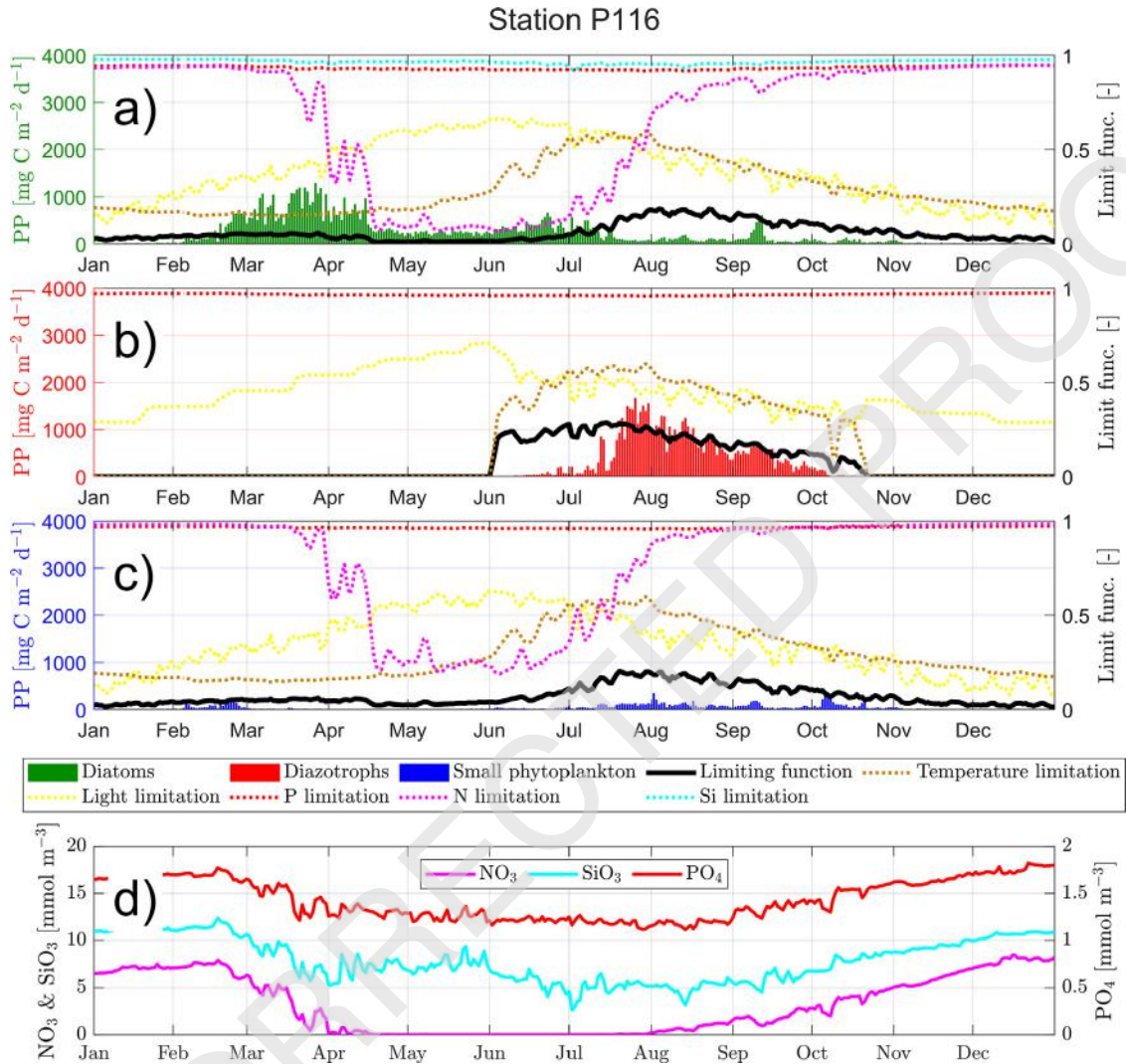


Figure 13 Primary production rate in 2021 for the entire water column at P116 station for a) diatoms, b) cyanobacteria, and c) small phytoplankton, compiled with limiting factors, and d) concentrations of nutrients.

672 This configuration of the model, combined with the mea- 673
 674 surement database, where most measurements come from 675
 676 shallow coastal locations, negatively affects the validation 677
 678 results.

679 Worse results in the validation of nutrients may be related 680
 681 to inaccurate data for rivers (especially the Vistula) 682
 683 and the constant concentrations adopted for some rivers 684
 685 (according to Pastuszak et al., 2018). The volume of fresh 686
 687 water carried into the Gulf of Gdańsk by rivers was determined 688
 689 on the basis of long-term averages, which can result in insufficiently 690
 691 accurate deposition modeling, especially during periods of high daily 692
 693 variability. To ensure the numerical stability of the *EcoFish* model, large 694
 695 rivers were subjected to distribution, that is, the volume of fresh water 696
 697 along with the nutrients carried by them was divided into several 698
 699 model cells (several dozen for the Vistula).

688 4.2. Nutrients

689 The oxygen present in seawater primarily comes from pho- 690
 691 tosynthesis and gas exchange with the atmosphere. How-

692 ever, when organic matter decomposes, oxygen is consumed, 693
 694 leading to potential deficits. In the central Baltic Sea, there are 695
 696 regular periods of stagnation in deep waters due to limited water 697
 698 exchange with the North Sea and consistent haline stratification 699
 700 (Conley et al., 2009, 2002; Meier et al., 2017). During these periods, 701
 702 nitrates are depleted, phosphates and ammonia concentrations 703
 704 increase, and dissolved oxygen levels decrease significantly at 705
 706 greater depths. Consequently, toxic hydrogen sulfide can emerge 707
 708 (Kuliński et al., 2022). The situation can improve temporarily 709
 710 when salty and oxygen-rich waters from the North Sea enter the 711
 712 Baltic Sea. However, such strong inflows have become increasingly 713
 714 infrequent in recent times, with only a few events occurring every 715
 716 decade (Mohrholz, 2018). In the deep basins of the Baltic Sea 717
 718 (including the area of the Gdańsk Deep), hypoxia and anoxia have 719
 720 increased significantly over the past century (Carstensen et al., 2014), 721
 722 and in 2019, the area of hypoxia covered approximately 32% of 723
 724 the surface of the Baltic Proper (Hansson et al., 2020). Despite 725
 726 efforts made to substantially decrease nutrient deposition in the 727
 728 waters of the Baltic Sea over the past few 729
 730 years, hypoxia remains a significant problem in the Baltic Sea 731
 732 region.

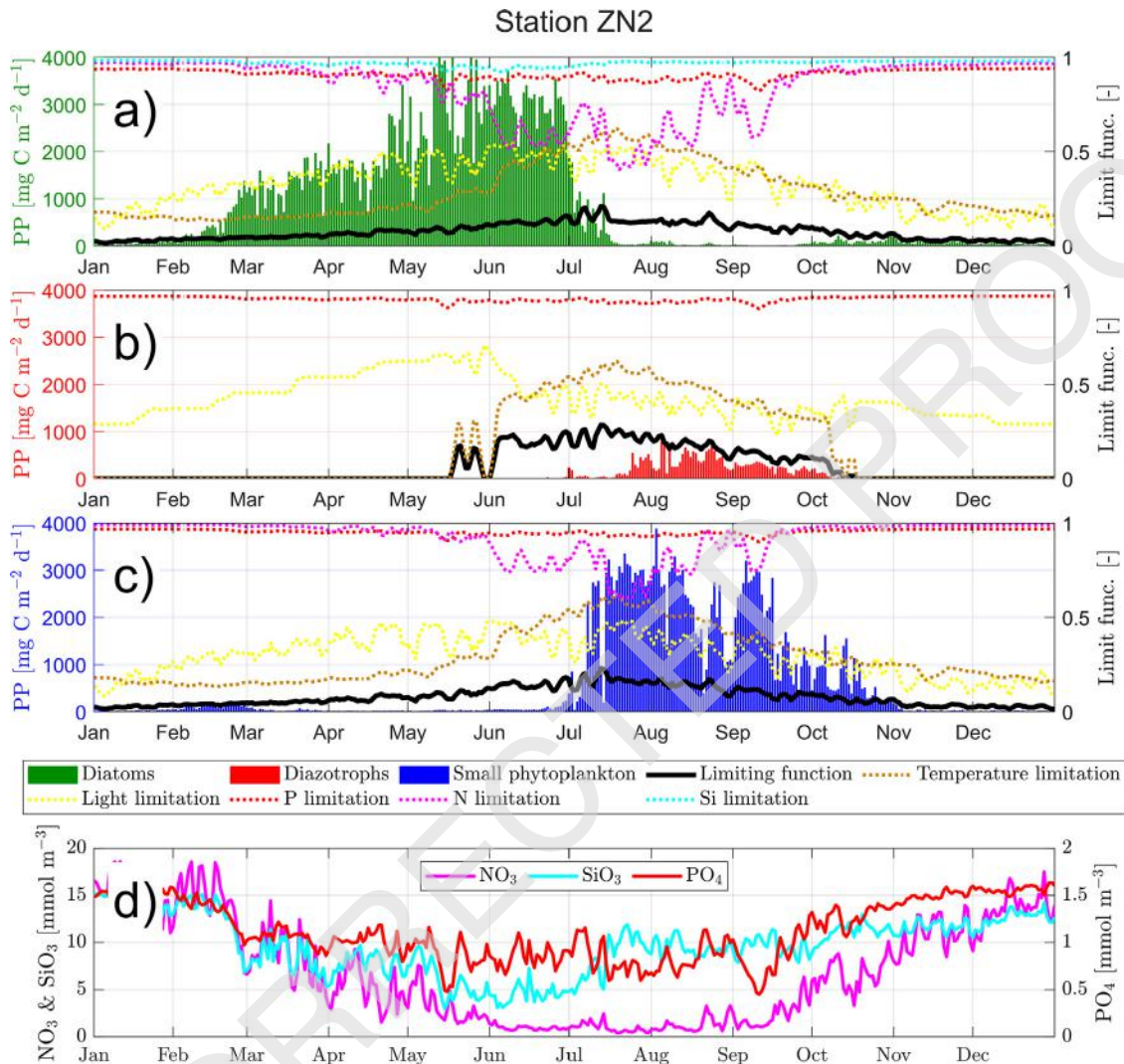


Figure 14 Primary production rate in 2021 for the entire water column at ZN2 station for a) diatoms, b) cyanobacteria, and c) small phytoplankton, compiled with limiting factors, and d) concentrations of nutrients.

712 decades, areas suffering from oxygen deficiency (mainly
713 caused by eutrophication) have not experienced reoxygena-
714 tion. This is because a considerable amount of nutrients has
715 accumulated in the sediments and is gradually released into
716 the water column, leading to prolonged oxygen depletion
717 (McCrackin et al., 2018).

718 Nitrogen is one of the main limiting factors for primary
719 production and an element causing eutrophication of the
720 marine environment (Andersen et al., 2015; Malone and
721 Newton, 2020). It is present in the water column in the form
722 of nitrates (NO_3), nitrites (NO_2) and ammonia (NH_4). Nitro-
723 gen concentrations in surface waters of the Gulf of Gdańsk
724 vary spatially – higher concentrations occur at the mouth
725 of the Vistula River, and lower in the central part of the
726 Gulf. These compounds show a strongly marked seasonal cycle.
727 The highest concentrations are recorded in early spring
728 (March), when the melting waters of the Vistula River flow
729 into the Gulf. Then, as a result of nitrogen consumption by
730 phytoplankton and underwater plants, nitrogen compound
731 concentrations decrease, eventually falling below the mea-
732 surement capabilities of the methods used.

The basic difference between nitrogen and phosphorus is
that the most plant-available forms (nitrates and nitrites)
are not as easily regenerated as phosphates (Paytan and
McLaughlin, 2007; Vitousek and Howarth, 1991). Therefore,
practically every year from May to the end of September,
seawater is devoid of nitrates and nitrites, which should
limit the development of phytoplankton in summer. How-
ever, existing phosphate resources promote the develop-
ment of Cyanobacteria, which can directly fixate nitrogen
(N_2) from the atmosphere. Among them are species that
produce toxins, such as *Nodularia spumigena* and *Aphanizomenon flos-aquae*,
which pose a potential threat to other organisms that live in the Gulf of Gdańsk
and to the health and lives of people resting by the sea.

Phosphorus, along with nitrogen, is the main element
that causes eutrophication of the marine environment
(Tamminen and Andersen, 2007). Phosphates in the Gulf
of Gdańsk exhibit a strong seasonal cycle, similar to that
of nitrates. The highest concentrations of phosphates are
recorded in winter and early spring, before the start of the
growing season. Then, as a result of the consumption of

754 phosphorus by phytoplankton and underwater vegetation, 814
755 phosphate concentrations decrease to low levels but are 815
756 not completely depleted, as is the case with nitrates. Phos- 816
757 phates are compounds with a short regeneration period, 817
758 which means that they are easily and quickly released by mi- 818
759 croorganisms (bacteria) from dead organic matter (Paytan 819
760 and McLaughlin, 2007). Therefore, shortly after the spring 820
761 bloom, they appear in marine waters in amounts sufficient 821
762 to provide a food base for species developing in the summer 822
763 (e.g., cyanobacteria). 823

764 Although chlorophyll *a* concentration is not a direct mea- 824
765 sure of phytoplankton biomass, it is one of the parameters 825
766 often used in oceanographic and limnological studies as an 826
767 indicator of the quantitative presence of phytoplankton in 827
768 water (Boyer et al., 2009; Gons et al., 2002; Randolph et al., 828
769 2008). The increase in phytoplankton biomass in the wa- 829
770 ters of the Gulf of Gdańsk has a seasonal cycle. The stages 830
771 of phytoplankton development are similar throughout the 831
772 area. The cycle begins in early spring (usually around Febru- 832
773 ary and March) with high nitrate concentrations and sea- 833
774 water temperatures of a few degrees Celsius. The rate of 834
775 primary production is usually very high during this period. 835
776 Due to the short life span of these microscopic plants and 836
777 the high productivity of the euphotic layer, phytoplankton 837
778 is the main source of energy for other components of the 838
779 ecosystem (Mosharov et al., 2022). Some phytoplankton is 839
780 directly consumed by herbivorous zooplankton, but a large 840
781 amount of phytoplankton sinks to the bottom. 841

782 4.3. Primary production cycle 842

783 The analysis of primary production (for the year 2021) is pre- 843
784 sented in Results (see 3.6. Primary production). The results 844
785 were compared with the limiting functions and concentra- 845
786 tions of nitrates, phosphates, and silicates, which are the 846
787 most important nutrients that limit the growth of phyto- 847
788 plankton. 848

789 As a result of this analysis, we confirm that in the first 849
790 weeks of the year, the factors determining the beginning of 850
791 the vegetation period are the availability of light and wa- 851
792 ter temperature. At each of the three locations analyzed 852
793 (PB1, P116, and ZN2), the first group that began the an- 853
794 nual production cycle in mid-February 2021 was diatoms. 854
795 However, the length and intensity of this bloom varied de- 855
796 pending on the location. The diatoms bloomed for the short- 856
797 est time (only until mid-March) at the PB1 station, where 857
798 the available nitrate was rapidly depleted due to the shal- 858
799 low depth. The availability of nitrates also determined the 859
800 end of the diatom bloom at station P116, but it lasted a 860
801 bit longer, until mid-April. After the spring diatom bloom, 861
802 there was a period without production (or with very low 862
803 production) at these stations until the water temperature 863
804 reached the optimal level for the start of cyanobacterial 864
805 blooms (June/July). These species can directly fix atmo- 865
806 spheric nitrogen, so their growth is not dependent on the 866
807 availability of nitrates in the water column. 867

808 A completely different situation prevailed at the ZN2 868
809 station, where due to the continuous supply of nutrients 869
810 (mostly nitrates and silicates) deposited with the Vistula 870
811 waters, the diatoms grew very intensively until July. Due 871
812 to this long growth period, diatoms consumed a very large 872
813 amount of phosphorus and, despite its continuous supply by

the Vistula, their level was lower than at the other stations, 814
effectively suppressing the intensity and duration of toxic 815
cyanobacterial blooms. 816

In the available scientific literature, many articles can be 817
found that analyze primary production in the Gulf of Gdańsk 818
(Mosharov et al., 2022; Ostrowska et al., 2022; Wasmund 819
et al., 2001; Witek et al., 1997; Zdun et al., 2021). In the 820
study by Ostrowska et al. (2022), the total yearly primary 821
production in the Gulf of Gdańsk (for the period 2010–2019) 822
ranged from 124 to 145 g C m⁻² year⁻¹. The values we ob- 823
tained for the year 2021 were higher, reaching 160.1 g C m⁻² 824
year⁻¹ at station P116, 168.2 g C m⁻² year⁻¹ at station PB1, 825
and 553.1 g C m⁻² year⁻¹ at station ZN2. 826

The lowest monthly means of daily primary production 827
occur in December, reaching 19.7 mg C m⁻² day⁻¹ at station 828
P116, 25.9 mg C m⁻² day⁻¹ at station PB1 and 64.9 mg C m⁻² 829
day⁻¹ at station ZN2. This result is consistent with previous 830
studies for this region (e.g., Ostrowska et al., 2022; Zdun 831
et al., 2021). 832

The highest monthly means of daily primary production 833
occur during the summer months. At station P116, it was 834
observed in August, with a value of 1021.6 mg C m⁻² day⁻¹. 835
The highest average of 1690.1 mg C m⁻² day⁻¹ was recorded 836
in July at station PB1. Station ZN2, on the other hand, ex- 837
hibited the highest primary production in June, with a value 838
of 3111.5 mg C m⁻² day⁻¹. 839

The maximum primary production in the Gulf of Gdańsk, 840
as reported by Ostrowska et al. (2022), is most often ob- 841
served in July and does not extend to August. The values 842
obtained in that study range from 603 mg C m⁻² day⁻¹ in 843
2017 to 1066 mg C m⁻² day⁻¹ in 2010. Zdun et al., 2021, 844
obtained the highest values in April and May, with primary 845
production exceeding 2000 mg C m⁻² day⁻¹. 846

The beginning of the vegetation period, as reported by 847
other studies (Ostrowska et al., 2022; Zdun et al., 2021), is 848
also in good agreement with our results. Furthermore, our 849
results agree with the experiment conducted by Sommer 850
et al. (2012), where it was confirmed that light availabil- 851
ity and temperature are the most important factors for the 852
timing of the spring bloom. 853

854 5. Conclusions 854

The *EcoFish* numerical model is part of the “*Knowledge 855*
transfer platform FindFISH” service, providing information 856
on hydrodynamic and biochemical variables for the Gulf 857
of Gdańsk area. Thanks to the numerical simulations from 858
the *EcoFish* model and the results for temperature, salinity 859
(presented in Janecki et al. 2021), and oxygen concentra- 860
tion, it is possible to operate the key element of the plat- 861
form, the *Fish Module*. Using these variables and the ap- 862
plied fuzzy logic method, the *Fish Module* allows the cre- 863
ation of maps of the most favorable environmental con- 864
ditions (Habitat Suitability Index) for the industrial fish- 865
ing of herring, sprat, and flounder in the Gulf of Gdańsk 866
area. 867

By presenting the most important biochemical variables 868
of the *EcoFish* model and conducting the validation, we have 869
confirmed that the results of numerical simulations are con- 870
sistent with in situ data and will provide a reliable set of 871
input data for the *Fish Module*. 872

873 In the analysis of primary production, we show that ge-
874 omorphological conditions and the deposition of nutrients
875 from rivers have a significant impact on its pattern and in-
876 tensity. The availability of nutrients can significantly alter
877 the biomass distribution of all phytoplankton groups.

878 An overly strong focus on limiting nitrate deposition in
879 river waters to inhibit marine eutrophication may ultimately
880 lead to the opposite situation, where short and small in-
881 tense diatom blooms in spring will be followed by long and
882 intense cyanobacterial blooms in summer. This is consistent
883 with the results obtained from a numerical experiment con-
884 ducted for Puck Bay by [Dybowski et al. \(2022\)](#). A reasonable
885 approach to any legislative decisions in this regard is partic-
886 ularly important in the era of climate change and increasing
887 water temperatures in seas and oceans, which will further
888 prolong the period of optimal temperature for the bloom of
889 this toxic and unwanted species from the perspective of the
890 region's specificity.

891 Uncited References

892 [Andersen et al., 2017](#), [Hansson et al., 2019](#), [Reckermann](#)
893 [et al., 2022](#), [von Storch, 2023](#)

894 Declaration of Competing Interest

895 The authors declare that they have no known competing fi-
896 nancial interests or personal relationships that could have
897 appeared to influence the work reported in this paper.

898 Acknowledgments

899 Calculations were carried out at the Academic Computer
900 Centre in Gdańsk.

901 We are grateful to the anonymous reviewers for valuable
902 comments on earlier versions of the manuscript.

903 Funding

904 Partial support for this study was provided by the project
905 "Knowledge transfer platform Find-Fish Numerical Forecast-
906 ing System for the Marine Environment of the Gulf of Gdańsk
907 for Fisheries," funded by the European Union through Euro-
908 pean Regional Development Fund Contract RPPM.01.01.01-
909 22-0025/16-00.

910 Some elements of the EcoFish model (i.e., river runoff
911 data) are based on the solutions developed during the Wa-
912 terPUCK project funded by National Centre for Research and
913 Development of Poland within the BIOSTRATEG III program
914 BIOSTRATEG3/343927/3/NCBR/2017.

915 Supplementary materials

916 Supplementary material associated with this article can be
917 found, in the online version, at doi:[10.1016/j.oceano.2023.](https://doi.org/10.1016/j.oceano.2023.05.001)
918 [05.001](https://doi.org/10.1016/j.oceano.2023.05.001).

References

- 920 Andersen, J.H., Carstensen, J., Conley, D.J., Dromph, K., Fleming-
921 Lehtinen, V., Gustafsson, B.G., Josefson, A.B., Norrko, A., Vill-
922 näs, A., Murray, C., 2017. Long-term temporal and spatial trends
923 in eutrophication status of the Baltic Sea. *Biol. Rev.* 92, 135–
924 149. <https://doi.org/10.1111/brv.12221>
- 925 Arheimer, B., Dahné, J., Donnelly, C., Lindström, G., Strömqvist, J.,
926 2012. Water and nutrient simulations using the HYPE model for
927 Sweden vs. the Baltic Sea basin – influence of input-data quality
928 and scale. *Hydrol. Res.* 43, 315–329. <https://doi.org/10.2166/nh.2012.010>
- 929 Blenckner, T., Möllmann, C., Stewart Lowndes, J., Griffiths, J.R.,
930 Campbell, E., De Cervo, A., Belgrano, A., Boström, C., Flem-
931 ing, V., Frazier, M., Neuenfeldt, S., Niiranen, S., Nilsson, A.,
932 Ojaveer, H., Olsson, J., Palmlov, C.S., Quaas, M., Rickels, W.,
933 Sobek, A., Viitasalo, M., Wikström, S.A., Halpern, B.S., 2021.
934 The Baltic Health Index (BHI): Assessing the social–ecological
935 status of the Baltic Sea. *People and Nature* 3, 359–375. <https://doi.org/10.1002/pan3.10178>
- 936 Boyer, J.N., Kelble, C.R., Ortner, P.B., Rudnick, D.T., 2009. Phy-
937 toplankton bloom status: Chlorophyll a biomass as an indicator
938 of water quality condition in the southern estuaries of Florida,
939 USA. *Ecol. Indic.* 9, 56–67. <https://doi.org/10.1016/j.ecolind.2008.11.013>
- 940 Carmichael, W., 2008. A world overview – One-hundred-twenty-
941 seven years of research on toxic cyanobacteria – Where do we
942 go from here? In: Hudnell, H.K. (Ed.), *Cyanobacterial Harmful*
943 *Algal Blooms: State of the Science and Research Needs*. Springer,
944 New York, NY, 619. *Adv. Exp. Med. Biol.* https://doi.org/10.1007/978-0-387-75865-7_4
- 945 Carstensen, J., Andersen, J.H., Gustafsson, B.G., Conley, D.J.,
946 2014. Deoxygenation of the Baltic Sea during the last century. *P.*
947 *Natl. Acad. Sci. USA* 111, 5628–5633. <https://doi.org/10.1073/pnas.1323156111>
- 948 Conley, D.J., Björck, S., Bonsdorff, E., Carstensen, J., Destouni, G.,
949 Gustafsson, B.G., Hietanen, S., Kortekaas, M., Kuosa, H.,
950 Markus Meier, H.E., Müller-Karulis, B., Nordberg, K., Norrko, A.,
951 Nürnberg, G., Pitkänen, H., Rabalais, N.N., Rosenberg, R.,
952 Savchuk, O.P., Slomp, C.P., Voss, M., Wulff, F., Zillén, L., 2009.
953 Hypoxia-Related Processes in the Baltic Sea. *Environ. Sci. Tech-*
954 *nol.* 43, 3412–3420. <https://doi.org/10.1021/es802762a>
- 955 Conley, D.J., Humborg, C., Rahm, L., Savchuk, O.P., Wulff, F., 2002.
956 Hypoxia in the Baltic Sea and Basin-Scale Changes in Phosphorus
957 Biogeochemistry. *Environ. Sci. Technol.* 36, 5315–5320. <https://doi.org/10.1021/es025763w>
- 958 Donnelly, C., Andersson, J.C.M., Arheimer, B., 2016. Using flow
959 signatures and catchment similarities to evaluate the E-HYPE
960 multi-basin model across Europe. *Hydrolog. Sci. J.* 61, 255–273.
961 <https://doi.org/10.1080/02626667.2015.1027710>
- 962 Dybowski, D., Dzierzbicka-Głowacka, L., 2022. Analysis of the im-
963 pact of nutrients deposited from the land side on the wa-
964 ters of Puck Lagoon (Gdańsk Basin, Southern Baltic): A model
965 study. *Oceanologia* 65 (2), 386–397. <https://doi.org/10.1016/j.oceano.2022.11.005>
- 966 Dybowski, D., Jakacki, J., Janecki, M., Nowicki, A., Rak, D.,
967 Dzierzbicka-Głowacka, L., 2019. High-Resolution Ecosystem
968 Model of the Puck Bay (Southern Baltic Sea)—Hydrodynamic
969 Component Evaluation. *Water-SUI* 11, 2057. <https://doi.org/10.3390/w11102057>
- 970 Dybowski, D., Janecki, M., Nowicki, A., Dzierzbicka-
971 Glowacka, L.A., 2020. Assessing the Impact of Chemical
972 Loads from Agriculture Holdings on the Puck Bay Envi-
973 ronment with the High-Resolution Ecosystem Model of
974 the Puck Bay, Southern Baltic Sea. *Water-SUI* 12, 2068.
975 <https://doi.org/10.3390/w12072068>
- 976 Dzierzbicka-Głowacka, L., Dybowski, D., Janecki, M., Woj-
977 978 979 980 981 982 983 984

- ciechowska, E., Szymczycha, B., Potrykus, D., Nowicki, A., Szymkiewicz, A., Zima, P., Jaworska-Szulc, B., Pietrzak, S., Pazikowska-Sapota, G., Kalinowska, D., Nawrot, N., Wielgat, P., Dembska, G., Matej-Lukowicz, K., Szczepańska, K., Puszkarczuk, T., 2022. Modelling the impact of the agricultural holdings and land-use structure on the quality of inland and coastal waters with an innovative and interdisciplinary toolkit. *Agr. Water Manage.* 263, 107438. <https://doi.org/10.1016/j.agwat.2021.107438>
- Dzierzbicka-Głowacka, L., Jakacki, J., Janecki, M., Nowicki, A., 2013a. Activation of the operational ecohydrodynamic model (3D CEMBS) – the hydrodynamic part. *Oceanologia* 55 (3), 519–541. <https://doi.org/10.5697/oc.55-3.519>
- Dzierzbicka-Głowacka, L., Janecki, M., Dybowski, D., Szymczycha, B., Obarska-Pempkowiak, H., Wojciechowska, E., Zima, P., Pietrzak, S., Pazikowska-Sapota, G., Jaworska-Szulc, B., Nowicki, A., Kłostowska, Ż., Szymkiewicz, A., Galer-Tatarowicz, K., Wichorowski, M., Białoskórski, M., Puszkarczuk, T., 2019. A New Approach for Investigating the Impact of Pesticides and Nutrient Flux from Agricultural Holdings and Land-Use Structures on Baltic Sea Coastal Waters. *Pol. J. Environ. Stud.* 28, 2531–2539. <https://doi.org/10.15244/pjoes/92524>
- Dzierzbicka-Głowacka, L., Janecki, M., Nowicki, A., Jakacki, J., 2013b. Activation of the operational ecohydrodynamic model (3D CEMBS) – the ecosystem module. *Oceanologia* 55 (3), 543–572. <https://doi.org/10.5697/oc.55-3.543>
- Dzierzbicka-Głowacka, L., Nowicki, A., Janecki, M., Szymczycha, B., Piotrowski, P., Piekiel, P., Łukasiewicz, G., 2018. Structure of the FindFish Knowledge Transfer Platform. *Fisheries & Aquatic Life* 26, 193–197. <https://doi.org/10.2478/aopf-2018-0021>
- Gons, H.J., Rijkeboer, M., Ruddick, K.G., 2002. A chlorophyll-retrieval algorithm for satellite imagery (Medium Resolution Imaging Spectrometer) of inland and coastal waters. *J. Plankton Res.* 24, 947–951. <https://doi.org/10.1093/plankt/24.9.947>
- Hansson, M., Viktorsson, L., Andersson, L., 2019. Oxygen Survey in the Baltic Sea 2019 - Extent of Anoxia and Hypoxia, 1960-2019 (No. 67), Report Oceanography. SMHI, Göteborg, Sweden.
- HELCOM, 2010. Ecosystem Health of the Baltic Sea 2003–2007: HELCOM Initial Holistic Assessment (No. 122). In: *Balt. Sea Environ. Proc.* Helsinki Commission. Helsinki, Finland.
- Janecki, M., Dybowski, D., Jakacki, J., Nowicki, A., Dzierzbicka-Głowacka, L., 2021. The Use of Satellite Data to Determine the Changes of Hydrodynamic Parameters in the Gulf of Gdańsk via EcoFish Model. *Remote Sens.-Basel.* 13, 3572. <https://doi.org/10.3390/rs13183572>
- Janecki, M., Dybowski, D., Rak, D., Dzierzbicka-Głowacka, L., 2022. A New Method for Thermocline and Halocline Depth Determination at Shallow Seas. *J. Phys. Oceanogr.* 52, 2205–2218. <https://doi.org/10.1175/JPO-D-22-0008.1>
- Kalinowska, D., Wielgat, P., Kolerski, T., Zima, P., 2018. Effect of GIS parameters on modelling runoff from river basin. The case study of catchment in the Puck District. In: *E3S Web Conf.*, 63, 00005. <https://doi.org/10.1051/e3sconf/20186300005>
- Kalinowska, D., Wielgat, P., Kolerski, T., Zima, P., 2020. Model of Nutrient and Pesticide Outflow with Surface Water to Puck Bay (Southern Baltic Sea). *Water-SUI* 12, 809. <https://doi.org/10.3390/w12030809>
- Kuliński, K., Rehder, G., Asmala, E., Bartosova, A., Carstensen, J., Gustafsson, B., Hall, P.O.J., Humborg, C., Jilbert, T., Jürgens, K., Meier, H.E.M., Müller-Karulis, B., Naumann, M., Olesen, J.E., Savchuk, O., Schramm, A., Slomp, C.P., Sofiev, M., Sobek, A., Szymczycha, B., Undeman, E., 2022. Biogeochemical functioning of the Baltic Sea. *Earth Syst. Dynam.* 13, 633–685. <https://doi.org/10.5194/esd-13-633-2022>
- Majewski, A., 1972. Hydrological characteristics of estuarine waters at the Polish Coast. Państwowy Instytut Hydrologiczno-Meteorologiczny, 3–40.
- Malone, T.C., Newton, A., 2020. The Globalization of Cultural Eutrophication in the Coastal Ocean: Causes and Consequences. *Front. Mar. Sci.* 7. <https://doi.org/10.3389/fmars.2020.00670>
- McCrackin, M.L., Muller-Karulis, B., Gustafsson, B.G., Howarth, R.W., Humborg, C., Svanbäck, A., Swaney, D.P., 2018. A Century of Legacy Phosphorus Dynamics in a Large Drainage Basin. *Global Biogeochem. Cy.* 32, 1107–1122. <https://doi.org/10.1029/2018GB005914>
- Meier, H.E.M., Höglund, A., Eilola, K., Almoth-Rosell, E., 2017. Impact of accelerated future global mean sea level rise on hypoxia in the Baltic Sea. *Clim. Dyn.* 49, 163–172. <https://doi.org/10.1007/s00382-016-3333-y>
- Mohrholz, V., 2018. Major Baltic Inflow Statistics – Revised. *Front. Mar. Sci.* 5. <https://doi.org/10.3389/fmars.2018.00384>
- Moore, J.K., Doney, S.C., Kleypas, J.A., Glover, D.M., Fung, I.Y., 2001. An intermediate complexity marine ecosystem model for the global domain. *Deep-Sea Res. Pt. II* 49, 403–462. [https://doi.org/10.1016/S0967-0645\(01\)00108-4](https://doi.org/10.1016/S0967-0645(01)00108-4)
- Mosharova, S.A., Mosharova, I.V., Dmitrieva, O.A., Semenova, A.S., Ulyanova, M.O., 2022. Seasonal Variability of Plankton Production Parameters as the Basis for the Formation of Organic Matter Flow in the Southeastern Part of the Baltic Sea. *Water-SUI* 14, 4099. <https://doi.org/10.3390/w14244099>
- O’Neil, J.M., Davis, T.W., Burford, M.A., Gobler, C.J., 2012. The rise of harmful cyanobacteria blooms: The potential roles of eutrophication and climate change. *Harmful Algae* 14, 313–334. <https://doi.org/10.1016/j.hal.2011.10.027>
- Ostrowska, M., Ficek, D., Stoltmann, D., Stoń-Egiert, J., Zdun, A., Kowalewski, M., Zapadka, T., Majchrowski, R., Pawlik, M., Dera, J., 2022. Ten years of remote sensing and analyses of the Baltic Sea primary production (2010–2019). *Remote Sensing Applications: Society and Environment* 26, 100715. <https://doi.org/10.1016/j.rsase.2022.100715>
- Pastuszek, M., Bryhn, A.C., Håkanson, L., Stålnacke, P., Zalewski, M., Wodzinowski, T., 2018. Reduction of nutrient emission from Polish territory into the Baltic Sea (1988–2014) confronted with real environmental needs and international requirements. *Oceanol. Hydrobiol. St* 47, 140–166. <https://doi.org/10.1515/ohs-2018-0015>
- Paytan, A., McLaughlin, K., 2007. The Oceanic Phosphorus Cycle. *Chem. Rev.* 107, 563–576. <https://doi.org/10.1021/cr0503613>
- Randolph, K., Wilson, J., Tedesco, L., Li, L., Pascual, D.L., Soyeux, E., 2008. Hyperspectral remote sensing of cyanobacteria in turbid productive water using optically active pigments, chlorophyll *a* and phycocyanin. *Remote Sens. Environ.* 112, 4009–4019. <https://doi.org/10.1016/j.rse.2008.06.002>
- Reckermann, M., Omstedt, A., Soomere, T., Aigars, J., Akhtar, N., Beldowska, M., Beldowski, J., Cronin, T., Czub, M., Eero, M., Hyttiäinen, K.P., Jalkanen, J.-P., Kiessling, A., Kjellström, E., Kuliński, K., Larsén, X.G., McCrackin, M., Meier, H.E.M., Oberbeckmann, S., Parnell, K., Pons-Seres de Brauer, C., Poska, A., Saarinen, J., Szymczycha, B., Undeman, E., Wörman, A., Zorita, E., 2022. Human impacts and their interactions in the Baltic Sea region. *Earth Syst. Dynam.* 13, 1–80. <https://doi.org/10.5194/esd-13-1-2022>
- Sato, N., 2021. Are Cyanobacteria an Ancestor of Chloroplasts or Just One of the Gene Donors for Plants and Algae? *Genes* 12 (6), 823. <https://doi.org/10.3390/genes12060823>
- Sommer, U., Aberle, N., Lengfellner, K., Lewandowska, A., 2012. The Baltic Sea spring phytoplankton bloom in a changing climate: an experimental approach. *Mar. Biol.* 159, 2479–2490. <https://doi.org/10.1007/s00227-012-1897-6>
- Szymczycha, B., Zaborska, A., Beldowski, J., Kuliński, K., Beszczyńska-Möller, A., Kędra, M., Pempkowiak, J., 2019. Chapter 4 - The Baltic Sea. In: Sheppard, C. (Ed.), *World Seas: An Environmental Evaluation*. Acad. Press, 85–111. <https://doi.org/10.1016/B978-0-12-805068-2.00005-X>
- Tamminen, T., Andersen, T., 2007. Seasonal phytoplankton nutrient

- 1121 limitation patterns as revealed by bioassays over Baltic Sea gra- 1151
1122 dients of salinity and eutrophication. *Mar. Ecol. Prog. Ser.* 340, 1152
1123 121–138. <https://doi.org/10.3354/meps340121>
- 1124 Tomczak, M.T., Szymanek, L., Pastuszak, M., Grygiel, W., Za- 1154
1125 lewski, M., Gromisz, S., Ameryk, A., Kownacka, J., Psuty, I., 1155
1126 Kuzebski, E., Grzebielec, R., Margoński, P., 2016. Evaluation of 1156
1127 Trends and Changes in the Gulf of Gdańsk Ecosystem – an Inte- 1157
1128 grated Approach. *Estuar. Coast.* 39, 593–604. [https://doi.org/](https://doi.org/10.1007/s12237-015-0026-4) 1158
1129 [10.1007/s12237-015-0026-4](https://doi.org/10.1007/s12237-015-0026-4)
- 1130 Verity, P.G., Smetacek, V., 1996. Organism life cycles, predation, 1159
1131 and the structure of marine pelagic ecosystems. *Mar. Ecol. Prog.* 1160
1132 *Ser.* 130, 277–293. <https://doi.org/10.3354/meps130277>
- 1133 Vitousek, P.M., Howarth, R.W., 1991. Nitrogen limitation on land 1161
1134 and in the sea: How can it occur? *Biogeochemistry* 13, 87–115. 1162
1135 <https://doi.org/10.1007/BF00002772>
- 1136 von Storch, H., 2023. Perceptions of an endangered Baltic Sea. 1163
1137 *Oceanologia* 65 (1), 44–49. [https://doi.org/10.1016/j.oceano.](https://doi.org/10.1016/j.oceano.2021.08.005) 1164
1138 [2021.08.005](https://doi.org/10.1016/j.oceano.2021.08.005)
- 1139 Voss, M., Liskow, I., Pastuszak, M., Rüb, D., Schulte, U., Dipp- 1165
1140 ner, J.W., 2005. Riverine discharge into a coastal bay: A stable 1166
1141 isotope study in the Gulf of Gdańsk, Baltic Sea. *J Marine Syst* 57, 1167
1142 127–145. <https://doi.org/10.1016/j.jmarsys.2005.04.002>
- 1143 Wasmund, N., Andrushaitis, A., Łysiak-Pastuszak, E., Müller- 1168
1144 Karulis, B., Nausch, G., Neumann, T., Ojaveer, H., Olenina, I., 1169
1145 Postel, L., Witek, Z., 2001. Trophic Status of the South-Eastern 1170
1146 Baltic Sea: A Comparison of Coastal and Open Areas. *Estuar.* 1171
1147 *Coast. Shelf. S.* 53 (6), 849–864. [https://doi.org/10.1006/ecss.](https://doi.org/10.1006/ecss.2001.0828) 1172
1148 [2001.0828](https://doi.org/10.1006/ecss.2001.0828)
- 1149 Wielgat, P., Kalinowska, D., Szymkiewicz, A., Zima, P., Jaworska- 1173
1150 Szulc, B., Wojciechowska, E., Nawrot, N., Matej-Lukowicz, K., 1174
1151 Dzierzbicka-Głowacka, L.A., 2021. Towards a multi-basin SWAT 1175
1152 model for the migration of nutrients and pesticides to Puck 1176
1153 Bay (Southern Baltic Sea). *Peer J* 9, e10938. [https://doi.org/](https://doi.org/10.7717/peerj.10938) 1177
1154 [10.7717/peerj.10938](https://doi.org/10.7717/peerj.10938)
- 1155 Witek, Z., Ochocki, S., Maciejowska, M., Pastuszak, M., 1178
1156 Nakonieczny, J., Podgórska, B., Kownacka, J.M., Mackiewicz, T., 1179
1157 Wrzesinska-Kwiecien, M., 1997. Phytoplankton primary produc- 1180
1158 tion and its utilization by the pelagic community in the coastal 1181
1159 zone of the Gulf of Gdansk (southern Baltic). *Mar. Ecol. Prog.* 1182
1160 *Ser.* 148, 169–186. <https://doi.org/10.3354/meps148169>
- 1161 Woźniak, B., Bradtke, K., Darecki, M., Dera, J., Dudzińska- 1183
1162 Nowak, J., Dzierzbicka-Głowacka, L., Ficek, D., 1184
1163 Furmańczyk, K., Kowalewski, M., Krężel, A., Majchrowski, R., 1185
1164 Ostrowska, M., Paszkuta, M., Stoń-Egiert, J., Stramska, M., 1186
1165 Zapadka, T., 2011a. SatBałtyk – A Baltic environmental satellite 1187
1166 remote sensing system – an ongoing project in Poland. Part 1: 1188
1167 Assumptions, scope and operating range. *Oceanologia* 53 (4), 1189
1168 897–924. <https://doi.org/10.5697/oc.53-4.897>
- 1169 Woźniak, B., Bradtke, K., Darecki, M., Dera, J., Dudzińska- 1190
1170 Nowak, J., Dzierzbicka-Głowacka, L., Ficek, D., 1191
1171 Furmańczyk, K., Kowalewski, M., Krężel, A., Majchrowski, R., 1192
1172 Ostrowska, M., Paszkuta, M., Stoń-egiert, J., Stramska, M., 1193
1173 Zapadka, T., 2011b. SatBałtyk – A Baltic environmental satellite 1194
1174 remote sensing system – an ongoing project in Poland. Part 2: 1195
1175 Practical applicability and preliminary results. *Oceanologia* 53 1196
1176 (4), 925–958. <https://doi.org/10.5697/oc.53-4.925>
- 1177 Zdun, A., Stoń-Egiert, J., Ficek, D., Ostrowska, M., 2021. Seasonal 1197
1178 and Spatial Changes of Primary Production in the Baltic Sea (Eu- 1198
1179 rope) Based on in situ Measurements in the Period of 1993–2018. 1199
1180 *Front. Mar. Sci.* 7. <https://doi.org/10.3389/fmars.2020.604532> 1200

5 Attachment

Janecki, M., Dzierzbicka-Glowacka, L., 2023. *Fish Module - A Prognostic Tool for Modeling the Optimal Environmental Conditions for Fish in the Gulf of Gdańsk (Southern Baltic Sea).* Manuscript submitted to Fish and Fisheries Journal

(IF¹ = 7.401; MEiN² = 200)

¹Journal (2021) Impact Factor (IF) according to the Journal Citation Reports

²Journal score according to the list of the Polish Ministry of Education and Science

ORIGINAL ARTICLE

Fish Module - A Prognostic Tool for Modeling the Optimal Environmental Conditions for Fish in the Gulf of Gdańsk (Southern Baltic Sea)

Maciej Janecki | Lidia Dzierzbicka-Głowacka

¹Ecohydrodynamics Laboratory, Physical Oceanography Department, Institute of Oceanology Polish Academy of Sciences, , Poland

Correspondence

Maciej Janecki, Institute of Oceanology Polish Academy of Sciences, Powstańców Warszawy 55, 81-712 Sopot, Poland.
Email: mjanecki@iopan.pl

Abstract

This article discusses the service called the *Fish Module* for the predictive determination of the optimal environmental conditions for the existence of sprat, herring, cod, and flounder found in the southern Baltic Sea (in particular in the Gulf of Gdańsk region). The *Fish Module* utilizes data from the *EcoFish* ecohydrodynamic model and fish preference data to calculate the Habitat Suitability Index (HSI). Data on fish preference were determined based on 587 expeditions during which physicochemical parameters of the sea were recorded. Our analysis determined threshold HSI values below which successful catches are unlikely for sprat, herring, and cod, confirming the system's effectiveness in identifying locations with favorable environmental conditions for these species. Fishermen are advised to select routes with specific HSI thresholds to achieve greater efficiency in fishing. Furthermore, the analysis revealed that fishing durations do not necessarily correlate with higher catches, emphasizing the importance of selecting suitable routes based on favorable environmental conditions for fish habitat. We expect the *Fish Module* to be the most demanded product of the *FindFISH* project.

KEYWORDS

Habitat suitability evaluation, HSI, Fuzzy Logic, EcoFish model, Fisheries, Gulf of Gdańsk

1 | INTRODUCTION

Commercial fishing plays a vital role in the global food chain, providing a source of food for millions of people around the world. However, with technological progress and population growth, fisheries face numerous challenges and difficulties that have a significant impact on the sustainable management of fish resources (Godfray et al., 2010). The fishing industry faces several problems that threaten marine life, the environment, and the economy (Hilborn et al., 2003). Overfishing can cause a decline not only in fish populations (Myers & Worm, 2003), but also lead to starvation of fish-eating birds (Camphuysen & Garthe, 2000), which can have ripple effects throughout the ecosystem. Bycatch (estimated at 40% of total global catch) can be seen as a waste of resources, leading to the deaths of many marine animals, including endangered species (Davies, Cripps, Nickson, & Porter, 2009). Another important issue is the degradation of the marine environment caused by oil pollution from fishing ships and the introduction of modern fishing methods, such as bottom trawling. According to the UN, even 95% of

global ocean damage can be a direct result of this fishing technique (UN, 2006). At the same time, it should be remembered that fishing is driven by living people (fishers), for whom it is often the only source of income. Regulations aimed at protecting declining or endangered species and the environment, make day-to-day fishing less and less profitable. This forces many fishermen to look for savings or to quit and change their profession. Trying to help overcome these problems, we decided to implement the project called "Knowledge Transfer Platform *FindFISH* – Numerical Forecasting System for the Marine Environment of the Gulf of Gdańsk for Fisheries" (Dzierzbicka-Głowacka et al., 2018; Dzierzbicka-Głowacka, 2023). The aim of *FindFISH* is to deal with the declining profitability of commercial fisheries, by reducing fishing time (fuel saving) and thus prevent environmental pollution. Our numerical modeling approach will enable fishers to optimize their catch and avoid bycatch. Furthermore, the project will improve maritime safety and working conditions. By catching the same amount of fish (or more) during shorter fishing expeditions, vessel crews will experience a reduced workload, what should improve safety. Decreased fuel consumption will lead to

additional cost savings and reduced environmental pollution. The result of the project is a user-friendly web service (www.findfish.pl) that provides accessible information regarding the physical and biochemical state of the Gulf of Gdańsk in the form of 48-hour forecasts. One of the key components of this system is the “Fish Module” designed to generate maps of the Habitat Suitability Index (HSI), indicating the locations of the best environmental conditions for fish in the Gulf of Gdańsk. It is implemented for four species: sprat (*Sprattus sprattus*), herring (*Clupea harengus*), cod (*Gadus morhua*), and flounder (*Platichthys flesus*). The assessment of habitat suitability is an important aspect of habitat conservation near river estuaries. There are several methodologies used in the literature that have been introduced to calculate the Habitat Suitability Index (Beecher, Caldwell, & DeMond, 2002; Bovee, 1986; Inglis, Hurren, Oldman, & Haskew, 2006; Poulos, Chernoff, Fuller, & Butman, 2012). These methods require a good understanding of the preferences of the analyzed species. Moreover, they rely on a substantial amount of highly accurate data. In ecology, numerous uncertainties emerge, including incomplete or inaccurate measurements and the utilization of estimations instead of direct measurements. These limitations have led to an interest in fuzzy logic, which is capable of effectively utilizing imprecise and uncertain measurements, as well as fuzzy expert knowledge. By expressing the uncertainty of habitat simulation, fuzzy sets employ imprecise or vague information. The available expert knowledge is represented as a preference data set (Fraternali, Castelletti, Soncini-Sessa, Vaca Ruiz, & Rizzoli, 2012; Prato, 2007). Models based on fuzzy rules have been applied in numerous studies, as they are designed to incorporate qualitative knowledge and possess a structure that facilitates result interpretation (Chou, Lin, & Lin, 2007; Fukuda et al., 2011; Legleiter & Goodchild, 2005; Mouton, De Baets, & Goethals, 2009; Rüger, Schlüter, & Matthies, 2005; Zhang, Sun, Shao, & Yang, 2016). The goals of the *FindFISH* project made the use of fuzzy logic a natural choice when designing the *Fish Module*. The purpose of this paper is to present the results provided by the *Fish Module* and to prove that using *in situ* data of habitat preferences and numerical modeling it is possible to determine the optimal environmental conditions for the existence of individual fish species found in the region of the southern Baltic Sea (in particular in the Gulf of Gdańsk). We expect the *Fish Module* to be the most demanded product of the *FindFISH* service.

2 | MATERIAL AND METHODS

2.1 | Fishing expeditions

The environmental data in the *FindFISH* project were collected during fishing expeditions conducted on vessels affiliated with the *Association of Sea Fishermen - Producers' Organization*[†] in Władysławowo (city in northern Poland). The research involved trawlers (mainly using pelagic trawls and pair trawls) and boats (using gillnets). Trawling in the Gulf

of Gdańsk focuses on the catch of herring, sprat, and cod (until 2021, when a total ban on cod fishing was implemented). The fishing boats are primarily targeting cod (until 2021), flounder, herring, and perch. Seven trawlers (JAS-74, WŁA-22, WŁA-65, WŁA-196, WŁA-207, WSG-22, ZAG-17) and four fishing boats (JAS-10, SZT-1, WŁA-16, WŁA-53) participated in these expeditions. To collect physicochemical data in the sea, the Valeport MIDAS CTD+ instrument was used. The instrument recorded crucial parameters for the *FindFISH* project, including oxygen saturation, salinity, and water temperature. During expeditions that used pelagic nets, the instrument was mounted to the upper edge of the fishing net or attached to the trawl wing (Figure 1a). In the case of the gillnet, MIDAS CTD+ was attached to a pole using a steel cable (Figure 1b). The instrument was always buoyed and weighted, ensuring its stability.

During each fishing expedition in which the MIDAS CTD+ instrument was used, the vessel's crew was required to complete a survey (Figure 2). The survey recorded the following information: vessel name, date and time of deployment and retrieval of fishing gear (start time for trawling gear), fishing square, position of gear deployment (initial and final position for trawling gear), gear code, wind speed and direction, cloud cover, precipitation, air temperature, sea surface temperature, sea state (wave height), as well as catch results (composition and weight of the catch).

The geographical coordinates of the fishing routes and the location of gillnets deployment were recorded using the user-friendly GARMIN GPS73 navigation tool. Data collection began in 2018 and took place during regular commercial fishing operations in the Gulf of Gdańsk. The fishing regulations (limitations and bans) and hydrometeorological conditions required adjustments to the schedule of expeditions. In January 2020, a ban on cod fishing was introduced, and a ban on pelagic fish lasted from June to August. In 2021, the fishing expeditions were greatly influenced by intense storms in January and February, bans on cod fishing (total ban) and pelagic fish (May to August, only for trawlers), as well as reduced catch quotas compared to previous years. From 2018 to 2022, a total of 587 fishing events were conducted using the MIDAS CTD+ instrument, with fishing boats completing 280 expeditions and trawlers completing 307. The catch consisted of 1,440,958 kg of sprat, 850,427 kg of herring, 22,861 kg of cod (during the permitted fishing period), and 4,780 kg of flounder.

The fishing expeditions targeting sprat took place in a wide strip that ran from the northwest part of the Gulf of Gdańsk to the mouth of the Vistula River (Figure 3a). Sprat was caught by seven fishing vessels: JAS-74, WSG-22, WŁA-196, WŁA-207, WŁA-22, WŁA-65, ZAG-17, using two types of fishing gear: pelagic trawl (tool code: OTM) and pelagic pair trawl (tool code: PTM). The locations where herring was caught (Figure 3b) overlapped with the sprat fishing grounds. These species coexist, and during most fishing expeditions, catches of both species were recorded simultaneously. Herring was also caught (in significantly smaller quantities) using gillnets (tool code: GNS) by WŁA-53 and SZT-1. Cod fishing was conducted only in the initial phase of the *FindFISH* project before the total ban on this species was implemented. Most of the cod catches were made using bottom otter trawls (tool code: OTB),

[†] <http://zrm-op.org/>

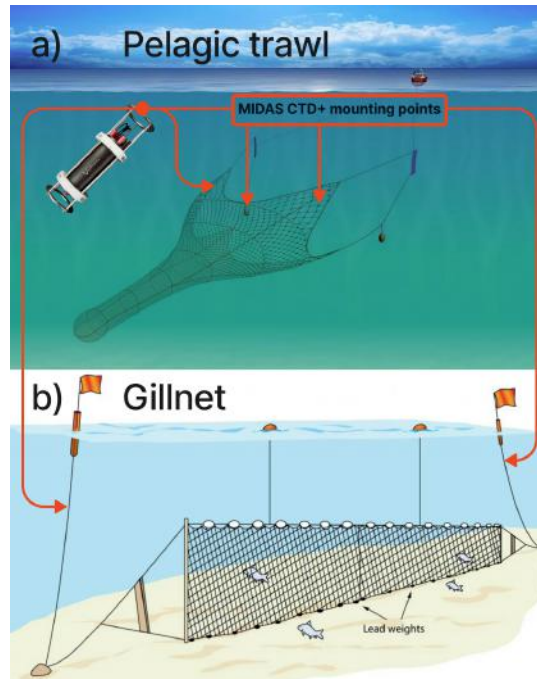


FIGURE 1 Mounting points of the MIDAS CTD+ instrument to a) pelagic trawl and b) gillnet during fishing expeditions (sources: seafish.org, smithsonianmag.com, valeport.co.uk; modified).

Ankieta dla narzędzi ciągnionych (FindFish)

Nazwa statku	WŁA-22
Data i godzina początku zaciągu	10.03.2021 07 ⁰⁰
Kwadrat rybacki (mały)	R-7
Pozycja początkowa zaciągu	54°58'20N 18°40'40E
Pozycja końcowa zaciągu	54°59'30N 18°33'00E
Kod narzędzia (według aktualnego rozporządzenia)	OTM 18
Siła wiatru (0 – cisza, 12 – huragan)	3
Kierunek wiatru (N, NE, E, SE, S, SW, W, NW)	SW
Zachmurzenie (0 – bezchmurnie, 8 – zachmurzenie całkowite)	0
Opad (0 – brak, 1 – mżawka, 2 – deszcz, 3 – ulewa)	0
Temperatura powietrza [st C]	10°
Temperatura wody powierzchniowej [st C]	5°
Stan morza (wysokość fali) (0 – 0 m; 1 – 0,0-0,1 m; 2 – 0,1-0,5 m; 3 – 0,5-1,25 m; 4 – 1,25-2,5 m; 5 – 2,5-4,0 m; 6 – 4,0-6,0 m; 7 – 6,0-9,0 m; 8 – 9,0-14,0 m; 9 – ponad 14 m)	2
Skład i masa połowu	SEPROT 9500kg ŚLEDZ 500

FIGURE 2 Completed survey (in Polish) from the fishing expedition of WŁA-22. From top to bottom: vessel name, date and time of the start of the haul, fishing square, initial and final position of the haul, gear code, wind speed and direction, cloud cover, precipitation, air temperature, sea surface temperature, sea state (wave height), catch composition, catch weight.

but there were also occasional expeditions where cod was caught using other gear (OTM, PTM, and GNS). Cod fishing took place mainly in the central part of the Gulf of Gdańsk (Figure 3c) conducted by the JAS-10, JAS-74, WŁA-196, WŁA-65, and ZAG-17. Most of the cod caught came from ZAG-17. Flounder was primarily caught using gillnets (tool code: GNS) and bottom otter trawls (tool code: OTB) by JAS-10, JAS-74,

WŁA-196, WŁA-65, and ZAG-17. Flounder fishing took place in shallow areas close to the coast (Figure 3d).

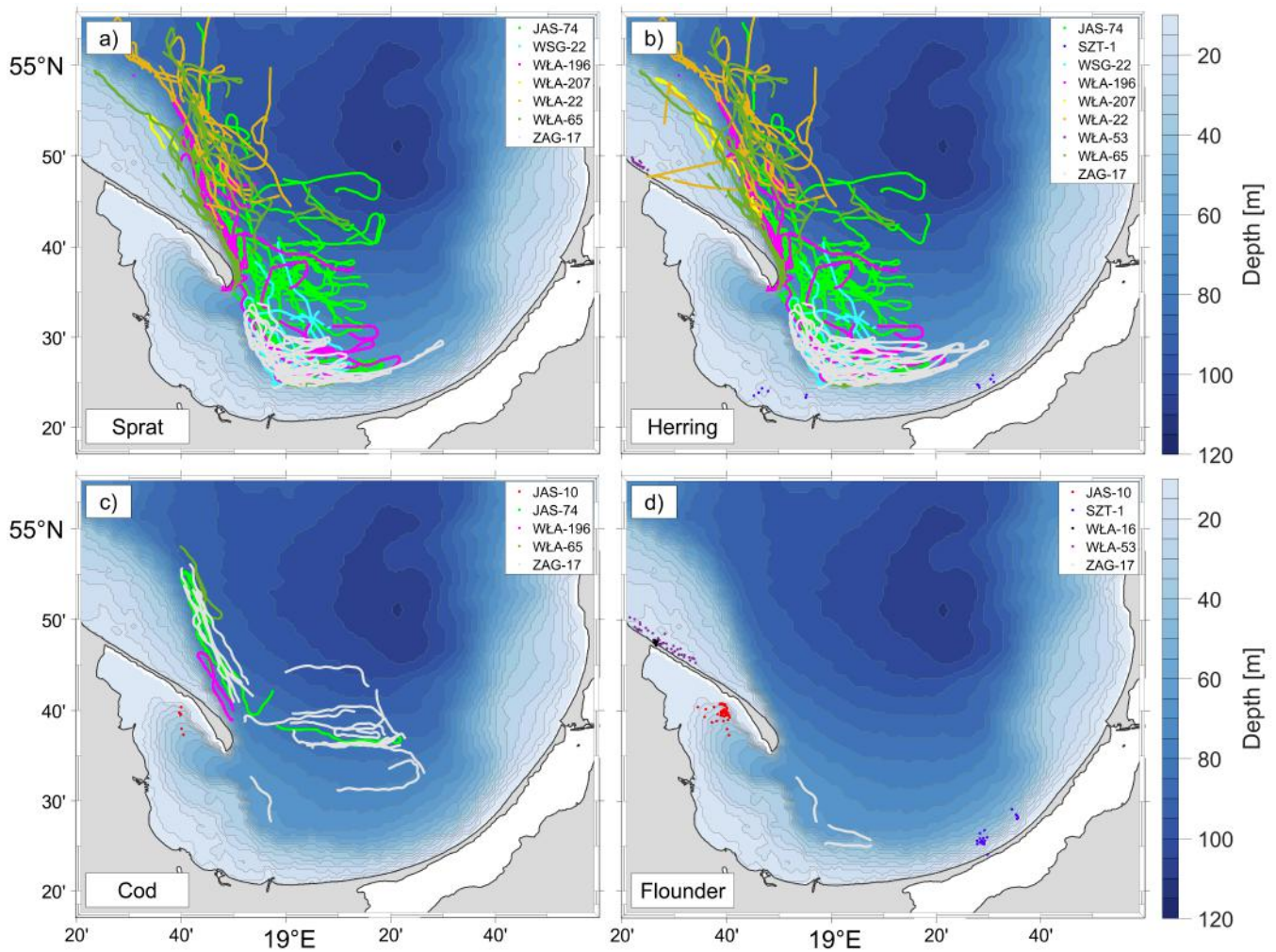


FIGURE 3 Topography of the *EcoFish* model domain with marked GPS traces of fishing vessels from expeditions targeting a) sprat, b) herring, c) cod, and d) flounder.

2.2 | The *EcoFish* model

For numerical simulations, we use a three-dimensional prognostic model called *EcoFish* (Janecki, Dybowski, Jakacki, Nowicki, & Dzierzbicka-Głowacka, 2021; Janecki, Dybowski, Rak, & Dzierzbicka-Głowacka, 2022; Janecki, Dybowski, & Dzierzbicka-Głowacka, 2023). It has been developed as part of the *FindFISH* project and adapted for the extended Gulf of Gdańsk domain. *EcoFish* provides 48-hour forecasts of hydrodynamic (water temperature, salinity, currents, sea surface height) and biochemical parameters (nitrate, phosphate, silicate, chlorophyll *a* concentration, phytoplankton and microzooplankton biomass, dissolved oxygen, and dissolved organic carbon concentration). *EcoFish* has a horizontal resolution of 575 m. Vertically it is a z-type model divided into 26 vertical levels, each with a thickness of 5 m. The main components of the model are:

- Hydrodynamic component - this is an ocean model based on the Parallel Ocean Program (POP) code, which has been described and validated in (Janecki et al., 2021, 2022).
- Biochemical component - this is an NPZD-type biochemical model based on the knowledge of the biological and chemical processes that occur in the marine environment and their mutual relationships (Dzierzbicka-Głowacka, Janecki, Nowicki, & Jakacki, 2013; Moore, Doney, Kleypas, Glover, & Fung, 2001) described and validated in (Janecki et al., 2023).

These components are dedicated to conducting numerical simulations (forecasts) of the modeled parameters. Additionally, the *EcoFish* model incorporates modules for processing input and output files, data assimilation (for surface temperature and chlorophyll *a* concentration), and coordinating the operational mode.

2.3 | Fish Module

The *Fish Module* is a computer algorithm that constitutes the final element of the *Knowledge Transfer Platform FindFISH* (Figure 4). Using expert knowledge and data on water temperature, salinity, oxygen saturation, fishing depth, and catch composition and weight (see 2.1 Fishing expeditions), we were able to determine the optimal conditions for the habitat of four commercially fished species in the Gulf of Gdańsk region. These species are herring, sprat, cod, and flounder. Subsequently, fuzzy rules were established that connect the input variables to the preferences of each species. This fuzzy system uses the *EcoFish* model data for temperature, salinity, and dissolved oxygen concentration to determine the Habitat Suitability Index (HSI) for the Gulf of Gdańsk. The HSI indicates the habitat conditions in the studied area and provides values that illustrate the optimal habitat conditions for a given species. The HSI ranges from 0 to 1, where 0 indicates that the habitat does not meet the conditions for the occurrence of a particular species, while 1 describes a habitat with optimal conditions for the existence of that species. The final stage involves visualizing the results on the *FindFISH* project web portal (www.findfish.pl) in the form of maps showing forecasts of environmental conditions.

2.3.1 | Membership functions

The determination of membership functions in the *Fish Module* involved the utilization of data defining the ranges of preferable values for each parameter governing the habitat of sprat, herring, cod, and flounder. These ranges were established based on physicochemical data (temperature, salinity, oxygen saturation, and fishing depth) and fishing data (catch composition and weight) collected during fishing expeditions. Several iterations were performed during the implementation of this system. In the initial version of the *Fish Module*, a division into four seasons was used (spring, summer, autumn, and winter). However, after the preliminary analysis of the results, it was determined that this approach was not sufficiently detailed, prompting actions to increase the temporal resolution to a monthly scale. In the second iteration of the *Fish Module*, the 25th and 75th percentiles were used as the range of optimal parameter values, with minimum and maximum values at the edges. However, the central intervals for the optimal values were too wide, preventing a detailed determination of the best parameter value for the habitat of each species in a given month, leading to low variability in HSI score. In the final iteration, the median of the optimal value was implemented along with a constant deviation C , and the minima/maxima at the edges (Figure 5). The preferences of each species implemented in the *Fish Module* were fuzzified in a way that the central trapezoid encompassed the optimal values of the respective parameter for the species' habitat, while lower and higher values represented conditions below and above the optimal range respectively.

The full table with the determined values of median, C , minimum, and maximum for sprat, herring, cod, and flounder is presented below

(Table 1). At the moment, the *Fish Module* generates HSI results for flounder only for the period from July to November. This is due to the lack of catch data necessary to determine flounder preferences in the remaining months, and an attempt to interpolate them from the available months could lead to wrong results.

2.3.2 | Fuzzy inference system and rules

The fuzzy inference system block performs calculations to determine the output membership function based on the input membership degrees. This function often exhibits a complex shape and its determination can be achieved through various mathematical inference methods. In the first stage of calculations within the fuzzy inference system (Figure 5), a set of membership functions is defined to convert the suitability of different species for various environments into linguistic terms. These terms serve as input to the fuzzy inference process. The "fuzzification" process involves transforming raw (crisp) values into linguistic quantities, ranging from "low" to "high" (Zadeh, 1965). Each linguistic value possesses a range of membership degrees represented by real numbers from 0 to 1. Membership functions enable the transformation of a regular set into a fuzzy one characterized by membership degrees. Moreover, a given value can belong to two adjacent fuzzy sets of different degrees due to the overlapping boundaries of the membership functions. In our study, trapezoidal membership functions are employed. They are shown to be effective in numerous studies (Muñoz-Mas, Martínez-Capel, Schneider, & Mouton, 2012; Van Broekhoven, Adriaenssens, De Baets, & Verdonschot, 2006; Zhang et al., 2016). All membership functions are defined by four parameters: median, C , minimum, and maximum (Table 1). The membership degree increases linearly from 0 to 1 between minimum and median - C , remains at 1 between median - C and median + C , and decreases from 1 to 0 between median + C and maximum (Figure 5). The next step in the calculations involves fuzzy logic inference using fuzzy rules. Inference rules connect the input variables (temperature, salinity, oxygen saturation, and depth) with the environmental conditions for species suitability (HSI) using a series of "IF-THEN" conditional statements. Fuzzy rules are defined based on expert knowledge, and fuzzy input can be transformed into fuzzy output data using these rules (Table 2).

Since we include four membership functions for each species in the *Fish Module*, the complete inference set consists of $3^4 = 81$ rules. However, for the presentation of the inference process (Figure 6f–6o), only two rules were used. The process of calculating the Habitat Suitability Index (HSI) using fuzzy logic inference is depicted in Figure 6. We employed the Maximum-Minimum inference method. Based on the fuzzy rule base, the resulting membership function is calculated (Figure 6j, 6o), and then, in the defuzzification process, the outcome is obtained as a

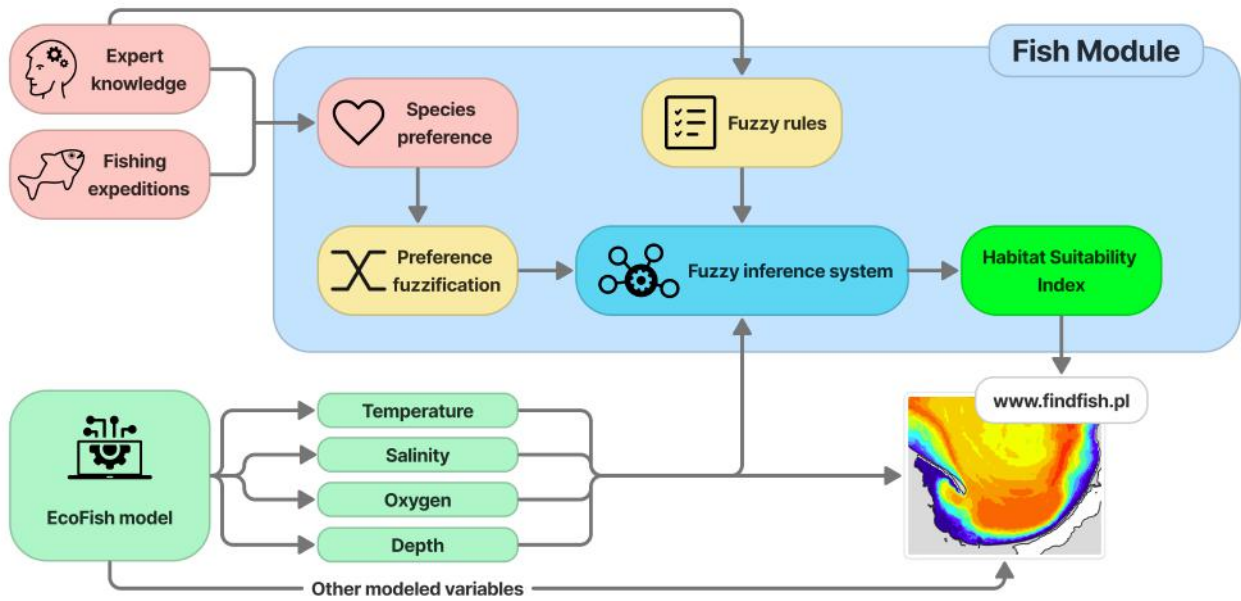


FIGURE 4 The general outline of the *Fish Module* algorithm along with the interdependencies between the elements implemented in the *FindFISH* project.

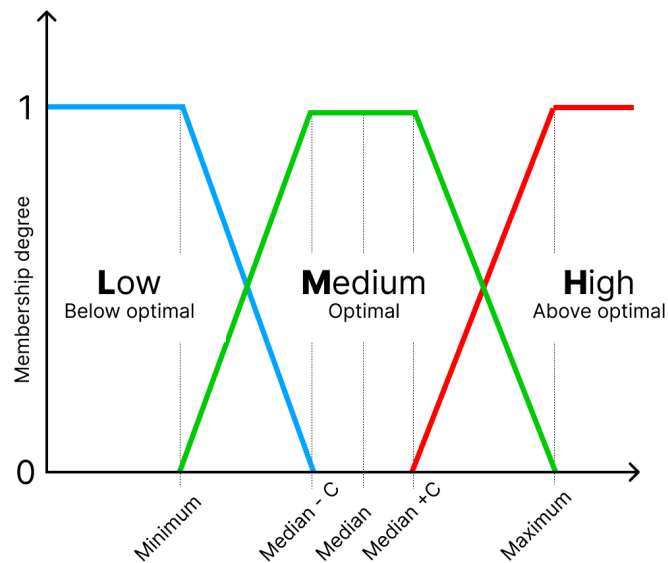


FIGURE 5 General outline of membership functions used to fuzzify the species preferences for water temperature, salinity, oxygen saturation, and depth.

single numerical value of the HSI. Defuzzification is performed using the Center of Gravity (COG) method (Figure 6p).

TABLE 1 Species preferences for water temperature, salinity, oxygen saturation and depth established based on the data from fishing expeditions.

Species	Month	Temperature [°C] C = 0.4 °C			Salinity C = 0.1			Oxygen saturation [%] C = 6 %			Depth [m] C = 4 m		
		Min	Med.	Max	Min	Med.	Max	Min	Med.	Max	Min	Med.	Max
Sprat	January	4.46	6.19	9.09	7.30	7.61	12.12	1.26	78.40	109.92	15.00	50.65	84.17
	February	2.41	5.16	9.22	7.36	7.77	12.89	3.62	78.30	109.99	15.01	55.55	85.67
	March	2.49	5.00	7.30	7.41	7.72	11.28	22.67	87.04	110.00	15.01	48.88	83.03
	April	3.79	5.50	7.26	5.06	7.78	11.79	4.52	74.55	109.79	15.00	54.12	75.91
	May	4.14	5.63	9.79	7.19	7.89	11.31	10.46	57.77	101.68	15.10	55.44	75.62
	June	5.64	7.13	11.29	6.97	7.67	11.09	9.26	58.00	102.25	9.70	50.04	70.22
	July	7.86	12.57	15.07	7.00	7.26	10.90	0.32	60.00	100.25	4.30	44.64	64.82
	August	8.50	10.00	17.60	7.00	7.47	10.80	1.09	60.00	100.60	14.00	20.13	60.00
	September	5.00	9.00	17.20	7.00	7.49	10.70	2.09	67.50	100.60	15.00	26.81	62.00
	October	4.60	8.50	16.00	7.08	7.39	10.67	11.09	90.64	101.68	15.00	25.72	68.81
	November	3.45	6.82	12.22	6.96	7.79	12.08	5.59	71.00	109.39	15.00	43.16	76.04
	December	6.12	6.95	8.36	7.30	7.61	11.05	7.28	31.00	107.31	15.05	42.32	76.54
Herring	January	4.46	6.24	9.09	7.44	7.63	12.12	1.26	78.40	109.92	15.00	48.90	84.17
	February	2.52	5.16	9.22	7.36	7.72	12.89	3.62	78.30	109.73	15.01	54.38	85.67
	March	0.87	6.11	10.22	7.26	7.65	12.27	26.09	87.20	98.29	15.00	47.24	85.67
	April	3.79	5.62	10.72	5.06	7.75	11.79	4.52	75.00	109.79	15.00	52.79	75.91
	May	4.14	5.63	11.32	7.19	7.89	11.31	10.46	58.70	109.99	15.10	55.44	75.62
	June	4.24	7.00	12.82	6.99	7.89	11.11	10.56	57.00	110.09	12.90	58.00	73.42
	July	4.23	9.00	14.97	6.59	7.51	10.71	10.06	50.00	93.47	15.12	40.00	60.84
	August	4.43	11.79	17.57	7.34	7.51	9.36	9.26	49.70	93.57	15.01	30.78	60.73
	September	3.32	5.84	18.00	6.95	7.66	10.84	8.23	80.40	97.62	15.00	46.52	60.26
	October	3.48	12.68	15.97	7.08	7.40	10.67	11.09	91.50	108.50	15.00	30.48	68.81
	November	3.45	6.57	12.22	6.96	7.89	12.08	5.59	71.40	109.39	15.00	46.48	76.04
	December	6.12	6.97	8.44	7.45	7.62	11.05	7.28	31.90	107.31	15.05	43.78	76.54
Cod	January	4.10	5.20	6.00	6.90	8.00	11.50	64.00	60.00	95.00	18.00	55.00	45.00
	February	4.30	5.10	6.10	6.90	8.00	10.90	66.00	70.00	92.00	9.00	57.00	45.00
	March	4.83	5.28	6.20	7.45	8.01	10.16	70.00	82.30	90.00	0.70	56.78	45.21
	April	5.11	5.58	6.40	7.60	7.74	8.14	73.23	80.10	85.47	42.90	63.26	54.83
	May	4.17	6.99	10.32	9.10	11.92	13.14	37.00	55.20	66.00	62.54	92.56	82.23
	June	4.41	6.14	8.12	9.80	11.41	12.61	5.00	44.70	48.79	71.21	86.09	80.32
	July	4.10	6.05	8.20	9.50	11.50	12.50	5.00	42.30	53.00	72.00	87.00	81.00
	August	4.00	6.00	8.30	8.80	11.00	12.30	2.00	51.76	54.00	71.00	86.00	81.00
	September	3.77	5.99	8.80	8.42	10.63	12.17	0.30	20.24	55.51	67.84	85.38	81.41
	October	3.40	5.92	15.93	4.06	9.26	11.13	0.39	31.18	102.38	38.53	72.36	57.66
	November	3.70	5.50	12.00	4.90	9.00	11.40	15.00	75.90	102.00	30.00	65.00	50.00
	December	3.90	5.30	8.00	5.50	8.00	11.60	29.00	84.30	101.00	23.00	57.00	45.00
Flounder	July	8.55	19.98	24.65	7.19	7.46	7.83	39.66	50.21	84.41	12.84	14.41	15.46
	August	4.76	16.71	20.99	7.26	7.47	7.67	39.66	50.21	84.41	0.11	20.56	44.57
	September	11.55	15.58	19.25	7.08	7.37	7.67	49.76	66.88	99.84	19.14	25.65	29.51
	October	8.84	13.84	16.90	7.17	7.47	7.90	56.26	84.07	98.17	0.11	24.90	40.43
	November	10.28	11.14	11.97	7.41	7.49	7.60	87.40	89.23	91.00	7.03	9.42	11.57

3 | RESULTS AND DISCUSSION

3.1 | Analysis of fishing expeditions. Fishing efficiency

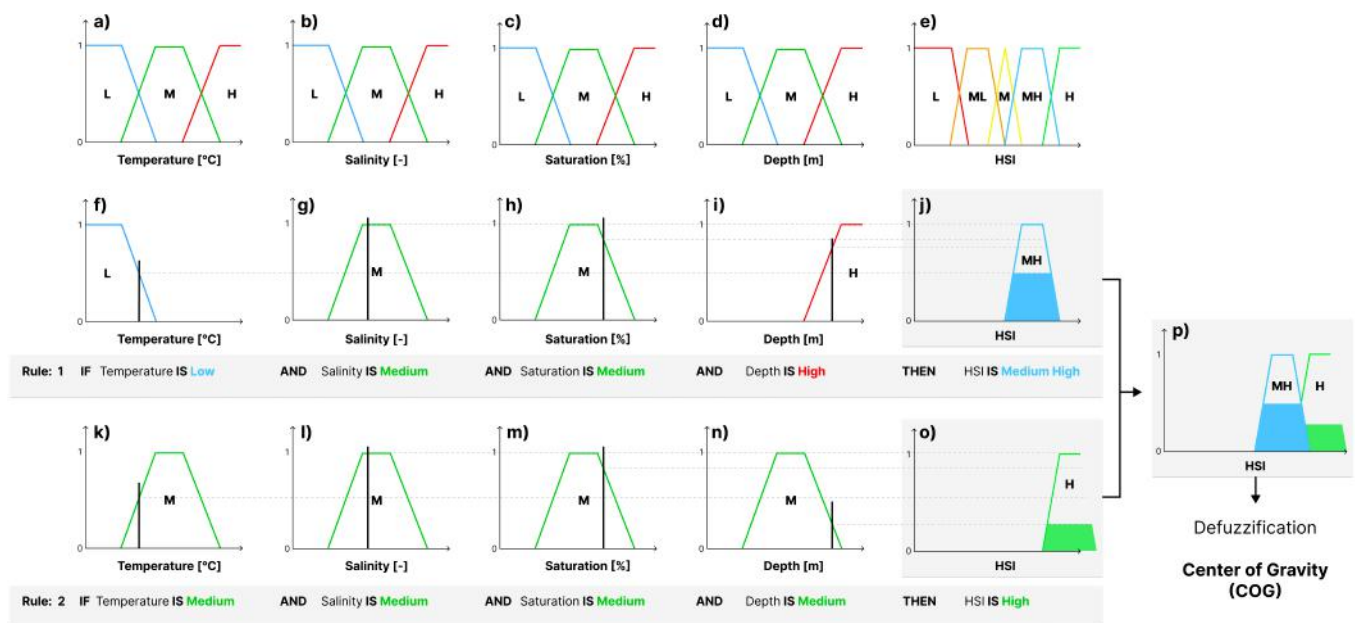
Data from 408 fishing expeditions conducted between September 13, 2018, and May 9, 2022, were analyzed to calculate detailed fishing efficiency (in kg per hour). Although there were more fishing data available, a portion of it was filtered out. Expeditions that exceeded the domain of the *EcoFish* model, as well as those with any issues in recording the fishing route by the GPS device, were excluded. The GPS traces of fishing vessels engaged in fishing activities for the *FindFISH* project

were trimmed to capture the periods of effective fishing. This involved manually filtering out information related to parking and net retrieval for each depth profile. The filtering method for depth profile information is presented in Figure 7, which originated from one of WŁA-207's expeditions.

The sections of a profile that were rejected from the fishing efficiency calculations are marked in red (Figure 7). The left side of the figure indicates the stage of the expedition associated with parking the pelagic trawl at the chosen fishing depth. On the right side of the chart, there is a rapid retrieval of the trawl from a depth of approximately 70 meters towards the surface, indicating the end of data recording by the measuring instrument. The effective fishing depth is marked in green and the

TABLE 2 Fragment of the fuzzy inference engine rules. L, ML, M, MH, H indicate low, medium low, medium, medium high, and high, respectively.

Rule number	Temperature	Salinity	Oxygen saturation	Fishing depth	HSI
1	L	M	M	H	MH
2	M	M	M	M	H
3	H	H	L	H	L
4	M	M	L	H	ML
5	L	H	H	H	L
6	M	M	H	H	M
7	H	H	L	L	L
8	M	M	H	L	MH
9	M	L	M	M	MH
10	H	M	M	M	L
11	M	L	H	H	ML
12	L	H	M	L	L

**FIGURE 6** Habitat Suitability Index inference and calculation. L represents the value of low/sub optimal environmental factor, M represents medium/optimal, H represents high/above optimal.

associated start and end times of fishing are determined. These fishing durations were then used to determine the fishing efficiency in all individual fishing expeditions. Fishing efficiency was determined by relating the reported composition and mass of the catch from the fishing survey (Figure 2) to the fishing duration established by the immersion time at the effective fishing depth.

Sprat was caught during 166 fishing expeditions, 134 of them using pelagic trawls (tool code: OTM) and 32 using pelagic pair trawls (tool code: PTM). The expeditions took place from January to the end of May, with a break during the summer months, followed by a resumption in September that continued until the end of the year (Figure 8a). The average catch of sprat for the OTM gear was 9193 kg, while for the PTM gear, it was 8322 kg. The fishing efficiency of the sprat using OTM gear averaged 1900 kg h⁻¹, while PTM gear had a slightly lower efficiency, averaging 1778 kg h⁻¹. These averages exhibited very large standard

deviations, exceeding 1000 kg h⁻¹. As shown in Figure 8a, there is no specific period of the year with significantly higher efficiency than others. The only distinguishable period is spring, from mid-April to mid-May, when the performances were relatively high, and no performances below 800 kg h⁻¹ were recorded.

Herring was caught during 218 fishing expeditions. 154 were conducted using pelagic trawls (OTM), 32 with pelagic pair trawls (PTM), and 32 with gillnets (GNS). The expeditions took place in the same months as the fishing expeditions targeting sprat (Figure 8b) on vessels JAS-74, SZT-1, WSG-22, WŁA-196, WŁA-207, WŁA-22, WŁA-53, WŁA-65, and ZAG-17. Herring and sprat are coexisting species and are usually caught together. However, the abundance of herring catches and fishing efficiency are about half lower compared to sprat catches. In the case of herring, pelagic pair trawls (PTM) were more efficient than pelagic trawls (OTM). The average catch abundance of herring for OTM

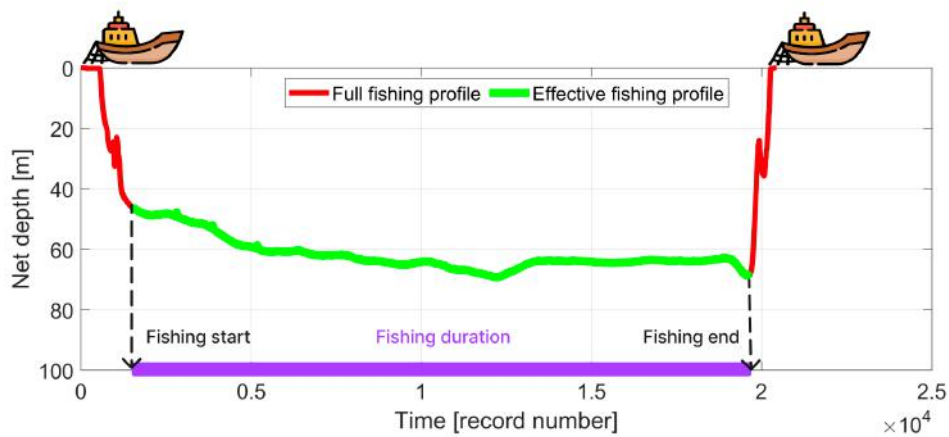


FIGURE 7 Example depth profile of the pelagic trawl (along with the MIDAS CTD+ instrument) during one of the fishing expeditions of WŁA-207.

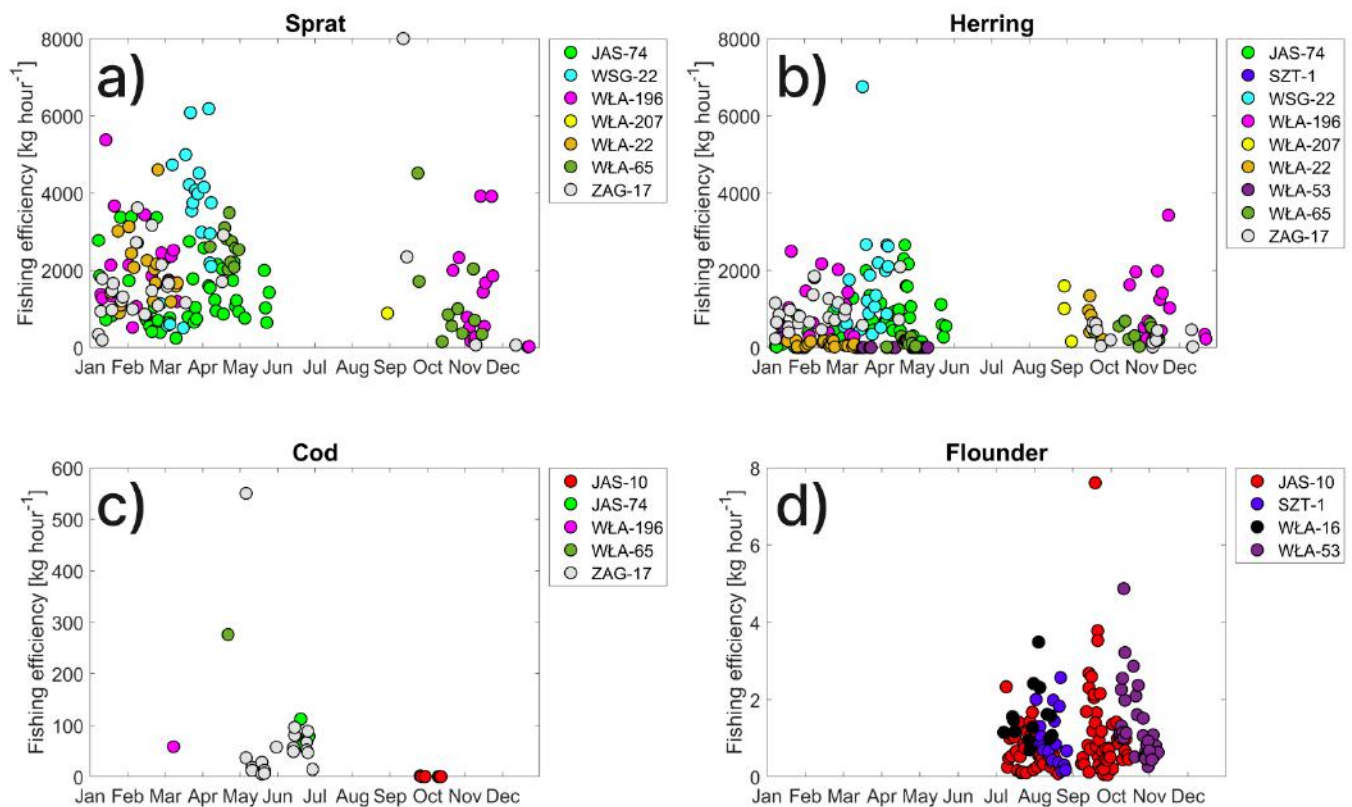


FIGURE 8 Fishing efficiency of vessels for a) sprat, b) herring, c) cod, and d) flounder.

gear was 3389 kg, while for PTM it was 4708 kg. Catches with GNS gear were very low, averaging around 25 kg. The fishing efficiency of herring for vessels using OTM gear was 698 kg h⁻¹ on average, while PTM vessels had a higher efficiency of about 1032 kg h⁻¹. These averages also exhibited very large standard deviations. The average fishing efficiency of herring using GNS gear didn't exceed 2 kg h⁻¹. Similar to sprat, there was no specific month with significantly higher efficiency.

Cod was caught 31 times using bottom trawls (OTB, 23 catches) and gillnets (GNS, 6 catches) by JAS-10, JAS-74, WŁA-196, WŁA-65, and ZAG-17. There was also an expedition using pelagic trawls (OTM) and pelagic pair trawls (PTM). The average catch abundance of cod for OTB gear was 421 kg, while for GNS, it was around 9 kg. The fishing efficiencies were 73 kg h⁻¹ for OTB and 0.5 kg h⁻¹ for GNS. Cod was caught primarily in May and June by ZAG-17 (Figure 8c) and in late September

and October by JAS-10. Single catches occurred in March (with PTM gear) and April (with OTM gear).

The flounder was caught 163 times, predominantly using gillnets (GNS, 160 catches) on JAS-10, SZT-1, WŁA-16, and WŁA-53. There were also 3 expeditions (WŁA-207 and ZAG-17) using bottom trawls (OTB). The average catch abundance of flounder for GNS gear was 25 kg, with a fishing efficiency of approximately 1 kg h^{-1} . Flounder catches were recorded from mid-June to mid-November (Figure 8d).

The duration of the fishing expeditions for sprat and herring using pelagic trawls was approximately 5 hours and 30 minutes. Expeditions with pelagic pair trawls were shorter, averaging around 5 hours. We also compared the duration of individual fishing expeditions with catch abundance for sprat and herring (Figure 9). For both species, undertaking very long fishing durations does not guarantee success in terms of catch mass. Similar catch sizes were observed for short 3-hour expeditions and those exceeding 7 hours.

3.2 | Results of the *Fish Module*. Habitat Suitability Index

Using data from the *EcoFish* model for temperature, salinity, and oxygen saturation (determined from dissolved oxygen concentrations), we analyzed a 5-year period from 2016 to 2020 to identify locations within the model domain that exhibit the most favorable environmental conditions for species investigated in the *FindFISH* project. There are certain limitations for flounder due to the lack of data on the preferred environmental parameters for this species from December to June. The analysis conducted below followed this procedure:

Step 1 For each grid cell in the model, we calculated the median of the Habitat Suitability Index (HSI) score in the water column for all days of the analyzed period.

Step 2 Monthly average medians were calculated next.

Step 3 Subsequently, long-term monthly averages were generated by averaging the medians of each month across consecutive years, that is, the monthly average HSI for January is the average of the medians from January 2016, 2017, 2018, 2019, and 2020.

Analyzing the long-term monthly average median HSI for sprat (Figure 10), it can be observed that the most favorable environmental conditions for this species, determined by the *Fish Module*, occur from December to April. From May to September, the environmental conditions exhibit a zonal pattern with a division into two sectors with distinct characteristics. The shallow coastal zone has noticeably worse environmental conditions compared to the deeper offshore areas. However, in November, the situation is reversed, and more favorable environmental conditions are observed in shallow waters.

The best environmental conditions for herring (as for sprat) occur from December to April (Figure 11). From May to September, there is a zonal distribution of environmental conditions. The shallow coastal zone is not a good habitat area for herring compared to deeper offshore

areas. In October and November, the situation is reversed, and the shallow transition areas are more favorable for herring than the open sea with greater depths. The herring spawning period begins in mid-March and lasts until the end of April. At this time, the herring migrates towards shallower coastal areas. It is particularly common in the southern part of the Gulf of Gdańsk. This is visible in Figure 11 for March and April with high HSI values near the mouth of the Vistula River.

Figure 12 presents the long-term monthly average median HSI for cod. It can be observed that the most favorable environmental conditions for this species, according to the *Fish Module* results, occur in autumn (October, November, and December). In the summer season from May to September, increased HSI values are also observed, but in the deep-water area around the Gdańsk Deep. In the shallow coastal zone and at intermediate depths, unfavorable environmental conditions prevail for cod habitat during these months.

Currently, the *Fish Module* generates HSI results for flounder only for the period from July 1 to November 30. This is due to the lack of the necessary catch data to determine flounder preferences in the remaining months, and attempting to interpolate them from the available months could yield inaccurate results. The missing period will be supplemented in the near future based on expert knowledge. The map of an average median HSI for flounder reveals that the most favorable environmental conditions for this species (for the months when results are available) occur in October and November in the shallow coastal zone of the southern part of the Gulf of Gdańsk and in an area north of the Hel Peninsula (Figure 13). Unfavorable environmental conditions for flounder are observed in the open sea, where greater depths are present.

3.3 | *Fish Module* validation. Relationship between fishing efficiency and Habitat Suitability Index values on the fishing profile

To validate the results of the *Fish Module*, we analyzed the relationship between fishing efficiency and the Habitat Suitability Index along the fishing profile. To achieve this, the vertical section of HSI was extracted from the model output data along the fishing route, and maximum and mean values were determined on the basis of the depths recorded by the MIDAS CTD+ instrument attached to the fishing net.

Figure 14 presents an example of a successful fishing expedition by the ZAG-17 vessel, which took place on February 28, 2020. The effective fishing time during this expedition lasted just over 5 hours and the vessel used pelagic trawl (OTM), resulting in a catch of 10,800 kg of sprat with a fishing efficiency of $2,146 \text{ kg h}^{-1}$. The vertical HSI profile along the fishing route (Figure 14b) clearly shows that the pelagic trawl operated at depths between 30 and 50 meters, corresponding to the maximum HSI values along this route. The average HSI was 0.76 with a maximum of 0.79 (Figure 14c). This indicates a well-chosen location and fishing depth by the skipper, resulting in a plentiful and efficient catch.

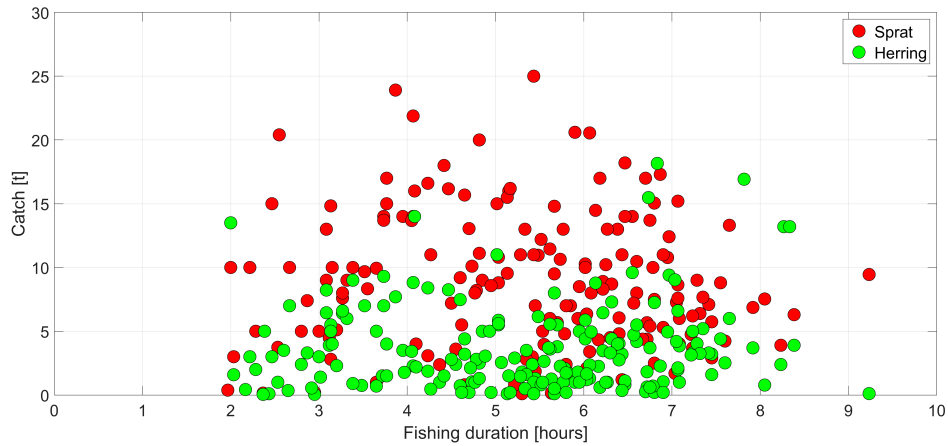


FIGURE 9 Relationship between fishing duration and catch for sprat (red) and herring (green).

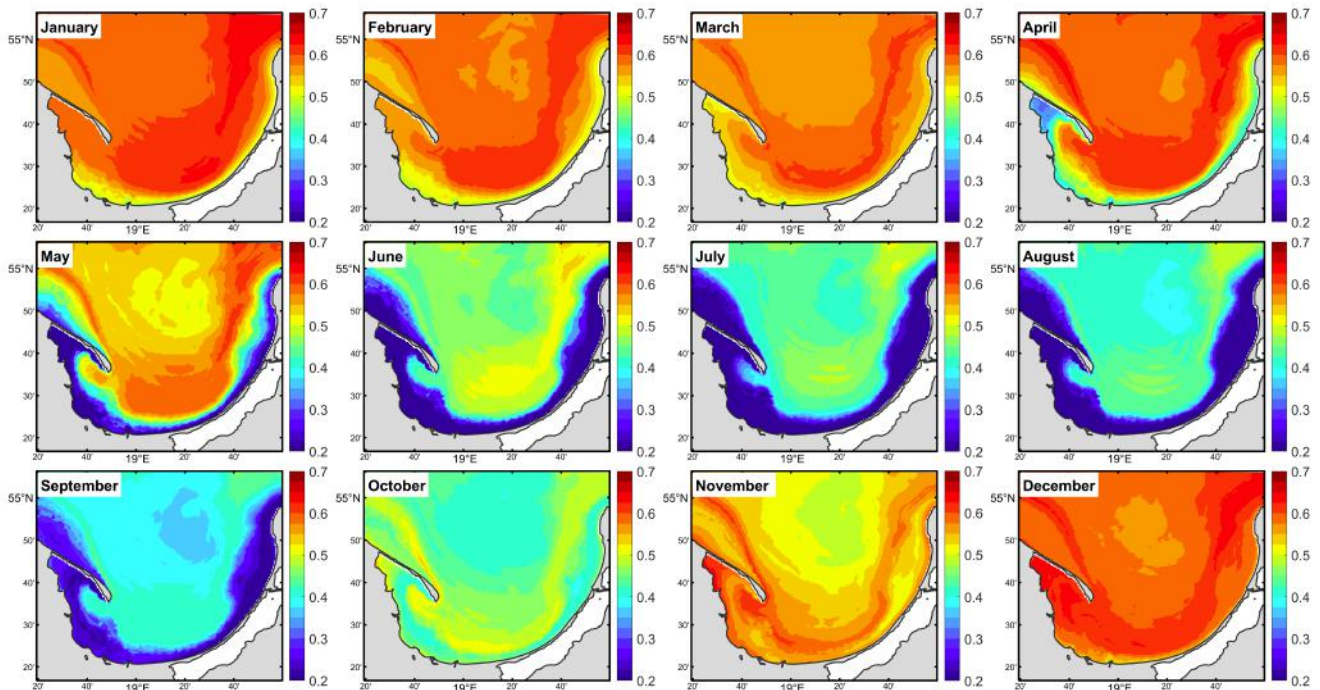


FIGURE 10 Sprat. Long-term (2016-2020) monthly average median HSI values.

The area north of the Vistula mouth has exceptionally good environmental conditions for sprat in February, which can be seen in Figure 10 (Figure 10, February).

Figure 15 presents another example of a fishing expedition, this time conducted by JAS-74, which took place on March 1, 2021 in the central part of the Gulf of Gdańsk. The effective fishing time during this expedition was 4 hours and 50 minutes, and the vessel also used pelagic trawl (OTM), yielding a catch of only 1,300 kg of herring with a low fishing efficiency of 270 kg h^{-1} . The vertical HSI section along the fishing route (Figure 15b) indicates that the pelagic trawl operated at depths between 60 and 75 meters, corresponding to low HSI values at this depth.

The mean HSI was only 0.45 with a maximum of 0.56 (Figure 15c). The HSI profile reveals that better conditions for herring habitat occurred at depths between 40 and 55 meters. It is possible that if the vessel had conducted fishing operations approximately 20 meters higher, it might have achieved fishing success.

Using the same technique, we calculated the mean HSI values for all the fishing expeditions and species analyzed and compared them with fishing efficiencies (Figure 16). Analyzing this comparison, it can be observed that for sprat, herring, and cod, there is a certain threshold value of HSI below which successful catches are unlikely to occur, with only

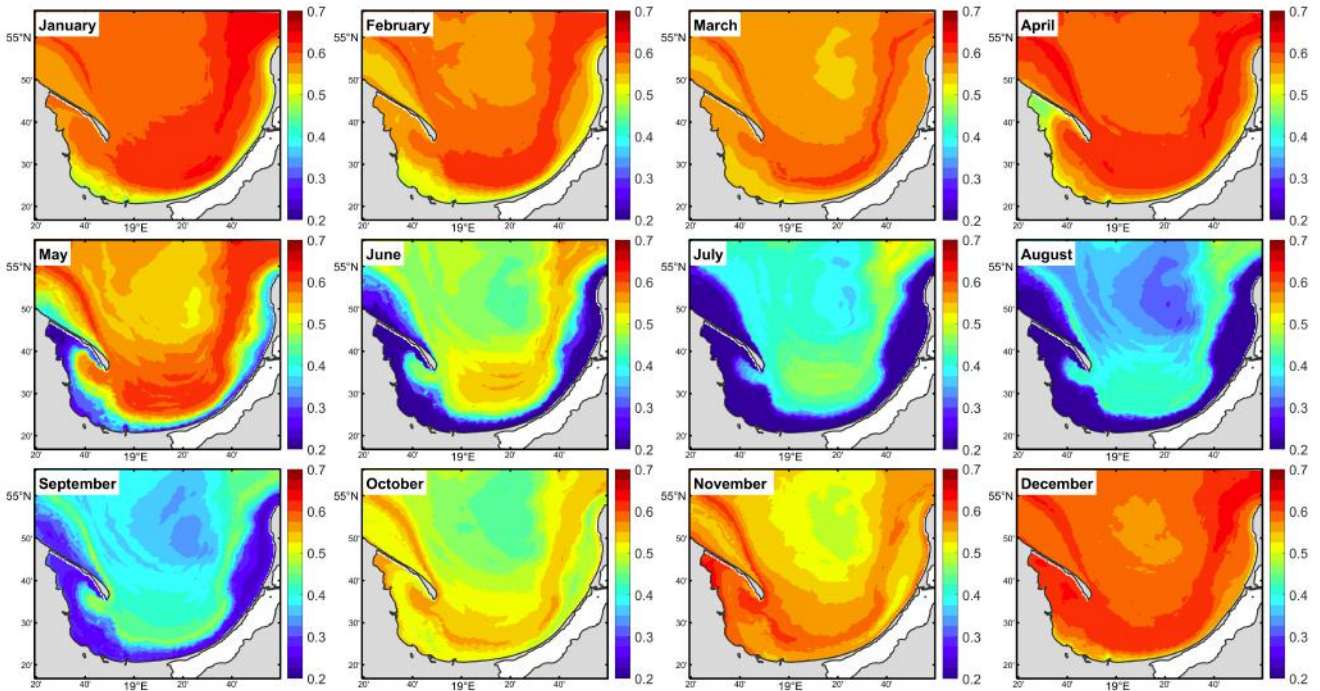


FIGURE 11 Herring. Long-term (2016-2020) monthly average median HSI values.

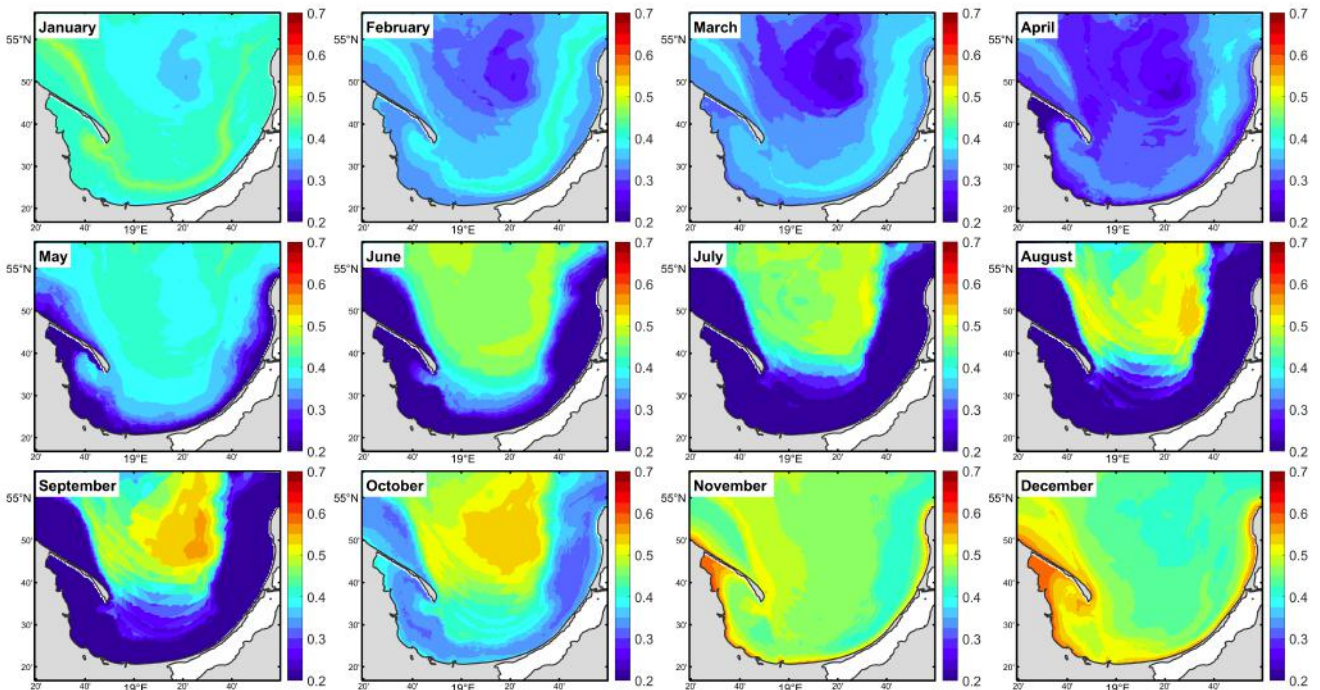


FIGURE 12 Cod. Long-term (2016-2020) monthly average median HSI values.

occasional exceptions. This indicates that the system accurately identifies locations with favorable environmental conditions for the habitat of these three species, and fishermen should choose routes where HSI is at least 0.5 for herring and sprat, and 0.4 for cod. A slight trend is also

visible for these three species (Figure 16a-c) indicating increased fishing efficiency with higher HSI values. This shows that selecting route with sufficiently high HSI score aids in achieving higher fishing efficiencies.

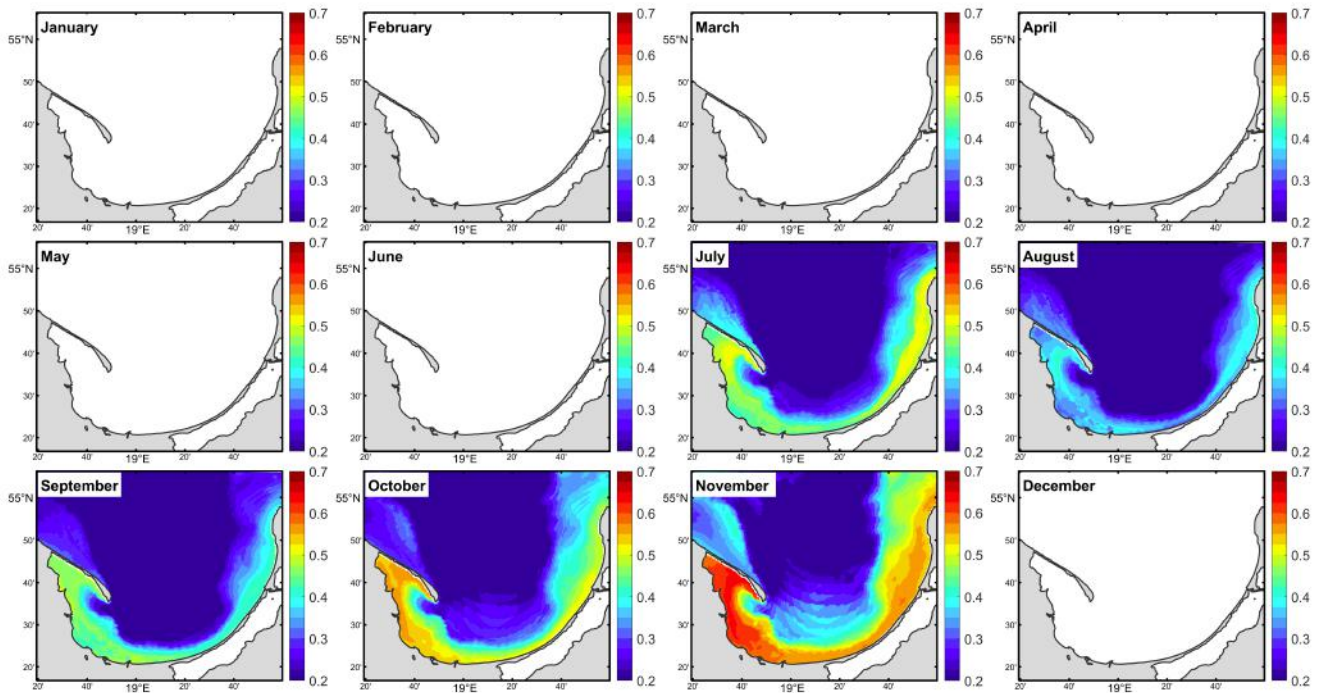


FIGURE 13 Flounder. Long-term (2016-2020) monthly average median HSI values.

However, the situation is not as straightforward for flounder. Here, the performances are scattered across the entire spectrum of HSI variations (Figure 16d). It is not possible to deduce the minimum HSI value from this graph below which fishing should be avoided. However, this does not imply that the system fails for this species. It can be associated with the specifics of flounder fishing itself, mainly using gillnets (GNS). Gillnet is anchored to the seabed in the same location, typically for around 24 hours. In the model, this fixed location corresponds to a single model cell with a single HSI value per unit of time. With such limited HSI variability, a significant dispersion in fishing efficiency can occur around all possible HSI values.

3.4 | Web portal. FindFISH Service

The results from the *EcoFish* model and the *Fish Module* are available through the *FindFISH* project website www.findfish.pl. This platform integrates all the results of the project. It involves free access to the data collected during the fishing expeditions (catch data and physicochemical data recorded by the MIDAS CTD+ instrument). Archived modeled results of hydrodynamic and biochemical parameters and maps of environmental conditions (HSI) for sprat, herring, cod, and flounder with the 48-hour forecasts are available upon registering and subscribing to the service. Forecasts are updated four times a day. The *EcoFish* model calculations are carried out on the *Tryton* supercomputer at the Academic Computer Centre in Gdańsk, Poland. *Fish Module* calculations, and website communication is conducted on the project server located at the Institute of Oceanology of the Polish Academy of Sciences in Sopot,

Poland. For all model products and variables, it is possible to generate raster maps for individual depths, representing the vertical layers of the model. Additionally, it is possible to create temporal and spatial series for specified periods in a selected location (after specifying or indicating the desired latitude and longitude) as well as data tables for selected model parameters. Regarding the *Fish Module*, there are several parameters available (Figure 17):

- Maximum HSI – field showing the maximum HSI values in the water column;
- HSI at the selected depth – a 3-dimensional field showing the HSI values at the selected depth;
- Depth for maximum HSI > 0.9 – a field showing the depths (in meters) at which the maximum HSI occurs in the water column (limited to HSI > 0.9 only);
- Depth for maximum HSI > 0.8 – a field showing the depths (in meters) at which the maximum HSI occurs in the water column (limited to HSI > 0.8 only);
- Depth for maximum HSI > 0.7 – a field showing the depths (in meters) at which the maximum HSI occurs in the water column (limited to HSI > 0.7 only);
- Depth for maximum HSI – a field showing the depths (in meters) at which the maximum HSI occurs in the water column.

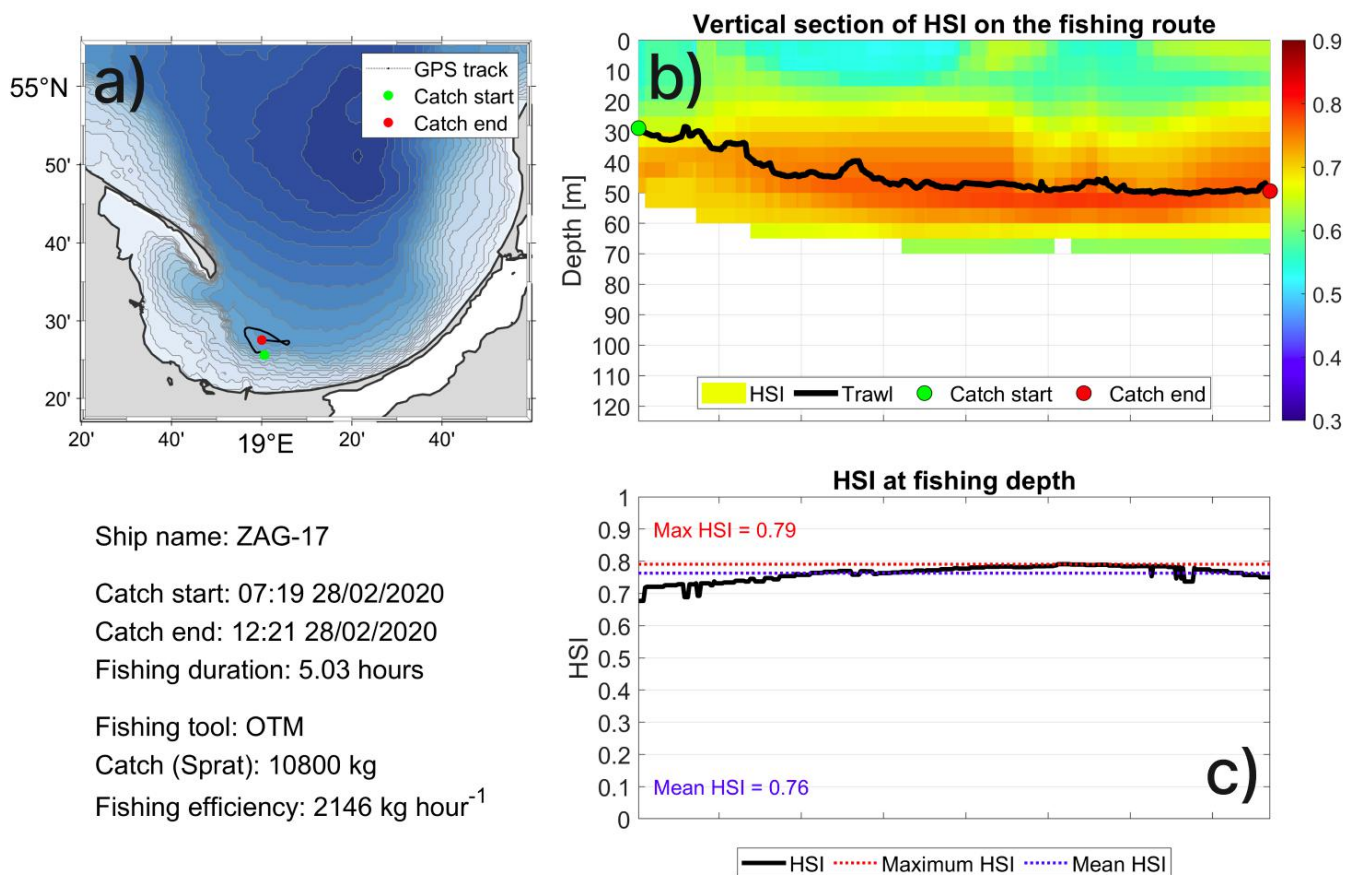


FIGURE 14 Panel displaying the details of successful fishing expedition of ZAG-17 on February 28, 2020; a) GPS track, b) vertical HSI section along the route, and c) HSI values during this expedition.

4 | CONCLUSIONS

The analysis of 408 fishing expeditions conducted in the *FindFISH* project focused on sprat, herring, cod, and flounder. Sprat catches were observed in 166 expeditions, with pelagic trawls (OTM) and pelagic pair trawls (PTM) being the primary gear used. The fishing efficiency for the sprat showed that the OTM gear performs better than the PTM, while for herring catches it was the other way around. Gillnets (GNS) were also used, but their efficiency was significantly lower. Cod catches were limited (as a result of a fishing ban), occurring mainly in May and June, with bottom trawls (OTB) being the primary gear used. Flounder catches occurred predominantly using gillnets (GNS) from mid-June to mid-November.

In general, the results indicate variations in catch abundance and fishing efficiency between different types of gear and species. The fishing efficiency did not show significant variations throughout specific months, except for relatively higher performances observed in spring. The findings provide valuable information on fishing dynamics and highlight the need for careful gear selection and understanding of species behavior to optimize fishing efficiency in the studied area.

The analysis also reveals that the average effective fishing durations for sprat and herring were between five and six hours. By comparing the duration of individual fishing expeditions with sprat and herring catch (Figure 9), it becomes evident that extended fishing durations do not guarantee higher catch. Interestingly, similar catch sizes were observed for both short 3-hour expeditions and those exceeding 7 hours. These findings emphasize that the key determinant in fishing planning lies not in the duration of the expedition itself, but rather in selecting a suitable route with favorable environmental conditions conducive to fish habitat. Thus, it underscores the critical importance of the *FindFISH Knowledge Transfer Platform and the Fish Module*, which, if utilized correctly, can support fishermen in fishing operations.

By calculating the mean HSI values for all the analyzed fishing expeditions and species and comparing them with fishing efficiencies, it was observed that there is a threshold HSI value below which successful catches are unlikely to occur for sprat, herring, and cod, with occasional exceptions. This indicates the system's accuracy in identifying locations with favorable environmental conditions for the habitat of these three species. Fishermen are advised to select routes where the HSI is at least 0.5 for herring and sprat, and greater than 0.4 for cod. Furthermore, a slight trend was observed for these three species, indicating an increase

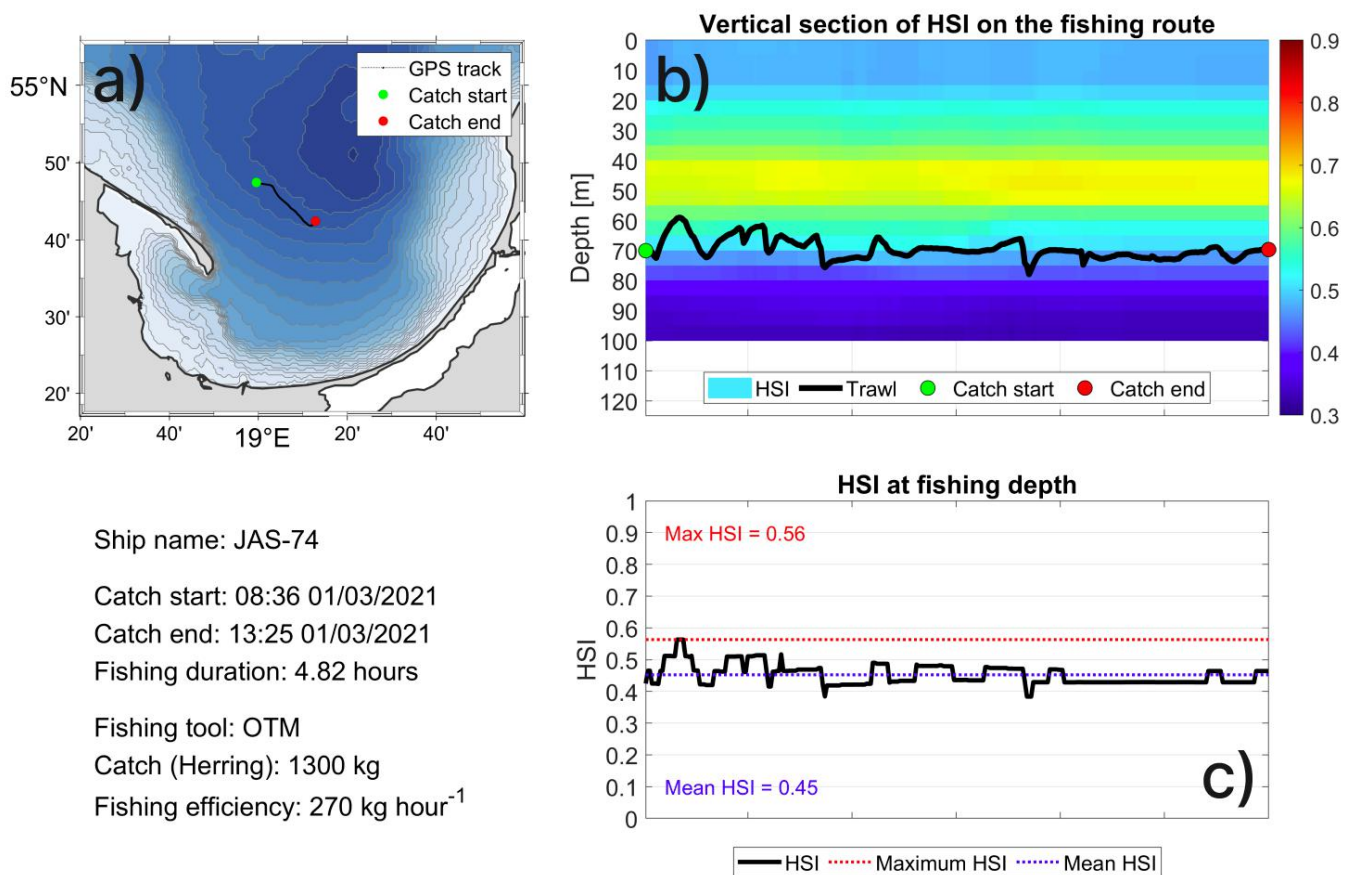


FIGURE 15 Panel displaying the details of an unsuccessful fishing expedition of JAS-74 on March 1, 2021; a) GPS track, b) vertical HSI section along the route, and c) HSI values during this expedition.

in fishing efficiency with higher HSI values. This shows that selecting routes with sufficiently high HSI values contributes to achieving higher fishing efficiencies.

Regarding flounder, the assessment based on comparing fishing efficiency with the mean HSI from the gillnet deployment position did not provide conclusive evidence regarding the system's ability to accurately identify locations with optimal environmental conditions for this species. Although there was a substantial amount of flounder data available, its spatial coverage was not as extensive as that of sprat or herring. The nets were deployed only within three specific areas: the southern part of the Gulf of Gdańsk, the vicinity of the Vistula Spit, and both sides of the Hel Peninsula.

To obtain more reliable validation, it is recommended to conduct dedicated fisheries experiments with and without the system and subsequently compare the catch results. However, since the system has been recently implemented, we currently lack feedback and access to such data. Future research should aim to gather the necessary information for a comprehensive evaluation of the system's performance in relation to flounder fishing.

From a technical standpoint, the implementation of the *FindFISH* platform enables the diagnosis and forecasting of marine environmental

conditions in the Gulf of Gdańsk. It facilitates quick access to essential information regarding the Gulf of Gdańsk environment, which can lead to the reduction of bycatch, improved selection of fishing locations based on specific numerical results presented in a clear and understandable format, easy data recording, and intuitive access and operation of the system through a web browser.

Considering the impact of fishing on the marine environment, we expect that the implementation of the *FindFISH* platform by fishermen will produce numerous positive effects. These effects are anticipated to include reduced fish mortality due to the limitation of unwanted catches, sustainable development of marine fisheries, protection of the Gulf of Gdańsk's marine ecosystem and protected areas, and enhanced self-control over fishing activities by fishermen. It will also help reduce fuel consumption costs for fishing vessels in search of fish and decrease the time that fishermen spend searching for fish.

The economic impact of implementing the *FindFISH* platform is expected to be immediately felt upon its commercialization and utilization by fishermen. On the other hand, significant environmental and fisheries impacts are likely to be observed within several years after the service's implementation. The *FindFISH* platform is estimated to be valuable not

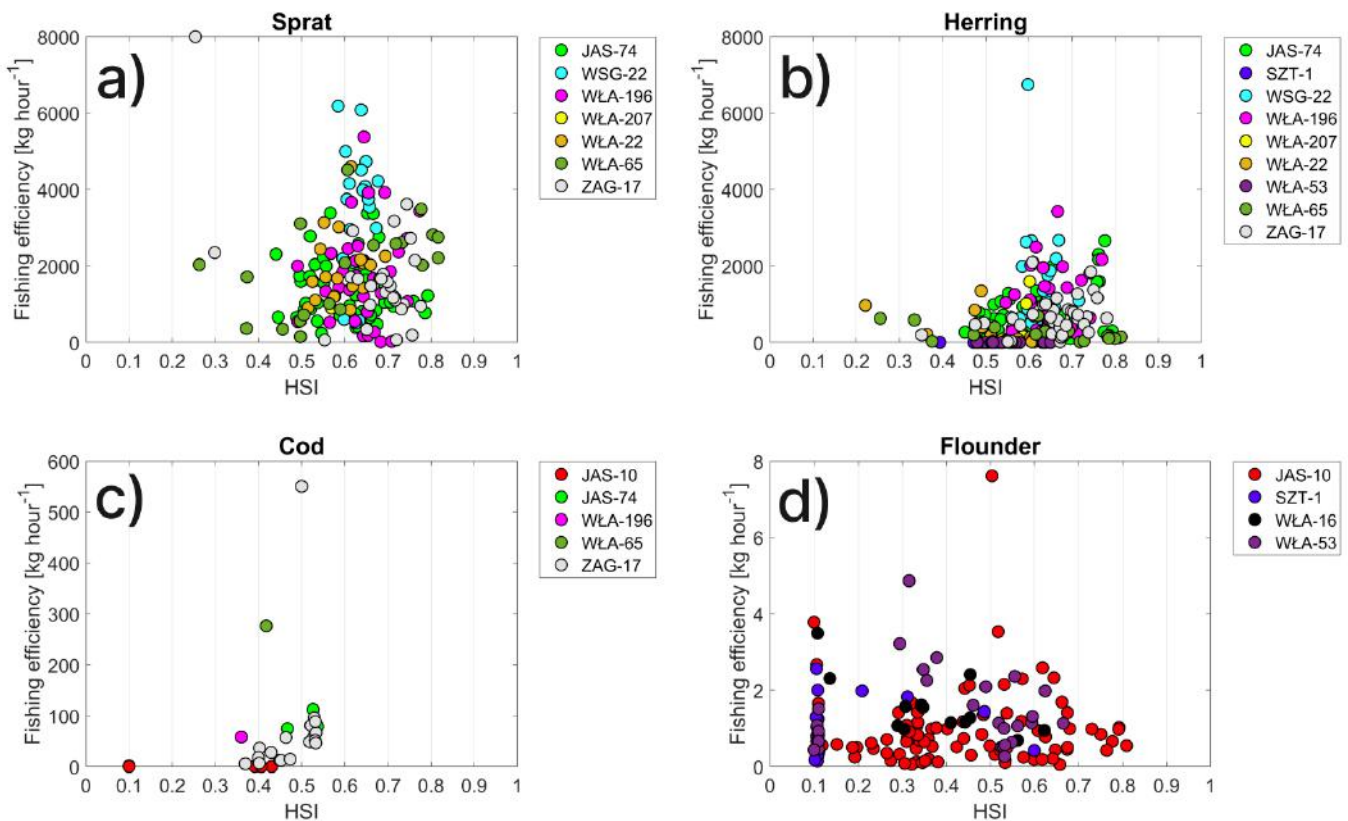


FIGURE 16 Fishing efficiency for a) sprat, b) herring, c) cod, and d) flounder related to the mean HSI value along the fishing route.

only for fishermen and scientists, but also for individuals responsible for shaping maritime and fisheries policies.

AUTHOR CONTRIBUTIONS

Maciej Janecki contributed in: conceptualization, methodology, software, validation, formal analysis, investigation, resources, data curation, writing, original draft preparation, visualization.

Lidia Dzierzbicka-Głowacka contributed in: conceptualization, formal analysis, investigation, original draft preparation, supervision, project administration, funding acquisition.

ACKNOWLEDGMENTS

Calculations were carried out at the Academic Computer Centre in Gdańsk. We are grateful to the anonymous reviewers for valuable comments on earlier versions of the manuscript.

FUNDING

Partial support for this study was provided by the project “Knowledge transfer platform Find-Fish Numerical Forecasting System for the Marine Environment of the Gulf of Gdańsk for Fisheries” funded by the European Union through the European Regional Development Fund Contract RPPM.01.01.01-22-0025/16-00.

Some elements of the EcoFish model (i.e., river runoff data) are based on the solutions developed during the WaterPUCK project funded by

the National Centre for Research and Development of Poland within the BIOSTRATEG III program BIOSTRATEG3/343927/3/NCBR/2017.

CONFLICT OF INTEREST

The authors declare no potential conflict of interests.

References

- Beecher, H. A., Caldwell, B. A., & DeMond, S. B. (2002). Evaluation of Depth and Velocity Preferences of Juvenile Coho Salmon in Washington Streams. *North American Journal of Fisheries Management*, 22(3), 785–795. doi: 10.1577/1548-8675(2002)022<0785:EODAVP>2.0.CO;2
- Bovee, K. D. (1986). *Development and evaluation of habitat suitability criteria for use in the instream flow incremental methodology* (Other Report FWS/OBS-86/7). Washington, D.C.: USDI Fish and Wildlife Service. Retrieved from <http://pubs.er.usgs.gov/publication/70121265>
- Camphuysen, C., & Garthe, S. (2000). Sea birds and commercial fisheries: population trends of piscivorous seabirds explained? In *Effects of Fishing on Non-Target Species and Habitats* (pp. 163–184). Oxford: Blackwell Science.
- Chou, W.-C., Lin, W.-T., & Lin, C.-Y. (2007). Application of

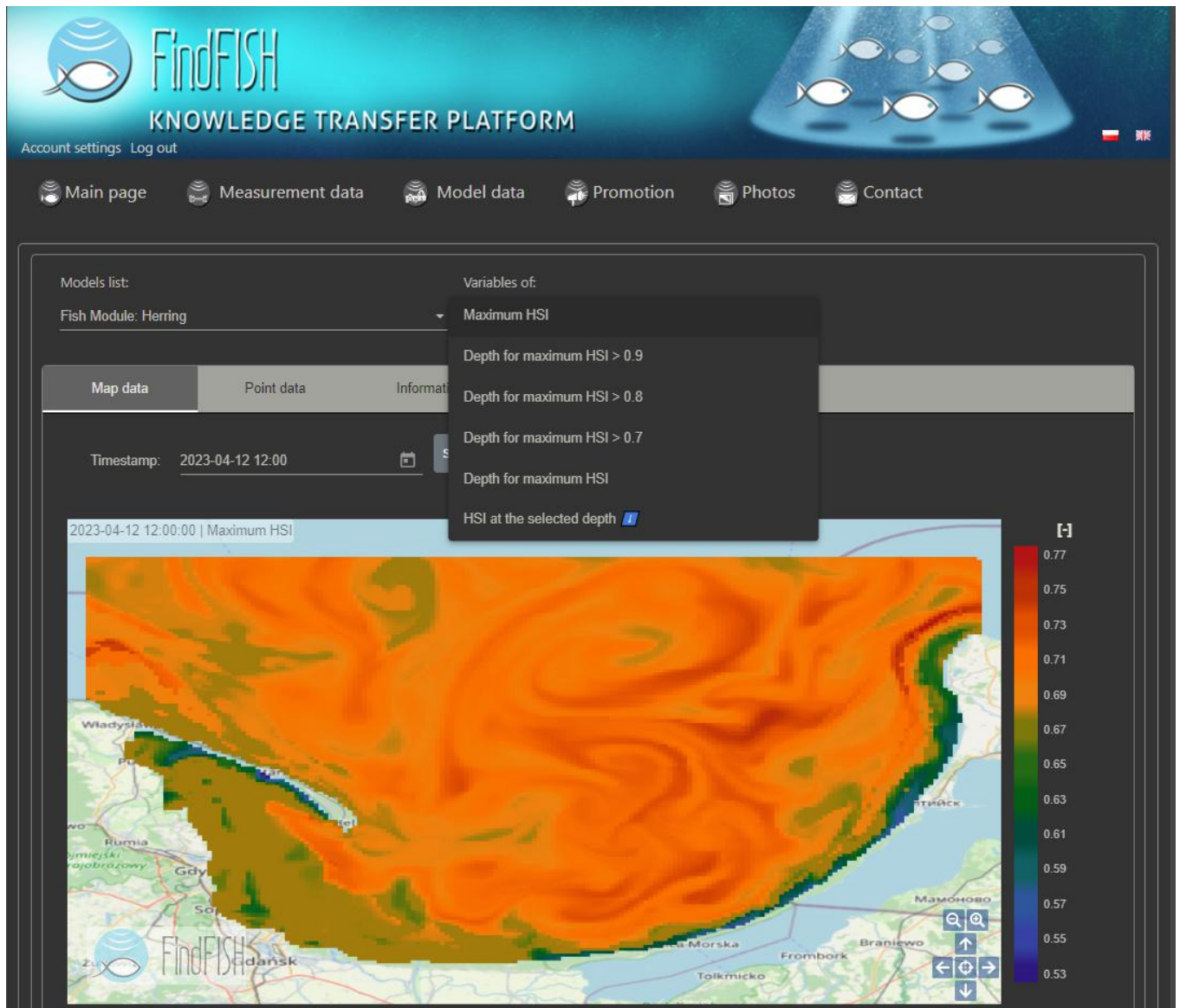


FIGURE 17 FindFISH project website. List of available parameters of the Fish Module, and the map of the Maximum HSI for herring on April 12, 2023.

fuzzy theory and PROMETHEE technique to evaluate suitable ecotechnology method: A case study in Shihmen Reservoir Watershed, Taiwan. *Ecological Engineering*, 31(4), 269–280. doi: 10.1016/j.ecoleng.2007.08.004

Davies, R. W. D., Cripps, S. J., Nickson, A., & Porter, G. (2009). Defining and estimating global marine fisheries bycatch. *Marine Policy*, 33(4), 661–672. doi: 10.1016/j.marpol.2009.01.003

Dzierzbicka-Głowacka, L. (2023). *Platforma transferu wiedzy FindFISH - Numeryczny System Prognozowania warunków środowiska morskiego Zatoki Gdańskiej dla Rybołówstwa*. Gdynia: Wydawnictwo Uniwersytetu Morskiego w Gdyni. Retrieved from <https://doi.org/10.26408/FindFISH>

Dzierzbicka-Głowacka, L., Janecki, M., Nowicki, A., & Jakacki, J.

(2013). Activation of the operational ecohydrodynamic model (3D CEMBS) – the ecosystem module. *Oceanologia*, 55(3), 543–572. doi: 10.5697/oc.55-3.543

Dzierzbicka-Głowacka, L., Nowicki, A., Janecki, M., Szymczycha, B., Piotrowski, P., Piecki, P., & Łukasiewicz, G. (2018). Structure of the FindFish Knowledge Transfer Platform. *Fisheries & Aquatic Life*, 26(3), 193–197. doi: 10.2478/aopf-2018-0021

Fraternali, P., Castelletti, A., Soncini-Sessa, R., Vaca Ruiz, C., & Rizzoli, A. E. (2012). Putting humans in the loop: Social computing for Water Resources Management. *Environmental Modelling & Software*, 37, 68–77. doi: 10.1016/j.envsoft.2012.03.002

Fukuda, S., De Baets, B., Mouton, A. M., Waegeman, W., Nakajima, J., Mukai, T., ... Onikura, N. (2011). Effect of model formulation on

- the optimization of a genetic Takagi–Sugeno fuzzy system for fish habitat suitability evaluation. *Ecological Modelling*, 222(8), 1401–1413. doi: 10.1016/j.ecolmodel.2011.01.023
- Godfray, H. C. J., Beddington, J. R., Crute, I. R., Haddad, L., Lawrence, D., Muir, J. F., ... Toulmin, C. (2010). Food Security: The Challenge of Feeding 9 Billion People. *Science*, 327(5967), 812–818. doi: 10.1126/science.1185383
- Hilborn, R., Branch, T. A., Ernst, B., Magnusson, A., Minte-Vera, C. V., Scheuerell, M. D., & Valero, J. L. (2003). State of the World's Fisheries. *Annual Review of Environment and Resources*, 28(1), 359–399. doi: 10.1146/annurev.energy.28.050302.105509
- Inglis, G. J., Hurren, H., Oldman, J., & Haskew, R. (2006). Using Habitat Suitability Index and Particle Dispersion Models for Early Detection of Marine Invaders. *Ecological Applications*, 16(4), 1377–1390. doi: 10.1890/1051-0761(2006)016[1377:UHSIAP]2.0.CO;2
- Janecki, M., Dybowski, D., & Dzierzbicka-Głowacka, L. (2023). The influence of biochemical parameters on primary production in the Gulf of Gdańsk region: A model study. *Oceanologia*. doi: 10.1016/j.oceano.2023.05.001
- Janecki, M., Dybowski, D., Jakacki, J., Nowicki, A., & Dzierzbicka-Głowacka, L. (2021). The Use of Satellite Data to Determine the Changes of Hydrodynamic Parameters in the Gulf of Gdańsk via EcoFish Model. *Remote Sensing*, 13(18), 3572. doi: 10.3390/rs13183572
- Janecki, M., Dybowski, D., Rak, D., & Dzierzbicka-Głowacka, L. (2022). A New Method for Thermocline and Halocline Depth Determination at Shallow Seas. *Journal of Physical Oceanography*, 52(9), 2205–2218. doi: 10.1175/JPO-D-22-0008.1
- Legleiter, C. J., & Goodchild, M. F. (2005). Alternative representations of in-stream habitat: classification using remote sensing, hydraulic modeling, and fuzzy logic. *International Journal of Geographical Information Science*, 19(1), 29–50. doi: 10.1080/13658810412331280220
- Moore, J. K., Doney, S. C., Kleypas, J. A., Glover, D. M., & Fung, I. Y. (2001). An intermediate complexity marine ecosystem model for the global domain. *Deep Sea Research Part II: Topical Studies in Oceanography*, 49(1), 403–462. doi: 10.1016/S0967-0645(01)00108-4
- Mouton, A. M., De Baets, B., & Goethals, P. L. M. (2009). Knowledge-based versus data-driven fuzzy habitat suitability models for river management. *Environmental Modelling & Software*, 24(8), 982–993. doi: 10.1016/j.envsoft.2009.02.005
- Muñoz-Mas, R., Martínez-Capel, F., Schneider, M., & Mouton, A. M. (2012). Assessment of brown trout habitat suitability in the Júcar River Basin (SPAIN): Comparison of data-driven approaches with fuzzy-logic models and univariate suitability curves. *Science of The Total Environment*, 440, 123–131. doi: 10.1016/j.scitotenv.2012.07.074
- Myers, R. A., & Worm, B. (2003). Rapid worldwide depletion of predatory fish communities. *Nature*, 423(6937), 280–283. doi: 10.1038/nature01610
- Poulos, H., Chernoff, B., Fuller, P., & Butman, D. (2012). Ensemble forecasting of potential habitat for three invasive fishes. In *Proceedings of the 17th International Conference on Aquatic Invasive Species* (pp. 59–72). San Diego, USA. doi: https://doi.org/10.3391/ai.2012.7.1.007
- Prato, T. (2007). Assessing ecosystem sustainability and management using fuzzy logic. *Ecological Economics*, 61(1), 171–177. doi: 10.1016/j.ecolecon.2006.08.004
- Rüger, N., Schlüter, M., & Matthies, M. (2005). A fuzzy habitat suitability index for *Populus euphratica* in the Northern Amudarya delta (Uzbekistan). *Ecological Modelling*, 184(2), 313–328. doi: 10.1016/j.ecolmodel.2004.10.010
- UN, S.-G. (2006). Impacts of fishing on vulnerable marine ecosystems :: actions taken by States and regional fisheries management organizations and arrangements to give effect to paragraphs 66 to 69 of General Assembly resolution 59/25 on sustainable fisheries, regarding the impact of fishing on vulnerable marine ecosystems : report of the Secretary-General. *Report of the Secretary-General*.
- Van Broekhoven, E., Adriaenssens, V., De Baets, B., & Verdonshot, P. F. M. (2006). Fuzzy rule-based macroinvertebrate habitat suitability models for running waters. *Ecological Modelling*, 198(1), 71–84. doi: 10.1016/j.ecolmodel.2006.04.006
- Zadeh, L. A. (1965). Fuzzy sets. *Information and Control*, 8(3), 338–353. doi: 10.1016/S0019-9958(65)90241-X
- Zhang, H., Sun, T., Shao, D., & Yang, W. (2016). Fuzzy Logic Method for Evaluating Habitat Suitability in an Estuary Affected by Land Reclamation. *Wetlands*, 36(1), 19–30. doi: 10.1007/s13157-014-0606-2

6 Authorship statements

Maciej Janecki

Institute of Oceanology of the Polish Academy of Sciences
Powstańców Warszawy 55
81-712 Sopot
Poland

Sopot, 1 June 2023

AUTHORSHIP STATEMENTS OF CO-AUTHOR OF THE ARTICLE

I confirm that I am co-author of the articles:

1. **Janecki, M.**, Dybowski, D., Jakacki, J., Nowicki, A., Dzierzbicka-Głowacka L., 2021. *The Use of Satellite Data to Determine the Changes of Hydrodynamic Parameters in the Gulf of Gdańsk via EcoFish Model*. Remote Sensing 13, 3572. <https://doi.org/10.3390/rs13183572>
2. **Janecki, M.**, Dybowski, D., Rak, D., Dzierzbicka-Głowacka L., 2022. *A New Method for Thermocline and Halocline Depth Determination at Shallow Seas*. Journal of Physical Oceanography 52, 2205–2218. <https://doi.org/10.1175/JPO-D-22-0008.1>
3. **Janecki, M.**, Dybowski, D., Dzierzbicka-Głowacka, L., 2023. *The influence of biochemical parameters on primary production in the Gulf of Gdańsk region: A model study*. Oceanologia. <https://doi.org/10.1016/j.oceano.2023.05.001>
4. **Janecki, M.**, Dzierzbicka-Głowacka, L., 2023. *Fish Module - A Prognostic Tool for Modeling the Optimal Environmental Conditions for Fish in the Gulf of Gdańsk (Southern Baltic Sea)*. Submitted to Fish and Fisheries Journal.

I declare that my contribution of **75%** to article No. 1, **80%** to article No. 2, **85%** to article No. 3, and **85%** to article No. 4 included participation in:

- studies conception
- data preparation and analysis
- interpretation of the results
- writing and revising manuscripts

Maciej Janecki

Lidia Dzierzbicka-Głowacka

Institute of Oceanology of the Polish Academy of Sciences
Powstańców Warszawy 55
81-712 Sopot
Poland

Sopot, 1 June 2023

AUTHORSHIP STATEMENTS OF CO-AUTHOR OF THE ARTICLE

I confirm that I am co-author of the article:

1. Janecki, M., Dybowski, D., Jakacki, J., Nowicki, A., **Dzierzbicka-Głowacka L.**, 2021. *The Use of Satellite Data to Determine the Changes of Hydrodynamic Parameters in the Gulf of Gdańsk via EcoFish Model*. Remote Sensing 13, 3572. <https://doi.org/10.3390/rs13183572>
2. Janecki, M., Dybowski, D., Rak, D., **Dzierzbicka-Głowacka L.**, 2022. *A New Method for Thermocline and Halocline Depth Determination at Shallow Seas*. Journal of Physical Oceanography 52, 2205–2218. <https://doi.org/10.1175/JPO-D-22-0008.1>
3. Janecki, M., Dybowski, D., **Dzierzbicka-Głowacka, L.**, 2023. *The influence of biochemical parameters on primary production in the Gulf of Gdańsk region: A model study*. Oceanologia. <https://doi.org/10.1016/j.oceano.2023.05.001>
4. Janecki, M., **Dzierzbicka-Głowacka, L.**, 2023. *Fish Module - A Prognostic Tool for Modeling the Optimal Environmental Conditions for Fish in the Gulf of Gdańsk (Southern Baltic Sea)*. Submitted to Fish and Fisheries Journal.

I declare that my contribution of **10%** to article No. 1, **10%** to article No. 2, **10%** to article No. 3, and **15%** to article No. 4 included participation in:

- studies conception
- interpretation of the results
- writing and revising manuscripts



Dawid Dybowski

Institute of Oceanology of the Polish Academy of Sciences
Powstańców Warszawy 55
81-712 Sopot
Poland

Sopot, 1 June 2023

AUTHORSHIP STATEMENTS OF CO-AUTHOR OF THE ARTICLE

I confirm that I am co-author of the article:

1. Janecki, M., **Dybowski, D.**, Jakacki, J., Nowicki, A., Dzierzbicka-Głowacka L., 2021. *The Use of Satellite Data to Determine the Changes of Hydrodynamic Parameters in the Gulf of Gdańsk via EcoFish Model*. Remote Sensing 13, 3572. <https://doi.org/10.3390/rs13183572>
2. Janecki, M., **Dybowski, D.**, Rak, D., Dzierzbicka-Głowacka L., 2022. *A New Method for Thermocline and Halocline Depth Determination at Shallow Seas*. Journal of Physical Oceanography 52, 2205–2218. <https://doi.org/10.1175/JPO-D-22-0008.1>
3. Janecki, M., **Dybowski, D.**, Dzierzbicka-Głowacka, L., 2023. *The influence of biochemical parameters on primary production in the Gulf of Gdańsk region: A model study*. Oceanologia. <https://doi.org/10.1016/j.oceano.2023.05.001>

I declare that my contribution of **5%** to article No. 1, **5%** to article No. 2, and **5%** to article No. 3 included participation in:

- studies conception
- interpretation of the results
- writing and revising manuscripts



Artur Nowicki

Institute of Oceanology of the Polish Academy of Sciences
Powstańców Warszawy 55
81-712 Sopot
Poland

Sopot, 1 June 2023

AUTHORSHIP STATEMENTS OF CO-AUTHOR OF THE ARTICLE

I confirm that I am co-author of the article:

1. Janecki, M., Dybowski, D., Jakacki, J., **Nowicki, A.**, Dzierzbicka-Glowacka L., 2021. *The Use of Satellite Data to Determine the Changes of Hydrodynamic Parameters in the Gulf of Gdańsk via EcoFish Model*. Remote Sensing 13, 3572. <https://doi.org/10.3390/rs13183572>

I declare that my contribution (5%) to this article included participation in:

- data preparation and analysis
- interpretation of the results
- writing and revising the manuscript





PODPIS ZAUFANY

JAROMIR
JAKACKI
10.06.2023 19:25:59 [GMT+2]
Dokument podpisany elektronicznie
podpisem zaufanym

Sopot, 1 June 2023

Jaromir Jakacki

Institute of Oceanology of the Polish Academy of Sciences
Powstańców Warszawy 55
81-712 Sopot
Poland

AUTHORSHIP STATEMENTS OF CO-AUTHOR OF THE ARTICLE

I confirm that I am co-author of the article:

1. Janecki, M., Dybowski, D., **Jakacki, J.**, Nowicki, A., Dzierzbicka-Glowacka L., 2021. *The Use of Satellite Data to Determine the Changes of Hydrodynamic Parameters in the Gulf of Gdańsk via EcoFish Model*. Remote Sensing 13, 3572. <https://doi.org/10.3390/rs13183572>

I declare that my contribution to this article is **5%**.

Daniel Rak

Institute of Oceanology of the Polish Academy of Sciences
Powstańców Warszawy 55
81-712 Sopot
Poland

Sopot, 1 June 2023

AUTHORSHIP STATEMENTS OF CO-AUTHOR OF THE ARTICLE

I confirm that I am co-author of the article:

1. Janecki, M., Dybowski, **D., Rak, D.**, Dzierzbicka-Głowacka L., 2022. *A New Method for Thermocline and Halocline Depth Determination at Shallow Seas*. Journal of Physical Oceanography 52, 2205–2218. <https://doi.org/10.1175/JPO-D-22-0008.1>

I declare that my contribution (5%) to this article included participation in:

- data acquisition and analysis
- interpretation of the results
- writing the manuscript

Daniel Rak

7 Acknowledgments

Presented studies were carried out in Marine Ecohydrodynamics Laboratory (Physical Oceanography Department) of the Institute of Oceanology of the Polish Academy of Sciences in Sopot, Poland.

This study was supported by :

- Project “Modelling of the impact of the agricultural holdings and land-use structure on the quality of inland and coastal waters of the Baltic Sea set up on the example of the Municipality of Puck region - Integrated info-prediction Web Service WaterPUCK” funded by the National Centre for Research and Development within BIOSTRATEG III Programme "Natural environment, agriculture and forestry" devoted to the Problem Area I "Rational management of natural resources with special regard to water management" (grant no. BIOSTRATEG3/343927/3/NCBR/2017).
- Project “Knowledge transfer platform FindFISH - Numerical Forecasting System for the Marine Environment of the Gulf of Gdańsk for Fisheries,” funded by the European Union through European Regional Development Fund Contract RPPM.01.01.01-22-0025/16-00.
- Institute of Oceanology of the Polish Academy of Sciences statutory task number II.1.

Computations were carried out using the computers of Centre of Informatics Tricity Academic Supercomputer & Network

First and foremost I am grateful to my supervisor Prof. Lidia Dzierzbicka-Głowacka for her guidance and support during this very interesting research that laid the foundation for this dissertation.

Special thanks are dedicated to the Colleagues and Organizations: IO PAN - Dawid Dybowski, Artur Nowicki, Jaromir Jakacki, Daniel Rak, Krzysztof Rutkowski, Agata Zaborska, Małgorzata Merchel, Natalia Szymańska; ZRM-OP – Jacek Wittbrodt, Grzegorz Krzemień, Grzegorz Łukasiewicz; Maritime Institute - Piotr Pieckiel, Tomasz Kuczyński, Michał Wójcik, Piotr Piotrowski; CI TASK - Bartosz Pliszka, Michał Białoskórski.

This journey would not have been possible without the dedicated support of my family and friends: Regina and Stanisław, Beata, Piotr and Ola, Michał, Anna and Piotr, Dominika and Dawid, Agata and Kamil, Ola and Mateusz, Beata and Max, Maciek, Mateusz, Marzena. Thank you for believing in me!

Last but not least, I would like to express my deepest gratitude to beloved fiance Maja for her constant support and belief.